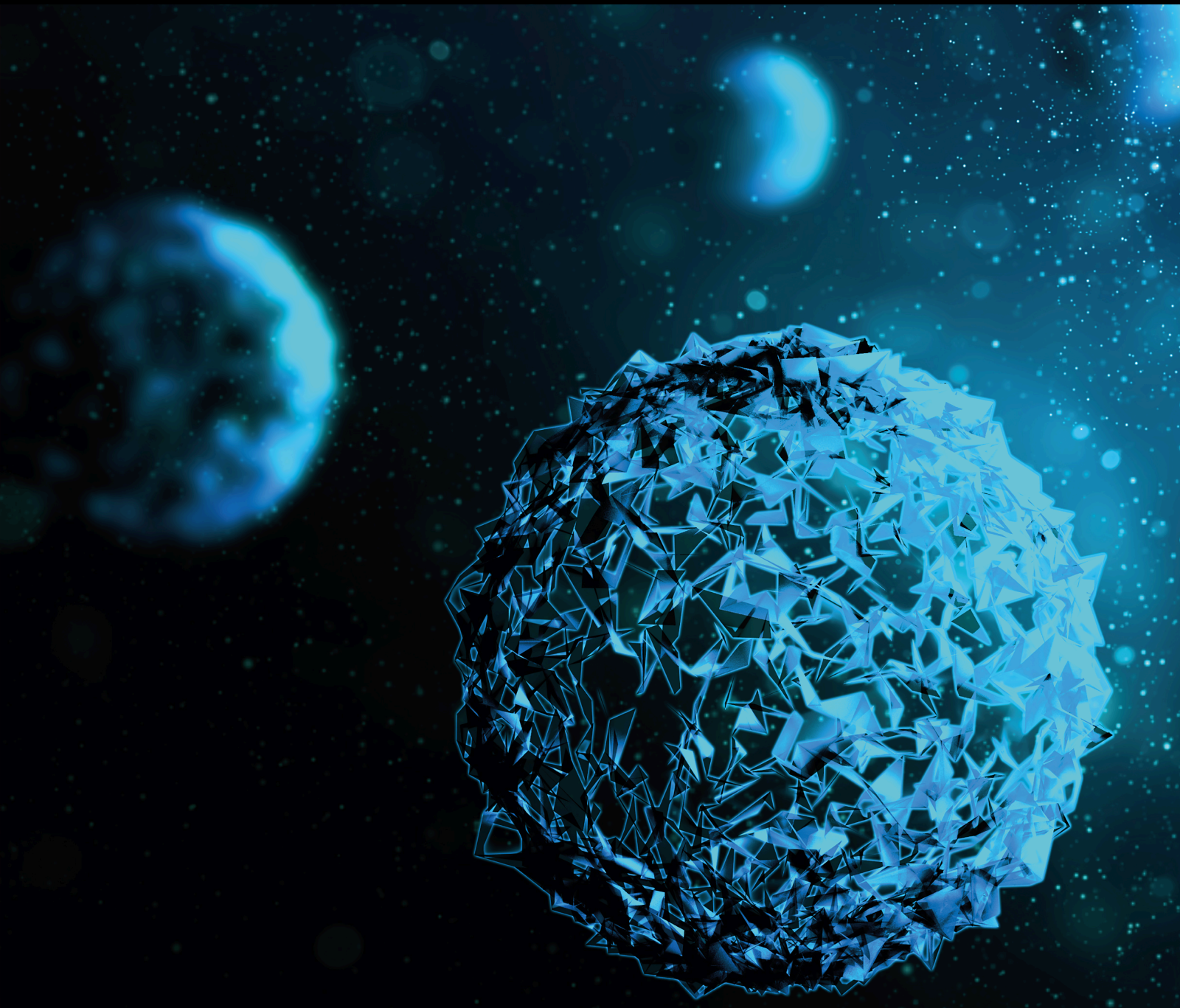


BioMed Research International

Implant Dentistry: New Materials and Technologies 2020

Lead Guest Editor: Luigi Canullo

Guest Editors: Henriette Lerner and Paolo Pesce





Implant Dentistry: New Materials and Technologies 2020

BioMed Research International

Implant Dentistry: New Materials and Technologies 2020

Lead Guest Editor: Luigi Canullo

Guest Editors: Henriette Lerner and Paolo Pesce



Copyright © 2021 Hindawi Limited. All rights reserved.

This is a special issue published in "BioMed Research International." All articles are open access articles distributed under the Creative Commons Attribution License, which permits unrestricted use, distribution, and reproduction in any medium, provided the original work is properly cited.

Editorial Board

Nadia Benkirane-Jessel, France
Adriana Bigi, Italy
Roya Dastjerdi, Iran
Marília G. de Oliveira, Brazil
Despina Deligianni, Greece
Nicholas Dunne, Ireland
Mirella Falconi, Italy
Victor Feitosa, Brazil
Milena Fini, Italy
Luca Fiorillo, Italy
Razvan Ghinea, Spain
Dong-Wook Han, Republic of Korea
Ming-Fa Hsieh, Taiwan
Elena Landi, Italy
Hwa-Liang Leo, Singapore
Jianshu Li, China
Joshua R. Mauney, USA
Konstantinos Michalakis, USA
Saeed Reza Motamedian, Iran
Sergio Murgia, Italy
Kee Woei Ng, Singapore
GuoXin Ni, China
Giuseppina Nocca, Italy
Changjiang Pan, China
Ravikiran Panakanti, USA
Georgios E. Romanos, USA
Mahmoud Rouabhia, Canada
Antonio Salgado, Portugal
Susan Sandeman, United Kingdom
Hélder A. Santos, Finland
Jan D. Schmitto, Germany
Andrea Scribante, Italy
Nick Silikas, United Kingdom
Gianrico Spagnuolo, Italy
Claudio Stacchi, Italy
Silvia Todros, Italy
Helena Tomas, Portugal
Mikael J. Turunen, Finland
Yu-Chang Tyan, Taiwan
cagri ulusoy, Turkey
Xiupeng Wang, Japan
Tetsuji Yamaoka, Japan

Chuan Ye, China
Hyuk Sang Yoo, Republic of Korea

Contents

Implant Dentistry: New Materials and Technologies 2020

Luigi Canullo , Henriette Lerner , and Paolo Pesce 

Editorial (1 page), Article ID 9852932, Volume 2021 (2021)

Dental Pulp Stem Cells on Implant Surface: An In Vitro Study

Luigi Laino, Marcella La Noce, Luca Fiorillo , Gabriele Cervino , Ludovica Nucci, Diana Russo, Alan Scott Herford, Salvatore Crimi, Alberto Bianchi, Antonio Biondi, Gregorio Laino, Antonino Germanà, and Marco Ciccù 

Research Article (12 pages), Article ID 3582342, Volume 2021 (2021)

The Alveolar Ridge Splitting Technique on Maxillae: A Biomechanical Human Cadaveric Investigation

Fabian Duttonhoefer , Peter Varga , Dominik Jenni, Leonard Grünwald, Luisa Thiemann, Boyko Gueorguiev , and Andres Stricker

Research Article (7 pages), Article ID 8894471, Volume 2020 (2020)

Environmental Disinfection of a Dental Clinic during the Covid-19 Pandemic: A Narrative Insight

Antonio Scarano , Francesco Inchingolo, and Felice Lorusso

Review Article (15 pages), Article ID 8896812, Volume 2020 (2020)

Digital vs. Freehand Anterior Single-Tooth Implant Restoration

D. Baldi, J. Colombo , F. Motta, F. M. Motta, A. Zillio, and N. Scotti

Research Article (6 pages), Article ID 4012127, Volume 2020 (2020)

Monolithic and Minimally Veneered Zirconia Complications as Implant-Supported Restorative Material: A Retrospective Clinical Study up to 5 Years

Markel Diéguez-Pereira , David Chávarri-Prado, Alejandro Estrada-Martínez, Esteban Pérez-Pevida, and Aritza Brizuela-Velasco

Research Article (6 pages), Article ID 8821068, Volume 2020 (2020)

Finite Element Method and Von Mises Investigation on Bone Response to Dynamic Stress with a Novel Conical Dental Implant Connection

Luca Fiorillo , Marco Ciccù , Cesare D'Amico , Rodolfo Mauceri , Giacomo Oteri , and Gabriele Cervino 

Research Article (13 pages), Article ID 2976067, Volume 2020 (2020)

Functionalized Scaffold and Barrier Membrane with Anti-BMP-2 Monoclonal Antibodies for Alveolar Ridge Preservation in a Canine Model

Seiko Min , Taewan Kim, Oksu Kim, Carames Goncalo, Tadahiko Utsunomiya, Takashi Matsumoto, Kayo Kuyama, and Nikola Angelov

Research Article (11 pages), Article ID 6153724, Volume 2020 (2020)

Failure Modes and Survival of Anterior Crowns Supported by Narrow Implant Systems

Edmara T. P. Bergamo , Everardo N. S. de Araújo-Júnior , Adolfo C. O. Lopes , Paulo G. Coelho , Abbas Zahoui , Ernesto B. Benalcázar Jalkh , and Estevam A. Bonfante 

Research Article (11 pages), Article ID 1057846, Volume 2020 (2020)

An Antibacterial Strategy of Mg-Cu Bone Grafting in Infection-Mediated Periodontics

Xue Zhao, Peng Wan, Hongyan Wang, Shuwei Zhang, Jingbo Liu, Chunrong Chang, Ke Yang , and Yaping Pan 

Research Article (9 pages), Article ID 7289208, Volume 2020 (2020)

Scientific Production in Dentistry: The National Panorama through a Bibliometric Study of Italian Academies

Felice Lorusso , Francesco Inchingolo, and Antonio Scarano 

Review Article (10 pages), Article ID 3468303, Volume 2020 (2020)

Influence of Implant Thread Morphology on Primary Stability: A Prospective Clinical Study

Maria Menini, Francesco Bagnasco, Ivan Calimodio, Nicolò Di Tullio, Francesca Delucchi , Domenico Baldi, and Francesco Pera

Research Article (8 pages), Article ID 6974050, Volume 2020 (2020)

Impact of Matching Point Selections on Image Registration Accuracy between Optical Scan and Computed Tomography

Hai Yen Mai  and Du-Hyeong Lee 

Research Article (7 pages), Article ID 3285431, Volume 2020 (2020)

The Effects of Titanium Surfaces Modified with an Antimicrobial Peptide GL13K by Silanization on Polarization, Anti-Inflammatory, and Proinflammatory Properties of Macrophages

Xuxi Chen , Lin Zhou, Dong Wu, Wenxiu Huang , Yanjun Lin, Bowei Zhou, and Jiang Chen 

Research Article (9 pages), Article ID 2327034, Volume 2020 (2020)

Editorial

Implant Dentistry: New Materials and Technologies 2020

Luigi Canullo ¹, **Henriette Lerner** ², and **Paolo Pesce** ³

¹University of Valencia, Valencia, Italy

²Johann Wolfgang Goethe-University, Frankfurt am Main, Germany

³University of Genova, Genova, Italy

Correspondence should be addressed to Luigi Canullo; luigicanullo@yahoo.com

Received 17 November 2021; Accepted 17 November 2021; Published 25 November 2021

Copyright © 2021 Luigi Canullo et al. This is an open access article distributed under the Creative Commons Attribution License, which permits unrestricted use, distribution, and reproduction in any medium, provided the original work is properly cited.

While osseointegration has become already clinically established concept in healthy patients, clinicians are facing a growing number of implant-supported rehabilitations on pathophysiologically impacted bone.

In these scenarios, moderately rough surfaces/traditional protocols might represent a *locus minoris resistentiae*. In fact, a high-performance surface might be requested for a long-standing integration of the fixture.

Bioactive surfaces with increased surface energy might respond to this requisite without encountering possible higher risk of bacterial contamination as rough-surfaced implants demonstrated.

Actually, the surface energy directly correlates with hydrophilicity and (on the contrary) indirectly with the presence of contaminants on the surface. In fact, it decreases with increased surface deposition of atmospheric elements or pollutants (present even on the “sterile” new implants).

As demonstrated, decontamination of the implant surface is an essential prerequisite for cell adhesion. However, even in optimal conditions of surface decontamination, the titanium fixture still remains hydrophobic and, then, less “tissue friendly.” This is correlated to the oxidation of the

external titanium layers due to the presence of oxygen into the implant sterile package.

The bioactivation through chemical or biophysical methods increases fixture surface energy and then wettability, removing the oxidized external layers.

The biological advantage of such activation is both qualitative (higher number of adhered cells) and quantitative (flat vs. spreaded arrangement), with a stronger adhesion, and this implies a faster cell adhesion and better cell stratification.

Translated to the clinics, this strategy promises to result in stronger osseointegration even in the initial stages of the treatment in physiological quality bone or after the traditional timing in compromised bone-quality patients.

Luigi Canullo
Henriette Lerner
Paolo Pesce

Conflicts of Interest

The authors declare there are no conflicts of interest.

Research Article

Dental Pulp Stem Cells on Implant Surface: An In Vitro Study

Luigi Laino,¹ Marcella La Noce,¹ Luca Fiorillo ^{1,2} Gabriele Cervino ² Ludovica Nucci,¹ Diana Russo,¹ Alan Scott Herford,³ Salvatore Crimi,⁴ Alberto Bianchi,⁴ Antonio Biondi,⁴ Gregorio Laino,¹ Antonino Germanà,⁵ and Marco Cicciù ²

¹Multidisciplinary Departments of Medical-Surgical and Dental Specialties, Second University of Naples, Naples 80100, Italy

²Department of Biomedical and Dental Sciences and Morphological and Functional Imaging, Messina University, Messina 98100, Italy

³Department of Maxillofacial Surgery, Loma Linda University, Loma Linda, CA 92354, USA

⁴Department of Surgical and Biomedical Sciences, Catania University, 95124 Catania, Italy

⁵Department of Veterinary Sciences, University of Messina, Messina, Italy

Correspondence should be addressed to Luca Fiorillo; lucafiorillo@live.it and Marco Cicciù; mcicciu@unime.it

Received 12 August 2020; Revised 28 October 2020; Accepted 14 March 2021; Published 24 March 2021

Academic Editor: Luigi Canullo

Copyright © 2021 Luigi Laino et al. This is an open access article distributed under the Creative Commons Attribution License, which permits unrestricted use, distribution, and reproduction in any medium, provided the original work is properly cited.

In the field of biology and medicine, one hears often about stem cells and their potential. The dental implant new surfaces, subjected to specific treatments, perform better and allow for quicker healing times and better clinical performance. The purpose of this study is to evaluate from a biological point of view the interaction and cytotoxicity between stem cells derived from dental pulp (DPSCs) and titanium surfaces. Through the creation of complex cells/implant, this study is aimed at analyzing the cytotoxicity of dental implant surfaces (Myth (Maipek Manufacturer Industrial Care, Naples, Italy)) and the adhesion capacity of cells on them and at considering the essential factors for implant healing such as osteoinduction and vasculogenesis. These parameters are pointed out through histology (3D cell culture), immunofluorescence, proliferation assays, scanning electron microscopy, and PCR investigations. The results of the dental implant surface and its interaction with the DPSCs are encouraging, obtaining results increasing the mineralization of the tissues. The knowledge of this type of interaction, highlighting its chemical and biological features, is certainly also an excellent starting point for the development of even more performing surfaces for having better healing in the oral surgical procedures related to dental implant positioning.

1. Introduction

1.1. Background. Stem cells are found in various body tissues: blood, muscles, skin, bone marrow, nerves, and liver. The key property of all stem cells is that they are undifferentiated; therefore, they can replicate indefinitely and replace/renew different types of damaged cells in the body [1–4]. Stem cells can divide and replicate over 200 types of specialized cells that are linked to the function of the immune system, heart, oxygen distribution, and others. Literature shows that stem cells from the dental pulp share behavioral characteristics similar to mesenchymal stem cells (MSCs) from other tissues [5–8]. MSCs are present in many tissues throughout the organism and can transform and replicate muscle, nerve, bone, and fat and cartilage cells. They also have the ability

to modify the behavior of the immune system and thus potentially treat a range of immune disorders [9]. Stem cells in the teeth could, in the future, be used to repair damage throughout the body and be used in regenerative medicine. The dental pulp is a connective tissue, contained within the pulp chamber and in root canals; it communicates with the periodontium through one or more apical foramina and through the lateral accessory channels of the roots [10, 11]. The pulp is composed of cells immersed in an intercellular matrix characterized by a fundamental substance and fibers (especially collagen fiber types I and III) [12]. The organic matrix represents about 25%, while the remaining 75% is made up of water. The central mass of the pulp is made up of cells and an intercellular matrix. The dental pulp plays the main role in tooth regeneration after an insult by

participating in the process known as dentinogenesis [13–15]. The direct capping of the pulp with Mineral Trioxide Aggregate (MTA) or calcium hydroxide, which promotes the activation of dentinogenesis with the production of tertiary dentin, is promoted by these tissues. This newly mineralized layer preserves pulp integrity and serves as a barrier to insult [16–19].

Inside the healthy pulp, there are fibroblasts, fibrocytes, mesenchymal stem cells, lymphocytes, macrophages-histiocytes, and rare mast cells. The intercellular matrix, which surrounds and supports the structures, is composed of collagen fibers, type I and to a lesser extent type III, and a fundamental substance, made up of water and proteoglycans. The fundamental substance represents the means by which metabolites and waste products are spread in the pulp [5–7]. With advancing age, there is a progressive decrease in the cell population and a numerical and volumetric increase in collagen fibers, especially in the 2/3 apical roots. Two different types of stem cells are distinguished: embryonic stem cells (ESCs) and adult stem cells (ASCs) [20].

ESCs are obtained directly from human embryos. Up to 3–4 days after fertilization (zygote and blastomeres of the morula), stem cells are totipotent: they have morphogenetic capacity. They are capable of giving rise to a complete individual, they have unlimited multiplicative and proliferative capacity (cell immortality), and they can differentiate into all cell types (differentiating ability) [21, 22]. At the implant surgery level, autologous bone derived from stem cells could replace the current materials used for guided bone regeneration (GBR) [23–26]. In addition, the possibility of having ligament-anchored implants, or implants surrounded by periodontal tissue, produced thanks to tissue engineering, between bone and implant surface, seems to arouse the interest of many researchers [27–29]. The characteristics of the implant surfaces have different implications in the integration that it will be possible to achieve, during rehabilitation, with both hard and soft tissues [7, 30]. A rough implant allows for greater osseointegration rates than a smooth surface one. Equally important is the management of soft tissues and the transmucosal portion of the implant [31, 32].

Over time, the study in the dental implant field has led to a change from smooth machined surfaces to roughened surfaces in order to improve osseointegration thanks to the osteoconductive properties of this type of texture [33, 34]. Scarano et al. recently demonstrated how a faster osseointegration could be achieved in the presence of specifically treated implant surfaces, promising encouraging clinical outcomes [35]. Other related researches highlighted how the presence of stem cells applied to a dental implant surface could increase and accelerate the physiological osteointegration processes [36, 37]. Scarano et al. [35] showed how the addition of bone marrow stromal stem cells could improve bone regeneration during bone porcine block regeneration techniques. Another study suggest that thermal treatment of dental implant surface could provide a better osseointegration [36]. The study evaluated the influence of this treatment of Ti6Al4V implant surfaces and the bone healing response in a rabbit model. They highlighted a statistically significant difference of bone-implant contact (BIC).

Other recent studies suggest that inflamed peri-implant tissues with associated progressive bone loss are becoming an increasingly frequent situation. One of the possible explanations for the phenomenon seems to derive from the fact that rough implants could favor the formation and deposit of bacterial plaque, which could then start the inflammatory process in the peri-implant tissues [37, 38].

1.2. Hypothesis. The aim of this scientific study is to evaluate the biological and interaction characteristics between Myth (Maipek Manufacturer Industrial Care, Naples, Italy) surface and stem cells derived from dental pulp (DPSCs). The clinical rationale of the study is to underline how the presence of MSCs and its interaction with the dental implant surface may increase the inflammatory tissue response with a quicker healing on the surgical site. This study was performed to evaluate the inflammatory response to novel dental implant surface, and the authors performed 2D and 3D cell culture, immunofluorescence, proliferation assays, scanning electron microscopy (SEM), and PCR (Polymerase Chain Reaction) investigations.

2. Materials and Methods

This work presents an *in vitro* study about the ability to stimulate the osteogenesis of DPSCs by Myth (Maipek Manufacturer Industrial Care, Naples, Italy) implant texture. Surface structure was viewed by SEM (scanning electron microscopy) and is reported in Figure 1, which highlights its roughness.

To conduct this study, complex cells/implant was realized: in particular, as Myth (Maipek Manufacturer Industrial Care, Naples, Italy) is aimed at a dental use, DPSCs, a lineage of mesenchymal stem cells extracted by dental pulp, were chosen. The methods of Naddeo et al. [39] have been followed.

2.1. Sample. Myth® (Maipek Manufacturer Industrial Care, Naples, Italy) is made of Grade 4 titanium. Titanium has a relative density of 4.5 g/cm [3] and a very low thermal conductivity and has a very high mechanical strength with an elongation at break equal to 12%. The modulus of elasticity is relatively low and similar to that of the bone. Grade 4 titanium within the four varieties of pure titanium (Ti cp) has the best overall characteristics, combining the workability and therefore precision typical of low grades with the superior mechanical properties of high grades. The fundamental characteristics of this metal are the high corrosion resistance and the high degree of biocompatibility. An atomic bombing with inert gas and magnetic fields were used to decontaminate the devices. About 18 implants were employed in this work.

2.1.1. Cell Extraction and 2D Culture. Mesenchymal stem cells were obtained by the extraction of dental pulp tissue from third molars. All subjects signed the ethical committee consent brochure (Second University Internal Ethical Committee). After mechanical and enzymatic digestion of the tissue with a collagenase I/dispase solution, the sample was filtered with 70 m Falcon strainers (BD Pharmingen,

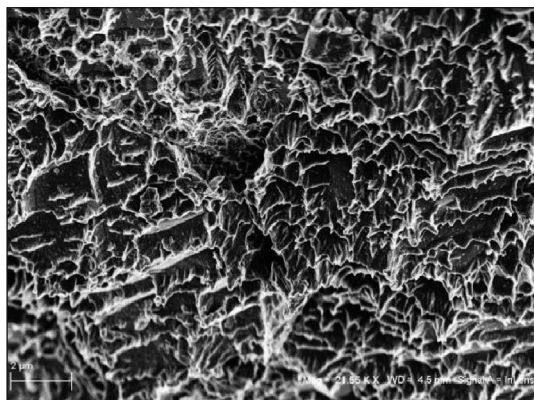


FIGURE 1: Myth (Maipek Manufacturer Industrial Care, Naples, Italy) implant texture observed by SEM.

Buccinasco, Milano, Italy) and centrifuged for 7 min at 1300 rpm. The pellets were then plated in T-25 flasks at 37°C and 5% CO₂ in DMEM culture medium supplemented with 10% fetal bovine serum (FBS), 2 mM l-glutamine, and 100 U/mL penicillin and 100 mg/mL streptomycin (all purchased from Gibco-Life Technologies, Monza, Italy). Adhered cells were expanded until they reached about 5 × 10⁵ cells/flask.

2.1.2. FACS Analysis and Sorting. Cells were detached using trypsin EDTA (GIBCO). At least 200,000 cells were incubated with fluorescent conjugated antibodies for 30 min at 4°C, washed, and resuspended in PBS. The antibodies used in this study were anti-CD34 PE (BD Pharmingen, Buccinasco, Milano, Italy) and anti-CD90 FITC (BD Pharmingen, Buccinasco, Milano, Italy). Isotypes were used as controls. Cells were analyzed with an Accuri C6 (BD Biosciences, San Jose, CA, USA) and the data collected with FCS Express version 3 (De Novo Software). Cells were sorted using simultaneous positivity for CD90 and CD34 using a FACS Aria III (BD, Franklin Lakes, NJ, USA). The purity of sorted populations was routinely 90%.

2.1.3. 3D Cell Culture: In Vitro Tissue Engineering. In order to achieve 3D tissue formation, cells were seeded at a density of 5 × 10⁵ cells/implant onto dental implants that had been previously washed in PBS. Cells were resuspended in 100 μL of culture medium and plated as a drop on the scaffold placed in a 12-well plate, taking care not to spill the medium at the bottom of the plate, to allow cell attachment. After 1 h of incubation, the cell implant devices were transferred to 15 mL tubes with a cap filter and incubated with osteogenic medium in a humidified atmosphere at 37°C and 5% CO₂ in a rotating culture apparatus (Wheaton Science Products, Millville, NJ, USA) at 6 rpm; cells plated in flasks were used as the control (2D culture). The 3D culture was performed for 30 days in osteogenic medium changed twice weekly; specimens were collected at 7, 14, and 30 days. Osteoinduction medium is composed of DMEM supplemented with 10% FBS, 1% Pen-Strep, 50 μg/mL L-ascorbic acid (Sigma, Gillingham, Dorset, UK), 10 mM glycerol phosphate disodium salt (β-glycerophosphate), and 10 nM dexamethasone

(Sigma, Gillingham, Dorset, UK). Experiments were performed in triplicate ($n = 3$ scaffolds/time point).

2.1.4. Cytotoxicity Test on Conditioned Medium. Cytotoxicity was evaluated on cells cultured in medium conditioned by the presence of implants. The conditioned medium was prepared by incubating each implant in 3 mL of DMEM without phenol red and supplemented with antibiotics (penicillin, streptomycin), glutamine, and FBS at 37°C for 3 days. DPSCs were seeded in 96-well plates at a density of 10 [4] cells per well and cultured in conditioned medium for 24 h and 48 h, and the cell viability was determined by MTT colorimetric assay. The values are expressed as the percentage of cell viability compared with control (cells incubated in unconditioned culture medium). The measurements were performed in triplicate.

2.1.5. Proliferation Assays. The MTT colorimetric assay was also performed to assess cell adhesion and proliferation. To this end, 5 × 10⁵ cells were plated on implants and incubated, as described above, in DMEM supplemented with FBS, l-glutamine, and antibiotics. Seeded implants were collected after 24 h and 48 h of 3D culture: medium was removed and cell implants incubated for 4 h in a solution of 5 mg/mL MTT. The same number of cells cultured in 2D was used as the control. After medium removal, 300 μL of DMSO was added to each well containing seeded implants or control cells for 10 min; supernatants collected were read at 540 nm with a spectrophotometer. Cell viability was calculated proportionally to the quantity of formazan salts produced by the enzymatic activity of cells. Values are given as percentage versus the control and normalized with respect to the number of cells and sample volumes.

2.1.6. Immunofluorescence. Expression of osteocalcin on seeded cells was evaluated at 3 and 30 days of culture. Implants seeded with 1 × 10⁶ cells/mL were washed in PBS and fixed with 4% paraformaldehyde (PFA) solution. Samples were incubated with primary antibodies: mouse monoclonal to osteocalcin (1:100, Abcam, Cambridge, UK), overnight at 4°C in the dark. This step was followed by incubation with the secondary antibody tetramethylrhodamine (TRITC-) conjugate (1:1000, Abcam). Nuclear counterstaining was performed with 4,6-diamidino-2-phenylindole (DAPI). After extensive washing with PBS, images were collected under a fluorescence microscope (Axiovert 100; Zeiss). In order to mimic the three-dimensional bone structure as much as possible (3D culture) and to assess whether the scaffolds were capable of inducing adhesion, about 250,000 cells were plated on 2 implants and incubated in rotating culture at 37°C in 5% CO₂. After 3 and 30 days of culture, the medium was removed and the implants were washed with Phosphate-Buffered Saline (PBS) and fixed in 4% paraformaldehyde (PFA). Then, fluorescence was performed by labeling with Hoechst, an intercalating-DNA dye that displays cell nuclei. The ability to express osteogenic specific markers was evaluated by immunofluorescence staining for osteocalcin, both at 3 and at 30 days of culture.

2.1.7. Scanning Electron Microscopy. Adhered cell morphology was assessed by SEM (Supra 40 ZEISS, Weimar, Germany). Seeded implants were deprived of medium, washed, fixed in PFA, and postfixed with 0.1% OsO₄ for 1 h. Thereafter, specimens were gradually dehydrated in an increasing ethanol concentration, treated by critical point drying, dry mounted on a stub, and sputter-coated with gold/palladium. DPSC/implant complexes, cultured for 3 and 30 days in the same conditions described above, after fixation were processed for SEM analyses, to obtain a clearer view of cell adhesion.

2.1.8. qRT-PCR. The osteoinduction capability of implants was evaluated by qRT-PCR analysis for genes involved in osteogenic differentiation on specimens collected after 7, 14, and 30 days of 3D cell culture. In particular, we examined the expression of genes involved in the production of molecules responsible for deposition of mineralized matrix: bone alkaline phosphatase (BAP), collagen I (COLL I), osteopontin (OPN), bone sialoprotein (BSP), and osteocalcin (OSTC). RNA extracted from pellets of cells cultured in 2D was used as control. RNA from cells adhered on implants was extracted by processing the entire sample according to the protocol of the Ambion RNA extraction kit (Life Technologies). cDNA was obtained after treatment with DNase (Promega, Italy) and reverse transcriptase (ImProm-II Reverse Transcriptase). Samples were analyzed using real-time quantitative PCR (qRT-PCR). PCR reactions were performed using a StepOne Thermocycler (Applied Biosystems, Monza, Italy), and the amplifications were done using the SYBR Green PCR Master Mix (Applied Biosystems, Monza, Italy). The thermal cycling conditions were 50°C for 2 min followed by an initial denaturation step at 95°C for 2 min and 40 cycles at 95°C for 30 s, 60°C or 58°C for 30 s, and 72°C for 60 s. Real-Time PCR was performed using the primer sequences shown in Table 1. An additional step starting from 60 to 95°C (0.05°C·s⁻¹) was performed to establish a melting curve. This was used to verify the specificity of the qRT-PCR reaction for each primer pair. For each measurement, a threshold cycle value (Ct) was determined. This was defined as the number of cycles necessary to reach a point at which the fluorescent signal is first recorded as being statistically significant above the background. Data were analyzed by using the 2^{-ΔΔCt} method to obtain the relative expression level, and each sample was normalized by using the GAPDH RNA expression. The ability of the implant texture to induce differentiation of DPSCs into the osteoblast to activate bone matrix deposition was evaluated by Real-Time Polymerase Chain Reaction (Real-Time PCR). The analyses were conducted on specimens collected after 7, 14, and 30 days of cell culture; in particular, the expression of genes encoding for molecules involved in matrix mineralization was examined: BAP, COLL I, OPN, BSP, and OSTC. RNA extracted from pellets of cells cultured in flasks (2D) was used as control. Quantitative Real-Time PCR was performed using the SYBR Green method. The amount of cDNA of the gene of interest has been normalized to that of the cDNA of

TABLE 1: Primers sequences for quantitative Real-Time Polymerase Chain Reaction (qRT-PCR).

Gene	Forward	Reverse	Ta
GAPDH	ggagtcaacggatttggctg	cttcccgttctcagccttga	60°C
BAP	tcaaaccgagatacaagcac	ggccagacgaaagatagagt	56°C
COLL I	gaggctctgaaggtcccca	caccagcaataccaggagca	58°C
OPN	gccgaggtgatagtgtggtt	tgaggtgatgtcctcgtctg	58°C
BSP	ctggcacagggtatacagggttag	actggtgccgtttatgccttg	60°C
OSTC	ctcacactcctcgcctattg	cttggacacaaggctgcac	60°C

GAPDH. The experiments were carried out in triplicate for each data point (Table 1).

2.1.9. Alizarin Red S Quantification. After 30 days of 3D culture, cell-implant biocomplexes were washed with PBS and fixed in 10% (v/v) formaldehyde (Sigma-Aldrich) at room temperature for 15 min. The samples were then washed twice with excess dH₂O prior to addition of 1 mL of 40 mM ARS (pH 4.1). Samples were incubated at room temperature for 20 min with gentle shaking. After aspiration of the unincorporated dye, the samples were washed four times with 4 mL dH₂O while shaking for 5 min and then stored at -20°C prior to dye extraction. For quantification of staining, 800 μL 10% (v/v) acetic acid was added to each sample, and the plate was incubated at room temperature for 30 min with shaking. Cells, now loosely attached to the implants, were then scraped with a cell scraper (Fisher Life Sciences) and transferred with 10% (v/v) acetic acid to a 1.5 mL microcentrifuge tube with a wide-mouth pipette. After vortexing for 30 s, the slurry was overlaid with 500 μL mineral oil (Sigma-Aldrich), heated to exactly 85°C for 10 min, and transferred to ice for 5 min. The slurry was then centrifuged at 20,000 g for 15 min, and 500 μL of the supernatant was removed to a new 1.5 mL microcentrifuge tube. Then, 200 μL of 10% (v/v) ammonium hydroxide was added to neutralize the acid. pH was measured to ensure that it was between 4.1 and 4.5. Aliquots (150 μL) of the supernatant were read in triplicate at 405 nm in 96-well format using opaque-walled, transparent-bottomed plates (Fisher Life Sciences). Cells seeded in 2D were used as control. In order to evaluate the ability to induce osteogenic differentiation, cells seeded on Myth (Maiepek Manufacturer Industrial Care, Naples, Italy) surfaces were cultured for three weeks in osteogenic medium in rotating culture. After PBS washing, the complexes were fixed and kept in a solution of Alizarin Red S 1% for 10 min. Alizarin is a red staining that binds calcium deposition by cells of an osteogenic lineage. Free calcium forms precipitates with alizarin and tissue containing calcium stain red immediately, when immersed in a solution containing it [40].

2.1.10. ELISA for h-OSTC and h-VEGF. In order to evaluate levels of human OSTC and VEGF produced by the cells and released into the culture medium, supernatant was collected from 3D cultures after 7, 14, and 30 days of

culture. After centrifugation to remove particulates, 2 mL aliquots of medium were stored at -20°C until processing for analysis. The evaluation was carried out with an ELISA kit (Human Osteocalcin ELISA kit, Invitrogen; Human VEGF ELISA kit, Invitrogen), and concentrations were read versus a standard curve at 450 nm using a spectrophotometer (DAS Plate Reader, Rome, Italy). The assays were performed in triplicate [41, 42].

3. Results

3.1. Cytotoxicity Test: Conditioned Medium. The high values of percentage showed in the graph (Figure 2) prove a total biocompatibility of the implants, suggesting that no particles that damage cells were released by them.

So, the Myth (Maipek Manufacturer Industrial Care, Naples, Italy) implant can be considered biologically safe.

3.2. Cell Proliferation Assay: MTT Tests. The amount is expressed in percentage versus the control cultured in the plate [43]. The implants promote cell proliferation approximately with the same values of the cell culture in standard conditions (Figure 3).

3.3. Cell Adhesion: Immunofluorescence. The images show the nuclei of adhered cells, evenly distributed on the implant's surfaces. Cells expressed osteocalcin as early as 3 days. The expression of osteocalcin is increased at 30 days, confirming the stability and osteogenic induction of the implant (Figure 4).

3.4. Cell Adhesion: Scanning Electron Microscopy (SEM). As the collected photos showed, adhered cells tended to spread onto Myth (Maipek Manufacturer Industrial Care, Naples, Italy) surfaces acquiring an osteoblastic morphology (Figure 5) [44].

3.5. Bone Matrix Formation: Histological Analysis. Alizarin Red S quantification has been performed because the thickness of the implant does not allow a quality image. As shown in Figure 6, cells seeded on Myth lay a quantity of calcified matrix greater than the control in which cells were grown in adhesion in the same condition described above (2D culture).

3.6. Osteoinduction: qRT-PCR. The image (Figure 7) in the upper left shows the temporal expression of markers involved in osteogenic differentiation; histograms display the activation of genes *BAP* (bone alkaline phosphatase), *COLLI* (collagen), *OPN* (osteopontin), *BSP* (bone sialoprotein), and *OSTC* (osteocalcin) in cells seeded on Myth (Maipek Manufacturer Industrial Care, Naples, Italy) implants versus a control 2D at 7, 14, and 30 days of culture.

The histograms show in cell-implant devices an upregulation of genes *BSP* and *OSTC* compared to the 2D system. Moreover, for the implants, the deposition of the matrix is already carried out after 7 days of culture (*COLL I*), compared to the control that, instead, presents the highest expression of *COLL I* just after 14 days of culture,

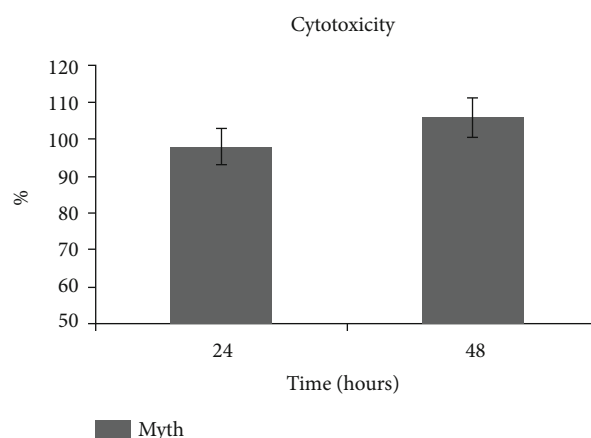


FIGURE 2: Cytotoxicity test on Myth (Maipek Manufacturer Industrial Care, Naples, Italy) implant by conditioned medium after 24 and 48 hours of incubation.

a growing trend of *OPN* and lower expression of *BSP* and *OSTC* with respect to Myth (Maipek Manufacturer Industrial Care, Naples, Italy) specimens. Then, the global analysis shows that the implant system enters early in a stage of matrix mineralization stimulating previously cell differentiation.

3.7. Matrix Mineralization: Human-Osteocalcin ELISA Test. Osteocalcin is the latest marker of the mature osteoblasts. It is the most abundant noncollagenous protein of the bone matrix. Once transcribed, osteocalcin undergoes posttranslational modifications within the osteoblast before its secretion. Osteocalcin is released by osteoblasts during bone formation and is bounded with the mineralized bone matrix.

The concentration of osteocalcin released in the culture medium by cells seeded on implants (3D) was evaluated by ELISA test, after 7, 14, and 30 days of culture, and as a control which was used the culture medium of cells plated in flasks (2D). The values of protein reported in Figure 8 show for the control (CTRL) a typical phasic trend, while the samples, collected by the implants, report an increase in concentrations at 30 days of culture with a value higher than the relative control (Figure 6).

3.8. Vasculogenesis: Human-VEGF ELISA Test. Vascular endothelial growth factor (VEGF) is a signal protein produced by cells that stimulate vasculogenesis and angiogenesis. The same protocol used for the h-OSTC ELISA test was performed for the evaluation of the concentration of VEGF released into the culture medium from DPSC/implant versus a control 2D. The values relative to Myth (Maipek Manufacturer Industrial Care, Naples, Italy) show an increasing trend during the time, with the highest peak at 30 days of culture, but the concentration is lower than that of the control for the respective times. The reason for that could be probably the search in the greater number of cells that the flask surface is able to contain with respect to implants (Figure 9).

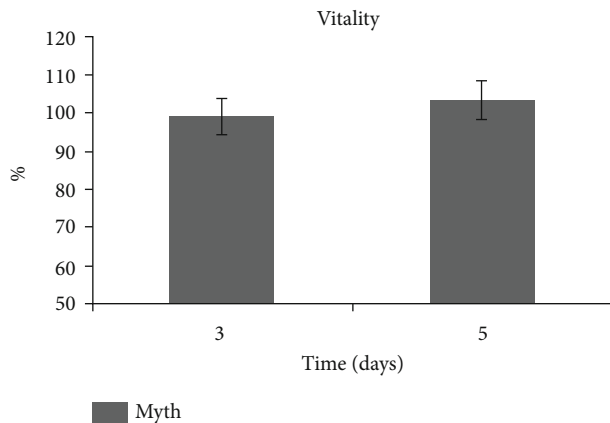


FIGURE 3: Proliferation assays on construct DPSCs/Myth (Maiepek Manufacturer Industrial Care, Naples, Italy) at 3 and 5 days of culture.

4. Discussion

The bone-implant interface plays a critical role for good and lasting osteointegration. Many implant surfaces have been studied over the last decades. Among these, titanium alloy is the material most used because of its mechanical strength and its resistance to corrosion. In this research project, the capability of the Myth (Maiepek Manufacturer Industrial Care, Naples, Italy) texture to induce the osteogenic process from DPSCs has been investigated; in particular, the fundamental aspects that regulate a full and long-term osseointegration at the bone-implant interface were examined.

The Myth (Maiepek Manufacturer Industrial Care, Naples, Italy) implant results are completely biocompatible: they preserved the cell viability stimulating their proliferation. Immunofluorescence and SEM analyses allow a detailed view of cells onto implant surfaces and prove that implant texture enables cell adhesion and DPSC differentiation into osteoblastic morphology. After differentiation, DPSC growth on Myth (Maiepek Manufacturer Industrial Care, Naples, Italy) surfaces implements extracellular matrix deposition and acts on the mineralization process, as the positivity for Alizarin Red staining revealed. The cell differentiation into the osteoblast and the activation of bone matrix formation were carried out in DPSCs seeded on Myth (Maiepek Manufacturer Industrial Care, Naples, Italy) surfaces in an earlier stage with respect to the control. In particular, the key protein for bone tissue formation, the osteocalcin was already produced and released to be bound to ECM for mineralization. Also, the vasculogenesis process was carried out by cell-Myth (Maiepek Manufacturer Industrial Care, Naples, Italy) devices, even if in a later stage with respect to the control [45–57].

DPSCs represent a suitable model for the study of bone differentiation thanks to their osteogenic capacity compared to other types of cells collected by the adult human body. This feature, together with their easy availability, high accessibility in the oral cavity, and resistance

to cryopreservation, makes DPSCs very interesting for use in bone tissue engineering procedures in combination with scaffolds. Therefore, it could be of interest, after DPSC seeding on implants, to test their differentiation performance in a 3D culture system and to analyze their genetic behavior. The proliferation of osteoblasts around the implant is the basis of the osseointegration process. The sowing surface is decisive in guiding cellular activities, such as adhesion, diffusion, migration, and rearrangement: the cells acutely perceive the variability in the microenvironment and adapt to it. Differentiation and production of mineralized matrix involves the expression of a considerable number of genes, as well as the production of many different proteins that guide the process. Osteogenic differentiation is known to develop through spatiotemporal changes in the expression of the genes involved in this process. During its progression, specific markers reach one or more expression peaks depending on the maturation stage in which the cell is located. The expression of molecular markers associated with cell differentiation studied and monitored the synthesis and/or release of key molecules involved in this process and in the deposition of matrices by analyzing the expression of BAP, OPN, and OSTC. It was shown that the cells sown on implants had a significantly better expression of all three genes examined than in the control. This is probably due to the fact that the 3D cell culture simulates the physiological cell environment more accurately. In this study, stem cells are strongly stimulated to differentiate into osteoblasts, and this occurs in a few days (7 days); the latter is obtained thanks to the 3D cell culture, which is an excellent system for performing stem cell differentiation, because it significantly improves bone differentiation, improving the phenotypic expression of cells and the synthesis of mineralized matrix, and both the structure and composition of the implant, which promotes bone differentiation. As a result, the differentiation and deposition of the previous matrix led to a decrease in the OPN and OSTC gene expressions, which usually (without the aforementioned tools) decrease by day 21. Osteocalcin is one of the most abundant proteins in the bone. Angiogenesis is a crucial stage in ossification. Osteogenesis and angiogenesis are two processes that share different key regulators such as the vascular endothelial growth factor (VEGF). It has been highlighted how the level of this factor influences the time of cell growth suggesting a possible role in vasculogenesis. Most of the studies are aimed at assessing the rate of cell growth and not long-term biocompatibility, without considering that faster may not necessarily mean better [58–61]. Klos et al. [62] evaluated cell adhesion on laser-induced periodic surface structures. Human mesenchymal stem cells were grown on simple nanostructured surfaces. This process could appear slower on complex surfaces. The authors' study demonstrated how human mesenchymal stem cells were spatially controlled and how nanoscale structures influence surface wettability and protein adsorption. All these features could promote osteogenic differentiation. Di Carlo et al. [63] evaluated a titanium modified surface; their study focused on graphene

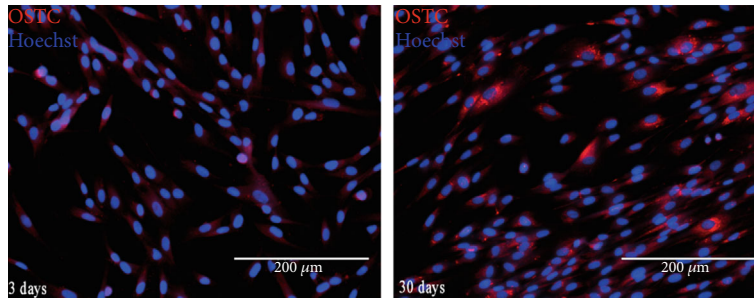


FIGURE 4: Immunofluorescence by Hoechst and OSTC on device DPSCs/Myth (Maipek Manufacturer Industrial Care, Naples, Italy) at 3 and 30 days of culture.

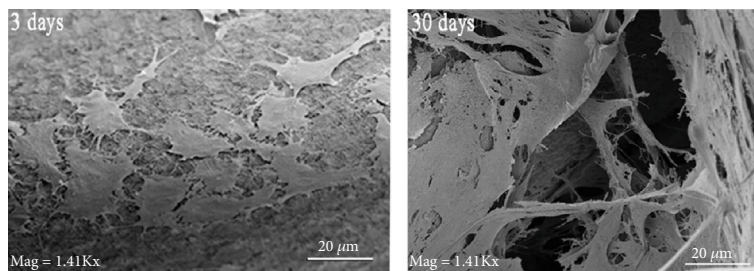


FIGURE 5: SEM photos of cells adhered on Myth (Maipek Manufacturer Industrial Care, Naples, Italy) surfaces after 3 days of culture. Cells form a monolayer after 30 days of culture.

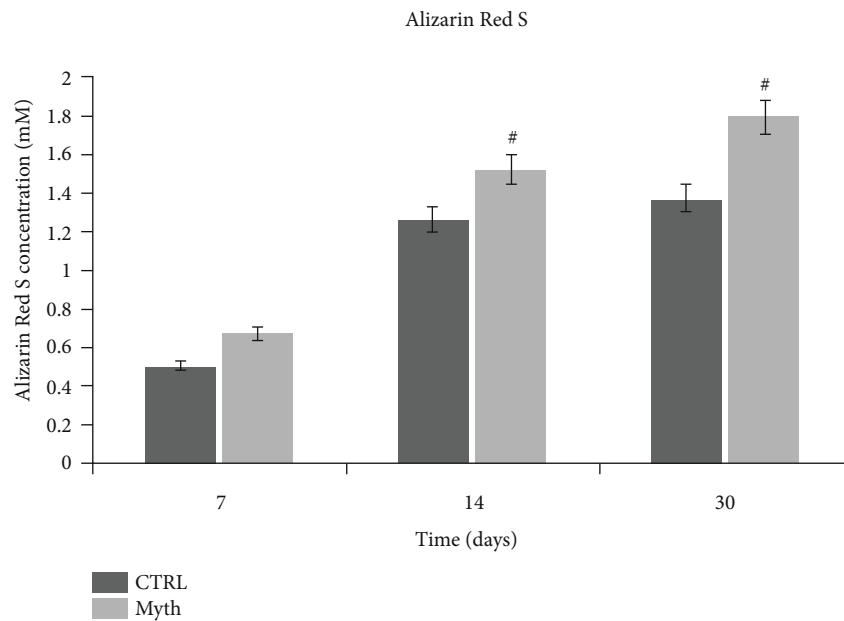


FIGURE 6: Alizarin Red S quantification.

oxide. The authors evaluated dental pulp stem cell viability, cytotoxicity, and osteogenic differentiation in the presence of graphene oxide-coated titanium surfaces. These surfaces demonstrated no significant differences with standard Ti disc surfaces [64–68]. The authors showed an increased secretion of PGE2 that could evidence a possible immunomodulatory role for graphene oxide. Diomed

et al. [69] investigated the interaction between human periodontal stem cells and titanium surfaces using vascular endothelial growth factor and runt-related transcription factor 2. The authors in these cases demonstrated how the growth factor could influence and improve cell adhesion, osteogenic and angiogenic events, and osseointegration process. Sunarso et al. [70] evaluated the osteogenic

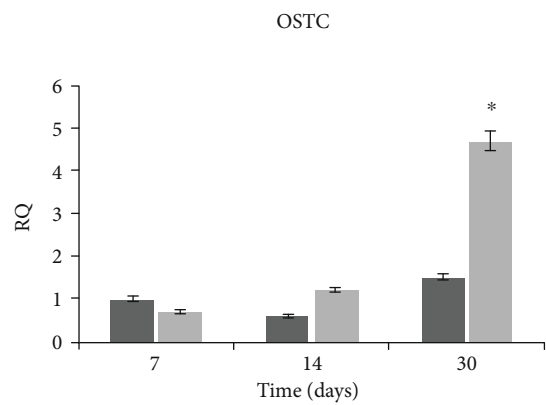
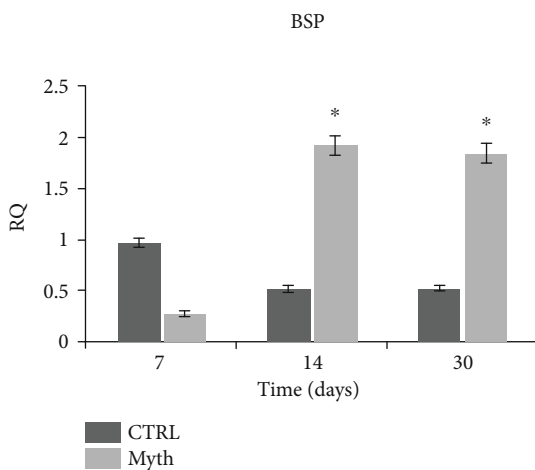
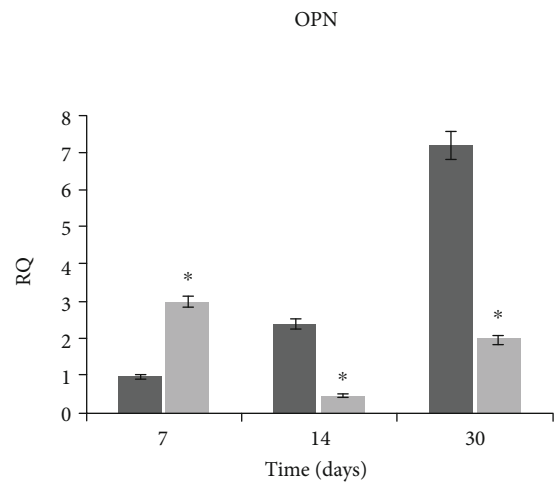
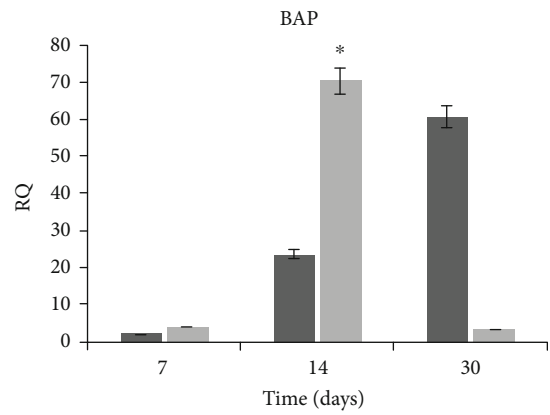
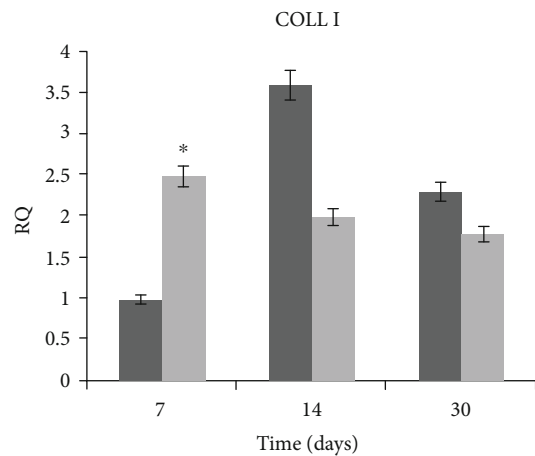
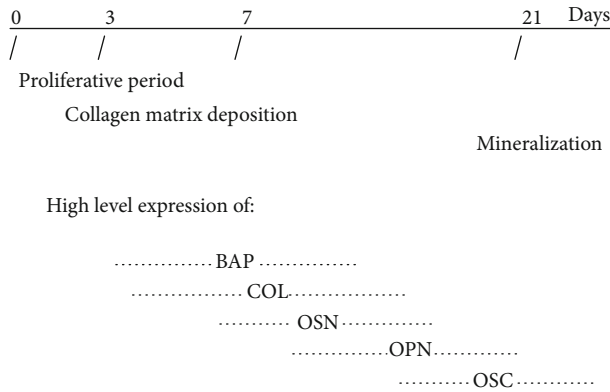


FIGURE 7: qRT-PCR of osteogenic genes BAP, COL1 I, OPN, BSP, and OSTC in cells seeded on Myth (Maiepek Manufacturer Industrial Care, Naples, Italy) versus a 2D control (CTRL) at 7, 14, and 30 days of culture.

capability of polyether-ether-ketone (PEEK). This study demonstrated that immobilization of phosphate or calcium increased the osteogenesis of rat mesenchymal stem cells compared with bare PEEK, including cell proliferation. Irastorza et al. [71] evaluated hDPSCs (human dental pulp stem cells), in combination with autologous plasma com-

ponents, for in vitro bone generation on biomimetic titanium dental implant materials. The authors demonstrated how a combination of biomimetic rough titanium surfaces, with autologous plasma-derived fibrin-clot membranes such as PRF and/or insoluble PRGF formulations, improves osteoblastic cell differentiation, bone generation,

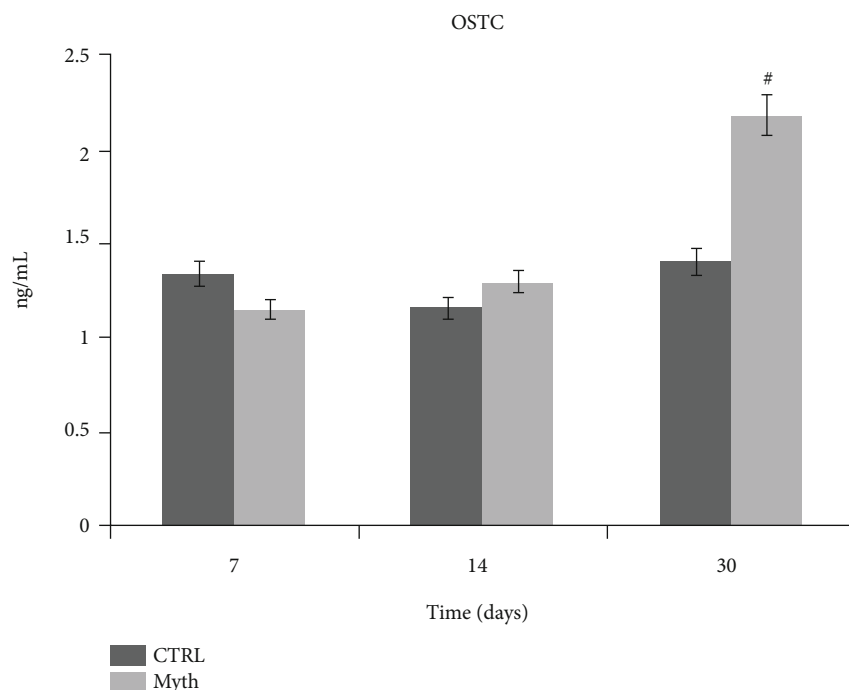


FIGURE 8: h-OSTC ELISA test of culture medium collected from 2D control (CTRL) and DPSC/Myth (Maipenk Manufacturer Industrial Care, Naples, Italy) devices after 7, 14, and 30 days of cell culture. The concentration was expressed in ng/mL.

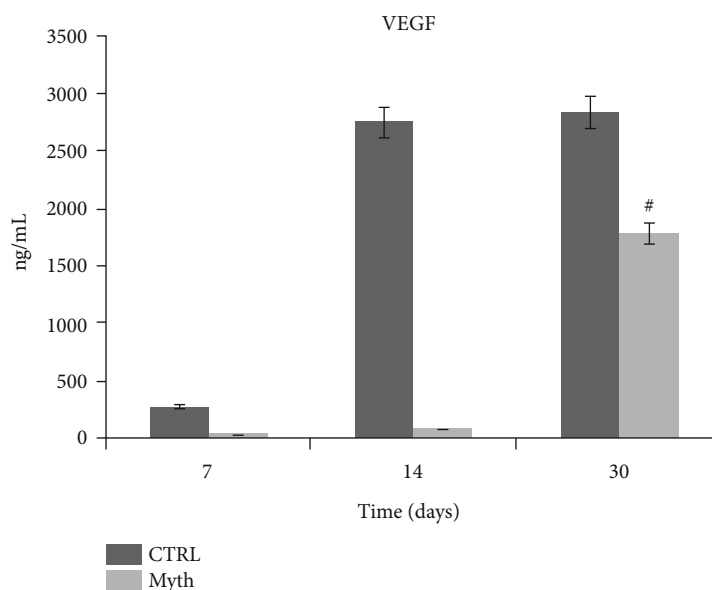


FIGURE 9: h-VEGF ELISA test of culture medium collected from 2D control (CTRL) and DPSC/Myth (Maipenk Manufacturer Industrial Care, Naples, Italy) devices after 7, 14, and 30 days of cell culture. The concentration was expressed in pg/mL.

anchorage, and osteointegration of titanium-made dental implants. Several modifications on the implant surfaces such as sandblasting, anodizing, acid attack, and calcium phosphate coverage have been designed in an attempt to improve the performance of the dental implant. Surface roughness is considered one of the most important characteristics for long-term implant stability. This study was conducted to test the osteoinductive potential of surfaces of dental implants on biological components.

Data Availability

The data used to support the findings of this study are included within the article.

Conflicts of Interest

The authors declare no conflict of interest.

Authors' Contributions

S.C. was responsible for the methodology; L.L. was responsible for the software, validation, and formal analysis; L.N. was responsible for the investigation; L.L. and D.R. were responsible for the data curation and writing—original draft preparation; L.F., G.C., and M.L.N. were responsible for the writing—review and editing; A.S.H. was responsible for the visualization; A.B., A.G., A.Bio., and G.L. were responsible for the supervision; and M.C. was responsible for the project administration. All authors have read and agreed to the published version of the manuscript.

References

- [1] T.-F. Chen, K.-W. Chen, Y. Chien et al., "Dental pulp stem cell-derived factors alleviate subarachnoid hemorrhage-induced neuroinflammation and ischemic neurological deficits," *International Journal of Molecular Sciences*, vol. 20, no. 15, p. 3747, 2019.
- [2] E. Inada, I. Saitoh, N. Kubota et al., "Increased expression of cell surface SSEA-1 is closely associated with Naïve-Like conversion from human deciduous teeth dental pulp cells-derived iPS cells," *International Journal of Molecular Sciences*, vol. 20, no. 7, p. 1651, 2019.
- [3] Y. Yamada, S. Nakamura-Yamada, K. Kusano, and S. Baba, "Clinical potential and current progress of dental pulp stem cells for various systemic diseases in regenerative medicine: a concise review," *International Journal of Molecular Sciences*, vol. 20, no. 5, p. 1132, 2019.
- [4] Y. Yamada, S. Nakamura-Yamada, E. Umemura-Kubota, and S. Baba, "Diagnostic cytokines and comparative analysis secreted from exfoliated deciduous teeth, dental pulp, and bone marrow derived mesenchymal stem cells for functional cell-based therapy," *International Journal of Molecular Sciences*, vol. 20, no. 23, p. 5900, 2019.
- [5] J. Pizzicannella, F. Diomedea, A. Gugliandolo et al., "3D printing PLA/gingival stem cells/ EVs upregulate miR-2861 and -210 during osteoangiogenesis commitment," *International Journal of Molecular Sciences*, vol. 20, no. 13, p. 3256, 2019.
- [6] C. H. Yang, Y. C. Li, W. F. Tsai, C. F. Ai, and H. H. Huang, "Oxygen plasma immersion ion implantation treatment enhances the human bone marrow mesenchymal stem cells responses to titanium surface for dental implant application," *Clinical Oral Implants Research*, vol. 26, no. 2, pp. 166–175, 2015.
- [7] F. Mastrangelo, S. Scacco, A. Ballini et al., "A pilot study of human mesenchymal stem cells from visceral and subcutaneous fat tissue and their differentiation to osteogenic phenotype," *European Review for Medical and Pharmacological Sciences*, vol. 23, no. 7, pp. 2924–2934, 2019.
- [8] M. Kurihara-Shimomura, T. Sasahira, H. Shimomura, C. Nakashima, and T. Kirita, "The oncogenic activity of miR-29b-1-5p induces the epithelial-mesenchymal transition in oral squamous cell carcinoma," *Journal of Clinical Medicine*, vol. 8, no. 2, p. 273, 2019.
- [9] Y.-C. Lee, Y.-H. Chan, S.-C. Hsieh, W.-Z. Lew, and S.-W. Feng, "Comparing the osteogenic potentials and bone regeneration capacities of bone marrow and dental pulp mesenchymal stem cells in a rabbit calvarial bone defect model," *International Journal of Molecular Sciences*, vol. 20, no. 20, p. 5015, 2019.
- [10] L. Erfanparast, P. Iranparvar, and A. Vafaei, "Direct pulp capping in primary molars using a resin-modified Portland cement-based material (TheraCal) compared to MTA with 12-month follow-up: a randomised clinical trial," *European Archives of Paediatric Dentistry*, vol. 19, no. 3, pp. 197–203, 2018.
- [11] A. Nowicka, G. Wilk, M. Lipski, J. Kofecki, and J. Buczkowska-Radlińska, "Tomographic evaluation of reparative dentin formation after direct pulp capping with Ca(OH)₂, MTA, biodentine, and dentin bonding system in human teeth," *Journal of Endodontics*, vol. 41, no. 8, pp. 1234–1240, 2015.
- [12] R. G. Triplett, M. Nevins, R. E. Marx et al., "Pivotal, randomized, parallel evaluation of recombinant human bone morphogenetic protein-2/absorbable collagen sponge and autogenous bone graft for maxillary sinus floor augmentation," *Journal of Oral and Maxillofacial Surgery*, vol. 67, no. 9, pp. 1947–1960, 2009.
- [13] J. Katz, H. Marc, S. Porter, and J. Ruskin, "Inflammation, periodontitis, and coronary heart disease," *The Lancet*, vol. 358, no. 9297, p. 1998, 2001.
- [14] E. Bjertness, B. F. Hansen, G. Berseth, and J. K. Gronnesby, "Oral hygiene and periodontitis in young adults," *The Lancet*, vol. 342, no. 8880, pp. 1170–1171, 1993.
- [15] C. Terada, S. Komasa, T. Kusumoto, T. Kawazoe, and J. Okazaki, "Effect of amelogenin coating of a nano-modified titanium surface on bioactivity," *International Journal of Molecular Sciences*, vol. 19, no. 5, p. 1274, 2018.
- [16] U. K. Vural, A. Kiremitci, and S. Gokalp, "Randomized clinical trial to evaluate MTA indirect pulp capping in deep caries lesions after 24-months," *Operative Dentistry*, vol. 42, no. 5, pp. 470–477, 2017.
- [17] B. N. Celik, M. S. Mutluay, V. Arikan, and S. Sari, "The evaluation of MTA and biodentine as a pulpotomy materials for carious exposures in primary teeth," *Clinical Oral Investigations*, vol. 23, no. 2, pp. 661–666, 2019.
- [18] H. Bakhtiar, M. H. Nekoofar, P. Aminishakib et al., "Human pulp responses to partial pulpotomy treatment with TheraCal as compared with biodentine and ProRoot MTA: a clinical trial," *Journal of Endodontics*, vol. 43, no. 11, pp. 1786–1791, 2017.
- [19] C. Ortiz and M. C. Boyce, "Materials science. Bioinspired structural materials," *Science*, vol. 319, no. 5866, pp. 1053–1054, 2008.
- [20] D. F. G. Poole and H. N. Newman, "Dental plaque and oral health," *Nature*, vol. 234, no. 5328, pp. 329–331, 1971.
- [21] C. Maiorana, M. Beretta, G. B. Grossi et al., "Histomorphometric evaluation of anorganic bovine bone coverage to reduce autogenous grafts resorption: preliminary results," *The Open Dentistry Journal*, vol. 5, no. 1, pp. 71–78, 2011.
- [22] M. Cicciù, A. S. Herford, G. Juodžbalys, and E. Stoffella, "Recombinant human bone morphogenetic protein type 2 application for a possible treatment of bisphosphonates-related osteonecrosis of the jaw," *Journal of Craniofacial Surgery*, vol. 23, no. 3, pp. 784–788, 2012.
- [23] R. E. Jung, S. I. Windisch, A. M. Eggenschwiler, D. S. Thoma, F. E. Weber, and C. H. F. Hämmerle, "A randomized-controlled clinical trial evaluating clinical and radiological outcomes after 3 and 5 years of dental implants placed in bone regenerated by means of GBR techniques with or without the addition of BMP-2," *Clinical Oral Implants Research*, vol. 20, no. 7, pp. 660–666, 2009.

- [24] O. Petrauskaite, P. de Sousa Gomes, M. H. Fernandes et al., "Biomimetic mineralization on a macroporous cellulose-based matrix for bone regeneration," *BioMed Research International*, vol. 2013, Article ID 452750, 9 pages, 2013.
- [25] R. E. Jung, R. Glauser, P. Schäfer, C. H. F. Hämmerle, H. F. Sailer, and F. E. Weber, "Effect of rhBMP-2 on guided bone regeneration in humans," *Clinical Oral Implants Research*, vol. 14, no. 5, pp. 556–568, 2003.
- [26] S. Degala and N. A. Bathija, "Evaluation of the efficacy of simvastatin in bone regeneration after surgical removal of bilaterally impacted third molars—a split-mouth randomized clinical trial," *Journal of Oral and Maxillofacial Surgery*, vol. 76, no. 9, pp. 1847–1858, 2018.
- [27] L. Ortensi, T. Vitali, R. Bonfiglioli, and F. Grande, "New tricks in the preparation design for prosthetic ceramic laminate veneers," *Prosthesis*, vol. 1, no. 1, pp. 29–40, 2019.
- [28] M. Ciccù, "Prosthesis: new technological opportunities and innovative biomedical devices," *Prosthesis*, vol. 1, no. 1, pp. 1–2, 2019.
- [29] L. Fiorillo, G. Cervino, A. Herford et al., "Interferon crevicular fluid profile and correlation with periodontal disease and wound healing: a systemic review of recent data," *International Journal of Molecular Sciences*, vol. 19, no. 7, p. 1908, 2018.
- [30] T. Traini, G. Murmura, B. Sinjari et al., "The surface anodization of titanium dental implants improves blood clot formation followed by osseointegration," *Coatings*, vol. 8, no. 7, p. 252, 2018.
- [31] D. Guadarrama Bello, A. Fouillen, A. Badia, and A. Nanci, "A nanoporous titanium surface promotes the maturation of focal adhesions and formation of filopodia with distinctive nanoscale protrusions by osteogenic cells," *Acta Biomaterialia*, vol. 60, pp. 339–349, 2017.
- [32] B. Bueno Rde, P. Adachi, L. M. S. de Castro-Raucci, A. L. Rosa, A. Nanci, and P. T. de Oliveira, "Oxidative nanopatterning of titanium surfaces promotes production and extracellular accumulation of osteopontin," *Brazilian Dental Journal*, vol. 22, no. 3, pp. 179–184, 2011.
- [33] M. Ciccù, L. Fiorillo, A. S. Herford et al., "Bioactive titanium surfaces: interactions of eukaryotic and prokaryotic cells of nano devices applied to dental practice," *Biomedicines*, vol. 7, no. 1, 2019.
- [34] G. Cervino, L. Fiorillo, G. Iannello, D. Santonocito, G. Risitano, and M. Ciccù, "Sandblasted and acid etched titanium dental implant surfaces systematic review and confocal microscopy evaluation," *Materials*, vol. 12, no. 11, p. 1763, 2019.
- [35] A. Scarano, V. Crincoli, A. Di Benedetto et al., "Bone regeneration induced by bone porcine block with bone marrow stromal stem cells in a minipig model of mandibular "critical size" defect," *Stem Cells International*, vol. 2017, Article ID 9082869, 9 pages, 2017.
- [36] A. Scarano, E. Crocetta, A. Quaranta, and F. Lorusso, "Influence of the thermal treatment to address a better osseointegration of Ti6Al4V dental implants: histological and histomorphometrical study in a rabbit model," *BioMed Research International*, vol. 2018, Article ID 2349698, 7 pages, 2018.
- [37] F. Variola, J. B. Brunski, G. Orsini, P. T. de Oliveira, R. Wazen, and A. Nanci, "Nanoscale surface modifications of medically relevant metals: state-of-the art and perspectives," *Nanoscale*, vol. 3, no. 2, pp. 335–353, 2011.
- [38] L. P. Maia, D. M. Reino, V. A. Muglia et al., "Influence of periodontal tissue thickness on buccal plate remodelling on immediate implants with xenograft," *Journal of Clinical Periodontology*, vol. 42, no. 6, pp. 590–598, 2015.
- [39] P. Naddeo, L. Laino, M. La Noce et al., "Surface biocompatibility of differently textured titanium implants with mesenchymal stem cells," *Dental Materials*, vol. 31, no. 3, pp. 235–243, 2015.
- [40] V. Corvino, G. Iezzi, O. Trubiani, T. Traini, and M. Piattelli, "Histological and histomorphometric evaluation of implant with nanometer scale and oxidized surface. In vitro and in vivo study," *Journal of biological regulators and homeostatic agents*, vol. 26, 2012.
- [41] F. R. Carbone and T. Gebhardt, "Immunology. A neighborhood watch upholds local immune protection," *Science*, vol. 346, no. 6205, pp. 40–41, 2014.
- [42] J. Lindhe, T. Berglundh, and N. P. Lang, *Parodontologia Clinica e Implantologia Orale*, Edi Ermes, Italy, 5th edition, 2009.
- [43] K. Bagri-Manjrekar, M. Chaudhary, G. Sridharan, S. R. Tekade, A. R. Gadbail, and K. Khot, "In vivo autofluorescence of oral squamous cell carcinoma correlated to cell proliferation rate," *Journal of Cancer Research and Therapeutics*, vol. 14, no. 3, pp. 553–558, 2018.
- [44] G. L. Giudice, G. Cutroneo, A. Centofanti et al., "Dentin morphology of root canal surface: a quantitative evaluation based on a scanning electronic microscopy study," *BioMed Research International*, vol. 2015, Article ID 164065, 7 pages, 2015.
- [45] E.-B. Bae, J.-H. Yoo, S.-I. Jeong et al., "Effect of titanium implants coated with radiation-crosslinked collagen on stability and osseointegration in rat tibia," *Materials*, vol. 11, no. 12, p. 2520, 2018.
- [46] J. Z.-C. Chang, P.-I. Tsai, M. Y.-P. Kuo, J.-S. Sun, S.-Y. Chen, and H.-H. Shen, "Augmentation of DMLS biomimetic dental implants with weight-bearing strut to balance of biologic and mechanical demands: from bench to animal," *Materials*, vol. 12, no. 1, p. 164, 2019.
- [47] D. Soto-Peñaloza, M. Caneva, J. Viña-Almunia, J. Martín-de-Llano, D. Peñarocha-Oltra, and M. Peñarocha-Diogo, "Bone-healing pattern on the surface of titanium implants at cortical and marrow compartments in two topographic sites: an experimental study in rabbits," *Materials*, vol. 12, no. 1, 2018.
- [48] M. Contaldo, D. Di Stasio, R. Santoro et al., "Non-invasive in vivo visualization of enamel defects by reflectance confocal microscopy (RCM)," *Odontology*, vol. 103, no. 2, pp. 177–184, 2015.
- [49] L. Fiorillo, L. Laino, R. De Stefano et al., "Dental whitening gels: strengths and weaknesses of an increasingly used method," *Gels*, vol. 5, no. 3, p. 35, 2019.
- [50] R. De Stefano, "Psychological factors in dental patient care: odontophobia," *Medicina*, vol. 55, 2019.
- [51] R. De Stefano, A. Bruno, M. R. Muscatello, C. Cedro, G. Cervino, and L. Fiorillo, "Fear and anxiety managing methods during dental treatments: a systematic review of recent data," *Minerva Stomatologica*, vol. 68, no. 6, 2019.
- [52] C. M. Schmitt, M. Koepfle, T. Moest, K. Neumann, T. Weisel, and K. A. Schlegel, "In vivo evaluation of biofunctionalized implant surfaces with a synthetic peptide (P-15) and its impact on osseointegration. A preclinical animal study," *Clinical Oral Implants Research*, vol. 27, no. 11, pp. 1339–1348, 2016.

- [53] R. N. Wakim, M. Namour, H. Nguyen et al., "Decontamination of dental implant surfaces by the Er:YAG laser beam: a comparative in vitro study of various protocols," *Dentistry Journal*, vol. 6, no. 4, 2018.
- [54] R. N. R. de Jesus, E. Carrilho, P. V. Antunes et al., "Interfacial biomechanical properties of a dual acid-etched versus a chemically modified hydrophilic dual acid-etched implant surface: an experimental study in beagles," *International journal of implant dentistry*, vol. 4, no. 1, pp. 28–28, 2018.
- [55] S. A. Gehrke, J. H. C. de Lima, F. Rodriguez et al., "Microgrooves and microrugosities in titanium implant surfaces: an in vitro and in vivo evaluation," *Materials*, vol. 12, no. 8, p. 1287, 2019.
- [56] L. Fiorillo and G. L. Romano, "Gels in medicine and surgery: current trends and future perspectives," *Gels*, vol. 6, 2020.
- [57] M. Cicciù, L. Fiorillo, G. Cervino, and M. B. Habal, "Bone morphogenetic protein application as grafting materials for bone regeneration in craniofacial surgery: current application and future directions," *Journal of Craniofacial Surgery*, vol. 32, no. 2, pp. 787–793, 2021.
- [58] G. Lucarini, A. Zizzi, C. Rubini, F. Ciolino, and S. D. Aspriello, "VEGF, microvessel density, and CD44 as inflammation markers in peri-implant healthy mucosa, peri-implant mucositis, and peri-implantitis: impact of age, smoking, PPD, and obesity," *Inflammation*, vol. 42, no. 2, pp. 682–689, 2019.
- [59] Z. Hu, D. Wu, Y. Zhao, S. Chen, and Y. Li, "Inflammatory cytokine profiles in the crevicular fluid around clinically healthy dental implants compared to the healthy contralateral side during the early stages of implant function," *Archives of Oral Biology*, vol. 108, article 104509, 2019.
- [60] B. Zavan, L. Ferroni, C. Gardin, S. Sivoilella, A. Piattelli, and E. Mijiritsky, "Release of VEGF from dental implant improves osteogenetic process: preliminary in vitro tests," *Materials*, vol. 10, no. 9, p. 1052, 2017.
- [61] L. Schorn, C. Sproll, M. Ommerborn, C. Naujoks, N. R. Kübler, and R. Depprich, "Vertical bone regeneration using rhBMP-2 and VEGF," *Head & Face Medicine*, vol. 13, no. 1, p. 11, 2017.
- [62] A. Klos, X. Sedao, T. E. Itina et al., "Ultrafast laser processing of nanostructured patterns for the control of cell adhesion and migration on titanium alloy," *Nanomaterials*, vol. 10, no. 5, p. 864, 2020.
- [63] R. Di Carlo, A. Di Crescenzo, S. Pilato et al., "Osteoblastic differentiation on graphene oxide-functionalized titanium surfaces: an in vitro study," *Nanomaterials*, vol. 10, no. 4, p. 654, 2020.
- [64] G. Cervino, M. Montanari, D. Santonocito et al., "Comparison of two low-profile prosthetic retention system interfaces: preliminary data of an in vitro study," *Prosthesis*, vol. 1, no. 1, pp. 54–60, 2019.
- [65] R. Scrascia, L. Fiorillo, V. Gaita, L. Secondo, F. Nicita, and G. Cervino, "Implant-supported prosthesis for edentulous patient rehabilitation. From temporary prosthesis to definitive with a new protocol: a single case report," *Prosthesis*, vol. 2, pp. 10–24, 2020.
- [66] C. D'Amico, S. Bocchieri, S. Sambataro, G. Surace, C. Stumpo, and L. Fiorillo, "Occlusal Load Considerations in implant-supported fixed restorations," *Prosthesis*, vol. 2, no. 4, pp. 252–265, 2020.
- [67] P. Iovino, A. Di Sarno, V. De Caro, C. Mazzei, A. Santonicola, and V. Bruno, "Screwdriver aspiration during oral procedures: a lesson for dentists and gastroenterologists," *Prosthesis*, vol. 1, no. 1, pp. 61–68, 2019.
- [68] L. Fiorillo, M. Cicciù, C. D'Amico, R. Mauceri, G. Oteri, and G. Cervino, "Finite element method and von Mises investigation on bone response to dynamic stress with a novel conical dental implant connection," *BioMed Research International*, vol. 2020, Article ID 2976067, 13 pages, 2020.
- [69] F. Diomedede, G. D. Marconi, M. F. X. B. Cavalcanti et al., "VEGF/VEGF-R/RUNX2 upregulation in human periodontal ligament stem cells seeded on dual acid etched titanium disk," *Materials*, vol. 13, no. 3, p. 706, 2020.
- [70] Sunarso, A. Tsuchiya, R. Toita, K. Tsuru, and K. Ishikawa, "Enhanced osseointegration capability of poly(ether ether ketone) via combined phosphate and calcium surface-functionalization," *International Journal of Molecular Sciences*, vol. 21, no. 1, p. 198, 2020.
- [71] I. Irastorza, J. Luzuriaga, R. Martinez-Conde, G. Ibarretxe, and F. Unda, "Adhesion, integration and osteogenesis of human dental pulp stem cells on biomimetic implant surfaces combined with plasma derived products," *European Cells and Materials*, vol. 38, pp. 201–214, 2019.

Research Article

The Alveolar Ridge Splitting Technique on Maxillae: A Biomechanical Human Cadaveric Investigation

Fabian Duttenhoefer ¹, Peter Varga ², Dominik Jenni,² Leonard Grünwald,² Luisa Thiemann,¹ Boyko Gueorguiev ² and Andres Stricker¹

¹University Hospital of Freiburg, Germany

²AO Research Institute Davos, Switzerland

Correspondence should be addressed to Fabian Duttenhoefer; fabian.duttenhoefer@uniklinik-freiburg.de

Received 11 September 2020; Revised 24 October 2020; Accepted 2 November 2020; Published 19 November 2020

Academic Editor: Paolo Pesce

Copyright © 2020 Fabian Duttenhoefer et al. This is an open access article distributed under the Creative Commons Attribution License, which permits unrestricted use, distribution, and reproduction in any medium, provided the original work is properly cited.

The alveolar ridge splitting technique (ARST) offers an alternative to classic ridge augmentation techniques for successful insertion of dental implants. However, the buccal lamella is at risk of fracturing during ARST distraction. To better understand the fracture mechanisms and displacement limits of the split lamella, this study conducted biomechanical tests on human cadaveric maxilla specimens having extremely atrophied alveolar ridges treated with ARST. A total of 12 standardized alveolar splits were prepared on the maxillae of 3 elderly female donors using an oscillating piezoelectric saw. Mimicking the surgical distraction process of the lamella, each split was tested to failure using a dental osteotome attached to the crosshead of an electromechanical testing system. All specimens were scanned by means of high-resolution peripheral quantitative computed tomography prior to and post testing to evaluate split geometries and failure modes. Split stiffness, failure force, and displacement were 27.4 ± 18.7 N/mm, 12.0 ± 8.4 N, and 0.97 ± 0.31 mm, with no significant differences between anatomical sides and split locations ($p \geq 0.17$). Stiffness correlated significantly with failure force ($R^2 = 0.71$, $p < 0.01$). None of the alveolar split widths correlated significantly with the outcomes from biomechanical testing ($p \geq 0.10$). The results suggest that simple geometrical measures do not predict the allowed extent of lamella distraction prior to failure. More sophisticated methods are required for surgical planning to optimize the ARST outcomes. Still, the present study may advocate a clinical protocol for the maxilla where the implant site is prepared directly after osteotomy setting and immediately before full lamella dislocation, when the lamella is still stable, resistant to mechanical stress, and bone loss caused by the abrasion of the burr is minimized.

1. Introduction

Rehabilitation of strongly atrophied alveolar ridge using dental implants usually requires complex augmentation techniques for their successful insertion. As an alternative to the classic augmentations through bone grafts or guided bone regeneration, the splitting and expansion of the alveolar ridge, so-called alveolar ridge splitting technique (ARST), offers the possibility of increasing the width of the alveolar ridge. This method is applied when the alveolar ridge exhibits sufficient vertical bone height but has insufficient horizontal width. After splitting and expansion of the bone, a sufficiently wide implantation site can be provided to allow full anchorage of the implant in the autologous bone [1–3]. Comparable

success rates to augmentations with bone blocks or guided bone regeneration can be achieved with this technique [4]. Further ARST advantages are that a second operation is avoided and the treatment duration is shortened due to simultaneous implant insertion [5].

The technical ARST implementation consists of setting a longitudinal osteotomy along the course of the alveolar ridge at the location of planned implant insertion and two vertical relief osteotomies. The enlarged alveolar width is then created by careful distraction of the outlined buccal segment [6, 7]. Subsequently, a drilling protocol is applied, and the implant is inserted.

The main risk of this surgical technique is related to fracturing of the buccal lamella during distraction. The risk

increases significantly in case of advanced alveolar ridge atrophy due to high bone resorption and poor bone quality [4, 8–14]. So far, little scientific knowledge exists about the fracture mechanisms and maximum possible extent of distraction before a lamella fracture occurs. Previous work investigated lamellar fracturing in porcine specimens [15]. Another *in vitro* animal study developed a biomechanical model to simulate the surgical procedure and fracture behavior during alveolar bone splitting [16]. However, both those previous investigations were limited by the use of porcine specimens which may differ from the human tissue. In particular, the good animal bone quality did not necessarily represent a situation with the most endangered patients, being the targeted group with atrophic alveolar ridge. Therefore, ARST and in particular the phenomenon of lamellar fracturing should be investigated on relevant human bone tissue.

The aim of this study was to perform biomechanical testing on human cadaveric specimens representing patients at the highest risk of lamellar fracturing during ARST implementation in order to investigate better the maximum extent of lamella displacement, draw conclusions about the predictability, and ultimately help prevent intraoperative lamellar fractures.

2. Materials and Methods

2.1. Specimen Preparation and Scanning. Fresh-frozen (-20°C) human cadaveric heads of three elderly female donors (76, 83, and 89 years old) with a long-standing complete edentulous intraoral condition were used. The donors gave their informed consent inherent within the donation of the anatomical gift statement during their lifetime. The maxillae were dissected from the skulls by Le Fort I osteotomy using an oscillating surgical saw (DePuy Synthes, Oberdorf, Switzerland), then separated and cleaned of soft tissues. Alveolar splits of 8 mm depth and 10 mm width were prepared using an oscillating piezoelectric saw with a blade thickness of 0.35 mm in two maxillae and 0.55 mm in the third one (PIEZOSURGERY® touch, Mectron, Carasco, Italia) (Figure 1). Vertical relief incisions were performed at both ends perpendicularly to the split plane. Twelve splits were prepared in total—four per maxilla: one in the canine and one in the premolar region of its left and right sides (Figure 1).

All prepared specimens were scanned by means of high-resolution peripheral quantitative computed tomography (HR-pQCT, XtremeCT, Scanco Medical AG, Brütisellen, Switzerland) to investigate the osteotomy lines. Scanning settings were 60 kV voltage, 900 μA current, and 82 μm isotropic voxel size. The dimensions of the alveolar bone were measured on the postoperative HR-pQCT images using Amira software package (Version 6.0, FEI, Hillsboro, USA) including the crestal and basal widths on the buccal and oral sides of the split, as well as the total crestal and basal widths (Figure 2).

2.2. Biomechanical Testing. The specimens were positioned in a custom-made adjustable holder. The cranial aspect of the maxillae was embedded in dental cement (True-Plast,

Superhartgips, Benzer Dental AG, Zurich, Switzerland) that cured at room temperature for approximately one hour. The embedding level was sufficiently far away from the splits in order to avoid its influence on the alveolar split behavior during the subsequent biomechanical tests (Figure 3, left).

Each split was tested to failure in a setup mimicking the surgical expansion process as follows. First, the plane of the split, identified by a thin plate inserted in the osteotomy, was carefully aligned with the horizontal plane by rotating the ball joint of the adjustable specimen holder (Figure 3, left). The aligned specimen was then mounted on an electro-mechanical material testing machine (Instron 5866, Instron, Norwood, USA). A dental osteotome (Ergoplant, Aesculap AG, Tuttlingen, Germany) was attached to a 1 kN load-cell mounted on the crosshead of the testing machine. The osteotome blade was aligned horizontally, and its height was adjusted to the split plane. The osteotome blade was then carefully inserted into the split at 3 mm depth by moving the specimen holder along the osteotome axis. The position of the specimen holder was then fixed. Quasi-static distraction test of the buccal lamella was performed by displacement-controlled vertical translation of the osteotome at a rate of 5 mm/min in vertical (i.e., vestibular) direction along the machine axis (Figure 3, right).

All specimens were rescanned post testing by means of HR-pQCT using the same settings as described above. Surface mesh of the segmented bone image region was used to visualize the fracture lines in Amira.

2.3. Data Acquisition and Analysis. Displacement of the machine crosshead and reaction force was recorded by the controllers of the testing system at a rate of 10 Hz. Stiffness (K , in N/mm) was evaluated from the steepest slope in the linear portion of the force-displacement curve. Failure was defined by a significant drop in the reaction force during testing. The corresponding failure force (F_{fx} , in N) and failure displacement (u_{fx} , in mm) were quantified.

2.4. Statistical Evaluation. Normality of data distribution among all geometrical alveolar widths and biomechanical outcomes was screened using the Shapiro-Wilk test. Friedman and Wilcoxon Signed-Rank tests were applied to detect significant differences among alveolar widths, as well as among biomechanical outcomes with respect to donors, anatomical sides, and anatomical locations. Spearman test was used to identify significant correlations between alveolar widths and biomechanical outcomes. Level of significance was set to $p = 0.05$ for all statistical tests.

3. Results

The measured alveolar widths of all prepared specimens (crestal-buccal, crestal-oral, crestal-total, basal-buccal, basal-oral, and basal-total) are summarized in Table 1. The dimensions of the splits were more standardized on the buccal side of the split and showed a larger scatter on the oral side. Overall, these geometrical parameters were significantly different for donor A compared with both donors B and C ($p \leq 0.03$) and did not differ significantly between donors B

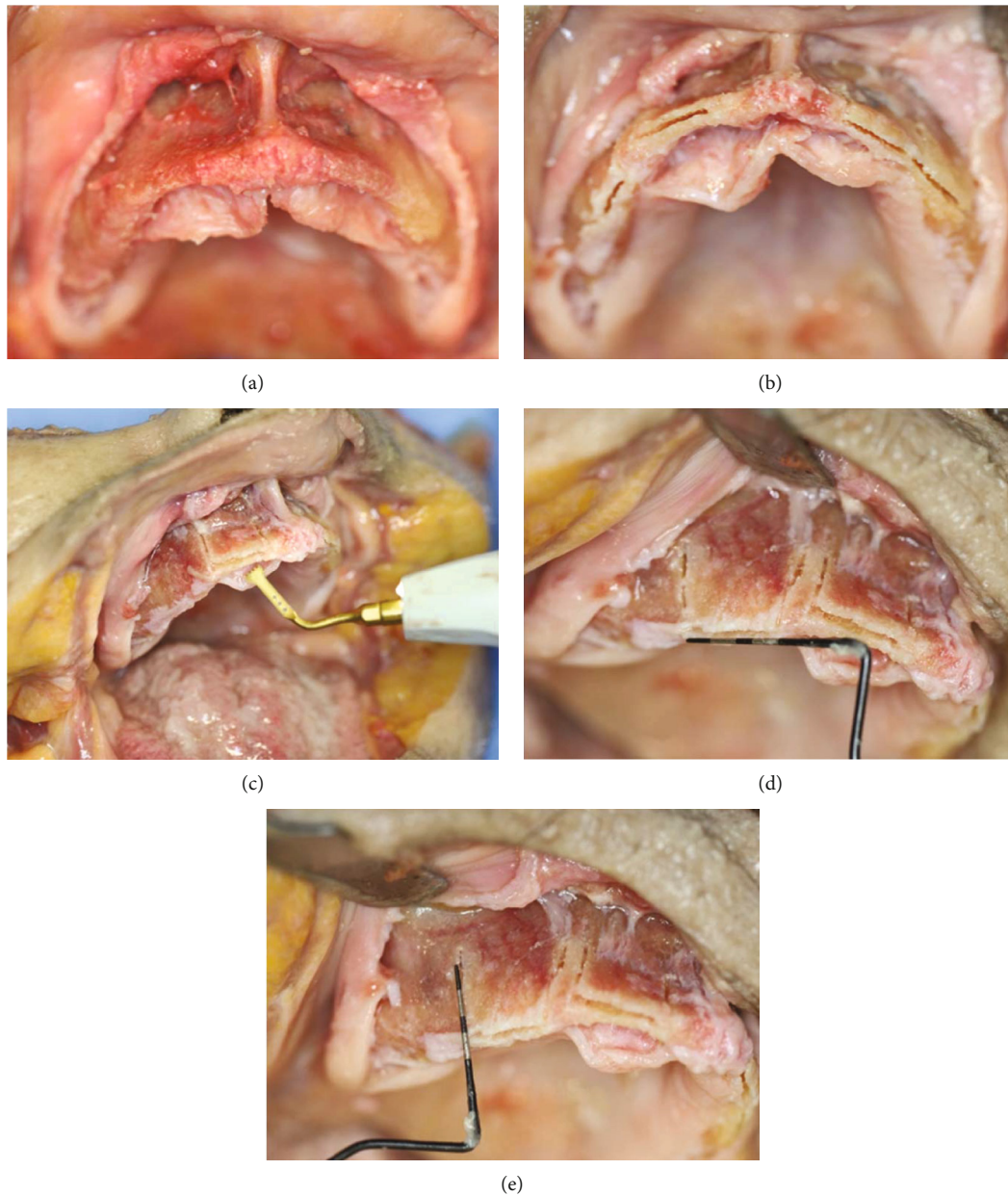


FIGURE 1: Surgical procedure: maxilla with deflected soft tissue (a); horizontal osteotomies created with the alveolar ridge splitting procedure (b); preparation of alveolar splits using an oscillating piezoelectric saw (c); controlling alveolar splits dimensions of 10 mm horizontal width (d) and 8 mm vertical depth (e) following the procedure.

and C ($p = 0.22$). No significant differences in the corresponding alveolar widths were detected between donors' right and left sides ($p = 0.11$). Moreover, the canine alveolar widths of the donors did not differ significantly from the corresponding premolar ones ($p \geq 0.34$).

A typical force-displacement curve of a biomechanically tested specimen is shown in Figure 4.

All biomechanical tests resulted in clinically relevant fracture modes with levels of the fracture lines ranging between the tip of the osteotome and the basal base of the splits (Figure 5).

The outcomes from biomechanical testing (stiffness, failure force, and failure displacement) are presented in Table 1. They differed significantly for donor B compared with both

donors A and C ($p < 0.01$) but did not differ significantly between donors A and C ($p = 0.31$). No significant differences in these outcomes were detected between donors' right and left sides ($p \geq 0.17$). Moreover, the outcomes for canine anatomical location did not differ significantly from the corresponding ones for premolar location ($p \geq 0.36$).

No significant correlations were detected between any of the measured alveolar widths and any of the outcomes from biomechanical testing ($p \geq 0.10$). Stiffness of the tested specimens correlated significantly with their failure force ($p < 0.01$, $R^2 = 0.71$, Figure 6), but not with the failure displacement ($p \geq 0.21$). No significant correlation was identified between failure force and failure displacement ($p \geq 0.10$).

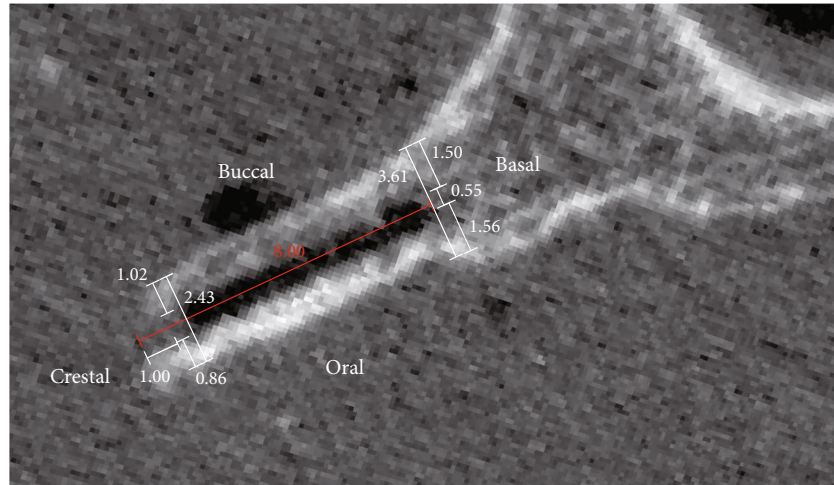


FIGURE 2: Geometrical measurements to quantify alveolar widths (crestal-buccal, crestal-oral, crestal-total, basal-buccal, basal-oral, and basal-total) on the high-resolution peripheral quantitative computed tomography images.

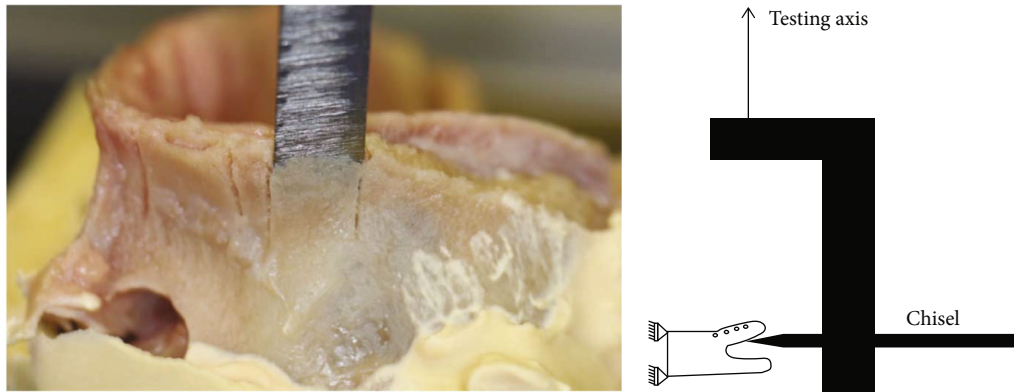


FIGURE 3: Setup for distraction testing of a split lamella. Photograph of an embedded specimen with a thin metal plate inserted in the split to identify the direction of positioning for biomechanical testing (left). Schematic illustration of the experimental setup (right).

4. Discussion

The most common complication of ARST is the intraoperative fracture of the buccal lamella [16]. It is therefore of essential importance to preoperatively estimate the maximum possible displacement of the lamella in order to adapt the surgical protocol accordingly. Still, the extension behavior of the buccal lamella and the related fracture mechanisms are not deciphered yet.

A pilot study by Stricker et al. successfully developed a biomechanical setup for relevant replication of lamellar fracturing applying ARST on porcine jaw specimens; a mean critical lamella displacement of 1.27 mm was reported for porcine mandibles osteotomized via piezosurgery and tested in lateral distraction with an osteotome [16]. Comparable results in alveolar ridge splitting of porcine mandibles were obtained in a study by Jung et al. [15] who analyzed lamella displacement by vertical force application utilizing either a mallet and chisel (control group) or an engine-driven ridge spreader (test group). The alveolar crest width could be significantly increased in both control (1.23 ± 0.45 mm) and test groups (0.98 ± 0.41 mm) [15]. Although the porcine model

exhibits a close similarity to human bone in terms of structure and bone mineral density [17, 18], the model has limited relevance for alveolar ridge splitting due to the pig anatomy [15, 16]. Moreover, the pristine bone of the applied pig models does not reproduce the clinical situation of severely atrophied and brittle human alveolar ridges. It is noteworthy to mention that the lack of cancellous bone often accounts for lamellar fractures, especially in the thicker and more mineralized cortical bone, such as the one seen in the mandible [19].

In the present work, the mechanical fracture simulation was transferred to human anatomy with strongly atrophied maxillae and was therefore able to reproduce a real clinical situation in the most endangered patients' group. We focused on the maxilla as the mandible in humans is less suited for alveolar ridge splitting due to its centrifugal atrophy pattern and a rather round-shaped cross-section as compared to the wedge-shaped pattern of the maxilla seen in the classification proposed by Cawood and Howell [20]. Moreover, implant placement in the atrophied maxilla aims to place the implant as far as buccally as possible. Due to the centripetal atrophy pattern of the maxilla, alveolar ridge splitting

TABLE 1: Measured alveolar widths of all prepared specimens (crestal-buccal, crestal-oral, crestal-total, basal-buccal, basal-oral, and basal-total) together with the outcomes from their biomechanical testing (stiffness, failure force, and failure displacement).

Donor ID	Specimen			Alveolar width						Outcomes biomechanical testing		
	Split ID	Side	Anatomical location	Crestal-buccal [mm]	Crestal-oral [mm]	Crestal-total [mm]	Basal-buccal [mm]	Basal-oral [mm]	Basal-total [mm]	Stiffness (K) [N/mm]	Failure force (F_{fx}) [N]	Failure displacement (U_{fx}) [mm]
A	1	L	Canine	1.36	0.67	2.38	2.47	0.70	3.52	60.9	34.8	0.88
A	2	L	Premolar	0.71	1.23	2.29	3.40	4.13	7.88	16.3	9.2	0.93
A	3	R	Premolar	0.88	0.82	2.05	1.90	2.51	4.76	42.1	14.9	0.9
A	4	R	Canine	0.96	0.87	2.18	1.16	2.16	4.12	31.2	15.7	0.93
B	1	L	Canine	1.02	0.86	2.43	1.50	1.56	3.61	11.4	8.6	1.27
B	2	L	Premolar	1.37	2.32	4.24	2.37	3.99	6.91	15	8.5	0.77
B	3	R	Premolar	1.22	2.22	3.99	1.99	3.05	5.59	23.1	5.1	0.5
B	4	R	Canine	1.15	1.00	2.70	1.75	2.68	4.98	5.4	4.6	1.18
C	1	L	Canine	1.05	0.70	2.10	3.50	6.55	10.40	24.2	9.8	0.59
C	2	L	Premolar	1.94	0.59	2.88	2.55	4.16	7.06	62.4	18.3	1.58
C	3	R	Premolar	0.99	0.43	1.77	2.27	3.32	5.94	23.9	6.6	0.77
C	4	R	Canine	1.03	1.13	2.51	2.90	7.15	10.41	13.3	7.6	1.3
Mean				1.14	1.07	2.63	2.31	3.50	6.27	28.7	12.0	0.97
Standard deviation				0.31	0.60	0.76	0.71	1.88	2.37	19.0	8.4	0.31

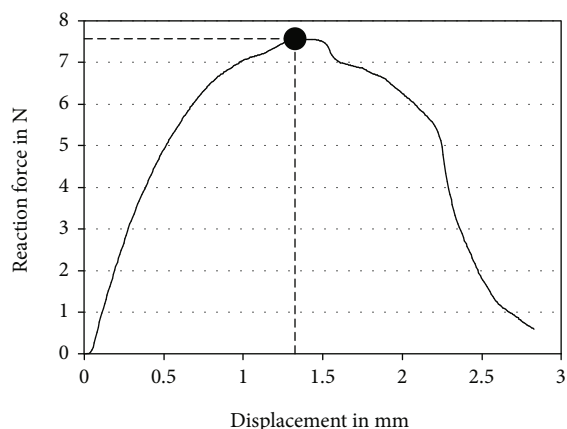


FIGURE 4: Exemplary force-displacement curve of a specimen during biomechanical testing, with a circle indicating fracturing.

with distraction of the buccal ridge aspect facilitates compensation of the centripetal bone loss.

In our previous porcine model, the osteotomy outlines varied between 4 and 8 mm depth being with a crestal cut between 7 and 10 mm in the mesiodistal direction [16]. The achieved displacement before permanent lamella dislocation, i.e., prior to reaching fracturing force, was 1.3 ± 0.9 mm. This considerable variation in the test results was probably related to the nonstandardized lamellar geometries. While relief height was found to correlate with fracture force, no correlations were found fracture displacement and the latter. Due to the small sample size, it could not be clearly concluded whether the scatter in the displacement results was related to the height, width, and/or the thickness of the lamella, the latter proportionally increasing with the height due to the

porcine anatomy. Hence, the split geometry in the present human cadaveric study was standardized to 8 mm depth and 10 mm width. Interestingly, although the utilized human specimens showed severe alveolar ridge atrophy, the average displacement when reaching fracturing force (0.97 mm) was close to the one reported in the porcine study (1.3 mm). Nevertheless, this may have been a coincidence. In turn, the standard deviation of the results could be efficiently reduced via the aforementioned standardization. In addition, the standardized depth and width of the splits allowed to investigate whether the lamellar thickness at the basal or crestal aspect would predict the biomechanical outcomes. No significant correlations were detected between the geometrical alveolar widths and the outcomes from biomechanical testing. However, similarly to a previous animal study, it could be shown that the stiffness correlated strongly with the failure force [16]. Nevertheless, the fracture line was not always located at the base, but often more crestal, assumedly at the local weakest region of the lamella (Figure 5). These findings suggest that simple geometrical measures may not suffice, and more sophisticated methods are necessary to preoperatively predict the biomechanical outcomes and especially the clinically relevant allowed extent of lamellar distraction. Finite element analysis, successfully applied on a small set of porcine specimens in our previous study [16], appears to be a promising technique for prediction of the biomechanical behavior and fracturing of the lamella. Future research is required to evaluate whether finite element models can better predict lamellar dislocation and possible implant placement in human alveolar bone based on computed tomography scans.

During the measurements performed in the present study, in agreement with previous work [16], the maximum force of the force-displacement curve was defined as failure

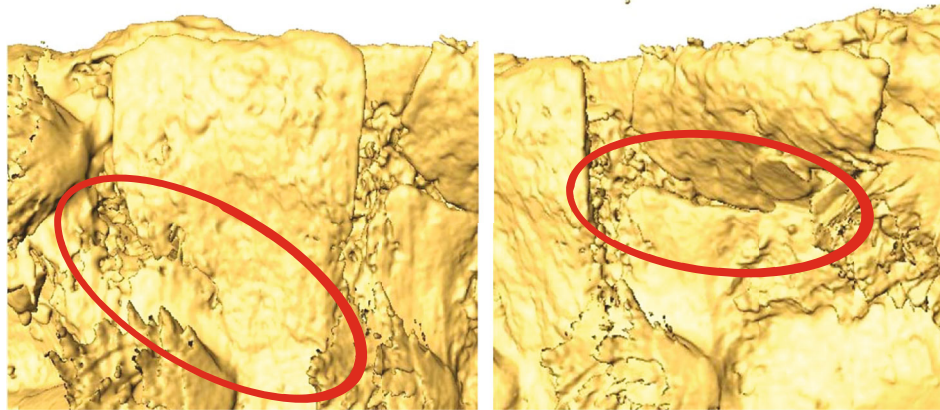


FIGURE 5: Exemplified fracture lines of alveolar split lamellae visualized on the surface renderings of segmented post-test high-resolution peripheral quantitative computed tomography images and highlighted with red ellipses.

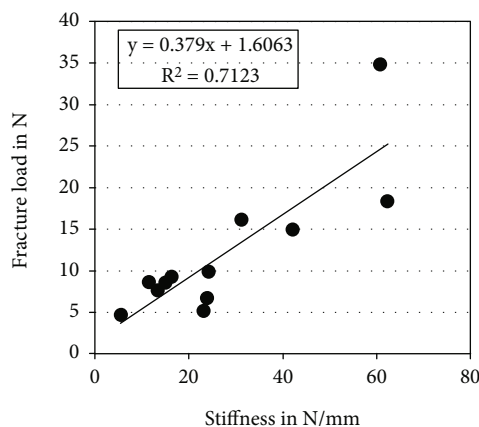


FIGURE 6: Linear regression plot between stiffness and failure force, visualizing a significant correlation between these two outcomes from biomechanical testing ($p < 0.01$).

force. However, this may not always correspond to what is described as “fracture of the lamella” in a clinical context. In a clinical situation, the term “fracture of the lamella” usually refers to a fully detached lamella or extensive dislocation inhibiting implantation. The definition used in this study implies that, beyond the state with maximum force, no further increase in the force is measured following increase of the applied displacement; however, the lamella could still be in place attached to the base, not extensively displaced and continuing to resist to further distraction. It remains unclear whether an implant could be inserted in a split at this state. To get further insight into the bone split technique, future studies may focus on fracture mechanisms and the clinical relevance of dislocating the alveolar lamella beyond the state defined by the maximum force in this study.

Yet, we have found some evidence that may lead to improvement of the surgical alveolar bone split protocol. Most of the clinical fractures of the bone split occur during instrumentation of the lamella, especially when using rota-

tion burs to prepare the implant site. According to our results, we propose to prepare the implant site after osteotomizing while the lamella is slightly dislocated right to the point prior to fracturing. The latter can be feasibly controlled by removing the utilized osteotome or chisel. At this point, the lamella is still stable and resistant to mechanical stress, with preformed gap and minimal bone loss caused by the abrasion of the burr.

4.1. Limitations. The limitations of the study are similar to those inherent for all biomechanical cadaveric investigations using a limited number of specimens. The sample size was modest, which was mainly due to restricted availability of relevant human cadaveric material. In addition, the lamellar displacement measured by the testing system may not have been accurate enough due to certain compliance of the experimental setup. Furthermore, the biomechanical in vitro testing approach may not have perfectly mimicked the split expansion during surgery. Finally, only ridge splitting with expansion was performed in the maxilla and without implantation that might have had further effects on the stability of the lamella.

4.2. Conclusions. The results from the current study suggest a clinical protocol during alveolar ridge splitting in highly atrophic maxilla, where the implant site can be minimal and adequately prepared directly after osteotomy setting and immediately before full lamella dislocation—identified by the maximum force before fracturing. In this state, the lamella is still stable and resistant to mechanical stress, while bone loss caused by the abrasion of the burr is minimal. More sophisticated methods are required for surgical planning to optimize the ARST outcomes, since simple geometrical measures do not predict the allowed extent of distraction prior to failure.

Data Availability

The data of the submitted paper is available upon e-mail request to the corresponding author.

Disclosure

The authors are not compensated, and there are no other institutional subsidies, corporate affiliations, or funding sources supporting this work unless clearly documented and disclosed.

Conflicts of Interest

The authors declare that they have no conflicts of interest.

Acknowledgments

This investigation was performed with the assistance of the AO Foundation. This study was supported by a grant from the ITI Foundation for the Promotion of Oral Implantology, Basel, Switzerland (grant No. 706-2010). The authors gratefully acknowledge Dieter Wahl, Benno Dicht, and Ivan Zderic for their assistance in preparing and conducting the biomechanical tests.

References

- [1] R. Bassetti, M. Bassetti, R. Mericske-Stern, and N. Enkling, "Piezoelectric alveolar ridge-splitting technique with simultaneous implant placement: a cohort study with 2-year radiographic results," *The International Journal of Oral & Maxillofacial Implants*, vol. 28, no. 6, pp. 1570–1580, 2013.
- [2] A. Stricker, J. Fleiner, M. Dard, P. Voss, S. Sauerbier, and D. D. Bosshardt, "Evaluation of a new experimental model to study bone healing after ridge expansion with simultaneous implant placement—a pilot study in minipigs," *Clinical Oral Implants Research*, vol. 25, no. 11, pp. 1265–1272, 2014.
- [3] M. Bassetti, R. Bassetti, and D. Bosshardt, "The alveolar ridge splitting/expansion technique: a systematic review," *Clinical Oral Implants Research*, vol. 27, no. 3, pp. 310–324, 2016.
- [4] M. Chiapasco, M. Zaniboni, and M. Boisco, "Augmentation procedures for the rehabilitation of deficient edentulous ridges with oral implants," *Clinical Oral Implants Research*, vol. 17, no. S2, pp. 136–159, 2006.
- [5] N. Altiparmak, S. S. Akdeniz, B. Bayram, S. Gulsever, and S. Uckan, "Alveolar ridge splitting versus autogenous onlay bone grafting: complications and implant survival rates," *Implant Dentistry*, vol. 26, no. 2, pp. 284–287, 2017.
- [6] S. Koo, S. Dibart, and H. Weber, "Ridge-splitting technique with simultaneous implant placement," *The Compendium of Continuing Education in Dentistry*, vol. 29, no. 2, pp. 106–110, 2008.
- [7] K. Funaki, T. Takahashi, and K. Yamauchi, "Horizontal alveolar ridge augmentation using distraction osteogenesis: comparison with a bone-splitting method in a dog model," *Oral Surgery, Oral Medicine, Oral Pathology, Oral Radiology, and Endodontology*, vol. 107, no. 3, pp. 350–358, 2009.
- [8] A. Scipioni, G. B. Bruschi, and G. Calesini, "The edentulous ridge expansion technique: a five-year study," *The International Journal of Periodontics & Restorative Dentistry*, vol. 14, no. 5, pp. 451–459, 1994.
- [9] A. Scipioni, G. B. Bruschi, G. Calesini, E. Bruschi, and C. De Martino, "Bone regeneration in the edentulous ridge expansion technique: histologic and ultrastructural study of 20 clinical cases," *The International Journal of Periodontics & Restorative Dentistry*, vol. 19, no. 3, pp. 269–277, 1999.
- [10] A. Sethi and T. Kaus, "Maxillary ridge expansion with simultaneous implant placement: 5-year results of an ongoing clinical study," *The International Journal of Oral & Maxillofacial Implants*, vol. 15, no. 4, pp. 491–499, 2000.
- [11] N. Ferrigno and M. Laureti, "Surgical advantages with ITI TE® implants placement in conjunction with split crest technique. 18-month results of an ongoing prospective study," *Clinical Oral Implants Research*, vol. 16, no. 2, pp. 147–155, 2005.
- [12] C. Blus and S. Szmukler-Moncler, "Split-crest and immediate implant placement with ultra-sonic bone surgery: a 3-year life-table analysis with 230 treated sites," *Clinical Oral Implants Research*, vol. 17, no. 6, pp. 700–707, 2006.
- [13] N. Elian, Z. Jalbout, B. Ehrlich et al., "A two-stage full-arch ridge expansion technique: review of the literature and clinical guidelines," *Implant Dentistry*, vol. 17, no. 1, pp. 16–23, 2008.
- [14] J. Y. Han, S. I. Shin, Y. Herr, Y. H. Kwon, and J. H. Chung, "The effects of bone grafting material and a collagen membrane in the ridge splitting technique: an experimental study in dogs," *Clinical Oral Implants Research*, vol. 22, no. 12, pp. 1391–1398, 2011.
- [15] G. U. Jung, J. H. Kim, N. H. Lim, G. H. Yoon, and J. Y. Han, "Biomechanical comparison of a novel engine-driven ridge spreader and conventional ridge splitting techniques," *Clinical Oral Implants Research*, vol. 28, no. 6, pp. 689–696, 2017.
- [16] A. Stricker, D. Widmer, B. Gueorguiev, D. Wahl, P. Varga, and F. Duttenehofer, "Finite element analysis and biomechanical testing to analyze fracture displacement of alveolar ridge splitting," *BioMed Research International*, vol. 2018, Article ID 3579654, 7 pages, 2018.
- [17] L. Mosekilde, J. Kragstrup, and A. Richards, "Compressive strength, ash weight, and volume of vertebral trabecular bone in experimental fluorosis in pigs," *Calcified Tissue International*, vol. 40, no. 6, pp. 318–322, 1987.
- [18] J. Aerssens, S. Boonen, G. Lowet, and J. Dequeker, "Interspecies differences in bone composition, density, and quality: potential implications for in vivo bone research," *Endocrinology*, vol. 139, no. 2, pp. 663–670, 1998.
- [19] M. Contessi, "The monocortical window (MCW): a modified split-crest technique adopting ligature osteosynthesis," *The International Journal of Periodontics & Restorative Dentistry*, vol. 33, no. 6, pp. e127–e139, 2013.
- [20] J. I. Cawood and R. A. Howell, "A classification of the edentulous jaws," *International Journal of Oral and Maxillofacial Surgery*, vol. 17, no. 4, pp. 232–236, 1988.

Review Article

Environmental Disinfection of a Dental Clinic during the Covid-19 Pandemic: A Narrative Insight

Antonio Scarano ¹, Francesco Inchingolo,² and Felice Lorusso¹

¹Department of Medical, Oral and Biotechnological Sciences, University of Chieti-Pescara, Via dei Vestini 31, 66100 Chieti, Italy

²Department of Interdisciplinary Medicine, University of Bari "Aldo Moro", 70121 Bari, Italy

Correspondence should be addressed to Antonio Scarano; ascarano@unich.it

Received 5 September 2020; Revised 27 September 2020; Accepted 16 October 2020; Published 29 October 2020

Academic Editor: Paolo Pesce

Copyright © 2020 Antonio Scarano et al. This is an open access article distributed under the Creative Commons Attribution License, which permits unrestricted use, distribution, and reproduction in any medium, provided the original work is properly cited.

Background. The control of biological hazard risk in health care and dental clinic environments represents a critical point in relation to the Covid-19 infection outbreak and international public health emergency. The purpose of the present review was to evaluate the scientific literature on the no-touch disinfection procedures in dental clinics aiming to limit transmission via airborne particles or fomites using no-touch procedures for environmental decontamination of dental clinics. **Methods.** An electronic database literature search was performed to retrieve research papers about Covid-19 and no-touch disinfection topics including full-length articles, editorials, commentaries, and outbreak studies. A total of 86 papers were retrieved by the electronic research. **Results.** No clinical article about the decontamination of a dental clinic during the Covid-19 pandemic was detected. About the topic of hospital decontamination, we found different no-touch disinfection procedures used in hospital against highly resistant organisms, but no data were found in the search for such procedures with respect to SARS-CoV-2: (1) aerosolized hydrogen peroxide, (2) H₂O₂ vapor, (3) ultraviolet C light, (4) pulsed xenon, and (5) gaseous ozone. One paper was retrieved concerning SARS-CoV-2; 32 documents focused on SARS and MERS. The cleaning and disinfection protocol of health care and dental clinic environment surfaces are essential elements of infection prevention programs, especially during the SARS-CoV-2 pandemic. **Conclusion.** The decontamination technique that best suits the needs of the dental clinic is peroxide and hypochlorous which can be sprayed via a device at high turbine speed with the ability of producing small aerosol particles, recommendable also for their low cost.

1. Background

A new coronavirus emerged in the central Chinese city of Wuhan in late 2019 [1] and spread rapidly around the world [2] causing the World Health Organization to declare pandemic infection on 11 March 2020 [2]. It is a coronavirus (SARS-CoV-2) that causes pneumonia, moderate to serious respiratory failure, septic shock, and higher risk of death in patients with other pathologies, especially in older people with underlying medical problems like chronic respiratory diseases, cancer, cardiovascular disease, and diabetes [1, 3]. The Covid-19 disease presents nonspecific symptoms such as conjunctivitis, diarrhea, vomiting, shortness of breath, sore throat, fatigue, and muscular pain, and then, there are also asymptomatic patients [4].

This coronavirus pneumonia has a high percentage mortality rate due to risk factors and mortality predictors such as age ≥ 65 years, concomitant cardiovascular pathologies, CD3 + CD8+ T cell count ≤ 75 cell· μL^{-1} , and cardiac troponin I ≥ 0.05 ng·mL⁻¹, [5, 6]. In Italy, the number of confirmed cases was 274.644, including 35.518 deaths as of 4 Sept. 2020, while the great spread of the number of infected cases has caused a lockdown of dental clinical activity and poses a significant risk to personnel dental health care (DHCP) and dental patients. Transmission of SARS-CoV-2 occurs mostly by respiratory droplets over a close distance. It is an aerosol-transmissible disease which can spread when infected people talk, cough, sneeze, or disperse mouth and nasal fomite secretions into the air. Droplets exhaled during speech, sneezes, coughs, and exhalations emit mucosalivary

droplets with semiballistic trajectories and a multiphase turbulent gas cloud that entrains ambient air and carries within its clusters of droplets with different droplet sizes. In fact, the exhaled air of infected humans is one of the prime sources of ambient contamination by pathogenic microorganisms. Larger droplets may rapidly settle on the ground or transmit disease to individuals in near proximity, while smaller droplets may remain suspended for a long time and can contribute to disease transmission over great distances [7] and for a long time [8]. Today, there is a worldwide pandemic SARS-CoV-2 agent of serious viral pneumonia in course which is being mitigated by lockdown (quarantine and isolation). The transmission routes of the novel coronavirus include direct transmission (aerosol-transmissible) via droplets that “settle” on another individual, while airborne transmission occurs via small droplets in suspension in the air. In particular, airborne transmission can occur without direct contact and at a long distance via air flows (e.g., if an infected person coughs in a room, leaves, and another person enters) as in the restaurant example presented by Lu et al. [9], while the fomite transmission refers to transmission via droplets (usually larger) that settle on surfaces and are then inoculated by contact of the hands with the contaminated surface which then touch nasal, oral, or eye mucous membranes.

Improving ventilation of health spaces will dilute and clear out potentially infectious aerosols [10, 11].

Viruses or bacteria take flight and remain in the air so that other people can breathe the airborne pathogenic organisms, or these can land on other surfaces. The locally humid and hot atmosphere within the turbulent gas cloud allows the contained droplets to elude evaporation for longer than occurs with isolated droplets [8].

So, for this reason, it is important to implement respiratory infection control with a good prevention strategy in dental practices and health care offices.

In fact, humans have a high-frequency face-touching habit with an average of 23 times in 1 hour, and hands are a common vector for the transmission of health care-associated infections [12]. When air containing pathogenic airborne microorganisms is inhaled by a human, it can cause tuberculosis or Legionella [13], mycoplasma, or influenza, which are great problems in dentistry practice [14]. In dental practices, droplets from infected patients can contaminate the equipment and surfaces with the risk of transferring microorganisms from contaminated surfaces to other patients through hand contact [14–16]. The high-touch equipment surfaces surrounding the patient increase the risk of contamination of these surfaces.

Furthermore, aerosolized virus, fungi, or bacteria in health care facilities can cause infection in the dentistry equipe and all health care workers [17].

So, it is very important that we adopt a proactive infection control approach to sanitation in the dental clinic between one patient and another to minimize the risk of transmission. We can use the disinfection agents through contact, but this procedure is too long and ineffective, because it is impossible to reach all hidden surfaces. The aims of this article are to discuss and suggest some of the novel no-touch disinfection methods in SARS-CoV-2 infection control

and prevention of viral transmission in the dental clinic setting, where droplets can be spread by dental tools that aerosolize particles from the mouth, and where surface disinfection is a priority.

In the present review, the scientific literature on the no-touch disinfection procedures in dental clinics aiming to limit transmission via airborne particles or fomites or using no-touch procedures for environmental decontamination of dental clinics was evaluated.

2. Methods

A 2-stage procedure was followed. The manuscript included for the evaluation was retrieved from PubMed and MEDLINE, and the data were collected on a specially designed Excel database (Microsoft, Redmond, WA, USA). The database search was performed by two expert reviewers (L.F. and A.S.). Moreover, a second step of the manual search was provided to identify manuscripts eligible for descriptive evaluation. The full text and abstract of the papers included were collected and analyzed. Information available from the literature on the no-touch disinfection of dental clinics in the SARS-CoV-2 pandemic era was acquired. A literature search was also performed to retrieve study articles regarding Covid-19 (SARS-CoV-2) and no-touch disinfection in dental clinics. In the present investigation clinical studies, retrospective and prospective trials and reviews in English full-length articles were included. The exclusion criteria were proceedings, short communications, and letters to the editors.

Data was then selected by focusing on the documentation of the measures of no-touch disinfection, and the actual situation of managing SARS-CoV-2 diffusion in the dental clinic. Also taken into consideration were the articles on the measures implemented in hospitals. The literature search was from database inception up to April 30, 2020. Editorials, commentaries, and outbreak studies were included. Studies in which no-touch disinfection methods were used to evaluate the efficacy of reducing contamination of surfaces were also included.

The Boolean search was performed according to the key words used: “disinfectants AND (Covid-19 OR SARS-CoV-2 infection)”, “no-touch disinfection”, “non-manual disinfection techniques”, “dentistry equipment surface”, “no-touch disinfection AND Covid-19”, “dentistry equipment surface contamination”, “vapor disinfectant AND dental clinic”, and “hospital surfaces contamination and dental clinic contamination”.

3. Results

A total of 86 papers were retrieved by the electronic research. No data on the clinical experience in the decontamination of dental clinics during the pandemic of Covid-19 were detected.

We found in literature different no-touch disinfection procedures used in hospitals against highly resistant organisms, but no data was found in the search for such procedures with respect to SARS-CoV-2 (Tables 1–9). Different no-touching disinfection systems have been

TABLE 1: Aerosolized hydrogen peroxide system (aHP) literature.

Author	Year	Aerosolized hydrogen peroxide systems (aHP) Design	Results
Chan et al. [24]	2011	Efficacy of hydrogen peroxide vapor decontamination on different surfaces of an Australian hospital, seeded with vancomycin-resistant <i>Enterococci</i> (VRE)	The 33.3% of the high-touch areas assessed had aerobic bacterial count below the detection limit post H ₂ O ₂ decontamination, with the highest microbial density of ≤3 c.f.u./cm
Fu et al. [26]	2012	Efficacy and safety of hydrogen peroxide vapor (HPV) and aerosolized hydrogen peroxide against 10(6) methicillin-resistant <i>Staphylococcus aureus</i> (MRSA), <i>Clostridium difficile</i> , and <i>Acinetobacter baumannii</i>	The HPV system was safer, faster, and more effective for biological inactivation
Orlando et al. [27]	2008	Different concentrations (1, 2, and 4 mL/m ³) of the hydrogen peroxide disinfectant were nebulized inside a 50 m ³ experimental environment	The reduction of mean bacterial loading at concentrations of 1, 2, and 4 mL/m ³ was 54.9%, 70.9%, and 86.9%
Holmdahl et al. [28]	2011	In vitro comparison of a hydrogen peroxide vapor (HPV) and aerosolized hydrogen peroxide (aHP)	ll BIs were inactivated for the 3 HPV tests, compared with only 10% in the first aHP test and 79% in the other 2 aHP tests

TABLE 2: H₂O₂ vapor heat-generated vapor system (aHP) literature.

Author	Year	H ₂ O ₂ vapor heat-generated vapor Design	Results
Sk et al. [29]	2011	Effect on high strength AISI 4340 steel after exposure to vaporized hydrogen peroxide	No effects were produced for samples exposed to vapor hydrogen peroxide for concentrations up to 1000 ppm H ₂ O ₂ and exposure times of 4.8h
Hall et al. [30]	2007	Effect of hydrogen peroxide vapor (HPV) disinfection on <i>M. tuberculosis</i> and <i>Geobacillus stearothermophilus</i>	Both groups were deactivated in all 10 locations following 90 min of HPV exposure
Otter et al. [31]	2013	No-touch automated room disinfection (NTD) system evaluation	NTD systems are a useful tool for infection prevention and control
Berrie et al. [32]	2011	Dried recombinant <i>adenovirus</i> (Ad5GFP) was tested before and after HPV exposure to determine the efficacy of hydrogen peroxide vapor HPV at inactivating adenovirus	HPV is effective for the inactivation of recombinant <i>adenovirus</i> and decontamination
Goyal et al. [33]	2010	Efficacy of hydrogen peroxide vapor (HPV) for the inactivation of <i>Feline calicivirus</i> (FCV)	The hydrogen peroxide resulted in a >3 log ₁₀ reduction in FCV infectivity and all but the 15 mL
Jeanes et al. [34]	2005	Hydrogen peroxide vapor (HPV) decontamination to eradicate MRSA environmental contamination in a surgical ward	Decontamination using HPV provides a rapid and cost-effective method for the eradication of environmental MRSA
Gopinath et al. [35]	2013	<i>NDM-1 Salmonella Senftenberg</i> (NDM-SS) drug resistance isolated in a patient. The environment was disinfected by hydrogen peroxide technology	Decontamination using hydrogen peroxide technology provides an effective method for <i>NDM-1 Salmonella Senftenberg</i> (NDM-SS)

TABLE 3: Dilute hydrogen peroxide (DHP) literature.

Author	Year	Dilute hydrogen peroxide (DHP) Design	Results
Oon et al. [36]	2011	Dilute hydrogen peroxide (DHP) in a critical care unit and measure the microbiological impact on surface contamination	Significant reduction in aerobic colony counts did not occur when the DHP was operating compared with baseline and control phases
OSHA guidelines [37]	2017	Samples are collected by drawing workplace air through two 25 mm quartz filters, coated with titanium oxysulfate, using personal sampling pumps	H ₂ O ₂ evaporated off the cassette wall and reacted with the titanium oxysulfate-coated quartz filter
ILO guidelines [38]	2017	Harmful contamination of the air can be reached rather quickly on evaporation of this substance at 20°C	Decomposes under the influence of light on warming producing oxygen. Increase of fire hazard and is a strong oxidant. Attacks many organic substances such as textiles and paper

TABLE 4: Surface disinfection via aerosol (SDVA) literature.

Surface disinfection via aerosol (SDVA)			
Author	Year	Design	Results
Boyce et al. [92]	2016	No-touch technologies include aerosol and vaporized hydrogen peroxide, mobile devices that emit continuous ultraviolet (UV-C) light, a pulsed-xenon UV light system, and use of high-intensity narrow-spectrum (405 nm) light	Environmental departments should consider the use of newer disinfectants and no-touch decontamination technologies to improve disinfection of surfaces in health care

TABLE 5: HOCl generated fog (VHOCl) literature.

		HOCl generated fog (VHOCl)	
Author	Year	Design	Results
Kim et al. [39]	2008	Human primary nasal epithelial cells treated with 3.5 ppm of hypochlorous acid for cell cytotoxicity	No cytotoxicity at 30 minutes or 2 hours after treatment with HOCl was recorded. More than 99% of bactericidal or fungicidal activity was noted for all species, except for <i>Candida albicans</i>
Park et al. [40]	2007	Efficacy of hypochlorous acid (HOCl) solution (HAS) to reduce NV in aqueous suspensions and inanimate carrier	Exposing virus-contaminated carriers of ceramic tile (porous) and stainless steel (nonporous) to 20 to 200 ppm of HOCl solution resulted in > or =99.9% (> or =3 log ₁₀) reductions of both infectivity and RNA titers of tested viruses within 10 min of exposure time
Russel et al. [41]	1999	Systematic review of sterilization methods, with uses and advantages outlined for each and valuation of disinfectants and their mechanisms of action with respect to current regulations	HOCl generated fog methods effective for the elimination or prevention/control of microbial growth
Yu et al. [42]	2011	Cells were infected with <i>human rhinovirus</i> for 24 hours and treated with HOCl three times, for 5 minutes each time, at 12-hour intervals	HOCl treatment significantly inhibited HRV-induced secretion of IL-6 and IL-8 and significantly reduced viral titer
Lister [43]	1952	The rate of decomposition of hypochlorous acid has been measured in an aqueous solution in the presence of much sodium hypochlorite	Values for the rate constants at different temperatures of all these reactions are given. Measurements are also reported on certain equilibria present in these solutions: the ionization of hypochlorous and chlorous acids, and the reaction
Hakim et al. [44]	2014	HOCl solutions containing 50, 100, and 200 ppm chlorine or their sprayed solutions were mixed with the virus with or without organic materials against a low pathogenic <i>avian influenza virus</i> (AIV), H7N1	In the indirect spray form, after 10 sec of spraying, the lids of the dishes were opened to expose the virus on rayon sheets to HOCl. In this form, the 200 ppm solution inactivated AIV within 10 min of contact, while 50 and 100 ppm could not inactivate the virus

proposed such as aerosolized hydrogen peroxide [18], hydrogen peroxide-producing systems [19], H₂O₂ vapor [20], hydrogen ultraviolet C light [21], pulsed xenon [22], and gaseous ozone [23].

We found more papers on the efficiency of disinfectant agents on other viruses such as severe acute respiratory syndrome (SARS), Middle East Respiratory Syndrome (MERS), mouse hepatitis virus (MHV), canine coronavirus (CCV), and human coronavirus (HCoV).

Aerosolized hydrogen peroxide systems (aHP) generate a dry-mist hydrogen peroxide aerosol of hydrogen peroxide and use a solution containing 5%–7% hydrogen peroxide with or without <50 ppm silver (Nocospay) (Figures 1 and 2) [24, 25]. The generator injects into a room a solution of HP

followed by passive aeration and water and is very active against microorganisms.

This device produces a variable particle size of 2–12 μm [26] or of 0.5 μm [27]. Generally, a dosage of 6 mL per m³ is recommended which, after erogation, should be left to decompose naturally. This technique uses a low concentration of hydrogen peroxide which, for this reason, metabolically inert spore and catalase-negative bacteria are less susceptible. It is able to reduce contamination of MRSA and *C. difficile* on work surfaces but has not been shown to eradicate pathogens in clinical practice. It is difficult to achieve the saturation of the environment because aHP is introduced via a unidirectional nozzle by gravity [28].

TABLE 6: UVC light (207–222 nm) literature.

Author	Year	UVC light (207–222 nm) Design	Results
Boyce et al. [45]	2011	<i>Clostridium difficile</i> aerobic colony counts were calculated for each of 5 standardized high-touch surfaces in the rooms before and after UV light decontamination (UVDL)	The mobile UV-C light unit significantly reduced aerobic colony counts and <i>C. difficile</i> spores on contaminated surfaces in patient rooms
Nerandzic et al. [46]	2010	Cultures for <i>C. difficile</i> , methicillin-resistant <i>Staphylococcus aureus</i> (MRSA), and vancomycin-resistant <i>Enterococcus</i> (VRE) were collected from commonly touched surfaces before and after the use of an automated ultraviolet radiation device	Efficient environmental disinfection technology that significantly reduces <i>C. difficile</i> , VRE, and MRSA contamination on commonly touched hospital surfaces
Conner-Kerr et al. [47]	1998	UV light (254 nm, 15.54 mW/cm ² output). Irradiation times were 0, 2, 5, 8, 15, 30, 45, 60, 90, or 120 seconds in killing antibiotic-resistant strains of <i>Staphylococcus aureus</i> and <i>Enterococcus faecalis</i> in vitro	Kill rates were 99.9 percent for the methicillin-resistant strain of <i>S. aureus</i> (MRSA) at 5, 8, 15, 30, 45, and 60 seconds and 100 percent at 90 and 120 seconds. Kill rates were 99.9 percent at 5, 8, 15, and 30 seconds for vancomycin-resistant <i>E. faecalis</i> (VRE) and 100 percent at 45, 60, 90, and 120 seconds
Setlow et al. [48]	1993	Irradiated groups of five 6-day-old fish with narrow wavelength bands at 302, 313, 365, 405, and 436 nm and scored the irradiated animals for melanomas 4 months later	The light energy absorbed in melanin is effective in inducing melanomas in this animal model and that, in natural sunlight, 90–95% of melanoma induction may be attributed to wavelengths >320 nm—the UV-A2 and visible spectral regions
Welch et al. [49]	2018	Far-UVC light (207–222 nm) efficiently inactivates bacteria without harm to exposed mammalian skin	Far-UVC efficiently inactivates aerosolized viruses, with a very low dose of 2 mJ/cm ² of 222 nm light inactivating >95% of aerosolized H1N1 influenza virus

H₂O₂ vapor heat-generated vapor. There are two types of HPV: condensing HPV technology and noncondensing vaporized hydrogen peroxide (VHP) technology. This technology uses a vaporizer heated to 120°C and circulates the HPV through the environmental chamber via a supply and return hose. Condensing systems inject hydrogen peroxide until the air in the room becomes saturated and HP begins to condense on the surfaces. The condensing of HP on surfaces can cause corrosion [29]. The HPV device injects at 2 mL/min for 1, 2, or 5 min followed by 1.5 mL/min for 15 min equating to three different volumes: 25, 27, and 33 mL.

The level of 1 ppm is the max level of exposure according to the Occupational Safety and Health Administration and International Labour Organisation. This procedure requires a first phase injection and second phase aeration for a total time of approximately 2–3 h, varying with the amount of hydrogen peroxide being vaporized.

Noncondensing systems produce dry gas by a vaporized hydrogen peroxide system that utilizes evaporation of 30%–35% aqueous hydrogen/peroxide (VHP) at high-velocity air. VHP systems have a generator which delivers until the air in the enclosure becomes saturated and hydrogen peroxide begins to condense on surfaces, and it is designed to achieve a humidity level set prior to the start of the cycle [30]. This system is noncondensing VHP because the vapor stream is dried as it is returned to the generator [31]. It is virucidal, bactericidal, sporicidal, and active against myco-

bacteria including *C. difficile* spores, MRSA, and a wide range of nosocomial pathogens [32, 33]. Its long cycle times have made it difficult to use this system in health care facilities. It is efficient against fungi, viruses, MRSA, VRE, *C. difficile*, Klebsiella, Serratia, Mycobacterium tuberculosis, and Acinetobacter [34, 35].

Dilute hydrogen peroxide (DHP). This technique uses water vapor and oxygen in the ambient air to continuously produce ozone-free hydrogen peroxide [36]. The environmental hydrogen peroxide produced is 0.02 ppm that is well below human safety thresholds. In fact, a level of 1 ppm is the max safety level of exposure according to the Occupational Safety and Health Administration and International Labour Organisation [37, 38]. DHP is active against a variety of viruses, bacteria, and fungi. It can be used during routine clinical practice in conjunction with established cleaning and decontamination methods. So, there are no restrictions on the use of a room for a period of time in practices.

Surface disinfection via aerosol (SDVA). The device produces dry fog through a turbine at high speed that atomized and sprays disinfectant. Usually, H₂O₂ and hypochlorous acid (HOCl) are used as a disinfectant (Figures 1 and 2). The disinfectant is atomized into ultrafine droplets, blown into the air, and, after 10–30 min, settles on all surfaces; these disinfectant droplets quickly begin to take effect. The generator produces on average size 5 μ particles of disinfectant and ensures a slow and completely uniform sedimentation on each square of the treated premises with no humidity. The

TABLE 7: PX-UV disinfection system literature.

Author	Year	PX-UV systems Design	Results
Stibich et al. [51]	2011	The use of pulsed-xenon ultraviolet (PX-UV) room disinfection by sampling frequently touched surfaces in <i>vancomycin-resistant enterococci</i> (VRE) isolation rooms	The PX-UV system showed a statistically significant reduction in microbial load and eliminated VRE on sampled surfaces when using a 12-minute multiposition treatment cycle
Jinadatha et al. [52]	2014	Standard manual room cleaning to PPX-UV disinfection technology for MRSA and bacterial heterotrophic plate counts (HPC) on high-touch surfaces in patient rooms	PPX-UV technology appears to be superior to manual cleaning alone for MRSA and HPC. Incorporating 15 minutes of PPX-UV exposure time to current hospital room cleaning practice can improve the overall cleanliness of patient rooms with respect to selected microorganisms
Ghantaji et al. [53]	2015	High-touch surfaces in rooms previously occupied by <i>C. difficile</i> -infected patients were sampled after discharge but before and after cleaning using either bleach or nonbleach cleaning followed by 15 min of PX-UV treatment	After disinfection, the mean level of contamination for bleach was 0.71 c.f.u. ($P = 0.1380$), and 1.19 c.f.u. ($P = 0.0017$) for PX-UV disinfected rooms
de Groot et al. [90]	2019	UV-C exposure times and distance in killing <i>C. auris</i> , using strains from different countries	A maximal effect of <i>C. auris</i> killing was found after 30 minutes of UV-C exposure at 2 m. With half the time or twice the distance, the efficacy strongly diminished to ~10 and ~50 fold
Li et al. [91]	2020	Portable pulsed-xenon ultraviolet (PX-UV) machine on samples was taken from the surface of research tables	PX-UV disinfection also significantly reduced residual bacterial counts
Yousif and Haddad [54]	2013	UV radiation causes photooxidative degradation which results in breaking of the polymer chains, produces free radical, and reduces the molecular weight, causing deterioration of mechanical properties and leading to useless materials, after an unpredictable time	Free hydrogen radicals diffuse very easily through the polymer matrix and combine in pairs or abstract hydrogen atoms from polymer molecule

dry fog is displaced at 15 m thanks to the venturi effect. This nonwetting and noncorrosive fog can be used for all surfaces including electronic ones and is environmentally friendly. There are two stages for completing disinfection, spraying, and contact time. When the disinfection cycles are completed, it is required to open the windows for almost 10 min. So, the total time required for completing the cycle is 10-30 min. The H_2O_2 is nontoxic because it degrades in H_2O and O_2 . Hypochlorous acid (HOCl) is a weak acid and has a virucidal power 300 times that of chlorine and is widely used for the decontamination of swimming pools. It is safe and used for nasal irrigation in patients affected by chronic sinusitis. A study showed a low (0.85%) concentration HOCl solution can be used as an effective nasal irrigation solution [39]. Hypochlorous acid (HOCl) has demonstrated broad-spectrum antimicrobial activity while being suitable for general use [40]. 20 to 200 ppm of HOCl solution resulted in $\geq 99.9\%$ reduction of noravirus contagion on inanimate surfaces and aqueous suspensions [40], with low potential to damage treated surface materials [41]. The generator produces droplets of size ranging between 20 and 50 μm . The HOCl fogs to concentrations ranging from 20 to 200 ppm and has virucidal effect against human norovirus [42]. Fogging is a mechanical action that produces small particles that can accelerate the interfacial mass transmission of chlorine gas. Low concentrations of hypochlorous acid (HOCl) have been demonstrated to exhibit both anti-influenza virus and

antibacterial activity, but HOCl is also used to kill human rhinovirus (HRV) [42]. HOCl is considered by the FDA the agent that has the highest bactericidal activity against a broad range of microorganisms (US FDA, 2015) [43]. Avian influenza (H5N1) virus inactivation through fog applications of HOCl was achieved in 10 seconds [44]. HOCl has a temporary and gentle chlorine smell that dissipates rapidly.

UVC light (207–222 nm) is not visible to the human eye. Ultraviolet C radiation (UVC) emits light (207–222 nm) with efficient bacteria inactivating deliver-specific doses at different powers, for vegetative bacteria 12,000 $\mu Ws/cm^2$ and high power at 22,000–36,000 $\mu Ws/cm^2$ for spores [45, 46].

The UV light also inactivates drug-sensitive and multi-drug-resistant bacteria and viruses [47].

This technology is very limited because conventional UVC light sources are a human safety hazard, with a carcinogenic effect [48]. For this reason, the power of UVC light has been lowered to 2 mJ/cm² and a recent study showed an efficiency when the lamps were positioned in public locations, reducing incidences of transmission of tuberculosis and influenza epidemics [49]. They are very efficient for the disinfection of health care environmental surfaces after manual cleaning has been performed. So, UVC irradiation treatments are effective for inactivating SARS-CoV. A continuous 30 min ultraviolet radiation is required to disinfect target surfaces and air [50].

TABLE 8: Gaseous ozone disinfection literature.

Author	Year	Design	Gaseous ozone	Results
Moat et al. [102]	2009	The efficacy of the approach using gaseous ozone for room sanitization was assessed		Application of the process in a 30 m ³ room showed similar reductions in viable counts for <i>Clostridium difficile</i> spores, <i>Escherichia coli</i> , and methicillin-resistant <i>Staphylococcus aureus</i>
Hudson et al. [55]	2009	Develop a practical method of utilizing the known antiviral properties of ozone in a mobile apparatus that could be used to decontaminate rooms in health care facilities		All 12 viruses tested, on different hard and porous surfaces, and in the presence of biological fluids, could be inactivated by at least 3 log ₁₀ , in the laboratory and in simulated field trials
Rowen [56]	2019	Ozone therapy, the most studied and least expensive to perform, is in itself a germicide, not an antibiotic, and improves several physiological parameters essential for infection defense		Very favorable responses to both bacterial and viral disease, inclusive of <i>Ebola</i> . Despite the lack of commercial profitability (not patentable), medicine would do well to revisit its preantibiotic era oxidation therapy roots, especially ozone in the current crisis
Hudson et al. [57]	2007	Ability of ozone gas to inactivate <i>norovirus</i> and its animal surrogate <i>Feline calicivirus (FCV)</i> in dried samples placed at various locations within a hotel room, a cruise liner cabin, and an office		QRT-PCR assays indicated similar decreases in both viral RNAs. Virus-containing samples dried onto hard surfaces (plastic, steel, and glass) and soft surfaces such as fabric, cotton, and carpet were equally vulnerable to the treatment
Miller et al. [58]	2018	Acute inhalation of ozone induces DNA methylation of apelin in the lungs and if a change in expression is related to altered DNA methylation in the lung		Ozone exposure reduced DNA cytosine-5-methyltransferase (DNMT) activity and Dnmt3a/b gene expression. Epigenetic modifications accompanied ozone-induced reduction of apelin expression and development of pulmonary edema
Ding et al. [103]	2019	Ozone disinfection of chlorine-resistant bacteria in drinking water		The ozone resistance of bacteria <i>Aeromonas jandaei</i> < <i>Vogesella perlucida</i> < <i>Pelomonas</i> < <i>Bacillus cereus</i> < <i>Aeromonas sobria</i> was lower than that of spores <i>Bacillus alvei</i> < <i>Lysinibacillus fusiformis</i> < <i>Bacillus cereus</i> at an ozone concentration of 1.5 mg/L. More than 99.9% of <i>Bacillus cereus</i> spores were inactivated by increasing ozone concentration and treatment duration

There is a problem that natural and synthetic polymers are attacked by ultraviolet radiation, materials that make up many parts of a dentist chair, and other medical devices that include polypropylene.

Pulsed-xenon (PX-UV) systems emit high-intensity broad-spectrum UV irradiation in the 200–320 nm range [51] and are a means of quickly producing germicidal UV [51].

Usually, this is a portable device used in empty patient rooms because prolonged exposure to UV-C can cause eye and skin irritation. Fifteen minutes of PPX-UV exposure time can eliminate the pathogenic microorganisms [52] against 45 min required to clean a room with bleach [53].

Gaseous ozone is used for environmental disinfection [54]. It has antimicrobial and antiviral properties inclusive of *Ebola* although its mechanisms of action are not well understood [55, 56]. The device generates ozone and increases the ozone gas peaking at 20–25 ppm and includes ozone's known corrosive properties [20]. This technology is more efficient when there is low relative humidity [23]. It only takes 3–4 ppm to reduce all viruses and bacteria [57], but at 25 ppm, it is a disinfectant, while at 50+ ppm, it sterilizes surfaces. Ozone can damage the lungs when inhaled, a recent study showed in a rat model that increased methylation of the apelin

promoter downstream of DNA damages the lungs, causing the development of pulmonary edema [58].

The generators are unable to elevate ozone levels near the required ppm range even in a small or average-sized room (<1–5 ppm). One to two hours of treatment are needed and 10–15 min of reentry after ventilation or open windows.

4. Discussion

During dentistry activity and the use of high-speed drills, droplets that are contaminated with the virus [59] can spread as far as two meters on to exposed surfaces [60] with environmental contamination and these remain infectious on workstation surfaces, medical instruments, etc. at room temperature for up to 9 days [61].

In fact, dental instruments such as rotating devices or ultrasonic devices use high-speed gas to drive the turbine to rotate at high speed and work with running water, and some dental procedures can cause coughing and, in any case, the patient breathes. The airborne droplets are of different dimensions and contain virus or bacteria pathogens which may survive on inanimate surfaces up to several months, and they may serve as a reservoir for cross-contamination

TABLE 9: Summary for each of the decontamination procedures for instance with the columns procedure, supply required, and threat to human health.

Procedure	Supply time	Decontamination procedure		Threat to human health
		Deposition time	Room ventilation	
Aerosolized hydrogen peroxide	6 min/100 m ²	1-2 h	15-30 min	Inhalation acute toxicity 1.93 mg/M ³ Inhalation long-term toxicity 0.21 mg/M ³
H ₂ O ₂ vapor heat-generated vapor	15-50 min cycle	~130 min	15-20 min	Eye irritation, odor threshold
Surface disinfection via aerosol	15 minutes at 20°C	~2 h	~10 min	Eye irritation and mucosal tissue irritation
HOCl generated fog	10 min	30 min to 2 h	20-30 min	At prolonged exposure mild inflammatory reactions to mucosal tissues. At free chlorine low concentration pH 7.0 no toxicity >3% hydrogen peroxide: mucosal tissue irritation,
Dilute hydrogen peroxide	Continuous	~2 h	Not required	vomiting and diarrhea. Chronic inhalation: upper respiratory tract inflammation
UVC light (207–222 nm)	60-120 sec/30 m ²	~	Not required	At direct exposure temporary damage and burns to the eyes, cornea, and potential carcinogen to the skin
PX-UV systems	12-30 min/30 m ²	~	Not required	Skin and mucosal damage at prolonged exposure
Gaseous ozone	10-30 min/30 m ³	~	10 min	Lungs damage, chest pain, coughing, shortness of breath, and throat irritation

with self-inoculation, as contaminated hands are a route for disseminating respiratory infections [62, 63].

In addition to the infected patients, there are the asymptomatic ones who can be negative to current health status investigations and/or the presence of risk factors for Covid-19 [64, 65]. For this reason, all patients must be treated during dental procedure as being Covid-19 positive. Hence, this is a timely topic, and dental clinics would be interested in the state of the art with respect to sanitization procedures. Several studies have found that hygiene quality management in the dental office may be problematic and surface microbial contamination has been found [66, 67]. All environment surfaces can become contaminated with infectious droplets from sprays of oral fluids or from touching them with contaminated fingers. The surfaces most frequently touched are drawer knobs, light handles, unit switches, dental radiograph equipment, reusable containers of dental materials, drawer handles, and dental chairside computers, and when these devices are touched, microbial agents can be transferred to other instruments [15]. General cleaning and disinfection with chemical or physical agents are recommended for device contact surfaces. It is very important to know material compatibility with physical or liquid chemical germicides. When wiping or scrubbing is used to remove microorganisms, any antimicrobial effect provided by the agent is reduced as there can still be a risk of creating another reservoir for microorganisms in the diluted solutions of the disinfectants themselves [68].

Disinfection of instruments and workstation surfaces against microbial contamination and inefficacy of environmental decontamination could be risk factors for cross-infection. Disinfection of surfaces is a method for reducing

the risk of contact to viruses and interrupting their spread [69]. In dentistry, conventional manual disinfection of medical device surfaces is used, and this needs a two-stage disinfection procedure which includes surface rehydration followed by disinfection, for effective inactivation of bacteria and viruses on dry surfaces [70]. It is important to improve ventilation of health care spaces to dilute and clear out potentially infectious aerosols [10, 11]. Ventilation can reduce virus concentration in the air, limiting airborne transmission, but also the settling of viral particles, causing fomite transmission, for example, in influenza viruses [71]. The use of high ventilation rates during and after aerosol-generating procedures, such as high-speed drills, or piezosurgery [72–75] or between two patients has the potential to efficiently reduce circulating concentration of viral particles.

Environmental disinfection of the dental clinic is very important because the coronavirus can persist on inanimate surfaces like metal, glass, or plastic for up to 9 days, but fortunately, it is very sensitive to the action of disinfectants [61]. A recent correspondence in *The New England Journal of Medicine* showed that the stability of SARS-CoV-2 was like that of SARS-CoV-1 and was more stable on plastic and stainless steel than on copper and cardboard, and viable virus was detected up to 72 hours after application on these surfaces [76]. Different disinfectant agents were used against severe acute respiratory syndrome (SARS), Middle East Respiratory Syndrome (MERS), mouse hepatitis virus (MHV), canine coronavirus (CCV), and human coronavirus (HCoV) such as ethanol [77], 2-propanol [78], benzalkonium chloride [79], dodecyl dimethyl ammonium chloride [80, 81], chlorhexidine digluconate [80], sodium hypochlorite [82], hydrogen peroxide [83], formaldehyde [78],

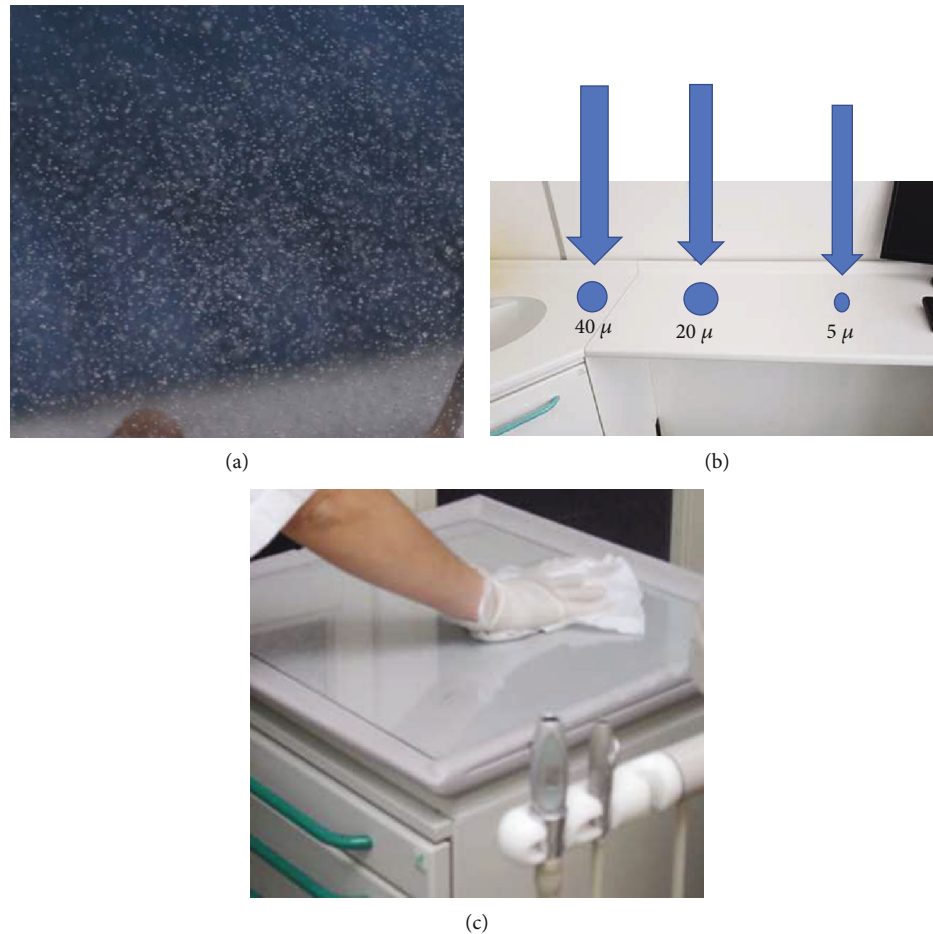


FIGURE 1: This is a schematic representation as there is no data referenced here in the present paper. (a) Aerosol generating during piezosurgery procedures. (b) Particles of different sizes. Smaller droplets ($5\ \mu$) may remain suspended for a long time and can settle on all environmental surfaces such as drawer knobs, light handles, unit switches, dental radiograph equipment, reusable containers of dental materials, drawer handles, and dental chairside computers and when these devices are touched, microbial agents can be transferred to other instruments. (c) Manual disinfection of medical device surfaces is very difficult.

glutaraldehyde [82], and povidone-iodine [84]. The WHO recommends environmental cleaning and disinfection procedures which must be followed correctly. Benzalkonium chloride and chlorhexidine digluconate are not very effective or basically ineffective.

The most effective disinfectants are ethanol at strong concentration while sodium hypochlorite and hydrogen peroxide require a minimal concentration to be effective with a low impact on human health. Also, ethanol at 62 and 71% is similarly efficacious against coronavirus but can be used for small surfaces [85]. Ethanol has been widely used for the decontamination of hands based on 80% ethanol or 75% 2-propanol, and these are sufficiently efficacious [86].

For cleaning the workstation surfaces, sodium hypochlorite is suitable at a concentration of 0.05% with efficient and sufficient procedures [85] and when used at a concentration of 0.1%, it is effective in 1 min. Also, hydrogen peroxide is effective with a low concentration of 0.5% and an action time of 1 min. It is used for cleaning and disinfection implant drills because it preserves the drill structure after 50 cycles of decontamination [87–89].

Thorough decontamination and disinfection of all workstation surfaces in the hospital are very often difficult to achieve on multiple surfaces and complex equipment with wiping or scrubbing and require a lot of time.

For this reason, systems have been proposed, which offer the potential to improve the efficacy and reliability in hospital disinfection of environment and surfaces such as aerosolized hydrogen peroxide [18], hydrogen peroxide-producing systems [19], H_2O_2 vapor [20], hydrogen ultraviolet C light [21], pulsed xenon [22], and gaseous ozone [23].

There are differences between these systems in terms of their effectiveness, technological aspects, and microbiological efficacy. No data were found in the Guidelines for Infection Control in Dental Health-Care Settings 2003 and 2016. UV-C activity against viruses and bacteria is strongly influenced by distance and exposure times and has the most critical parameters; for this reason, a mobile ultraviolet-C device has been introduced [90]. A recent study showed that 6 min PX-UV disinfection is required to disinfect target surfaces and air, so it is fast and effective disinfection [91]. PX-UV disinfection is an effective agent for decontaminating the

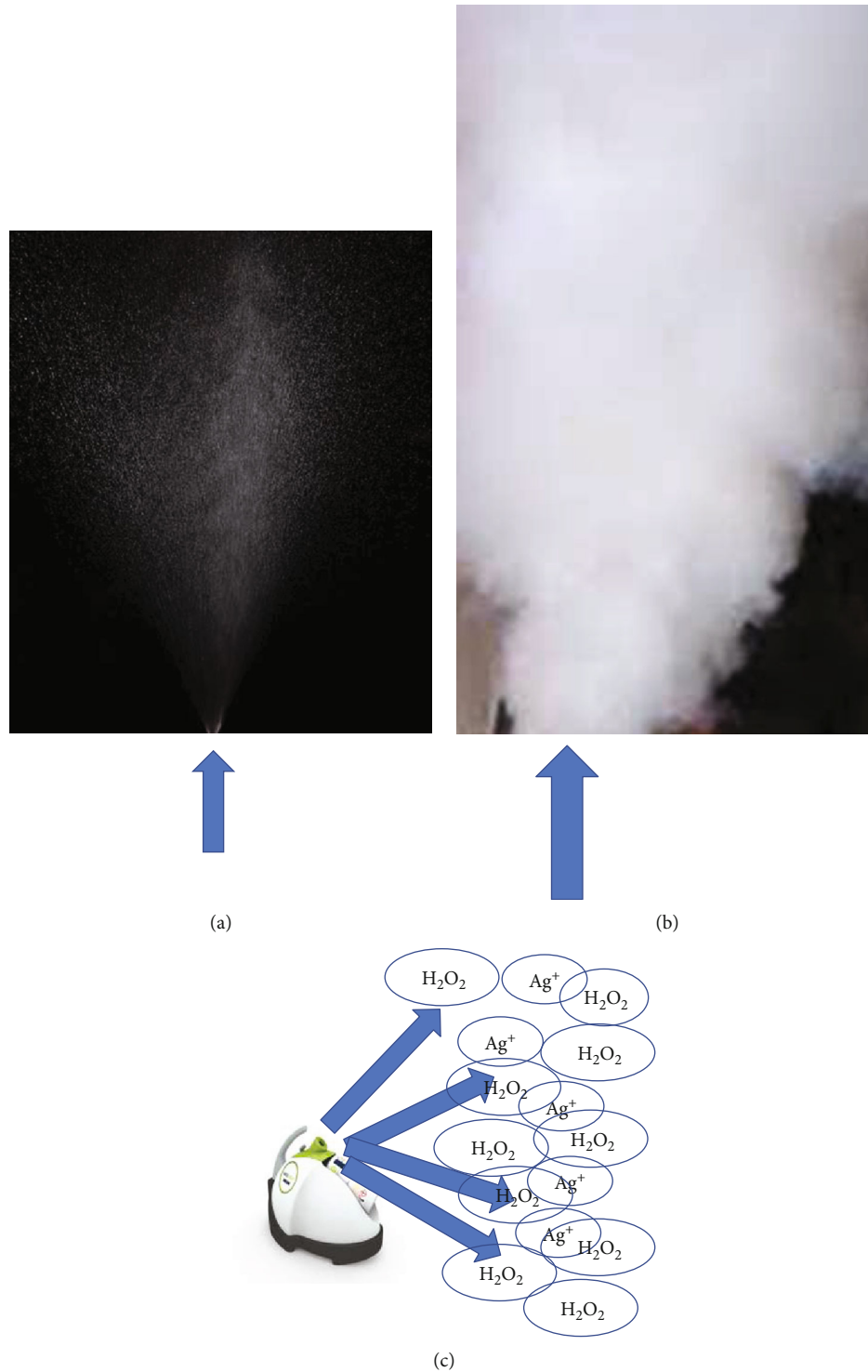


FIGURE 2: (a) Difference between nebulization. (b) Generator of dilute hydrogen peroxide. (c) Dry fog generated through a turbine at high speed that atomized and sprays disinfectant (arrows).

workroom. However, UV radiation may cause a significant degradation of synthetic polymers such as polystyrene which results in breaking the polymer chains [54].

The performance of different systems must be evaluated for use in dental practice. The UVC light and PX-UV systems are efficacious methods for decontamination

of a room, but both systems attack synthetic polymer materials and many parts of dentist chairs and other medical devices can be damaged. The gaseous ozone requires a high concentration and in practice is very difficult to achieve without sealing the doors. So, the most interesting techniques for decontamination in clinical practice are

VHP and aHP both of which use HP vapor or aerosol and are widely used for environmental decontamination in hospitals [92]. It is desirable that these techniques are also applied to dentistry.

Manual disinfection of work surfaces can result in poor disinfection of work stations with the risk of spreading pathogens from one surface to another [93]. However, there are many variables that influence the efficacy of the manual disinfection process such as distribution and contact time of the agent, which further limit the repeatability and reliance for an operator. For example, quarternary ammonium is an efficacious agent but when used with cotton or wipes containing substantial amounts of cellulose, the antimicrobial efficacy of the disinfectant may be reduced [94, 95]; therefore, it is recommended to use microfiber [96]. Another error is inappropriate overdilution of disinfectant solutions resulting in inappropriately low concentrations.

Outbreaks and rapid transmission of some viral diseases like rhinovirus, influenza, avian influenza, SARS, and infectious bronchitis, with their elevated morbidity and mortality rates, are generally attributed to infection via aerosol. Droplets produced during the use of high-speed handpieces and air/water syringes with the patient's saliva contaminate the air and floor, all work surface walls, and the objects that are nearby. Then, a no-touch or automatic disinfection approach to disinfection is needed to improve disinfection of surfaces in the dental clinic.

The major problem in clinical practice is that many enteric and respiratory viruses can be shed at great concentrations and contaminate and survive for long periods on environmental and medical device surfaces; this has been shown to play a role in their transmission [97]. HPV is a vapor-phase disinfection method. It is virucidal, including against influenza, and hence can be considered for the environment decontamination and disinfection of virus-contaminated surfaces in the dental clinic.

This technique is also very safe; in fact, it has also been used for the disinfection of N95 respirators with a residual level of H_2O_2 on the inner facial filter respirator at a very low level, 0.6 ppm at 2 hours and undetectable at 3 hours when the safety limit is actually lower, being <1 ppm [98]. Also, HOCl is a fast and simple technique that can be implemented in the dental clinic, since slightly acidic hypochlorous acid water has very fast and strong efficacy against pathogens [99].

Biosecurity programs have a critical role in the control of all infectious diseases. The main way to control and prevent those diseases that are airborne in the hospital or dental clinic is inactivation of infectious agents by spraying disinfectants in the air. HOCl is very popular for its broad and strong disinfection ability, demonstrating a very fast and strong efficacy against avian influenza and many viruses in a short contact time (5 sec), in vitro [44]. It has shown activity also against many bacteria and other microorganisms such as *Staphylococcus aureus* and *Pseudomonas aeruginosa*. Application of HOCl in low concentrations 20-200 ppm, by a spraying system with high turbine speed with the ability of producing aerosol particles (3-10 μ) inside dental clinics, is able to

reduce the chances of aerogenic infection causing outbreaks and can limit virus transmission from one site to another. This powerful weapon is 100 percent safe for humans as it occurs naturally in our bodies. Neutrophils are white blood cells that are the first to arrive on site when an invading microorganism is detected. Neutrophils will chase down and engulf the pathogen through phagocytosis. Upon contact, neutrophils release a burst of bactericidal chemicals including its most effective oxidizing agent, HOCl. This inactivates the pathogen by destroying the cell membranes and proteins [100]. All the articles discussed in this review concern the control of infections of very resistant agents (such as norovirus, Ebola, methicillin-resistant *Staphylococcus aureus*, and *C. difficile*); for this reason, we can deduce that they are also active against influenza viruses which are much more sensitive to common disinfectants. Very few studies on dental clinics and the identified potential methods to achieve decontamination are detected in literature. So the decontamination technique that best suits the needs of the dental clinic is peroxide and hypochlorous which can be sprayed via a device at high turbine speed with the ability of producing small aerosol particles, recommendable also for their low cost.

These procedures do not replace the correct use of personal protective equipment [101, 102]. The lower the shed quantity (via the use of masks and safety glasses to limit shedding), the easiest it is to reach noninfectious doses after disinfection, and the lower the exposure dose, the lower the probability to get infected (via the use of masks to limit inoculation) [103, 104]. Although all dentistry procedures cannot be realized with a mask on the patient, it is important for the dentist to wear correctly one, in addition to colleagues entering the room, and patients in the waiting room for instance. We believe that no-touch methods augment manual cleaning but cannot replace it.

5. Conclusions

Dentists should consider the use of these disinfectants and no-touch decontamination technologies to improve disinfection of surfaces in dental clinics. In conclusion, manual cleaning and disinfection of environmental surfaces in health care facilities (daily and at patient discharge) are essential elements of infection prevention programs, especially during the SARS-CoV-2 pandemic.

Abbreviations

SARS-CoV-2:	Severe acute respiratory syndrome coronavirus
Covid-19:	Coronavirus 19
UV:	Ultraviolet light
HAS:	Hypochlorous acid solution.

Conflicts of Interest

The authors declare that they have no conflicts of interest.

References

- [1] N. Zhu, D. Zhang, W. Wang et al., "A novel coronavirus from patients with pneumonia in China, 2019," *The New England Journal of Medicine*, vol. 382, no. 8, pp. 727–733, 2020.
- [2] Organization, WH, *Coronavirus disease 2019 (COVID-19): situation report*, no. 70, 2020.
- [3] J. Chen, "Pathogenicity and transmissibility of 2019-nCoV—a quick overview and comparison with other emerging viruses," *Microbes and Infection*, vol. 22, no. 2, pp. 69–71, 2020.
- [4] N. Chen, M. Zhou, X. Dong et al., "Epidemiological and clinical characteristics of 99 cases of 2019 novel coronavirus pneumonia in Wuhan, China: a descriptive study," *Lancet*, vol. 395, no. 10223, pp. 507–513, 2020.
- [5] V. J. Lee, X. Aguilera, D. Heymann et al., "Preparedness for emerging epidemic threats: a lancet infectious diseases commission," *The Lancet Infectious Diseases*, vol. 20, no. 1, pp. 17–19, 2020.
- [6] R.-H. Du, L.-R. Liang, C.-Q. Yang et al., "Predictors of mortality for patients with COVID-19 pneumonia caused by SARS-CoV-2: a prospective cohort study," *The European Respiratory Journal*, vol. 55, no. 5, p. 2000524, 2020.
- [7] X. Xie, Y. Li, H. Sun, and L. Liu, "Exhaled droplets due to talking and coughing," *Journal of The Royal Society Interface*, vol. 6, Supplement_6, pp. S703–S714, 2009.
- [8] L. Bourouiba, "Turbulent gas clouds and respiratory pathogen emissions," *JAMA*, 2020.
- [9] J. Lu, J. Gu, K. Li et al., "COVID-19 outbreak associated with air conditioning in restaurant, Guangzhou, China, 2020," *Emerging Infectious Diseases*, vol. 26, no. 7, pp. 1628–1631, 2020.
- [10] G. A. Somsen, C. van Rijn, S. Kooij, R. A. Bem, and D. Bonn, "Small droplet aerosols in poorly ventilated spaces and SARS-CoV-2 transmission," *The Lancet Respiratory Medicine*, vol. 8, no. 7, pp. 658–659, 2020.
- [11] M. Meselson, "Droplets and aerosols in the transmission of SARS-CoV-2," *The New England Journal of Medicine*, vol. 382, no. 21, p. 2063, 2020.
- [12] Y. L. A. Kwok, J. Gralton, and M.-L. McLaws, "Face touching: a frequent habit that has implications for hand hygiene," *American Journal of Infection Control*, vol. 43, no. 2, pp. 112–114, 2015.
- [13] M. T. Montagna, M. L. Cristina, O. D. Giglio et al., "Serological and molecular identification of *Legionella* spp. isolated from water and surrounding air samples in Italian healthcare facilities," *Environmental Research*, vol. 146, pp. 47–50, 2016.
- [14] X. Peng, X. Xu, Y. Li, L. Cheng, X. Zhou, and B. Ren, "Transmission routes of 2019-nCoV and controls in dental practice," *International Journal of Oral Science*, vol. 12, no. 1, p. 9, 2020.
- [15] D. G. Maki, C. J. Alvarado, C. A. Hassemer, and M. A. Zilz, "Relation of the inanimate hospital environment to endemic nosocomial infection," *The New England Journal of Medicine*, vol. 307, no. 25, pp. 1562–1566, 1982.
- [16] V. Russotto, A. Cortegiani, T. Fasciana et al., "What healthcare workers should know about environmental bacterial contamination in the intensive care unit," *BioMed Research International*, vol. 2017, Article ID 6905450, 7 pages, 2017.
- [17] R. Tellier, Y. Li, B. J. Cowling, and J. W. Tang, "Recognition of aerosol transmission of infectious agents: a commentary," *BMC Infectious Diseases*, vol. 19, no. 1, p. 101, 2019.
- [18] W. A. Rutala and D. J. Weber, "Are room decontamination units needed to prevent transmission of environmental pathogens?," *Infection Control & Hospital Epidemiology*, vol. 32, no. 8, pp. 743–747, 2011.
- [19] M. E. Falagas, P. C. Thomaidis, I. K. Kotsantis, K. Sgouros, G. Samonis, and D. E. Karageorgopoulos, "Airborne hydrogen peroxide for disinfection of the hospital environment and infection control: a systematic review," *The Journal of Hospital Infection*, vol. 78, no. 3, pp. 171–177, 2011.
- [20] A. Davies, T. Pottage, A. Bennett, and J. Walker, "Gaseous and air decontamination technologies for *Clostridium difficile* in the healthcare environment," *The Journal of Hospital Infection*, vol. 77, no. 3, pp. 199–203, 2011.
- [21] K. Bedell, A. H. Buchaklian, and S. Perlman, "Efficacy of an automated multiple emitter whole-room ultraviolet-C disinfection system against coronaviruses MHV and MERS-CoV," *Infection Control and Hospital Epidemiology*, vol. 37, no. 5, pp. 598–599, 2016.
- [22] P. G. Vianna, C. R. Dale, S. Simmons, M. Stibich, and C. M. Licitra, "Impact of pulsed xenon ultraviolet light on hospital-acquired infection rates in a community hospital," *American Journal of Infection Control*, vol. 44, no. 3, pp. 299–303, 2016.
- [23] D. Zoutman, M. Shannon, and A. Mandel, "Effectiveness of a novel ozone-based system for the rapid high-level disinfection of health care spaces and surfaces," *American Journal of Infection Control*, vol. 39, no. 10, pp. 873–879, 2011.
- [24] H.-T. Chan, P. White, H. Sheorey, J. Cocks, and M.-J. Waters, "Evaluation of the biological efficacy of hydrogen peroxide vapour decontamination in wards of an Australian hospital," *The Journal of Hospital Infection*, vol. 79, no. 2, pp. 125–128, 2011.
- [25] D. Mosci, G. W. Marmo, L. Sciolino et al., "Automatic environmental disinfection with hydrogen peroxide and silver ions versus manual environmental disinfection with sodium hypochlorite: a multicentre randomized before-and-after trial," *The Journal of Hospital Infection*, vol. 97, no. 2, pp. 175–179, 2017.
- [26] T. Y. Fu, P. Gent, and V. Kumar, "Efficacy, efficiency and safety aspects of hydrogen peroxide vapour and aerosolized hydrogen peroxide room disinfection systems," *The Journal of Hospital Infection*, vol. 80, no. 3, pp. 199–205, 2012.
- [27] P. Orlando, M. L. Cristina, M. Dalleria, G. Ottria, A. Vitale, and G. Badolati, "Surface disinfection: evaluation of the efficacy of a nebulization system spraying hydrogen peroxide," *Journal of Preventive Medicine and Hygiene*, vol. 49, no. 3, pp. 116–119, 2008.
- [28] T. Holmdahl, P. Lanbeck, M. Wullt, and M. H. Walder, "A head-to-head comparison of hydrogen peroxide vapor and aerosol room decontamination systems," *Infection Control and Hospital Epidemiology*, vol. 32, no. 9, pp. 831–836, 2011.
- [29] M. H. Sk, R. A. Overfelt, R. L. Haney, and J. W. Fergus, "Hydrogen embrittlement of 4340 steel due to condensation during vaporized hydrogen peroxide treatment," *Materials Science and Engineering: A*, vol. 528, no. 10–11, pp. 3639–3645, 2011.
- [30] L. Hall, J. A. Otter, J. Chewins, and N. L. Wengenack, "Use of hydrogen peroxide vapor for deactivation of *Mycobacterium*

- tuberculosis in a biological safety cabinet and a room,” *Journal of Clinical Microbiology*, vol. 45, no. 3, pp. 810–815, 2007.
- [31] J. A. Otter, S. Yezli, T. M. Perl, F. Barbut, and G. L. French, “The role of “no-touch” automated room disinfection systems in infection prevention and control,” *The Journal of Hospital Infection*, vol. 83, no. 1, pp. 1–13, 2013.
- [32] E. Berrie, L. Andrews, S. Yezli, and J. A. Otter, “Hydrogen peroxide vapour (HPV) inactivation of adenovirus,” *Letters in Applied Microbiology*, vol. 52, no. 5, pp. 555–558, 2011.
- [33] S. M. Goyal, Y. Chander, S. Yezli, and J. A. Otter, “Hydrogen peroxide vapor (HPV) inactivation of Feline calicivirus, a surrogate for norovirus,” in *In Proceedings of the Hospital Infection Society (HIS) Conference*, 2010.
- [34] A. Jeanes, G. Rao, M. Osman, and P. Merrick, “Eradication of persistent environmental MRSA,” *Journal of Hospital Infection*, vol. 61, no. 1, pp. 85–86, 2005.
- [35] R. Gopinath, P. Savard, K. C. Carroll, L. E. Wilson, B. M. Landrum, and T. M. Perl, “Infection prevention considerations related to New Delhi metallo- β -lactamase Enterobacteriaceae: a case report,” *Infection Control and Hospital Epidemiology*, vol. 34, no. 1, pp. 99–100, 2013.
- [36] A. Oon, E. Reading, J. K. Ferguson, S. J. Dancer, and B. G. Mitchell, “Measuring environmental contamination in critical care using dilute hydrogen peroxide (DHP) technology: an observational cross-over study,” *Infection, Disease & Health*, vol. 25, no. 2, pp. 107–112, 2020.
- [37] O. Safety and H. Administration, “Occupational safety and health guideline for hydrogen peroxide,” *Hydrogen Peroxide*, 2000, <https://www.cdc.gov/niosh/docs/81-123/pdfs/0335.pdf>.
- [38] International Labour Organisation, *Hydrogen peroxide (>60% solution in water)*, 2017.
- [39] H. J. Kim, J.-G. Lee, J. W. Kang et al., “Effects of a low concentration hypochlorous acid nasal irrigation solution on bacteria, fungi, and virus,” *Laryngoscope*, vol. 118, no. 10, pp. 1862–1867, 2008.
- [40] G. W. Park, D. M. Boston, J. A. Kase, M. N. Sampson, and M. D. Sobsey, “Evaluation of liquid- and fog-based application of Sterilox hypochlorous acid solution for surface inactivation of human norovirus,” *Applied and Environmental Microbiology*, vol. 73, no. 14, pp. 4463–4468, 2007.
- [41] A. D. Russel, W. B. Hugo, and J. Ayliffe, *Disinfection, Preservation and Sterilization*, Blackwell Science, Osney Mead, Oxford, United, 3rd edition edition, 1999.
- [42] M. S. Yu, H. W. Park, H. J. Kwon, and Y. J. Jang, “The effect of a low concentration of hypochlorous acid on rhinovirus infection of nasal epithelial cells,” *American Journal of Rhinology & Allergy*, vol. 25, no. 1, pp. 40–44, 2011.
- [43] M. W. Lister, “The decomposition of hypochlorous acid,” *Canadian Journal of Chemistry*, vol. 30, no. 11, pp. 879–889, 1952.
- [44] H. Hakim, C. Thammakarn, A. Suguro et al., “Evaluation of sprayed hypochlorous acid solutions for their virucidal activity against avian influenza virus through in vitro experiments,” *Journal of Veterinary Medical Science*, vol. 77, no. 2, pp. 211–215, 2015.
- [45] J. M. Boyce, N. L. Havill, and B. A. Moore, “Terminal decontamination of patient rooms using an automated mobile UV light unit,” *Infection Control and Hospital Epidemiology*, vol. 32, no. 8, pp. 737–742, 2011.
- [46] M. M. Nerandzic, J. L. Cadnum, M. J. Pultz, and C. J. Donskey, “Evaluation of an automated ultraviolet radiation device for decontamination of *Clostridium difficile* and other healthcare-associated pathogens in hospital rooms,” *BMC Infectious Diseases*, vol. 10, no. 1, p. 197, 2010.
- [47] T. A. Conner-Kerr, P. K. Sullivan, J. Gaillard, M. E. Franklin, and R. M. Jones, “The effects of ultraviolet radiation on antibiotic-resistant bacteria in vitro,” *Ostomy/Wound Management*, vol. 44, pp. 50–56, 1998.
- [48] R. B. Setlow, E. Grist, K. Thompson, and A. D. Woodhead, “Wavelengths effective in induction of malignant melanoma,” *Proceedings. National Academy of Sciences. United States of America*, vol. 90, no. 14, pp. 6666–6670, 1993.
- [49] D. Welch, M. Buonanno, V. Grilj et al., “Far-UVC light: a new tool to control the spread of airborne-mediated microbial diseases,” *Scientific Reports*, vol. 8, no. 1, p. 2752, 2018.
- [50] T. Dai, M. S. Vrahas, C. K. Murray, and M. R. Hamblin, “Ultraviolet C irradiation: an alternative antimicrobial approach to localized infections?,” *Expert Review of Anti-Infective Therapy*, vol. 10, no. 2, pp. 185–195, 2014.
- [51] M. Stibich, J. Stachowiak, B. Tanner et al., “Evaluation of a pulsed-xenon ultraviolet room disinfection device for impact on hospital operations and microbial reduction,” *Infection Control and Hospital Epidemiology*, vol. 32, no. 3, pp. 286–288, 2011.
- [52] C. Jinadatha, R. Quezada, T. W. Huber, J. B. Williams, J. E. Zeber, and L. A. Copeland, “Evaluation of a pulsed-xenon ultraviolet room disinfection device for impact on contamination levels of methicillin-resistant *Staphylococcus aureus*,” *BMC Infectious Diseases*, vol. 14, no. 1, p. 187, 2014.
- [53] S. S. Ghantaji, M. Stibich, J. Stachowiak et al., “Non-inferiority of pulsed xenon UV light versus bleach for reducing environmental *Clostridium difficile* contamination on high-touch surfaces in *Clostridium difficile* infection isolation rooms,” *Journal of Medical Microbiology*, vol. 64, no. 2, pp. 191–194, 2015.
- [54] E. Yousif and R. Haddad, “Photodegradation and photostabilization of polymers, especially polystyrene: review,” *Springerplus*, vol. 2, no. 1, p. 398, 2013.
- [55] J. B. Hudson, M. Sharma, and S. Vimalanathan, “Development of a practical method for using ozone gas as a virus decontaminating agent,” *Ozone: Science & Engineering*, vol. 31, no. 3, pp. 216–223, 2009.
- [56] R. J. Rowen, “Ozone and oxidation therapies as a solution to the emerging crisis in infectious disease management: a review of current knowledge and experience,” *Medical Gas Research*, vol. 9, no. 4, p. 0, 2019.
- [57] J. B. Hudson, M. Sharma, and M. Petric, “Inactivation of norovirus by ozone gas in conditions relevant to healthcare,” *Journal of Hospital Infection*, vol. 66, no. 1, pp. 40–45, 2007.
- [58] C. N. Miller, J. A. Dye, M. C. Schladweiler et al., “Acute inhalation of ozone induces DNA methylation of apelin in lungs of Long-Evans rats,” *Inhalation Toxicology*, vol. 30, no. 4–5, pp. 178–186, 2018.
- [59] J. Wei and Y. Li, “Airborne spread of infectious agents in the indoor environment,” *American Journal of Infection Control*, vol. 44, no. 9, pp. S102–S108, 2016.
- [60] R. Rautemaa, A. Nordberg, K. Wuolijoki-Saaristo, and J. H. Meurman, “Bacterial aerosols in dental practice - a potential hospital infection problem?,” *The Journal of Hospital Infection*, vol. 64, no. 1, pp. 76–81, 2006.

- [61] G. Kampf, D. Todt, S. Pfaender, and E. Steinmann, "Persistence of coronaviruses on inanimate surfaces and their inactivation with biocidal agents," *The Journal of Hospital Infection*, vol. 104, no. 3, pp. 246–251, 2020.
- [62] J. Gu, Y. Zhong, Y. Hao et al., "Preventive behaviors and mental distress in response to H1N1 among university students in Guangzhou, China," *Asia Pacific Journal of Public Health*, vol. 27, no. 2, pp. NP1867–NP1879, 2015.
- [63] H. Nishimura, S. Sakata, and A. Kaga, "A new methodology for studying dynamics of aerosol particles in sneeze and cough using a digital high-vision, high-speed video system and vector analyses," *PLoS One*, vol. 8, no. 11, article e80244, 2013.
- [64] L. Meng, F. Hua, and Z. Bian, "Coronavirus disease 2019 (COVID-19): emerging and future challenges for dental and oral medicine," *Journal of Dental Research*, vol. 99, no. 5, pp. 481–487, 2020.
- [65] Z. Y. Li and L. Y. Meng, "The prevention and control of a new coronavirus infection in department of stomatology," *Zhonghua Kou Qiang Yi Xue Za Zhi*, vol. 55, article E001, 2020.
- [66] A. Smith, S. Creanor, D. Hurrell, J. Bagg, and M. McCowan, "Management of infection control in dental practice," *The Journal of Hospital Infection*, vol. 71, no. 4, pp. 353–358, 2009.
- [67] C. Pasquarella, L. Veronesi, C. Napoli et al., "Microbial environmental contamination in Italian dental clinics: a multicenter study yielding recommendations for standardized sampling methods and threshold values," *Science of the total environment*, vol. 420, pp. 289–299, 2012.
- [68] R. Y. Chinn and L. Sehulster, *Guidelines for environmental infection control in health-care facilities; recommendations of CDC and Healthcare Infection Control Practices Advisory Committee (HICPAC)*, 2003.
- [69] M. Dettenkofer and R. C. Spencer, "Importance of environmental decontamination—a critical view," *Journal of Hospital Infection*, vol. 65, pp. 55–57, 2007.
- [70] J. Barker, I. B. Vipond, and S. F. Bloomfield, "Effects of cleaning and disinfection in reducing the spread of norovirus contamination via environmental surfaces," *The Journal of Hospital Infection*, vol. 58, no. 1, pp. 42–49, 2004.
- [71] W. Yang and L. C. Marr, "Dynamics of airborne influenza A viruses indoors and dependence on humidity," *PLoS One*, vol. 6, no. 6, article e21481, 2011.
- [72] A. Scarano, F. Carinci, F. Lorusso et al., "Ultrasonic vs drill implant site preparation: post-operative pain measurement through VAS, swelling and crestal bone remodeling: a randomized clinical study," *Materials (Basel)*, vol. 11, no. 12, p. 2516, 2018.
- [73] A. Scarano, A. Piattelli, G. Murmura, G. Iezzi, B. Assenza, and C. Mancino, "Delayed expansion of the atrophic mandible by ultrasonic surgery: a clinical and histologic case series," *The International Journal of Oral & Maxillofacial Implants*, vol. 30, no. 1, pp. 144–149, 2015.
- [74] A. Scarano, F. Carinci, B. Assenza, M. Piattelli, G. Murmura, and A. Piattelli, "Vertical ridge augmentation of atrophic posterior mandible using an inlay technique with a xenograft without miniscrews and miniplates: case series," *Clinical Oral Implants Research*, vol. 22, no. 10, pp. 1125–1130, 2011.
- [75] A. Scarano, P. Di Domizio, G. Petrone, G. Iezzi, and A. Piattelli, "Implant periapical lesion: a clinical and histologic case report," *The Journal of Oral Implantology*, vol. 26, no. 2, pp. 109–113, 2000.
- [76] N. van Doremalen, T. Bushmaker, D. H. Morris et al., "Aerosol and surface stability of SARS-CoV-2 as compared with SARS-CoV-1," *The New England Journal of Medicine*, vol. 382, no. 16, pp. 1564–1567, 2020.
- [77] H. F. Rabenau, G. Kampf, J. Cinatl, and H. W. Doerr, "Efficacy of various disinfectants against SARS coronavirus," *The Journal of Hospital Infection*, vol. 61, no. 2, pp. 107–111, 2005.
- [78] H. F. Rabenau, J. Cinatl, B. Morgenstern, G. Bauer, W. Preiser, and H. W. Doerr, "Stability and inactivation of SARS coronavirus," *Medical Microbiology and Immunology*, vol. 194, no. 1-2, pp. 1–6, 2005.
- [79] A. Wood and D. Payne, "The action of three antiseptics/disinfectants against enveloped and non-enveloped viruses," *The Journal of Hospital Infection*, vol. 38, no. 4, pp. 283–295, 1998.
- [80] M. Saknimit, I. Inatsuki, Y. Sugiyama, and K.-I. Yagami, "Virucidal efficacy of physico-chemical treatments against coronaviruses and parvoviruses of laboratory animals," *Experimental Animals*, vol. 37, no. 3, pp. 341–345, 1988.
- [81] A. Pratelli, "Action of disinfectants on canine coronavirus replication in vitro," *Zoonoses and Public Health*, vol. 54, no. 9-10, pp. 383–386, 2007.
- [82] N. Omidbakhsh and S. A. Sattar, "Broad-spectrum microbicidal activity, toxicologic assessment, and materials compatibility of a new generation of accelerated hydrogen peroxide-based environmental surface disinfectant," *American Journal of Infection Control*, vol. 34, no. 5, pp. 251–257, 2006.
- [83] C. Dellanno, Q. Vega, and D. Boesenberg, "The antiviral action of common household disinfectants and antiseptics against murine hepatitis virus, a potential surrogate for SARS coronavirus," *American Journal of Infection Control*, vol. 37, no. 8, pp. 649–652, 2009.
- [84] H. Kariwa, N. Fujii, and I. Takashima, "Inactivation of SARS coronavirus by means of povidone-iodine, physical conditions and chemical reagents," *Dermatology*, vol. 212, no. 1, Supplement 1, pp. 119–123, 2006.
- [85] G. Annex, "Infection Prevention and Control of Epidemic- and Pandemic-Prone Acute Respiratory Infections in Health Care," in *Use of disinfectants: alcohol and bleach*, Geneva, 2014.
- [86] A. Siddharta, S. Pfaender, N. J. Vielle et al., "Virucidal activity of World Health Organization-recommended formulations against enveloped viruses, including Zika, Ebola, and emerging coronaviruses," *The Journal of Infectious Diseases*, vol. 215, no. 6, pp. 902–906, 2017.
- [87] A. Scarano, M. Petrini, F. Mastrangelo, S. Noubissi, and F. Lorusso, "The effects of liquid disinfection and heat sterilization processes on implant drill roughness: energy dispersion X-ray microanalysis and infrared thermography," *Journal of Clinical Medicine*, vol. 9, no. 4, p. 1019, 2020.
- [88] A. Scarano, A. Piattelli, B. Assenza et al., "Infrared thermographic evaluation of temperature modifications induced during implant site preparation with cylindrical versus conical drills," *Clinical Implant Dentistry and Related Research*, vol. 13, no. 4, pp. 319–323, 2011.
- [89] A. Scarano, S. Noubissi, S. Gupta, F. Inchingolo, P. Stilla, and F. Lorusso, "Scanning electron microscopy analysis and energy dispersion X-ray microanalysis to evaluate the effects of decontamination chemicals and heat sterilization on implant surgical drills: zirconia vs. steel," *Applied Sciences*, vol. 9, no. 14, p. 2837, 2019.

- [90] T. de Groot, A. Chowdhary, J. F. Meis, and A. Voss, "Killing of *Candida auris* by UV-C: importance of exposure time and distance," *Mycoses*, vol. 62, no. 5, pp. 408–412, 2019.
- [91] J.-J. Li, S.-N. Wang, J.-J. Qiao et al., "Portable pulsed xenon ultraviolet light disinfection in a teaching hospital animal laboratory in China," *Journal of Photochemistry and Photobiology B: Biology*, vol. 207, article 111869, 2020.
- [92] J. M. Boyce, "Modern technologies for improving cleaning and disinfection of environmental surfaces in hospitals," *Antimicrobial Resistance and Infection Control*, vol. 5, no. 1, 2016.
- [93] J. L. Cadnum, K. N. Hurlless, S. Kundrapu, and C. J. Donskey, "Transfer of *Clostridium difficile* spores by nonsporicidal wipes and improperly used hypochlorite wipes: practice + product = perfection," *Infection Control and Hospital Epidemiology*, vol. 34, no. 4, pp. 441–442, 2013.
- [94] K. Engelbrecht, D. Ambrose, L. Sifuentes, C. Gerba, I. Weart, and D. Koenig, "Decreased activity of commercially available disinfectants containing quaternary ammonium compounds when exposed to cotton towels," *American Journal of Infection Control*, vol. 41, no. 10, pp. 908–911, 2013.
- [95] J. M. Boyce, L. Sullivan, A. Booker, and J. Baker, "Quaternary ammonium disinfectant issues encountered in an environmental services department," *Infection Control and Hospital Epidemiology*, vol. 37, no. 3, pp. 340–342, 2016.
- [96] S. Ali, G. Moore, and A. P. R. Wilson, "Effect of surface coating and finish upon the cleanability of bed rails and the spread of *Staphylococcus aureus*," *The Journal of Hospital Infection*, vol. 80, no. 3, pp. 192–198, 2012.
- [97] B. Stephens, P. Azimi, M. S. Thoemmes, M. Heidarinejad, J. G. Allen, and J. A. Gilbert, "Microbial exchange via fomites and implications for human health," *Current Pollution Reports*, vol. 5, no. 4, pp. 198–213, 2019.
- [98] V. C. C. Cheng, S.-C. Wong, G. S. W. Kwan, W.-T. Hui, and K.-Y. Yuen, "Disinfection of N95 respirators by ionized hydrogen peroxide during pandemic coronavirus disease 2019 (COVID-19) due to SARS-CoV-2," *The Journal of Hospital Infection*, vol. 105, no. 2, pp. 358–359, 2020.
- [99] D. J. Alexander, "Newcastle disease and other avian paramyxovirus," *Revue Scientifique et Technique de l'OIE*, vol. 19, no. 2, pp. 443–462, 2000.
- [100] A. Degrossoli, A. Müller, K. Xie et al., "Neutrophil-generated HOCl leads to non-specific thiol oxidation in phagocytized bacteria," *eLife*, vol. 7, 2018.
- [101] A. Scarano, F. Inchingolo, and F. Lorusso, "Facial skin temperature and discomfort when wearing protective face masks: thermal infrared imaging evaluation and hands moving the mask," *International Journal of Environmental Research and Public Health*, vol. 17, no. 13, p. 4624, 2020.
- [102] J. Moat, J. Cargill, J. Shone, and M. Upton, "Application of a novel decontamination process using gaseous ozone," *Canadian Journal of Microbiology*, vol. 55, no. 8, pp. 928–933, 2009.
- [103] W. Ding, W. Jin, S. Cao et al., "Ozone disinfection of chlorine-resistant bacteria in drinking water," *Water Research*, vol. 160, pp. 339–349, 2019.
- [104] F. Lorusso, F. Inchingolo, and A. Scarano, "The impact of the novel Covid-19 on the scientific production spread: a five-month bibliometric report of the worldwide research community," *Acta Medica Mediterranea*, vol. 36, pp. 1–4, 2020.

Research Article

Digital vs. Freehand Anterior Single-Tooth Implant Restoration

D. Baldi,¹ J. Colombo ,¹ F. Motta,¹ F. M. Motta,¹ A. Zillio,¹ and N. Scotti²

¹Department of Surgical Sciences (DISC), Division of Prosthetic Dentistry, University of Genoa, Genoa, Italy

²Department of Surgical Sciences, University of Turin, Turin, Italy

Correspondence should be addressed to J. Colombo; jacopocolo@tiscali.it

Received 11 June 2020; Revised 25 September 2020; Accepted 6 October 2020; Published 23 October 2020

Academic Editor: Luigi Canullo

Copyright © 2020 D. Baldi et al. This is an open access article distributed under the Creative Commons Attribution License, which permits unrestricted use, distribution, and reproduction in any medium, provided the original work is properly cited.

Replacing a single tooth in the anterior maxilla is one of the greatest challenges in dentistry. Both functional and aesthetic results are to be strictly pursued. Planning and executing such a case through a totally digital methodology eventually guarantee many advantages, above all patient's operative and postoperative comfort. To ascertain this, a BOP analysis was performed which allowed us to evaluate soft tissues health, and more; crestal bone resorption was measured to evaluate hard tissues stability. This assumption was studied through four cases in which patients were alternatively treated with analogic and digital techniques. Four homogeneous patients were recruited. They all needed to extract one of the upper incisors, due to different clinical reasons, and then to replace it with an implant. Each patient was treated with an immediate postextractive implant which was immediately loaded, and finally, analogical and digital techniques were compared. All patients underwent a preoperative CBCT examination. After surgery, patients were checked by the surgeon after 10 days and one month to evaluate the progress of healing and to exclude any prosthetic problem. At 6 months (T1), one year (T2), and three years (T3), intraoral x-rays were performed using customized centring devices, according to the parallel beam technique. All data have been collected in a table and statistically processed; mean and standard deviation were measured. All patients entered an oral hygiene program with six months recall. Dental hygienist checked the BOP at T1, T2, and T3. At every step, similar levels of BOP were recorded. About interproximal bone loss, all patients showed an initial moderate loss (between T1 and T2), followed by stable values between T2 and T3. Despite the important limitations of a study with few cases, these results show a similar outcome comparing digital and analogical methods.

1. Introduction

Oral health seems to be of paramount importance for individuals [1, 2]. Replacing an anterior tooth in the maxillary area is one of the greatest rehabilitative challenges in dentistry [3–5]. In oral therapy, functional and aesthetic aims cannot be separated [6]. The great challenge for the dentist lies in perfectly blending surgery with the prosthetics in order to get an overall satisfactory result [7–9]. Furthermore, therapy must guarantee stability over time. The first step is a good surgical planning. A complete analysis of the implant site, a correct choice of the fixture [10–14], and its positioning are fundamental steps. Eventually, the choice of both temporary and definitive prosthesis accomplishes the path so that an optimal result is achievable. In recent years, new digital instruments would contribute to optimize all these steps, making the path predictable at all. Moreover, guided surgery

let us achieve decidedly higher levels of precision compared to traditional techniques [15–19]. Furthermore, using an optical impression also optimize prosthetic steps [20–22]. Transition from a completely analogical to a completely digital execution makes these complex therapies more predictable, because these procedures become less operator depending. In particular, planning surgery through a dedicated software allows to pursue all parameters leading to long-term success. Differently, even in the hands of very experienced operators, traditional surgery can expose to inevitable errors due to anatomical and human factors. Restoration guides our digital planning in which every aspect can be optimize, including the abutment shape, the profile of the crown, and choice of materials [23, 24].

Furthermore alternative surgical methods, like Piezosurgery [25–28], would add patient's comfort. Various methods are analyzed starting from the assumption that

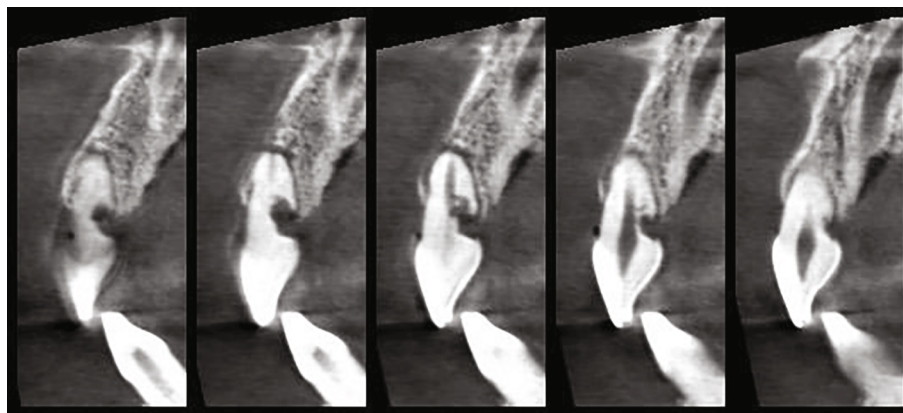


FIGURE 1: Preoperative CBCT of the patient.



FIGURE 2: Final situation of patient 1.

they all biologically valid. For this reason, a BOP analysis was also performed to evaluate the health of soft tissues and interproximal crestal bone resorption to evaluate the stability of hard tissues [29]. The aim of the article is to analyze them with the help of four cases in which analog and digital modes alternate.

2. Materials and Methods

Four patients have been recruited for the study, everyone being required for the extraction of an upper incisor and a related implant rehabilitation. All patients were in good health, and none presented contraindications to implant surgery. Informed consent was collected for all patients, and all possible methods of treatment were proposed. This prospective protocol has been led in accordance with the Good Clinical Practice Guidelines (GCPs) and following the recommendations of the Declaration of Helsinki as revised in Fortaleza (2013) for investigations into human subjects. Patient 1 underwent the extraction of tooth 1.1 because of an external resorption in the palatine area (Figure 1). The implant was inserted freehand immediate postextraction mode (Shelta 3.8 X 11.5, Sweden & Martina, Due Carrare, Italy), and then, it was immediately loaded with a temporary resin crown built after a traditional impression. At 6 months, a definitive screwed ceramic zirconia crown was made still after taking a traditional polyether impression (Figure 2). Patient 2 underwent 1.1

extraction caused by a root fracture. A freehand postextraction implant was inserted (Nobel Active 3.5 X 15, Nobel Biocare, Zurich, Switzerland). The implant was immediately loaded with a temporary crown made by taking a traditional impression. At 6 months, a definitive ceramic zirconia crown was built. In patient 3 was placed in an immediate postextractive implant (Nobel Active 3.5 X 13, Nobel Biocare, Zurich, Switzerland) in seat 22 for palatine destructive caries. Implant was placed with guided surgery (Implant Studio, 3Shape, Copenhagen, Denmark). Optical impression for temporary (one-time one abutment) and final crown (zirconia-ceramic) was cemented directly from the immediate abutment file without performing a new impression (only position impression of the zirconia coping to detect soft tissues after healing). In patient 4 was placed in an immediate postextractive implant in site 12 for a coronoradicular fracture (Nobel Active 3.5 X 13, Nobel Biocare, Zurich, Switzerland) (Figure 3). Implant was positioned with guided surgery (Implant Studio, 3Shape, Copenhagen, Denmark) and loaded with an immediate provisional made before surgery and already luted to the abutment (specifying the planned position) (Figures 4 and 5). Final optical impression was taken to build a screwed zirconia-ceramic crown (Figures 6 and 7). All implants were inserted in postextractive mode with a 1.5mm subcrestal position, to compensate a predictable bone resorption due to tooth extraction [30]. Immediate loading with screwed temporaries was performed in all



FIGURE 3: Preoperative situation of patient 4.

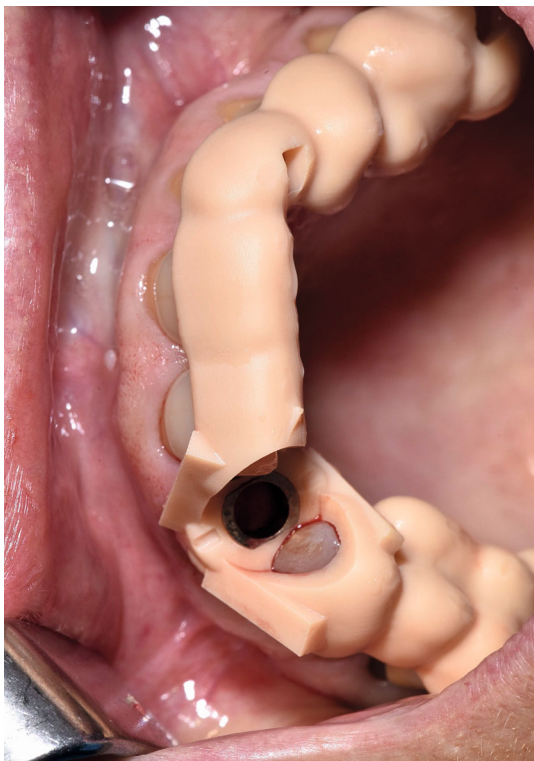


FIGURE 4: Surgical guide of patient 4.

patients. Every patient was checked at 10 days and one month by the surgeon to evaluate the progress of healing and to look at any prosthetic problems. All patients underwent



FIGURE 5: Provisional crown digital project of patient 4.

a preoperative CBCT examination. At 6 months (T1), 1 year (T2), and 3 years (T3), plates with Rx-customized centring devices were used according to the parallel beam technique, and with these, a radiologist measured the peri-implant bone loss in relation to mesial and distal peaks of the adjacent teeth. All data have been inserted in a table and have been subjected to a statistical investigation with measurement of mean and standard deviation. The patients entered into a tight professional hygiene program with 6-month calls, which were preferably performed with the use of powders [31]. At 6 months (T1), 1 year (T2), and 3 years (T3) of recalls, a dental hygienist performed the BOP (bleeding on probing) measurement, pinning the result on the patient's medical record. The bleeding sites have been expressed as a percentage of the total of the surveyed sites (6 per implant). Data were entered into two tables, and the mean and standard deviation were calculated.

3. Results

The BOP measurements have been inserted in a table (Table 1). The observed data showed almost the same level of gingival inflammation in all 4 cases, at T1, T2, and T3 after the insertion of the final manufacture.

The loss of interproximal bone with respect to the peak of the adjacent teeth was inserted in a table (Table 2).

In all 4 cases, the loss of interproximal bone, after a more sensible loss between T1 and T2, has stabilized on almost constant values between T2 and T3. The average of T1 bone levels was 0.0125 mm (standard deviation + -0.15 mm). The T2 mean was 1.03 mm (standard deviation + -0.12 mm). The mean at T3 was 1.3 mm (standard deviation + -0.09 mm).

No patient at 3 years old dropped out the recall and control sessions.

4. Discussion

Analyzing the BOP data, it has been observed that all patients showed an excellent level of oral hygiene with a very low

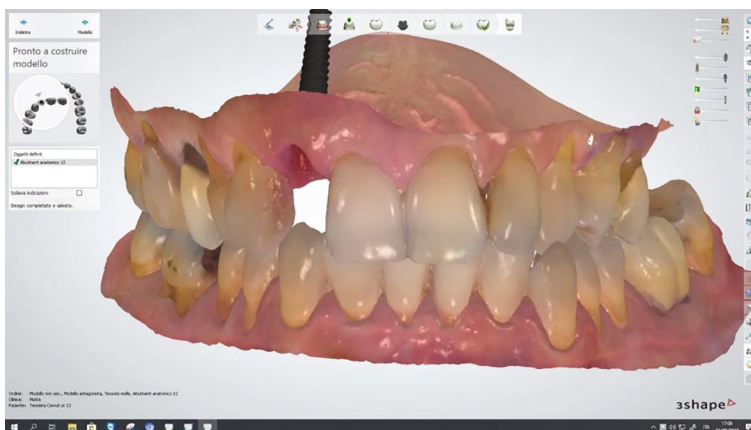


FIGURE 6: Definitive crown digital impression of patient 4.

FIGURE 7: Final restoration *in situ* (patient 4).

TABLE 1: BOP index on implant site at T1, T2, and T3.

	T1 (6 months)	T2 (1 year)	T3 (3 years)
Case 1	0	0	0
Case 2	0	16.6	0
Case 3	16.6	16.6	16.6
Case 4	0	0	16.6

TABLE 2: Interproximal bone loss from T1 to T3.

	T1		T2		T3	
	medial	distal	medial	distal	medial	distal
Case 1	0.1	0.2	1	1.1	1.2	1.2
Case 2	0	-0.2	1.1	1.1	1.3	1.4
Case 3	-0.2	-0.1	0.9	0.8	1.2	1.3
Case 4	0	0.1	1.1	1.1	1.4	1.4

inflammatory index. Right after surgery, all patients underwent oral hygiene sessions and strict home instructions. It could be possible that the presence of an important rehabili-

tation in the aesthetic area may increase patient's compliance about hygienic maintenance.

Interproximal bone loss data reflected the trend of bone resorption expected from the literature data [32]. The most important resorption has been occurred between T1 and T2, therefore within a year since an implant insertion.

As suggested by Schwartz-Arad et al. [31], a natural contraction of the alveolus has been compensated by a the subcrestal insertion of about 1.5 mm of the implant in immediate postextractive mode, in order to obtain a final iuxtaosseous positioning of the head of the implant at T1.

Between T2 and T3, the bone rearrangement is extremely limited, according to Van Steenberghe [33].

From a biological point of view, using a completely analogical or a completely digital technique does not seem to determine differences. Instead, it is very interesting to focus on the predictability of the intervention. According to several authors, the three-dimensional position of the implant is one of the most important factors for the long-term stability of the peri-implant tissues [34, 35]. In the analogical insertion mode, success is strongly delegated to the surgeon's manual ability. In particular, some parameters such as the axis and the insertion depth of the implant require precise capabilities that are not easily

reproducible. On the opposite, the choice of guided surgery allows you to completely plan the intervention. Even with the intrinsic limits of this method, for example the precision of CBCT exams or the precision of the surgical masks, there is no doubt that the operations can be performed with a clearly superior reproducibility of some parameters [30, 36]. Choosing a digital prosthetic flow allows more advantages. For example, in immediate loading, the use of a definitive abutment right after surgery, applying the concept of “one time, one abutment” proposed by Degidi et al. [37, 38]. Patients’ comfort is also very important [39], because they must not undergo a traditional intraoperative impression. In fact, the clinician has both the possibility of already getting the temporary crown ready before surgery and the possibility of performing a scan of the implant after positioning it and getting the temporary in a very short time. A digital flow allows the clinician greater rigor in the surgical field and flexibility in the prosthetic field, with the possibility of planning the prosthesis since the preoperative setting and even of modifying the project with extremely simple steps. Obviously, the transition from analogical to digital techniques requires an important learning curve, which, however, once addressed allows a significant simplification of any clinical procedures.

5. Conclusions

Despite limitations of a study with few cases, results show a substantial overlap between analogical and digital implant-prosthetic techniques about peri-implant tissues health.

The prosthetic workflow also offers several advantages related to ergonomics and comfort; in addition, digital techniques would seem guarantee greater stability of peri-implant tissues in the long term.

Monitoring patients over time and designing new clinical trials with a larger sample are needed to confirm these results.

Data Availability

All data of the present article are available on request by contacting corresponding author.

Conflicts of Interest

The authors do not have any financial interest in the companies whose materials are included in this article.

References

- [1] Organization WH, *International Classification of Functioning, Disability and Health*, ICF: World Health Organization, 2001.
- [2] P. E. Petersen, D. Bourgeois, H. Ogawa, S. Estupinan-Day, and C. Ndiaye, “The global burden of oral diseases and risks to oral health,” *Bulletin of the World Health Organization. Supplement*, vol. 83, no. 9, pp. 661–669, 2005.
- [3] G. Heydecke, D. Locker, M. A. Awad, J. P. Lund, and J. S. Feine, “Oral and general health-related quality of life with conventional and implant dentures,” *Community Dentistry and Oral Epidemiology*, vol. 31, no. 3, pp. 161–168, 2003.
- [4] K. Fueki, K. Kimoto, T. Ogawa, and N. R. Garrett, “Effect of implant-supported or retained dentures on masticatory performance: a systematic review,” *The Journal of Prosthetic Dentistry*, vol. 98, no. 6, pp. 470–477, 2007.
- [5] N. Khzam, H. Arora, P. Kim, A. Fisher, N. Mattheos, and S. Ivanovski, “Systematic review of soft tissue alterations and esthetic outcomes following immediate implant placement and restoration of single implants in the anterior maxilla,” *Journal of Periodontology*, vol. 86, no. 12, pp. 1321–1330, 2015.
- [6] R. E. Jung, L. Heitz-Mayfield, F. Schwarz, and on behalf of the Groups of the 2nd Osteology Foundation Consensus Meeting, “Evidence-based knowledge on the aesthetics and maintenance of peri-implant soft tissues: Osteology Foundation Consensus Report Part 3-aesthetics of peri-implant soft tissues,” *Clinical Oral Implants Research*, vol. 29, Supplement, pp. 14–17, 2018.
- [7] J. Y. K. Kan, K. Rungcharassaeng, M. Deflorian, T. Weinstein, H. L. Wang, and T. Testori, “Immediate implant placement and provisionalization of maxillary anterior single implants,” *Periodontology 2000*, vol. 77, no. 1, pp. 197–212, 2018.
- [8] W. C. Martin, A. Pollini, and D. Morton, “The influence of restorative procedures on esthetic outcomes in implant dentistry: a systematic review,” *The International Journal of Oral & Maxillofacial Implants*, vol. 29, Supplement, pp. 142–154, 2014.
- [9] A. T. Lugas, M. Terzini, E. M. Zanetti et al., “In vitro impact testing to simulate implant-supported prosthesis retrievability in clinical practice: influence of cement and abutment geometry,” *Materials*, vol. 13, no. 7, p. 1749, 2020.
- [10] D. Baldi, T. Lombardi, J. Colombo et al., “Correlation between insertion torque and implant stability quotient in tapered implants with knife-edge thread design,” *BioMed Research International*, vol. 2018, Article ID 7201093, 7 pages, 2018.
- [11] D. Baldi, M. Longobardi, C. Cartiglia et al., “Dental implants osteogenic properties evaluated by cDNA microarrays,” *Implant Dentistry*, vol. 20, no. 4, pp. 299–305, 2011.
- [12] M. Menini, E. Dellepiane, D. Chvartzaid, D. Baldi, I. Schiavetti, and P. Pera, “Influence of different surface characteristics on peri-implant tissue behavior: a six-year prospective report,” *The International Journal of Prosthodontics*, vol. 28, no. 4, pp. 389–395, 2015.
- [13] M. Menini, E. Dellepiane, D. Baldi, M. G. Longobardi, P. Pera, and A. Izzotti, “Microarray expression in peri-implant tissue next to different titanium implant surfaces predicts clinical outcomes: a split-mouth study,” *Clinical Oral Implants Research*, vol. 28, no. 9, pp. e121–e134, 2017.
- [14] D. Baldi, J. Colombo, S. Verardi, A. Rebaudi, F. Rebaudi, and C. Makary, “Clinical osseointegration of bone level implants with conical shape and textured surface with low primary stability,” *Minerva Stomatologica*, vol. 69, no. 1, pp. 8–13, 2020.
- [15] T. Fortin, J. L. Bosson, M. Isidori, and E. Blanchet, “Effect of flapless surgery on pain experienced in implant placement using an image-guided system,” *The International Journal of Oral & Maxillofacial Implants*, vol. 21, no. 2, pp. 298–304, 2005.
- [16] J. D’haese, J. Ackhurst, D. Wismeijer, H. de Bruyn, and A. Tahmaseb, “Current state of the art of computer-guided implant surgery,” *Periodontology 2000*, vol. 73, no. 1, pp. 121–133, 2017.
- [17] F. Bover-Ramos, J. Viña-Almunia, J. Cervera-Ballester, M. Peñarrocha-Diago, and B. García-Mira, “Accuracy of

- implant placement with computer-guided surgery: a systematic review and meta-analysis comparing cadaver, clinical, and in vitro studies," *The International Journal of Oral & Maxillofacial Implants*, vol. 33, no. 1, pp. 101–115, 2018.
- [18] M. Colombo, C. Mangano, E. Mijiritsky, M. Krebs, U. Hauschild, and T. Fortin, "Clinical applications and effectiveness of guided implant surgery: a critical review based on randomized controlled trials," *BMC Oral Health*, vol. 17, no. 1, p. 150, 2017.
- [19] D. P. Laverty, J. Buglass, and A. Patel, "Flapless dental implant surgery and use of cone beam computer tomography guided surgery," *British Dental Journal*, vol. 224, no. 8, pp. 601–611, 2018.
- [20] K. Aswani, S. Wankhade, A. Khalikar, and S. Deogade, "Accuracy of an intraoral digital impression: a review," *The Journal of Indian Prosthodontic Society*, vol. 20, no. 1, pp. 27–37, 2020.
- [21] L. Arcuri, C. Lorenzi, A. Vanni, N. Bianchi, A. Dolci, and C. J. Arcuri, "Comparison of the accuracy of intraoral scanning and conventional impression techniques on implants: a review," *Journal of Biological Regulators & Homeostatic Agentss*, vol. 34, 1 Supplement 1, pp. 89–97, 2020.
- [22] T. Joda, F. Zarone, and M. Ferrari, "The complete digital workflow in fixed prosthodontics: a systematic review," *BMC Oral Health*, vol. 17, no. 1, p. 124, 2017.
- [23] T. Joda, M. Ferrari, G. O. Gallucci, J. G. Wittneben, and U. Brägger, "Digital technology in fixed implant prosthodontics," *Periodontology 2000*, vol. 73, no. 1, pp. 178–192, 2017.
- [24] D. L. Guichet, "Digital workflows in the management of the esthetically discriminating patient," *Dental Clinics of North America*, vol. 63, no. 2, pp. 331–344, 2019.
- [25] C. Stacchi, F. Bassi, G. Troiano et al., "Piezoelectric bone surgery for implant site preparation compared with conventional drilling techniques: a systematic review, meta-analysis and trial sequential analysis," *The International Journal of Oral Implantology*, vol. 13, no. 2, pp. 141–158, 2020.
- [26] D. Baldi, M. Menini, J. Colombo, E. Lertora, and P. Pera, "Evaluation of a new ultrasonic insert for prosthodontic preparation," *The International Journal of Prosthodontics*, vol. 30, no. 5, pp. 496–498, 2017.
- [27] G. Schierano, T. Vercellotti, F. Modica et al., "A 4-year retrospective radiographic study of marginal bone loss of 156 titanium implants placed with ultrasonic site preparation," *The International Journal of Periodontics & Restorative Dentistry*, vol. 39, no. 1, pp. 115–121, 2019.
- [28] C. Stacchi, T. Lombardi, D. Baldi et al., "Immediate loading of implant-supported single crowns after conventional and ultrasonic implant site preparation: a multicenter randomized controlled clinical trial," *BioMed Research International*, vol. 2018, Article ID 6817154, 8 pages, 2018.
- [29] B. Musante, F. Romano, D. Baldi, P. Pera, F. Grillo, and E. Fulcheri, "Methodological approach for the evaluation of homologous bone graft use in post-extractive atrophic alveolar ridges," *Journal of Biological Research*, vol. 86, no. 1, 2013.
- [30] G. S. Unsal, I. Turkyilmaz, and S. Lakhia, "Advantages and limitations of implant surgery with CAD/CAM surgical guides: a literature review," *Journal of Clinical and Experimental Dentistry*, vol. 12, no. 4, pp. e409–e417, 2020.
- [31] D. Schwartz-Arad and G. Chaushu, "The ways and wherefores of immediate placement of implants into fresh extraction sites: a literature review," *Journal of Periodontology*, vol. 68, no. 10, pp. 915–923, 1997.
- [32] K. W. Slagter, L. den Hartog, N. A. Bakker, A. Vissink, H. J. A. Meijer, and G. M. Raghoebar, "Immediate placement of dental implants in the esthetic zone: a systematic review and pooled analysis," *Journal of Periodontology*, vol. 85, no. 7, pp. e241–e250, 2014.
- [33] D. Van Steenberghe, I. Naert, R. Jacobs, and M. Quirynen, "Influence of inflammatory reactions vs. occlusal loading on peri-implant marginal bone level," *Advances in Dental Research*, vol. 13, no. 1, pp. 130–135, 2016.
- [34] T. Albrektsson, G. Zarb, P. Worthington, and A. R. Eriksson, "The long-term efficacy of currently used dental implants: a review and proposed criteria of success," *The International Journal of Oral & Maxillofacial Implants*, vol. 1, no. 1, pp. 11–25, 1986.
- [35] P. Paspaspyridakos, C. J. Chen, M. Singh, H. P. Weber, and G. O. Gallucci, "Success criteria in implant dentistry: a systematic review," *Journal of Dental Research*, vol. 91, no. 3, pp. 242–248, 2012.
- [36] D. N. Tatakis, H. H. Chien, and A. O. Parashis, "Guided implant surgery risks and their prevention," *Periodontology 2000*, vol. 81, no. 1, pp. 194–208, 2019.
- [37] M. Degidi, D. Nardi, G. Daprile, and A. Piattelli, "Nonremoval of immediate abutments in cases involving subcrestally placed postextractive tapered single implants: a randomized controlled clinical study," *Clinical Implant Dentistry and Related Research*, vol. 16, no. 6, pp. 794–805, 2014.
- [38] M. Degidi, D. Nardi, and A. Piattelli, "One abutment at one time: non-removal of an immediate abutment and its effect on bone healing around subcrestal tapered implants," *Clinical Oral Implants Research*, vol. 22, no. 11, pp. 1303–1307, 2011.
- [39] J. Feine, S. Abou-Ayash, M. al Mardini et al., "Group 3 ITI Consensus Report: patient-reported outcome measures associated with implant dentistry," *Clinical Oral Implants Research*, vol. 29, Supplement 16, pp. 270–275, 2018.

Research Article

Monolithic and Minimally Veneered Zirconia Complications as Implant-Supported Restorative Material: A Retrospective Clinical Study up to 5 Years

Markel Diéguez-Pereira ¹, David Chávarri-Prado,¹ Alejandro Estrada-Martínez,¹ Esteban Pérez-Pevida,^{2,3} and Aritza Brizuela-Velasco¹

¹Department of Surgery and Medical-Surgical Specialties, Faculty of Medicine, University of Oviedo, Av. Julián Clavería 6, 33006 Oviedo, Spain

²Department of Surgery, Faculty of Medicine, University of Salamanca, Campus Miguel de Unamuno, 37007 Salamanca, Spain

³Faculty of Health Sciences, Miguel de Cervantes European University, C/Padre Julio Chevalier 2, 47012 Valladolid, Spain

Correspondence should be addressed to Markel Diéguez-Pereira; markeldieguez@hotmail.com

Received 3 September 2020; Revised 1 October 2020; Accepted 7 October 2020; Published 20 October 2020

Academic Editor: Paolo Pesce

Copyright © 2020 Markel Diéguez-Pereira et al. This is an open access article distributed under the Creative Commons Attribution License, which permits unrestricted use, distribution, and reproduction in any medium, provided the original work is properly cited.

Objective. Long-term clinical data on the success and complication rates of monolithic or minimally veneered zirconia implant-supported restorations are lacking. Hence, the purpose of this retrospective clinical study was to analyze the complications of monolithic or partially veneered zirconia implant-supported restorations up to 5 years follow-up. **Material and Methods.** Single crowns, bridges, and full-arch rehabilitations were included. The selection process was achieved by reviewing data from the prosthetic laboratory and excluding cases in which zirconium and full-ceramic coating restorations were used. A total of 154 restorations were included (82 monolithic and 72 with buccal ceramic stratification). All the complications encountered, and the solutions applied, were explained. **Results.** A total of 93 restorative units had a follow-up of between 24 and 60 months, and 61 restoration units had a follow-up of between 12 and 24 months. A total of 7 complications were encountered (14.58% of cases; 95.45% per prosthetic unit). The technical complication rate was 2.08% (one case of minor chipping in one prosthetic unit); regarding the mechanical complications, four decementations (8.33% of the cases) and two screw loosening (4.17% of the cases) were encountered. **Conclusions.** Considering the limitations of this study, it can be concluded that monolithic or partially veneered zirconia implant-supported restorations have a good clinical behavior during a follow-up period of up to 5 years.

1. Introduction

In the past, metal-ceramics have been the restorative material of choice for tooth- and implant-supported fixed prostheses [1]. Attempts to improve the esthetic properties of these materials led to the development of all-ceramics, either by combining a ceramic core and veneer or using a single monolithic block [2]. Feldspathic porcelain was introduced first; it has a high proportion of vitreous phase in its structure, resulting in good esthetic properties, but it is mechanically inadequate in some cases [2]. Later, the fracture resistance of ceramics was improved by increasing their crystalline phase content—lithium disilicates or zirconium

dioxide (ZrO_2)—which can be used as a ceramic core with feldspathic veneer or in monolithic form. Zirconium (Zr) is a periodic table metal with properties common to the group of metals in terms of resistance and optical and chemical behavior.

Restorations with a zirconia core and ceramic veneer are widely used with good clinical results for both teeth and implants [3, 4]. In addition to providing a survival similar to metal-ceramics, they have better esthetic properties. However, one of the most common complications is a minor veneer debonding or chipping, while extensive fractures of the structure are less common [3, 4]. Different strategies have been described to prevent this limitation of the material, such

as changing the structural design or using different sintering methods, but chipping remains a major problem [5, 6]. In recent years, a new type of zirconia with higher translucency has appeared; this can be used as a monolithic material without ceramic veneer, thus avoiding chipping [7, 8]. Despite the decrease in fracture resistance compared with the conventional zirconia core of prosthetic structures, its mechanical behavior is superior to metal-ceramic or zirconia ceramic restorations [9, 10]. Also, one of the main advantages of this material is the simplicity of the working process, which requires less preparation time by the laboratory technician and has a lower economic cost.

However, the upper-anterior region has higher esthetic demands, so a cut-back technique can be used on the buccal surface of the restorations to veneer feldspathic porcelain in this region. Even after adding this ceramic layer, the risk of chipping is lower, since it is only placed in nonfunctional areas [11].

Additionally, the increased use of computer-aided design and computer-aided manufacturing (CAD-CAM) technology has also improved the cost-benefit ratio. Another important factor when choosing this material is that it causes less wear on the opposing dentition than any other suitable restorative material [12, 13]. However, at present, there are not many clinical studies with a long follow-up period assessing the reliability of such material. Therefore, the aim of the present retrospective clinical study was to analyze the complications of implant-supported crowns, bridges, and full arches of monolithic or partially veneered zirconia.

The null hypothesis tested was that implant-supported crowns, bridges, and full-arches made of monolithic or partially veneered zirconia have high success rates (over 90%).

2. Materials and Methods

2.1. Data Collection. For this study, patients who consented to receive single crowns, bridges, and full-arch prostheses of monolithic or partially veneered zirconia from 2013 to May 2019 were reviewed. Patients of all ages and with different prosthetic needs at two different private clinics located in Bilbao and Vitoria (Spain) participated in the study (Table 1).

Implant placement and prosthetic protocols were carried out in the same clinical way by two skilled operators (MD and DC). Patients who underwent treatments with implant-supported prostheses ranging from single crowns to fixed partial dentures and full arches were included. Participant selection was conducted by reviewing the data of the clinic history of the patient and including those cases restored with monolithic zirconia and buccal ceramic-veneered zirconia restorations. The following data were considered: age, sex, number of prosthetic units, crowns or bridges, number of abutments and pontics, cantilever units, anterior or posterior, use of monolithic or partially veneered zirconia, zirconia trademark, use of an occlusal splint, time in mouth from placement to the last examination, mechanical and technical complications (screw loosening, decementation of the restoration, chipping, or fractures of the framework), and its solutions. The exclusion criteria were as follows: teeth-supported prosthesis, peri-implantitis in some of the implants that supported the prosthesis, implant-supported restorations

TABLE 1: Distribution of the restorations per patient's gender and age.

Age	Men	Women	Number of restorations
20s	2	0	3
30s	0	2	2
40s	4	4	14
50s	8	10	57
60s	10	3	51
70s	2	2	15
80s	0	1	12
Total	26	22	154

made of any material other than monolithic or buccal ceramic-veneered zirconia, and restorations which had not been cement-screw-retained.

2.2. Clinical Procedures. Tapered bone and tissue level Klockner implants were inserted (Soadco S.L., Escaldes Engordany, Andorra). The implant position was based on a previous prosthetic-guided planning and an exhaustive clinical and radiologic examination. All implant-supported restorations were planned to be hybrid cement-screw-retained. In all the cases, cone beam computed tomography (CBCT) images in combination with three-dimensional (3D) planning software were used (Carestream Dental LLC, Atlanta, USA). All implants were placed with an open flap procedure and following a drilling protocol according to the recommendations of the manufacturer.

A healing time of 8 weeks was applied. If guided bone regeneration procedures were carried out simultaneously to the implant placement, or primary stability values were not enough (insertion torque < 35 Ncm² or ISQ < 65), a healing time of 4 up to 6 months was maintained.

Once the implant was osseointegrated (ISQ values ≥ 70), prosthetic treatments were performed. The standard clinical procedure for placement of implant-supported prostheses with the one-step pick-up technique and with individual tray was applied. The obtained casts were scanned; next, the design was developed using the Trios software (3Shape Dental System, Copenhagen, Denmark) and later milled in acrylic material (Degos Dental GmbH, Regenstauf, Deutschland). These preliminary restorations served to check esthetics and occlusion. Then, the test result was sent back to the dental laboratory technician for rescanning and virtually superimposing onto the previous design using the same software (3Shape Dental System, Copenhagen, Denmark).

Finally, the final structure was milled in monolithic zirconia (Zahn Dental Labs, Melville, USA) according to the performed clinical modifications with a minimum thickness of 0.5 mm. If feldspathic porcelain would be added on the buccal side, a last intraoral test was achieved with the zirconia milled restoration with the buccal cut-back applied, and finally, it was sent back to the laboratory for finishing. All reconstructions were fabricated by the same dental technician in a private laboratory.

Before placing the restoration, a try-in occlusion check was performed. If any adjustment was done, restoration

was sent back to the laboratory for polishing. For single crowns, hybrid cement-screw retention with antirotational cementing abutments with at least 2 mm of gingival height was used. In bridges, and full arches, nonengaging titanium bases with 1 mm of gingival height and 3.5 mm of cementing surface (Soadco S.L., Escaldes Engordany, Andorra) were used for hybrid cement-screw-retained restorations.

The crowns were cemented on the abutment outside of the mouth with a Maxcem Elite™ Self-Etch, Self-Adhesive Resin Dental Cement (KerrHawe, Bioggio, Switzerland). Then, in all cases, restorations were screwed into the implant at 30 N/cm² according to the manufacturer's recommendations. The screw access hole was closed with flowable composite (Clearfil Majesty, Kuraray Europe, Hattersheim am Main, Deutschland).

Patients were followed up at one month, 6 months, and finally each year except in cases requiring more attention, for example, patients with periodontal diseases who need shorter periodic follow-ups (Figure 1).

In this routine recall sessions, clinical and radiographic examination with bitewings and periapical radiographs was performed, and mechanical (decementations or screw loosening) and/or technical complications (chipping or fractures) occurred were written in the clinic history.

Due to sample heterogeneity and the impossibility of performing analytical statistics, descriptive statistics were performed and all data were collected in an Excel file, and statistical analysis was performed with computerized software (STATA/SE version 13.1, Stata Corporation).

3. Results

The study analyzed 154 restorations, including 34 pontics and 8 cantilevers (82 monolithic zirconia and 72 partially veneered zirconia) in 48 patients (26 men and 22 women) between the ages of 20 and 83 (mean age 56.3 years) (Table 1), yielding 65 cases and a total of 112 implants. Follow-up periods varied from 12 months to 60 months.

Of these restorations, 80 were posterior, 16 anterior, and 58 full-arch. An overview of all included zirconia implant-supported restorations is given in Table 2.

The follow-up period ranged from 24 to 60 months for 93 prosthetic units and 12 to 24 months for 61 prosthetic units. A total of 7 complications occurred. Five of the complications occurred in the group with a follow-up from 24 to 60 months (94.62% of success rate per restoration and 76.19% per case), and the remaining two complications belonged to the group with a follow-up from 12 to 24 months (96.72% of success rate per restoration and 92.59% per case). There was a single case of minor chipping that occurred in one prosthetic unit out of all the placed with partially veneered zirconia, which was resolved by polishing the ceramic surface, as it was only a minor chipping without exposing the zirconia core.

Regarding mechanical complications, four decementations occurred, which were resolved by recementation; the screw loosened in two implant-supported splinted restorations, which were fixed by retightening the screws at 30 N/cm². All these complications are detailed in Table 3. All the success rates are shown in Table 4.

4. Discussion

This study investigated the complications of implant-supported crowns, bridges, and full arches of monolithic or partially veneered zirconia. The null hypothesis tested must be accepted for single crowns (anterior and posterior) and for posterior crowns when this group is analyzed in ratios per case.

This success rate is consistent with clinical studies such as that of Degidi et al., with 88.2% success rates in restorations placed on implants with conical abutments [14]. However, other similar clinical study related 98.4% of survival rate without any mechanical or technical complication [15]. The present study has a smaller sample size and similar follow-up periods than the first study and a longer follow-up period and a larger sample size than the second study cited. Moscovitch published a retrospective study with 600 implant-supported prosthetic units of monolithic or partially veneered zirconia with up to 68 months of follow-up and reported that one cement-retained restoration was lost to zirconia abutment fracture and replaced with a single screw-retained implant-supported zirconia restoration with a titanium base (99.83% success rate per prosthetic unit up to 68 months) [16]. The results in terms of the success of the present study agree with the results exhibited by Degidi et al. However, they found the wear of the occlusal surface as the main observed complication; on the other hand, they did not report any debonding of the restoration, because a cone-in-cone connection without cement was used. Other prospective studies in the literature reported success rates ranging between 91.1% and 98.5% and follow-up periods from 12 to 41 months [17, 18]. Regarding full-arch rehabilitations, one systematic review reported a success rate of 83.9% [19]. In this study, there were complications in 2/5 of full-arch implant-supported rehabilitations placed, resulting in 60% complication-free total cases. When considering the number of prosthetic units included in these full rehabilitations, the success rate changed to 81.03%.

In this study, only 4 of 49 patients that were rehabilitated with implant-supported FDPs used an occlusal splint. An occlusal splint was prescribed only in patients with bruxism and various joint and/or muscle disorders but not as a general measure to prevent restoration fracture.

Most studies published on zirconia describe ceramic-veneered restorations. The most commonly reported technical problem in these cases was a minor ceramic delamination or chipping. Nevertheless, it should be noted this chipping rate is very similar to that reported in the latest published reviews comparing this material with implant-supported metal-ceramic crowns [4]. This remains a significant problem, especially in bridges [3]. It almost disappeared after high translucency zirconia became available and enabled monolithic restorations with good esthetic results.

In all of the studied cases in this research, the restorative material in contact with opposing teeth was monolithic zirconia, since the feldspathic ceramic was only placed on the buccal surface of the upper teeth. The opposing teeth characteristics (natural teeth, restored teeth, or implants)



FIGURE 1: (a) Example of a single monolithic zirconia crown in 4.6. (b) Double full-arch monolithic zirconia rehabilitation. (c) 1.2-2.2 FDP made of monolithic zirconia with buccal porcelain veneered.

TABLE 2: Zirconia implant-supported restorations included.

Prosthetic restoration	Area	No. of cases	No. of restorations	No. of implants	No. of pontics and cantilevers	Monolithic	Partially veneered	Total
Single crowns	Posterior	35	35	35	-	33	2	39
	Anterior	4	4	4	-	0	4	
Fixed dental prostheses	Posterior	18	45	38	7	35	10	57
	Anterior	3	12	8	4	0	12	
Full-arch restoration	-	5	58	27	31	14	44	58
Total		65	154	112	42	82	72	154

TABLE 3: Complications encountered during follow-ups.

	Minor chipping		Decementation			Screw loosening	
Age	69	72	56	59	68	47	74
Gender	W	W	M	W	M	W	M
Affected teeth	1.1	1.4-2.5	2.4-2.5	1.6-1.4	2.4-2.6	3.6-3.7	4.6-4.7
Prosthetic design	Full arch	Full arch	FDP	FDP	FDP	FDP	FDP
Abutments/pontics	5/6	4/5	1/1	2/1	2/1	2/0	2/0
Cantilever	0	0	1 (mesial)	1 (distal)	1 (distal)	0	0
Buccal ceramic veneering	Yes	Yes	No	No	No	No	No
Occlusal splint	No	No	No	No	No	No	No
Complication time (months)	12	24	11	9	18	12	14
Follow-up time (months)	36	42	56	42	42	16	23
Solution	Polishing ceramic surface		Recementation			Retightening	

TABLE 4: Success rates per case and per restoration in all the prosthetic modalities studied.

	Success rate per case			Success rate per restoration		
	Total	Anterior	Posterior	Total	Anterior	Posterior
Single crown	100%	100%	100%	100%	100%	100%
FDP	76.19%	100%	72.22%	82.46%	100%	77.78%
Full arch	60%	-	-	81.03%	-	-
Total	89.23%	100%	90.57%	86.36%	100%	88.89%

were not selected as exclusion criteria to choose the final sample of the study, and this could be a limitation. However, when a prosthetic complication was detected, the opposing teeth were registered. In this sense, only one technical complication occurred—one case of minor chipping in a buccal feldspathic porcelain-veneered crown (tooth 1.1) on an upper full-arch implant-supported rehabilitation. In this case, the antagonist was a natural teeth arch without any restoration and with a mutually protected occlusal scheme with anterior guidance.

Regarding decementation and screw loosening, multiple factors could have affected: type of cement employed, size of the cementable abutment, passive fit of the restoration, and occlusal forces [20–22]. Nevertheless, all the decemented cases had a cantilever as a common factor (three of them were distal and the other one mesial), and this could be a possible cause of excessive load and leverage.

In respect of screw loosening, both cases observed were splinted posterior restorations. In theory, this could make the screw loosening more difficult. However, the higher difficulty to achieve passive fit in FDPs is well known. Hence, the lack of passive fit could have been the cause of this complication. However, a new screw loosening was not observed after retightening in successive recall sessions.

Another property of monolithic zirconia is its lower abrasion rate of the opposing tooth compared with other ceramics [12, 13]. In this regard, wear of the opposing dentition was not observed in any case at the follow-up sessions. Moreover, zirconia is highly biocompatible with adjacent tissues and presents lower bacterial adhesion than other restorative materials, resulting in a good response of periodontal and peri-implant soft tissues [23, 24]. In relation to this, no peri-implant disease was observed in any of the implant-supported restorations studied.

Furthermore, one medium- or long-term problem of monolithic zirconia is its low-temperature degradation (LTD) related to hydrothermal aging; this could cause the material to transform spontaneously from the metastable tetragonal phase to the monolithic phase. This change could affect the mechanical properties of zirconia. This initial phase transformation would facilitate that of adjacent particles because of the increase in the associated volume, thereby increasing stress in these grains and causing microcracking. Microcracks would create a path for water to penetrate the ceramic. The mechanism by which oral environmental factors (saliva, acids, temperature, moisture, and stress) affect the transformation rate is not yet clear [25]. Despite the effects of hydrothermal aging, the mechanical properties of this material are still superior to metal-ceramics and

zirconia-ceramics [26, 27]. Nevertheless, it is mandatory to avoid grinding of the surface of the monolithic zirconia restorations to prevent the formation of microcracks. In this sense, it is recommended to apply an optimal prosthetic planning and a try-in with a PMMA material that allows to make all necessary esthetic and occlusal adjustments in this trial. If minimal occlusal adjustments were made in the definitive restoration try-in, it would be sent back to the technician for further surface polishing.

The retrospective nature of the present study and the different observation periods are its main limitation.

5. Conclusions

Considering the limitations of this study, but taking into account the use of a high number of restorations, long follow-up, and use of the same working protocols, we could affirm that monolithic or partially veneered zirconia is a material with good clinical behavior on implant-supported restorations in follow-up periods of up to 5 years. However, although many *in vitro* studies have been conducted in this field, a greater number of clinical studies are needed with a longer follow-up period to confirm the results of the present study.

Data Availability

The data used to support the findings of this study are available from the corresponding author upon request.

Conflicts of Interest

The authors declare that there is no conflict of interest regarding the publication of this paper.

References

- [1] K. Tan, B. E. Pjetursson, N. P. Lang, and E. S. Y. Chan, “A systematic review of the survival and complication rates of fixed partial dentures (FPDs) after an observation period of at least 5 years,” *Clinical Oral Implants Research*, vol. 15, no. 6, pp. 654–666, 2004.
- [2] B. E. Pjetursson, I. Sailer, N. A. Makarov, M. Zwahlen, and D. S. Thoma, “All-ceramic or metal-ceramic tooth-supported fixed dental prostheses (FDPs)? A systematic review of the survival and complication rates. Part II: multiple-unit FDPs,” *Dental Materials*, vol. 31, no. 6, pp. 624–639, 2015.
- [3] B. E. Pjetursson, N. A. Valente, M. Strasding, M. Zwahlen, S. Liu, and I. Sailer, “A systematic review of the survival and complication rates of zirconia-ceramic and metal-ceramic

- single crowns,” *Clinical Oral Implants Research*, vol. 29, Supplement 16, pp. 199–214, 2018.
- [4] I. Sailer, M. Strasding, N. A. Valente, M. Zwahlen, S. Liu, and B. E. Pjetursson, “A systematic review of the survival and complication rates of zirconia-ceramic and metal-ceramic multiple-unit fixed dental prostheses,” *Clinical Oral Implants Research*, vol. 29, Supplement 16, pp. 184–198, 2018.
- [5] M. Rosentritt, D. Steiger, M. Behr, G. Handel, and C. Kolbeck, “Influence of substructure design and spacer settings on the in vitro performance of molar zirconia crowns,” *Journal of Dentistry*, vol. 37, no. 12, pp. 978–983, 2009.
- [6] J. P. Tan, D. Sederstrom, J. R. Polansky, E. A. McLaren, and S. N. White, “The use of slow heating and slow cooling regimens to strengthen porcelain fused to zirconia,” *The Journal of Prosthetic Dentistry*, vol. 107, no. 3, pp. 163–169, 2012.
- [7] F. Beuer, M. Stimmelmayer, J. F. Gueth, D. Edelhoff, and M. Naumann, “In vitro performance of full-contour zirconia single crowns,” *Dental Materials*, vol. 28, no. 4, pp. 449–456, 2012.
- [8] Y. Zhang, H. Chai, J. J. W. Lee, and B. R. Lawn, “Chipping resistance of graded zirconia ceramics for dental crowns,” *Journal of Dental Research*, vol. 91, no. 3, pp. 311–315, 2011.
- [9] A. Brizuela-Velasco, M. Diéguez-Pereira, Á. Álvarez-Arenal et al., “Fracture resistance of monolithic high translucency zirconia implant-supported crowns,” *Implant Dentistry*, vol. 25, no. 5, pp. 624–628, 2016.
- [10] Y. Zhang, Z. Mai, A. Barani, M. Bush, and B. Lawn, “Fracture-resistant monolithic dental crowns,” *Dental Materials*, vol. 32, no. 3, pp. 442–449, 2016.
- [11] C. W. Cheng, C. H. Chien, C. J. Chen, and P. Papaspyridakos, “Complete-mouth implant rehabilitation with modified monolithic zirconia implant-supported fixed dental prostheses and an immediate-loading protocol: a clinical report,” *The Journal of Prosthetic Dentistry*, vol. 109, no. 6, pp. 347–352, 2013.
- [12] J. W. Choi, I. H. Bae, T. H. Noh et al., “Wear of primary teeth caused by opposed all-ceramic or stainless steel crowns,” *The Journal of Advanced Prosthodontics*, vol. 8, no. 1, pp. 43–52, 2016.
- [13] U. Lohbauer and S. Reich, “Antagonist wear of monolithic zirconia crowns after 2 years,” *Clinical Oral Investigations*, vol. 21, no. 4, pp. 1165–1172, 2017.
- [14] M. Degidi, D. Nardi, S. Gianluca, and A. Piattelli, “The conometric concept: a 5-year follow-up of fixed partial monolithic zirconia restorations supported by cone-in-cone abutments,” *The International Journal of Periodontics & Restorative Dentistry*, vol. 38, no. 3, pp. 363–371, 2018.
- [15] A. Worni, J. Katsoulis, L. Kolgeci, M. Worni, and R. Mericske-Stern, “Monolithic zirconia reconstructions supported by teeth and implants: 1- to 3-year results of a case series,” *Quintessence International*, vol. 48, no. 6, pp. 459–467, 2017.
- [16] M. Moscovitch, “Consecutive case series of monolithic and minimally veneered zirconia restorations on teeth and implants: up to 68 months,” *The International Journal of Periodontics & Restorative Dentistry*, vol. 35, no. 3, pp. 315–323, 2015.
- [17] C. W. Cheng, C. H. Chien, C. J. Chen, and P. Papaspyridakos, “Clinical results and technical complications of posterior implant-supported modified monolithic zirconia single crowns and short-span fixed dental prostheses: a 2-year pilot study,” *Journal of Prosthodontics*, vol. 27, no. 2, pp. 108–114, 2018.
- [18] C. W. Cheng, C. H. Chien, C. J. Chen, and P. Papaspyridakos, “Randomized controlled clinical trial to compare posterior implant-supported modified monolithic zirconia and metal-ceramic single crowns: one-year results,” *Journal of Prosthodontics*, vol. 28, no. 1, pp. 15–21, 2019.
- [19] A. S. Bidra, P. Rungruanant, and M. Gauthier, “Clinical outcomes of full arch fixed implant-supported zirconia prostheses: a systematic review,” *European Journal of Oral Implantology*, vol. 10, Supplement 1, pp. 35–45, 2017.
- [20] M. Emms, C. J. Tredwin, D. J. Setchell, and D. R. Moles, “The effects of abutment wall height, platform size, and screw access channel filling method on resistance to dislodgement of cement-retained, implant-supported restorations,” *Journal of Prosthodontics*, vol. 16, no. 1, pp. 3–9, 2007.
- [21] D. A. Covey, D. K. Kent, H. A. St. Germain Jr., and S. Koka, “Effects of abutment size and luting cement type on the uniaxial retention force of implant-supported crowns,” *The Journal of Prosthetic Dentistry*, vol. 83, no. 3, pp. 344–348, 2000.
- [22] J. Katsoulis, T. Takeichi, A. Sol Gaviria, L. Peter, and K. Katsoulis, “Misfit of implant prostheses and its impact on clinical outcomes. Definition, assessment and a systematic review of the literature,” *European Journal of Oral Implantology*, vol. 10, Supplement 1, pp. 121–138, 2017.
- [23] F. Zarone, S. Russo, and R. Sorrentino, “From porcelain-fused-to-metal to zirconia: clinical and experimental considerations,” *Dental Materials*, vol. 27, no. 1, pp. 83–96, 2011.
- [24] H. Y. Kim, I. S. Yeo, J. B. Lee, S. H. Kim, D. J. Kim, and J. S. Han, “Initial in vitro bacterial adhesion on dental restorative materials,” *The International Journal of Artificial Organs*, vol. 35, no. 10, pp. 773–779, 2018.
- [25] K. Nakamura, A. Harada, T. Kanno et al., “The influence of low-temperature degradation and cyclic loading on the fracture resistance of monolithic zirconia molar crowns,” *Journal of the Mechanical Behavior of Biomedical Materials*, vol. 47, pp. 49–56, 2015.
- [26] D. P. Lameira, W. A. B. Silva, F. A. Silva, and G. M. de Souza, “Fracture strength of aged monolithic and bilayer zirconia-based crowns,” *BioMed Research International*, vol. 2015, Article ID 418641, 7 pages, 2015.
- [27] G. K. R. Pereira, T. Silvestri, M. Amaral, M. P. Rippe, C. J. Kleverlaan, and L. F. Valandro, “Fatigue limit of polycrystalline zirconium oxide ceramics: effect of grinding and low-temperature aging,” *Journal of the Mechanical Behavior of Biomedical Materials*, vol. 61, pp. 45–54, 2016.

Research Article

Finite Element Method and Von Mises Investigation on Bone Response to Dynamic Stress with a Novel Conical Dental Implant Connection

Luca Fiorillo ¹, Marco Ciccù ¹, Cesare D'Amico ¹, Rodolfo Mauceri ²,
Giacomo Oteri ¹ and Gabriele Cervino ¹

¹Department of Biomedical and Dental Sciences, Morphological and Functional Images, University of Messina, Policlinico G. Martino, Via Consolare Valeria, 98100 Messina, Italy

²Department of Surgical Oncological and Oral Sciences, University of Palermo, 90127 Palermo, Italy

Correspondence should be addressed to Luca Fiorillo; lucafiorillo@live.it

Received 14 July 2020; Revised 14 August 2020; Accepted 24 August 2020; Published 8 October 2020

Guest Editor: Paolo Pesce

Copyright © 2020 Luca Fiorillo et al. This is an open access article distributed under the Creative Commons Attribution License, which permits unrestricted use, distribution, and reproduction in any medium, provided the original work is properly cited.

The bioengineering and medical and biomedical fields are ever closer, and they manage to obtain surprising results for the development of new devices. The field of simulations and studies in silica has undergone considerable development in recent years, favoring the advancement of medicine. In this manuscript, a study was carried out to evaluate the force distribution on the implant components (In-Kone® Universal) and on the peri-implant tissues subjected to loading. With the finite element analysis and the Von Mises method, it was possible to evaluate this distribution of forces both at 0 degrees (occlusal force) and at 30 degrees; the applied force was 800 N. The obtained results on this new type of connection and on all the implant components are satisfactory; the distribution of forces appears optimal even on the peri-implant tissues. Surely, studies like this help to obtain ever more performing devices, improving both the clinic and the predictability of rehabilitations.

1. Introduction

The finite element technique, also known with the acronym FEM (finite element method) has historically established itself for the study of structural phenomena related to stiffness, strength, and elastic stability of bodies. Thanks to the experience gained over the years, manufacturers are able to perform structural calculations on complete machines, boats, cars, aeronautical structures, consumer goods, and industrial plants. Modeling and computational analysis are giving medical engineering a significant competitive advantage by reducing risks, lowering costs, and accelerating innovation [1–5]. FEM analysis is a computer simulation technique applicable to many engineering sectors. The FEM analysis allows to describe a real system accurately and reliably, in order to obtain the physical quantities of interest [6–12]. Depending on the applications, these quantities could be displacements, temperatures, stresses, deformations, electric/

magnetic fields, pressure, etc. The advantage of integrating FEM analysis into the design method lies in the possibility of studying complex physical phenomena that could otherwise be addressed with an experimental approach, more expensive. FEM allows us to identify any problems before the prototype is even made and therefore to review the design quickly and economically. In addition to identifying malfunctions, with FEM, it is possible to optimize a structure by removing excess material and improving weight distribution. Applied to fluid dynamics, the same methodology allows to limit pressure and flow losses by refining the profiles of grids, fans, and pipes. In most biomechanical finite element analyses, the linear elastic behavior of biological tissues is assumed [13, 14].

The analyst's true ability lies in building a model that simulates reality well without exceeding in the finesse of discretization in points of little structural interest and in identifying the constraints and loads that reflect the physics of the



FIGURE 1: Reverse engineering of prostheses.

problem. The application of this method therefore requires a good basic theoretical knowledge that allows a targeted choice of the elements to be used, in relation to the analysis to be conducted, and a critical interpretation of the results obtained in light of the limitations and approximations of the method. It is also necessary to pay constant attention to experimental analyses that allow validating the hypothesized approximations. The bioengineering and biomedical investigations are of great help in the prosthetic field and especially in the dental field [7, 15]. Considerable studies have been conducted to evaluate the stress of dental implants on the different biomechanical forces present in the oral cavity.

Stages of the realization of a finite element model are as follows:

(i) Preparation of the geometric model

- (ii) Discretization of the entire volume in finite elements (tetrahedra or parallelepipeds)
- (iii) Assignment of the mechanical properties of the materials
- (iv) Identification of loads and constraint points
- (v) Choice of the type of solution (static or dynamic analysis, linear or nonlinear, etc.)
- (vi) Analysis of the results [16, 17]

The aim of this study is to evaluate the biomechanical behavior of the In-Kone® dental implant connection. This device has been studied under the action of the mandibular force that is exercised during chewing cycles. The study was divided into three steps:



FIGURE 2: Acquisition of missing measures from the real component.

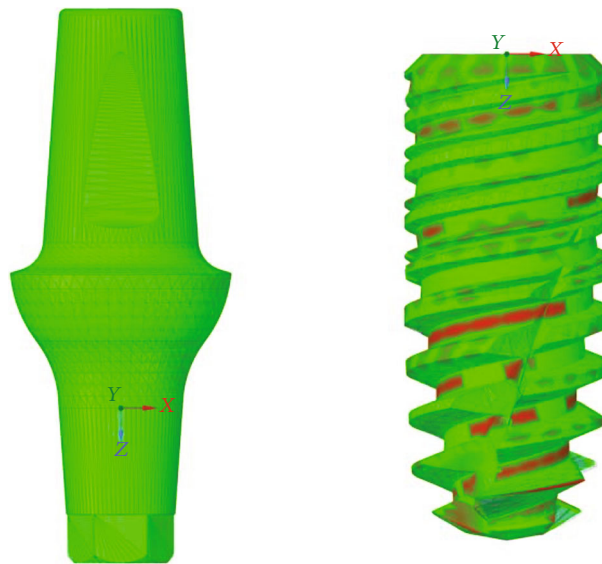


FIGURE 3: Maximum deviation equal to 0.09 mm of the CAD with respect to the STL.

TABLE 1: Properties of the tested materials.

Properties	Cortical bone	Cancellous bone	Ti6Al4V
Density	1.8 g/cm ³	1.2 g/cm ³	4.510 g/cm ³
E _{xx}	9.6 GPa	0.144 GPa	105 GPa
E _{yy}	9.6 GPa	0.099 GPa	105 GPa
E _{zz}	17.8 GPa	0.344 GPa	105 GPa
v _{xx}	0.55	0.23	0.37
v _{yy}	0.30	0.11	0.37
v _{zz}	0.30	0.13	0.37
G _{xx}	3.10 GPa	0.053 GPa	38.32 GPa
G _{yy}	3.51 GPa	0.063 GPa	38.32 GPa
G _{zz}	3.51 GPa	0.045 GPa	38.32 GPa

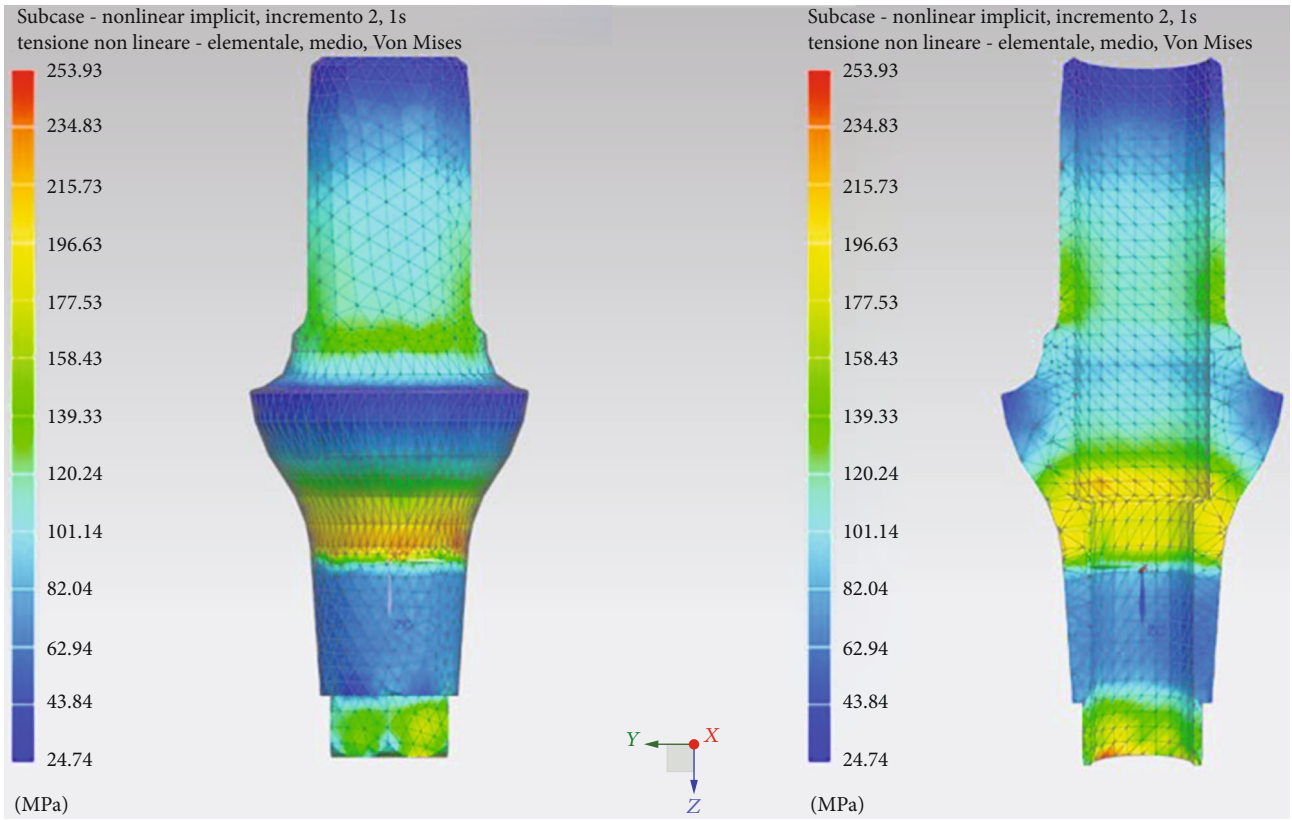
E: elasticity module; *G*: tangential elasticity module, *v*: Poisson coefficient; each module is reflected in the three space directions.

- (i) The first step was the reverse engineering of the prosthesis, which allowed the transformation of a STL scan into a three-dimensional CAD model
- (ii) The second step was the creation of the mechanical model, with applications of the boundary conditions of loads and constraints
- (iii) Finally, results on mechanical behavior are obtained, i.e., on the distribution of stresses in the three prosthodontics [18–20]

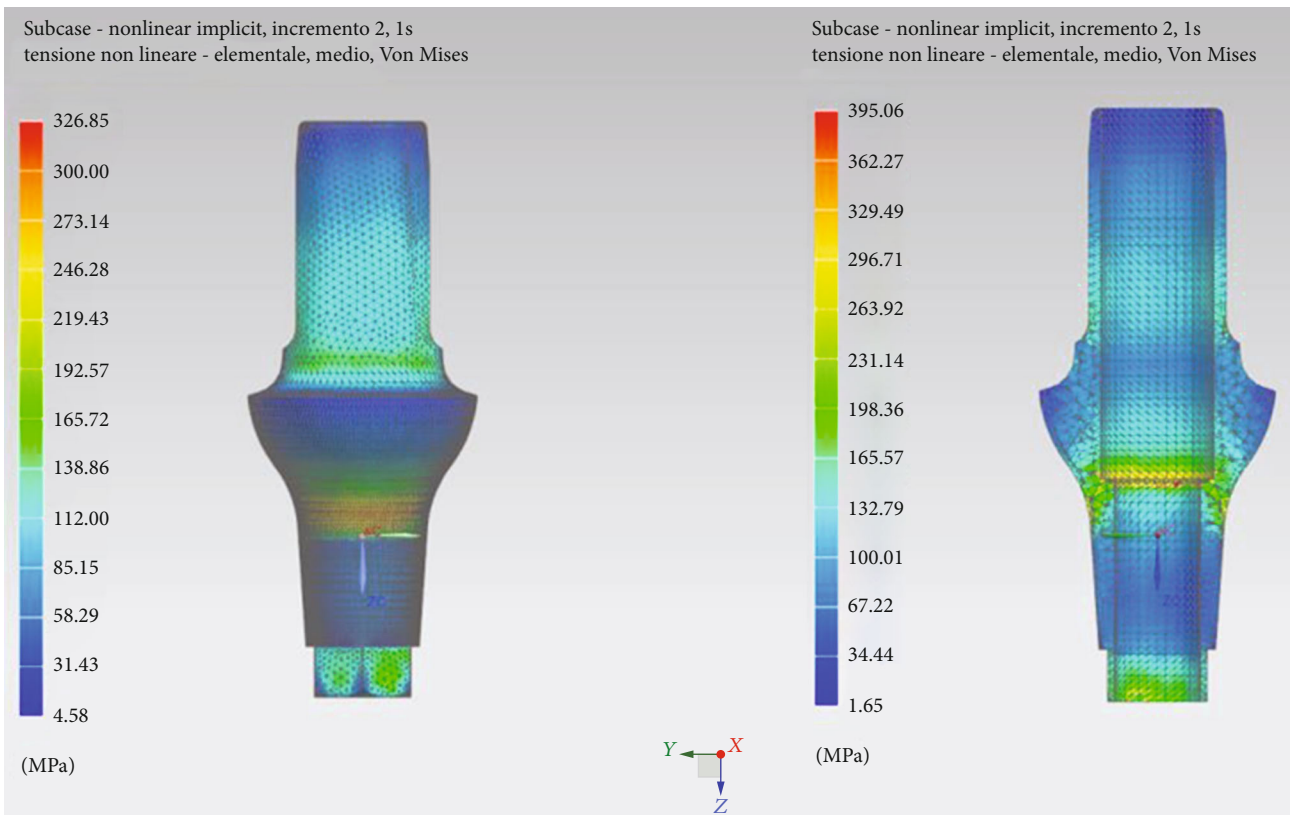
The null hypothesis was assumed that there are no clinical differences between in silica studies and in vivo conditions.

2. Materials and Methods

The first step in setting up the FEM was to perform Reverse reverse Engineering engineering of the In-Kone® Universal



(a)



(b)

FIGURE 4: Continued.

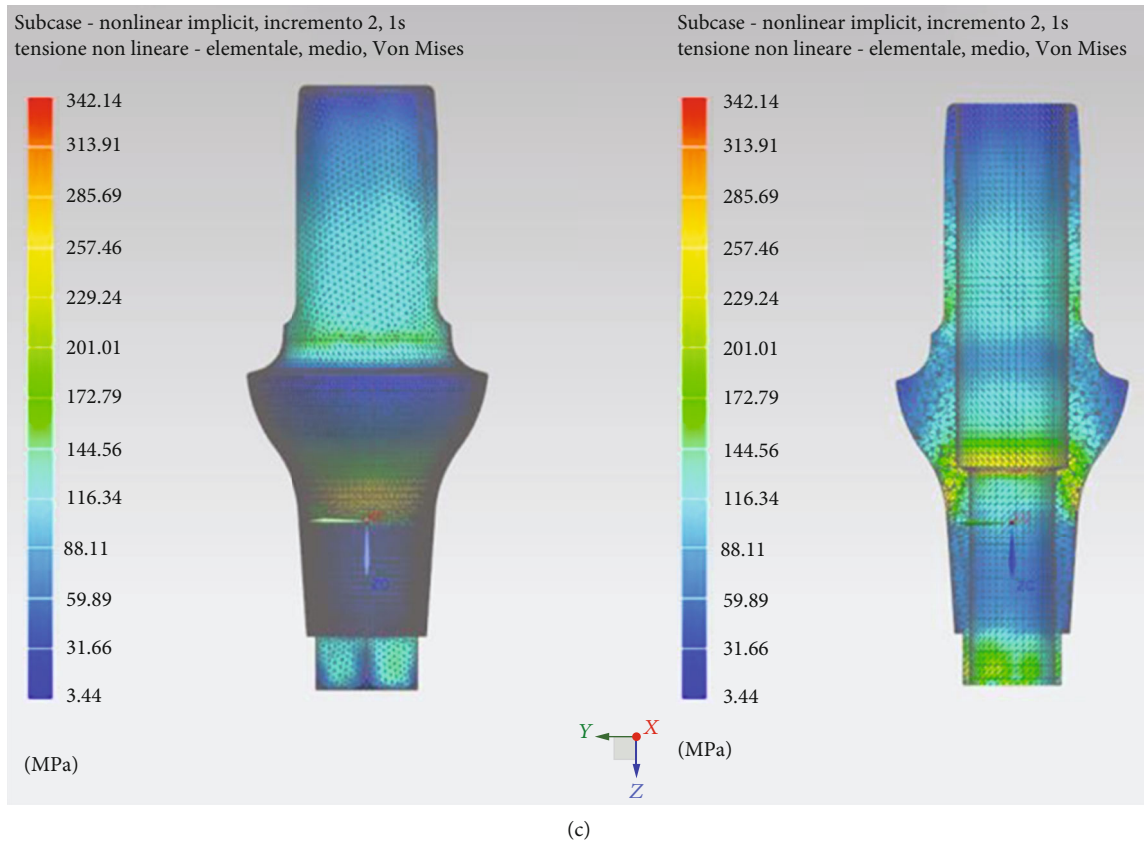


FIGURE 4: Mesh sensitivity study 0.4 mm elements (a), 0.2 mm (b), and 0.1 mm (c).

TABLE 2: Comparison values between the various dimensions of the element.

Element size (mm)	Stress (MPa)	Error (%)
0.1	342.14	/
0.2	326.85	4.47
0.3	299.42	12.49
0.4	274.42	19.79
0.5	253.93	25.78

prosthesis so as to obtain a CAD CAD-type file from the STL source file, and finally, a rendering was done on the CAD reconstructed through the Keyshot® software.

The missing measurements were acquired using a digital microscope on the prosthesis from the real. The supplied STLs have a low resolution as can be seen in Figure 1; moreover, the retention screw did not respect the real dimension measured through a gauge on the piece from the truth. This difficulty has been overcome by reconstructing the geometry of this component through the use of a digital microscope. In Figure 2, there is an example of measurements taken on the real pieces, which were missing in the STL files.

The reverse was carried out maintaining maximum deviations with respect to the geometry of the STL file of the order of a tenth of a millimeter (Figure 3).

Figure 1 shows reverse engineering and a sagittal section, along the y axis, and rendering of the three components.

The FEM simulation was performed through the Siemens NX Nastran® software. The properties of the materials have been specified in terms of Young’s modulus, Poisson’s ratio, and density. In particular, the titanium alloy Ti6Al4V was considered homogeneous, linear, and isotropic, while the cortical and cancellous bone tissues were considered as orthotropic (Table 1). The data obtained in the literature were used as mechanical characteristics of the materials.

The mesh was made with 4-node solid tetrahedral elements, of the CTETRA 4 type; this allows considerable computational resource savings compared to the 10-node tetrahedral. The cell size fell on 0.2 mm elements. This value was chosen after performing the convergence analysis of the mesh (Figure 4).

This study makes it possible to find the right compromise between simulation calculation speed and reliable stress values. As the size of the elements changes, the stress converges to a value that remains stable even at 0.2 mm. In Table 2, it is possible to observe the estimated error taking as a reference to the element size of 0.1 mm.

The chosen value of 0.2 mm induces a 4.47% error on the stress value, which can be considered an acceptable compromise as less than 5%.

Figure 5 shows the prosthesis mesh implanted on a parallelepiped (the latter mechanically characterized as cortical and cancellous bone tissue), with an element size of 0.2 mm.

2.1. Zero-Degree Boundary Conditions. The boundary conditions of the system concern the application of the preload

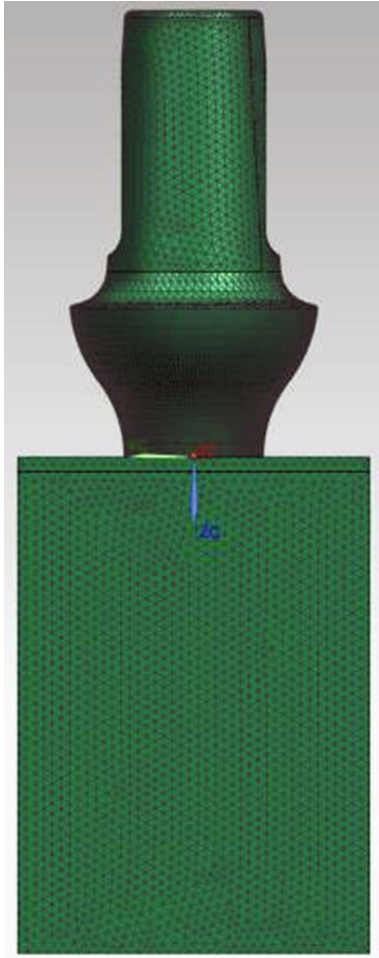


FIGURE 5: Prosthetic mesh.

force of the internal tightening screw and of the maximum chewing force on the prosthetic stump. The force value of the preload 430 N is relative to a tightening torque of 15 Ncm. This force was calculated through the following empirical formula:

$$M = KDP, \quad (1)$$

where M is the tightening torque (expressed in Nmm), K is a global coefficient that takes into account the friction coefficients on the thread, diameter, and pitch of the screw (in the case under examination, it is equal to 0.2), D is the diameter of the thread (expressed in mm), and P is the axial preload applied to the screw (expressed in N). To model the clamping force, the practical NX Nastran[®] tool was used to apply this force to the 3D bolt or screw model. Its functioning is easy to understand; at the beginning of the simulation, the software first applies the preload force gradually up to the maximum value, then applies the remaining load acting on the model [15, 21, 22]. Figure 6 shows the section of the internal screw with the traction forces applied by the preload on the geometry.

The second force applied to the model is a compression force, equal to 800 N, equally reparted on the apex of the

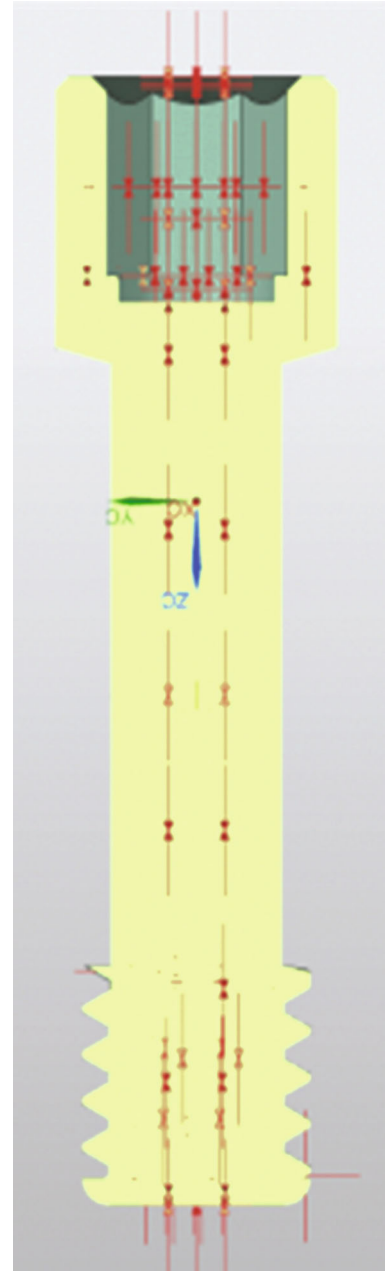


FIGURE 6: Preload on a screw.

prosthesis. It stimulates the jaw force. The two forces are applied along the y axis (Figure 7).

The contacts between the various parts were modeled with nonlinear contact functions. The conditions of contact between bone and prosthesis were considered as “bonded,” to simulate a perfect osseointegration, and therefore a mechanical continuity. As for the contact between the metal surfaces of the prosthesis, they were considered as separate surfaces and in the presence of friction, with a value of the friction coefficient equal to 0.3. The outer surfaces of the bone block have been fixed.

2.2. 30-Degree Boundary Conditions. The boundary conditions are the same as in the previous report, i.e., a tightening

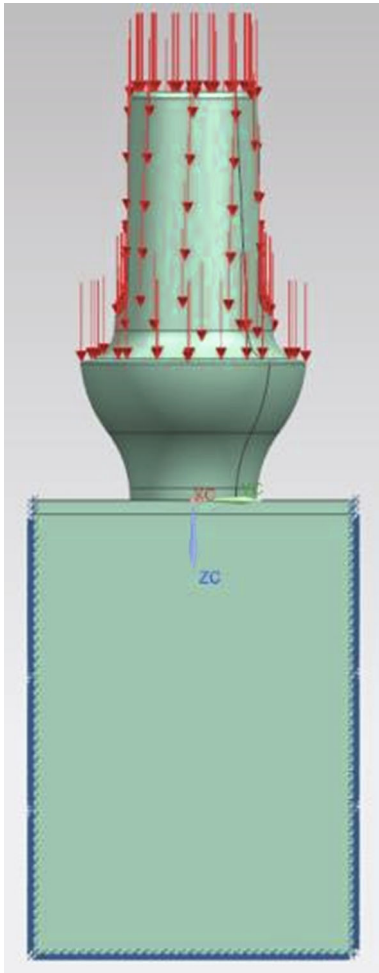


FIGURE 7: Loading and constraint conditions.

preload on the screw, the constraints, and the same mesh size. The difference is in the direction of application of the load (800 N); indeed, it has an angle of 30° with respect to the vertical axis z (Figure 8).

The material of the dental prosthetic retention and the contacts are the same as in the previous paragraph.

3. Results

3.1. Zero-Degree Boundary Conditions. The use of finite element analysis allows the evaluations of the stresses that arise in the bone after a prosthetic implant. To perform a correct simulation, the reverse engineering phase is of fundamental importance. The geometric modeling of the prosthesis allows a correct setting of the contacts and frictions and therefore the interactions between the various components of the prosthesis. Another important factor is the inclusion of operating parameters such as the model of the bone tissue material, the preloading of the tightening screw, and the osseointegration of the implant. In Table 3, the maximum equivalent stress value of Von Mises recorded in the prosthesis during the masticatory cycle was inserted. As it is possible to see, the prosthesis reaches a maximum value lower than the titanium yielding stress, thus avoiding plasticization phenomena of

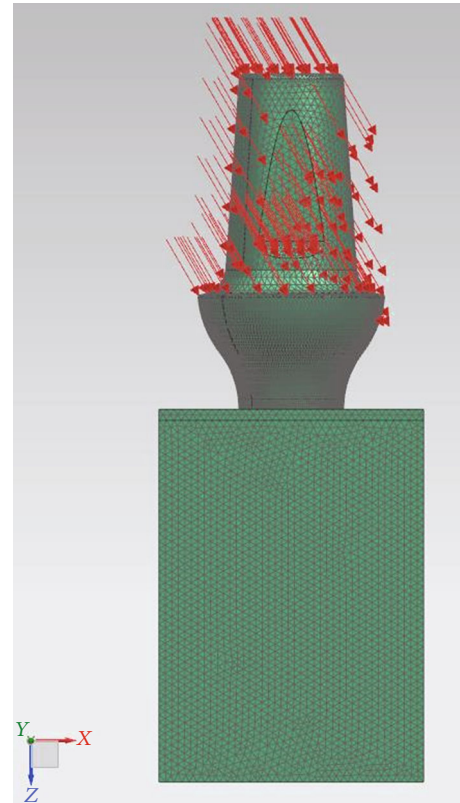


FIGURE 8: Load direction.

the material and above all the static breaking of the prosthesis.

Instead, the values of the stresses acting in the bone tissue are reported. It is possible to see that the maximum stress values are below the static resistance of the bone. In Table 3, instead, the values of the stresses acting in the bone tissue are reported. It is possible to see that the maximum stress values are the static resistance of the bone.

In Figure 9, the trends of the equivalent Von Mises stresses in cancellous and cortical bone tissue are reported. It is possible to see how the distribution of stresses in the bone is located around the implant where the maximum tension is recorded in the cortical bone. With regard to the cancellous bone tissue, the tensions are lower and their distribution on the whole contact surface is generally homogeneous.

Figure 10 shows the equivalent Von Mises stresses in detail for each component and its sagittal section. The most stressed components of the entire prosthetic device are the internal tightening screws, with the most stressed areas located at the contact interface between the head of the screw itself and the hole of the abutment; the highest value is recorded in the threaded area in particular in the first fillets. As for the bone implant, here too the distribution is greater in the first three threads.

3.2. 30-Degree Boundary Conditions. The use of finite element analysis has allowed to evaluate the stresses that arise in the bone after a prosthetic implant. The extreme operating conditions, due to the force applied at 30° , produce a high

TABLE 3: The maximum stress Von Mises and Von Mises tension in bone tissue.

	Maximum stress value (MPa)	Static resistance of titanium (MPa)	%
In-Kone® Universal	471.25	1020	53.8%
	Maximum tension on bone tissue (MPa)	Static bone resistance (MPa)	%
In-Kone® Universal	143.19	180	20.45%

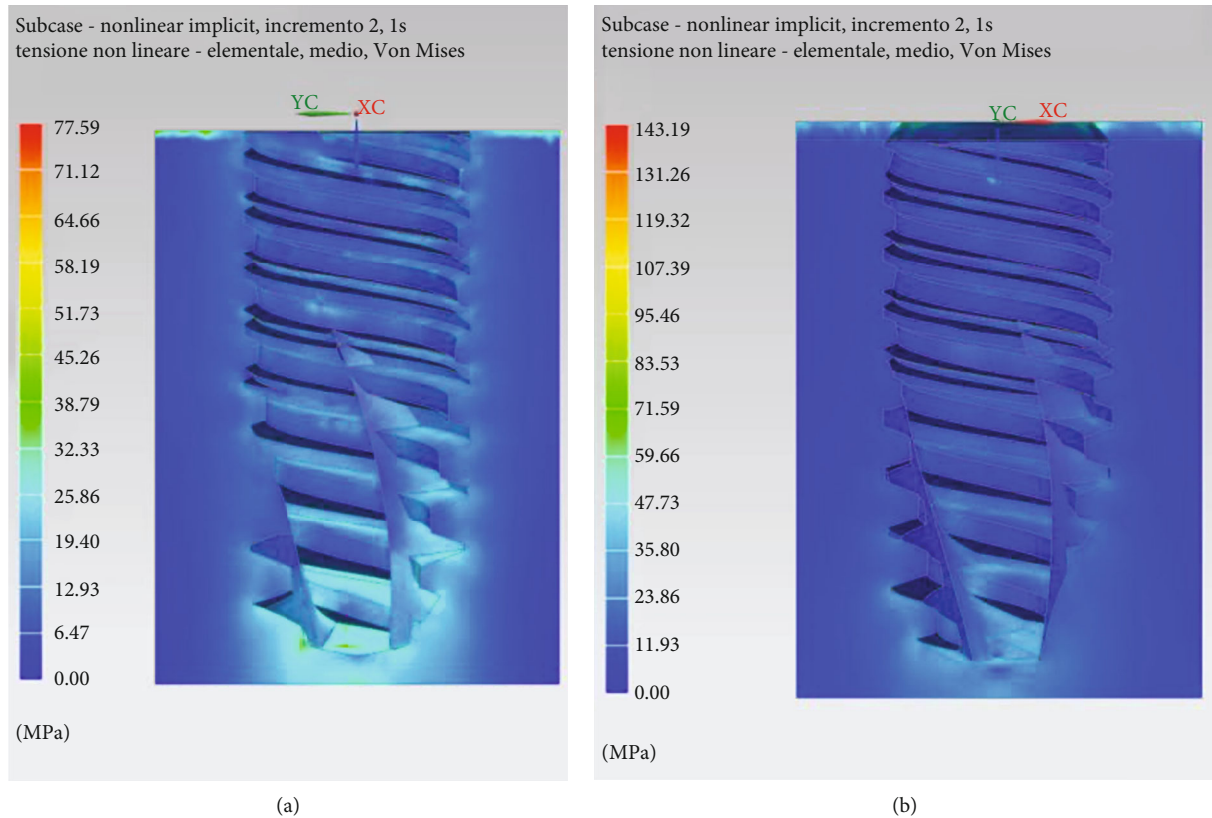


FIGURE 9: Distribution of stress in cancellous (a) and cortical/cancellous bone tissue. In this second case, two types of bone with different features have been considered (b).

concentrated stress on the side of the implant, but always remaining within at about the 90% of the yield condition. This condition is unlikely to happen during the masticatory cycle, but it is convenient to take this into account for precautionary purposes, since its dangerousness. In Table 4, the maximum equivalent stress value of Von Mises was compared with the static resistance value.

In Table 4, the maximum values of the stresses acting on the bone are reported.

In Figures 11(a) and 11(b), the trends of Von Mises stress in the cancellous bone tissue are reported. In particular, it is worth considering the trend of the stresses on the xy plane and the sagittal section on the zx plane. The stress distribution is influenced by the applied load.

Figures 11(c) and 11(d) shows the stress patterns in cancellous and cortical bone tissue.

Figure 12 shows the Von Mises stresses in detail for each component and its sagittal section. In this case, the most stressed part is the side of the upper abutment, where a lever arm acts that concentrates the stresses.

4. Discussion

Finite element analysis (FEM) is a technique that virtually reproduces, from a physical-mechanical point of view, a real condition for studying the interaction between different objects and predicting their mutual behavior under certain load conditions and stress. It is a technique that derives from engineering and is still applied to many fields of the mechanical and aeronautical industry and also in the biomedical sector. Normally, this type of analysis, given its difficulty, is limited to biomedical devices before their industrial production to verify their mechanical properties in relation to their shape. There are various typologies of prosthesis: these are examined by FEM before their production to verify their correspondence with the biomechanical criteria that they must face once implanted [16, 23]. However, the use of FEM has gradually expanded also in the medical sector for the study of mechanically active anatomical parts. Among the applications of finite element analysis in medicine, the simulation of the opening of endovascular stents and the simulation of loads on an orthopedic prosthesis could be made.

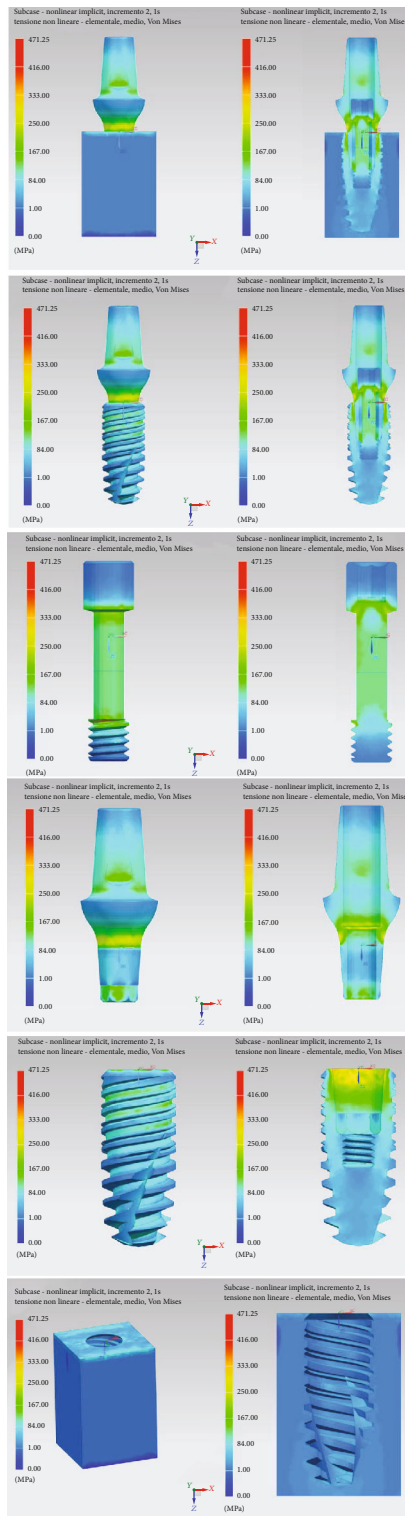


FIGURE 10: Von Mises tension results in detail.

The study conducted on this novel dental implant connection therefore includes an analysis of the forces with a load of 800 N at 0 and 30 degrees of angulation, as shown in Figure 12. It is evident however that from the first experiment, the occlusal load provides a release of forces in the apical area of the dental implant, on the medullary

bone. In the peri-implant cortex, the distribution of forces appears uniform, without reaching point peaks around the neck of the dental implant. The same applies to the implant components, where the forces are discharged more on the neck of the abutment and on the first turns of the passant screw. In the second experiment, while there are no important differences in the medullary bone, on the cortex this occurs, showing peaks around the neck of the dental implant based on the orientation of the mechanical load, the same is also reflected on the prosthetic components, showing a peak on the hexagon of the abutment and on the neck of the abutment.

Different studies have been conducted using this method on dental implants and implant connections. Based on Kitagawa et al. [24] in comparing different connections, it was found that the external hexagonal joint model had a greater movement than the conical connection model. The external hexagonal model showed a rotation movement, while the movement of the conical connection model showed no rotation. It was concluded that the nonlinear dynamic analysis used in this study clearly demonstrated the rotation differences of the components in dental implant systems with tapering or external hexagonal connections. According to Pournasrollah et al. [25], screw loosening is less likely to occur in the morse hexagonal connection compared to the octagon connection due to the lack of separation of the screw from the internal surface of the abutment.

In the literature, there is a good amount of material that reports FEM studies also carried out in dentistry as an evaluation of the mechanical response of the dental elements subjected to loads of various kinds. In the biomechanical field, the distribution of voltage is analyzed with particular attention, both in biological structures to see how the coupling with an artificial structure (e.g., prosthesis and implant) changes their structural response to external stresses and in artificial structures for check its resistance. The identification in a structure of the distribution and extent of the tensions is important as it highlights which areas are most stressed and therefore most at risk of breaking or, in the case of biological tissues, of necrosis or hypertrophy and which are the areas less stressed which, in the case of biological tissues, could induce atrophy [26–30]. It is necessary to consider that the insertion of implants in the maxillary bones always requires a high precision surgical event, which must be conducted taking into consideration the prosthetic rehabilitation of our patient. Often, the bone or tissue conditions of the jaws do not allow an ideal insertion, and in this case, it may be necessary to conduct further regenerative maneuvers [31, 32]. The innovativeness of this study lies mainly in the fact that all the implant-prosthetic components were evaluated, with a force of 800 N and different angles. The strength of 800 N was taken into consideration following a literature review of previous FEM studies. Furthermore, testing different angles has the purpose of simulating closely the biological conditions created in vivo during chewing. Different studies conducted by Cicciù et al. [1, 15, 22, 33, 34] confirmed the widespread use of finite element methods for calculating the distribution of forces in oral and implant-supported and nonsupported rehabilitations. Knowing the distribution of forces on the

TABLE 4: The maximum stress of Von Mises at 30 degrees.

	Maximum equivalent stress (MPa)	Static resistance of titanium alloy (MPa)	%
In-Kone® Universal	936.93	1020	91.8%
	Maximum equivalent tension value on bone tissue (MPa)	Static bone resistance (MPa)	%
In-Kone® Universal	162.52	180	90.3%

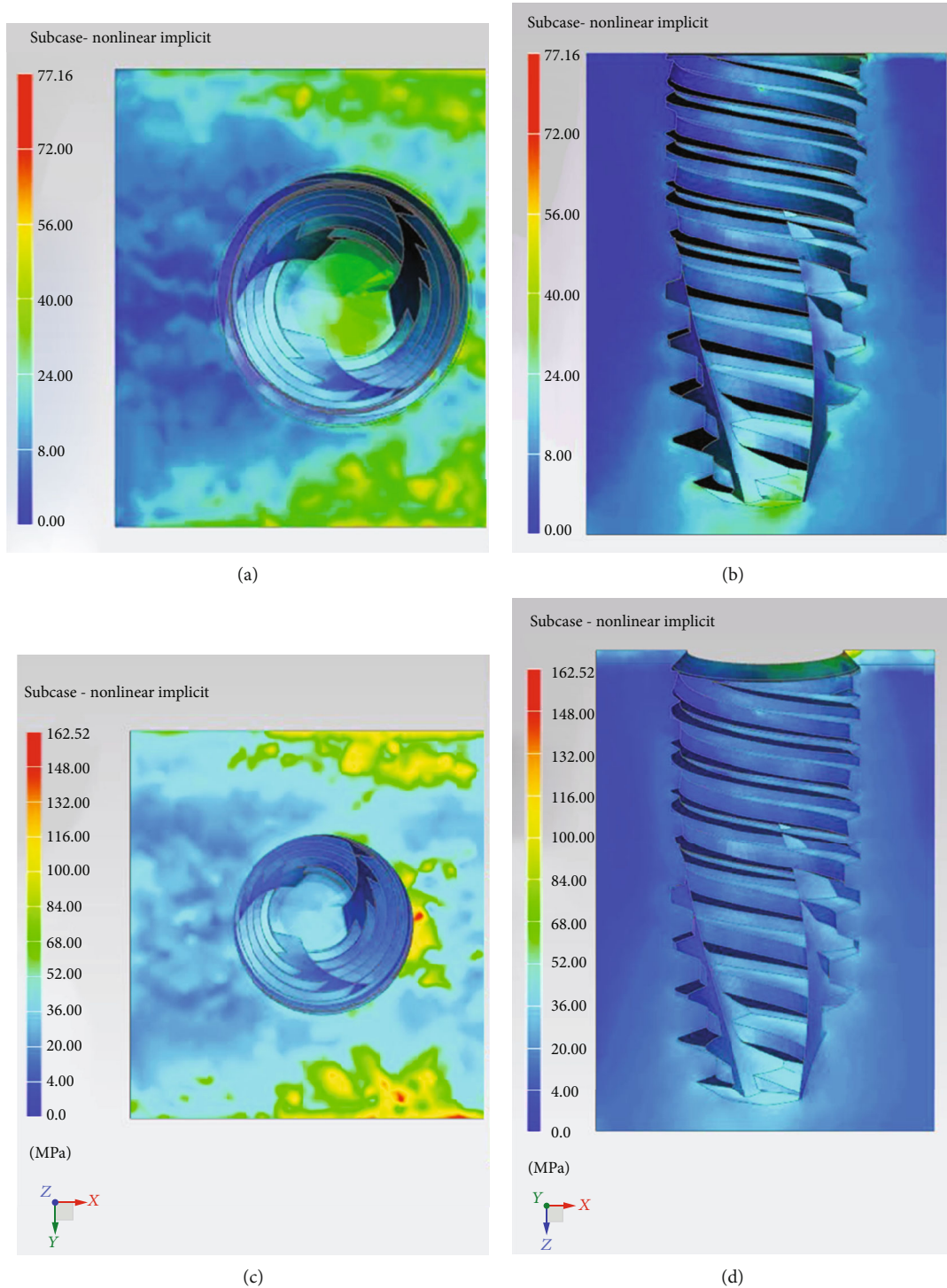


FIGURE 11: Distribution of stresses in cancellous bone (a, b) and cortical bone (c, d).

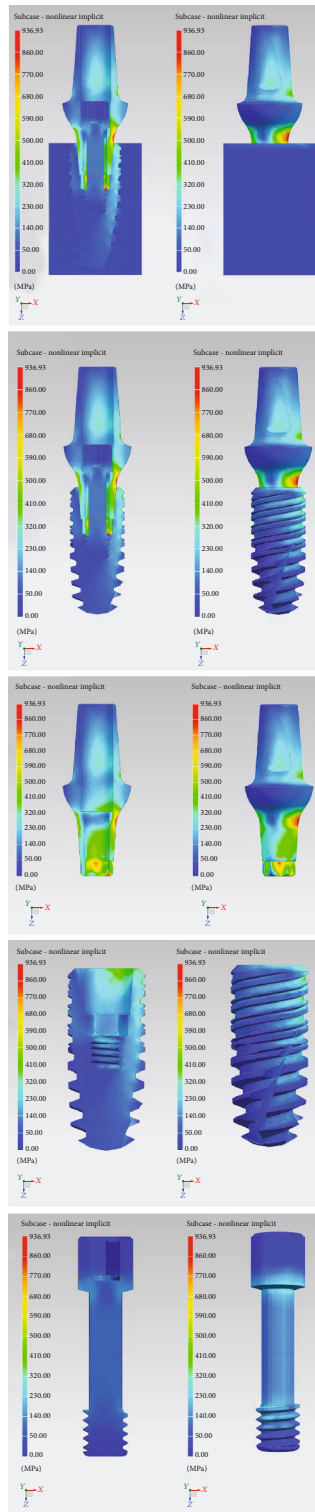


FIGURE 12: Von Mises tensions at 30-degree results in detail.

implant-prosthetic components is an excellent starting point for improving and modifying the latter in such a way as to respond positively to stresses. From a clinical point of view, it is also useful to know how different angles can affect these components. In fact, implant surgery, which tends to be pros-

thetically guided, can be further helped by these types of studies.

5. Conclusions

The fields of bioengineering come together in the development of new devices for the medical field and medical rehabilitation. Surely, the tested connection shows how studies of this type are able to improve dental implants even before they are fabricated. Being able to perform simulations and thus improve the device is a significant advantage. These new connections guarantee a correct distribution of forces both on the implant components and on the peri-implant tissues. The continuous evolution in the bioengineering field will certainly lead to obtaining ever more performing dental implants.

Data Availability

The data used to support the findings of this study are included within the article. The data that support the findings of this study are available from the corresponding author upon reasonable request.

Conflicts of Interest

The authors declare no conflict of interest.

Authors' Contributions

L.F. wrote and prepared the original draft; C.D.A. wrote, reviewed, and edited the manuscript; G.O. and R.M. visualized the study; M.C. supervised the study; G.C. administered the project. All authors have read and agreed to the published version of the manuscript.

References

- [1] M. Beretta, P. P. Poli, S. Pieriboni et al., "Peri-implant soft tissue conditioning by means of customized healing abutment: a randomized controlled clinical trial," *Materials*, vol. 12, no. 18, p. 3041, 2019.
- [2] P. Castrogiovanni, M. Di Rosa, S. Ravalli et al., "Moderate physical activity as a prevention method for knee osteoarthritis and the role of synoviocytes as biological key," *International Journal of Molecular Sciences*, vol. 20, no. 3, p. 511, 2019.
- [3] G. Cervino, L. Fiorillo, G. Spagnuolo et al., "Interface between Mta and dental bonding agents: scanning electron microscope evaluation," *Journal of International Society of Preventive and Community Dentistry*, vol. 7, no. 1, pp. 64–68, 2017.
- [4] G. Cervino, et al.U. Romeo, F. Lauritano et al., "Fem and Von Mises analysis of Osstem® dental implant structural components: evaluation of different direction dynamic loads," *The Open Dentistry Journal*, vol. 12, no. 1, pp. 219–229, 2018.
- [5] G. Cervino, L. Fiorillo, A. V. Arzukanyan, G. Spagnuolo, P. Campagna, and M. Ciccù, "Application of bioengineering devices for stress evaluation in dentistry: the last 10 years Fem parametric analysis of outcomes and current trends," *Minerva Stomatologica*, vol. 69, no. 1, pp. 55–62, 2020.
- [6] M. Ciccù, E. Bramanti, F. Cecchetti, L. Scappaticci, E. Guglielmino, and G. Risitano, "Fem and Von Mises analyses

- of different dental implant shapes for masticatory loading distribution,” *ORAL and Implantology*, vol. 7, no. 1, pp. 1–10, 2014.
- [7] M. Cicciù, E. Bramanti, G. Maticena, E. Guglielmino, and G. Risitano, “Fem evaluation of cemented-retained versus screw-retained dental implant single-tooth crown prosthesis,” *International Journal of Clinical and Experimental Medicine*, vol. 7, no. 4, pp. 817–825, 2014.
 - [8] M. Cicciù, G. Cervino, E. Bramanti et al., “Fem analysis of mandibular prosthetic overdenture supported by dental implants: evaluation of different retention methods,” *Computational and Mathematical Methods in Medicine*, vol. 2015, Article ID 943839, p. 16, 2015.
 - [9] M. Cicciù, G. Risitano, C. Maiorana, and G. Franceschini, “Parametric analysis of the strength in the “Toronto” osseous-prosthesis system,” *Minerva stomatologica*, vol. 58, no. 1-2, pp. 9–23, 2009.
 - [10] M. Cicciù, G. Cervino, D. Milone, and G. Risitano, “Fem analysis of dental implant-abutment interface overdenture components and parametric evaluation of Equator® and Locator® prosthodontics attachments,” *Materials*, vol. 12, no. 4, p. 592, 2019.
 - [11] M. Cicciù, G. Cervino, D. Milone, and G. Risitano, “Fem investigation of the stress distribution over mandibular bone due to screwed overdenture positioned on dental implants,” *Materials*, vol. 11, no. 9, p. 1512, 2018.
 - [12] M. Cicciù, G. Risitano, G. Lo Giudice, and E. Bramanti, “Periodontal health and caries prevalence evaluation in patients affected by Parkinson’s disease,” *Parkinson’s Disease*, vol. 2012, article 541908, 6 pages, 2012.
 - [13] G. de la Rosa Castolo, S. V. Guevara Perez, P.-J. Arnoux, L. Badih, F. Bonnet, and M. Behr, “Mechanical strength and fracture point of a dental implant under certification conditions: a numerical approach by finite element analysis,” *The Journal of Prosthetic Dentistry*, vol. 119, no. 4, pp. 611–619, 2018.
 - [14] V. E. de Souza Batista, F. R. Verri, D. A. d. F. Almeida, J. F. Santiago Junior, C. A. A. Lemos, and E. P. Pellizzer, “Finite element analysis of implant-supported prosthesis with pontic and cantilever in the posterior maxilla,” *Computer Methods in Biomechanics and Biomedical Engineering*, vol. 20, no. 6, pp. 663–670, 2016.
 - [15] O. Eraslan, O. Inan, and A. Secilmis, “The effect of framework design on stress distribution in implant-supported Fpds: a 3-D Fem study,” *European Journal of Dentistry*, vol. 4, no. 4, pp. 374–382, 2010.
 - [16] B. Jin, Y. G. Hu, and L. Han, “Progress in finite element analysis of meniscus,” *Zhongguo Gu Shang*, vol. 32, no. 5, pp. 485–488, 2019.
 - [17] D. Jörn, P. Kohorst, S. Besdo, M. Rücker, M. Stiesch, and L. Borchers, “Influence of lubricant on screw preload and stresses in a finite element model for a dental implant,” *The Journal of Prosthetic Dentistry*, vol. 112, no. 2, pp. 340–348, 2014.
 - [18] N. Kaleli, D. Sarac, S. Külünk, and Ö. Öztürk, “Effect of different restorative crown and customized abutment materials on stress distribution in single implants and peripheral bone: a three-dimensional finite element analysis study,” *The Journal of Prosthetic Dentistry*, vol. 119, no. 3, pp. 437–445, 2018.
 - [19] M. Cicciù, M. Beretta, G. Risitano, and C. Maiorana, “Cemented-retained vs screw-retained implant restorations: an investigation on 1939 dental implants,” *Minerva stomatologica*, vol. 57, no. 4, pp. 167–179, 2018.
 - [20] W. Kim, E. Song, K. Ju et al., “Finite element analysis of novel separable fixture for easy retrieval in case with peri-implantitis,” *Materials*, vol. 12, no. 2, p. 235, 2019.
 - [21] T. Kitagawa, Y. Tanimoto, M. Odaki, K. Nemoto, and M. Aida, “Influence of implant/abutment joint designs on abutment screw loosening in a dental implant system,” *Journal of Biomedical Materials Research Part B: Applied Biomaterials*, vol. 75B, no. 2, pp. 457–463, 2005.
 - [22] C. G. Liu, Y. J. Lu, J. Gao, and Q. Liu, “Application of finite element method in traffic injury and its prospect in forensic science,” *Fa Yi Xue Za Zhi*, vol. 32, no. 3, pp. 196–199, 2016.
 - [23] J. P. Macedo, J. Pereira, J. Faria et al., “Finite element analysis of stress extent at peri-implant bone surrounding external hexagon or Morse taper implants,” *Journal of the Mechanical Behavior of Biomedical Materials*, vol. 71, pp. 441–447, 2017.
 - [24] G. Mailath, B. Stoiber, G. Watzek, and M. Matejka, “Bone resorption at the entry of osseointegrated implants—a biomechanical phenomenon. finite element study,” *Zeitschrift für Stomatologie*, vol. 86, no. 4, pp. 207–216, 1989.
 - [25] P. Marcián, L. Borák, J. Valášek, J. Kaiser, Z. Florian, and J. Wolff, “Finite element analysis of dental implant loading on atrophic and non-atrophic cancellous and cortical mandibular bone - a feasibility study,” *Journal of Biomechanics*, vol. 47, no. 16, pp. 3830–3836, 2014.
 - [26] A. Mohammadi, A. Ahmadian, S. Rabbani, E. Fattahi, and S. Shirani, “A combined registration and finite element analysis method for fast estimation of intraoperative brain shift: phantom and animal model study,” *The International Journal of Medical Robotics and Computer Assisted Surgery*, vol. 13, no. 4, article e1792, 2017.
 - [27] A. Pirjamalineisiani, M. Sarafbidabad, N. Jamshidi, and F. A. Esfahani, “Finite element analysis of post dental implant fixation in drilled mandible sites,” *Computers in Biology and Medicine*, vol. 81, pp. 159–166, 2017.
 - [28] A. Pournasrollah, R. Negahdari, V. Gharekhani, A. Torab, and S. Jannati Ataei, “Investigating the effect of abutment-implant connection type on abutment screw loosening in a dental implant system using finite element methods,” *Journal of Dental Research, Dental Clinics, Dental Prospects*, vol. 13, no. 4, pp. 289–297, 2019.
 - [29] R. Razaghi, H. Biglari, and A. Karimi, “Dynamic finite element simulation of dental prostheses during chewing using muscle equivalent force and trajectory approaches,” *Journal of Medical Engineering & Technology*, vol. 41, no. 4, pp. 314–324, 2017.
 - [30] A. D. Schwitalla, M. Abou-Emara, T. Spintig, J. Lackmann, and W. D. Müller, “Finite element analysis of the biomechanical effects of peek dental implants on the peri-implant bone,” *Journal of Biomechanics*, vol. 48, no. 1, pp. 1–7, 2015.
 - [31] B. Vafaeian, L. H. le, T. N. H. T. Tran, M. el-Rich, T. el-Bialy, and S. Adeeab, “Micro-scale finite element modeling of ultrasound propagation in aluminum trabecular bone-mimicking phantoms: a comparison between numerical simulation and experimental results,” *Ultrasonics*, vol. 68, pp. 17–28, 2016.
 - [32] R. C. Van Staden, H. Guan, and Y. C. Loo, “Application of the finite element method in dental implant research,” *Computer Methods in Biomechanics and Biomedical Engineering*, vol. 9, no. 4, pp. 257–270, 2006.

- [33] R. Vayron, V. H. Nguyen, R. Bosc, S. Naili, and G. Haïat, "Assessment of the biomechanical stability of a dental implant with quantitative ultrasound: a three-dimensional finite element study," *The Journal of the Acoustical Society of America*, vol. 139, no. 2, pp. 773–780, 2016.
- [34] R. C. Vercio and H. G. Basmajian, "Fracture of a carbon fiber reinforced intramedullary femoral nail," *Journal of the American Academy of Orthopaedic Surgeons*, vol. 27, no. 12, pp. e585–e588, 2019.

Research Article

Functionalized Scaffold and Barrier Membrane with Anti-BMP-2 Monoclonal Antibodies for Alveolar Ridge Preservation in a Canine Model

Seiko Min¹, Taewan Kim,² Oksu Kim,³ Carames Goncalo,⁴ Tadahiko Utsunomiya,⁵ Takashi Matsumoto,⁶ Kayo Kuyama,⁵ and Nikola Angelov¹

¹Department of Periodontics and Dental Hygiene, University of Texas Health Science Center at Houston, Houston, TX, USA

²Department of Periodontics, University of Pennsylvania School of Dental Medicine, Philadelphia, PA, USA

³Department of Periodontology, Dental Research Institute, School of Dentistry, Chonnam National University, Gwangju, Republic of Korea

⁴Department of Periodontology, Implantology Institute, Lisbon, Portugal

⁵Department of Pathology, School of Dentistry, Nihon University at Matsudo, Chiba, Japan

⁶Division of Diagnostic Pathology, Nihon University Hospital School of Dentistry at Matsudo, Chiba, Japan

Correspondence should be addressed to Seiko Min; seiko.s.min@uth.tmc.edu

Received 6 June 2020; Accepted 4 August 2020; Published 23 September 2020

Guest Editor: Paolo Pesce

Copyright © 2020 Seiko Min et al. This is an open access article distributed under the Creative Commons Attribution License, which permits unrestricted use, distribution, and reproduction in any medium, provided the original work is properly cited.

Introduction. The aim of this study was to investigate the ability of anti-bone morphogenetic protein 2 monoclonal antibody (anti-BMP-2 mAb) to functionalize scaffolds to mediate bone regeneration in a canine model. **Materials and Methods.** The mandibular right premolar 4 (PM4) was extracted in eight beagle dogs and grafted with anti-BMP-2 mAb+anorganic bovine bone mineral with 10% collagen (ABBM-C) and porcine bilayer native collagen membrane (CM). The ABBM-C and CM were functionalized with either anti-BMP-2 mAb (test group) or an isotype matched control mAb (control group). Animals were euthanized at 12 weeks for radiographic, histologic, and histomorphometric analyses. Outcomes were compared between groups. **Results.** 3D imaging using cone beam computed tomography (CBCT) revealed that sites treated with ABBM-C and CM functionalized with anti-BMP-2 mAb exhibited significantly more remaining bone width near the alveolar crest, as well as buccal bone height, compared with control groups. Histologic and histomorphometric analyses demonstrated that in anti-BMP-2 mAb-treated sites, total tissue volume was significantly higher in the coronal part of the alveolar bone crest compared with control sites. In anti-BMP-2 mAb-treated sites, bone formation was observed under the barrier membrane. **Conclusion.** Functionalization of the ABBM-C scaffold and CM appeared to have led to bone formation within healing alveolar bone sockets.

1. Introduction

Numerous studies have demonstrated that significant bone resorption occurs as an inevitable biological event following tooth extraction without additional intervention [1–11]. The rates of loss of alveolar bone width and height in the first three months following extraction are approximately 0.25 mm and 0.2 mm, respectively [7]. A systematic review concluded that in the first six months, the dimensional changes in the alveolar ridge after tooth extraction lead to a mean horizontal width loss of 3.8 mm and a mean vertical

height loss of 1.24 mm [12]. Moreover, spontaneous postextraction healing leads to significant alveolar bone contour loss [13].

The magnitude of bone resorption appears more prominent when the initial thickness of the buccal bone wall is less than 1.0 mm [6]. The prevalence of a thin buccal wall was investigated and a study revealed that most teeth in the anterior maxilla have a thin buccal bone [14].

The subsequent dimensional loss of the alveolar ridge following tooth extraction often results in different complications, including insufficient bone volume for dental implant

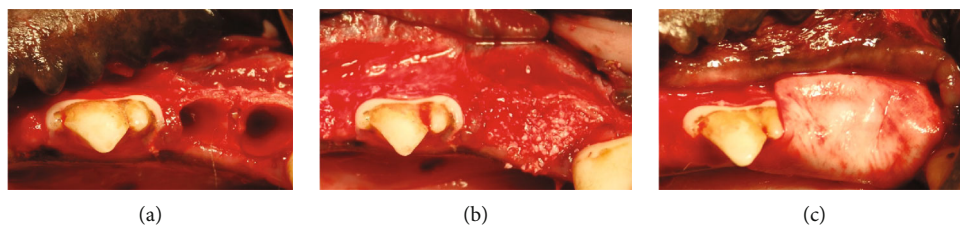


FIGURE 1: (a) The mandibular right premolar 4 (PM4) was extracted with flap elevation as atraumatically as possible. (b) The sockets were filled with anorganic bovine bone mineral with 10% collagen (ABBM-C) functionalized with either anti-bone morphogenetic protein 2 monoclonal antibody (anti-BMP-2 mAb, test group) or isotype matched control mAb (control group). (c) The sockets filled with ABBM-C were covered by porcine bilayer native collagen membrane (CM) functionalized with either anti-BMP-2 mAb or isotype matched control mAb. The marginal gingiva was then approximated to achieve primary wound closure with a nonresorbable suture.

placement in the optimal position and an esthetic defect. The esthetic complication such as a peri-implant soft tissue deficiency can be caused mostly by implant malposition [15].

To minimize the postextraction alveolar ridge dimensional loss, systematic reviews have recommended socket grafting at the time of extraction for ridge preservation [16, 17]. Various biomaterials used for ridge preservation have been evaluated including autograft [18, 19], allograft [20], xenograft [18, 21–25], and alloplast [24, 26–28]. These graft materials have been protected by different barrier devices, including resorbable membranes [20, 29, 30], nonresorbable membranes [31], autogenous soft tissue plugs [32], and extraction socket devices [7–11].

Tissue engineering strategies that combine osteoconductive scaffolds with osteoinductive mediators, such as recombinant human bone morphogenetic protein 2 (rhBMP-2), have been reported [33–37]. Application of rhBMP-2 has been expanded for bone repair; however, the numbers of reported complications have been increasing [38–48].

As an alternative approach to using rhBMP-2, the application of anti-bone morphogenetic protein 2 monoclonal antibody (anti-BMP-2 mAb) was proposed to capture endogenous BMP-2 and homologous ligands in an approach known as antibody-mediated osseous regeneration (AMOR) [49]. Anti-BMP-2 mAbs are able to mediate differentiation of local progenitor stem cells into osteoblast-like cells, thereby promoting bone repair and regeneration. Anti-BMP-2 mAbs can capture endogenous BMPs that supply the signals for repairing different types of bony defects, such as BMP-2, BMP-4, and BMP-7. The capability of AMOR has been tested in various defect models [49–57].

This exploratory study used an AMOR approach in a canine model to investigate a potential therapeutic intervention for preserving the alveolar ridge following tooth extraction. The anti-BMP-2 mAb was employed to functionalize both a scaffold and a barrier membrane.

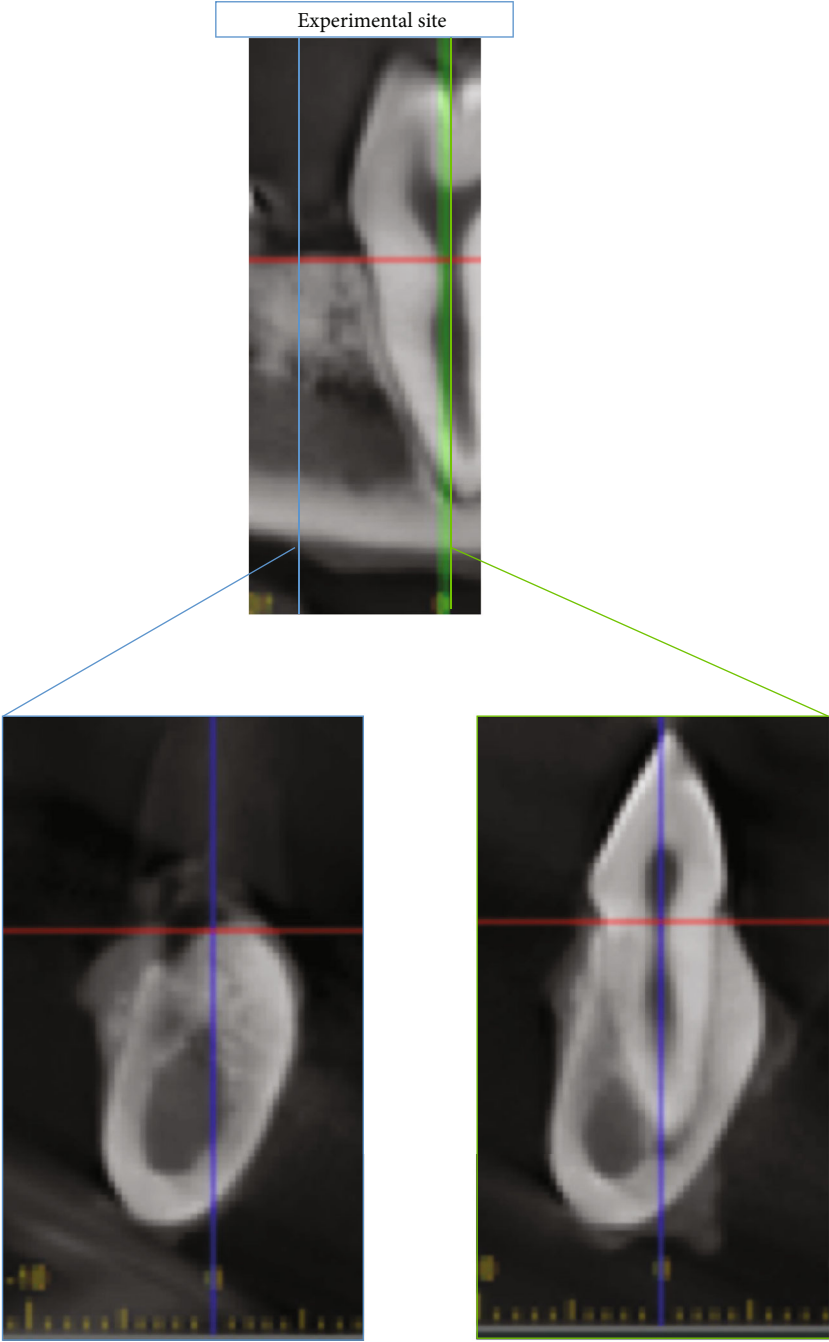
2. Materials and Methods

2.1. Animals. The research protocol of this study was approved by the Institutional Animal Care and Use Committee (IACUC) of the University of Southern California (USC, Los Angeles, CA, USA). Eight beagle dogs (four years old, weighing 10 to 11 kg) were used in this study and maintained on a soft diet with food and water *ad libitum*.

2.2. Materials

2.2.1. Antibodies and Scaffold. The experimental mAb was a chimeric anti-BMP-2 mAb with cross-reactivity to BMP-4 and BMP-7. The control mAb was an isotype matched mAb specific for the KLH peptide that had no specific affinity for BMP-2 [54]. A concentration of 25 $\mu\text{g/ml}$ of mAb was chosen based on the results of our previous studies [54]. Anti-BMP-2 mAb and isotype matched control mAb were immobilized on deproteinized anorganic bovine bone mineral with 10% collagen (ABBM-C; Bio-Oss Collagen®, Geistlich, Pharma AG, Wolhusen, Switzerland) as well as porcine bilayer native collagen membrane (CM; Bio-Gide® membrane, Geistlich, Pharma AG, Wolhusen, Switzerland) as previously described [54]. Briefly, the ABBM-C and CM were incubated at room temperature with mAb diluted with phosphate-buffered saline (PBS) for one hour prior to implantation into the sockets after tooth extraction. All antibody preparations were made by two of the coauthors (S.M., O.K.).

2.2.2. Surgical Protocol. Preoperatively, animals were given atropine (0.05 mg/kg) and sedated with ketamine (10 mg/kg subcutaneously). Ketamine/xylazine was administered to induce anesthesia. Animals were intubated and ventilated with an isoflurane/oxygen machine. Anesthesia was maintained by isoflurane (1–4%). Animals were draped and then periorally swabbed with cetrimide (1% solution), followed by chlorhexidine gluconate (0.05% solution). Before surgeries, dental prophylaxis was performed and all surgical sites were swabbed with chlorhexidine gluconate (0.12% solution). After intravenous ketamine (5 mg/ml) and intramuscular tiletamine-zolazepam (5–10 mg/kg) were administered, local anesthesia was achieved by using lidocaine HCl (2%) with 1:100,000 epinephrine. The mandibular right premolar 4 (PM4) was then extracted with flap elevation as atraumatically as possible in each of the eight dogs (Figure 1(a)). Then, the sockets were filled with ABBM-C functionalized with either anti-BMP-2 mAb or isotype matched control mAb (Figure 1(b)). After the sockets were filled with ABBM-C, they were covered by functionalized CM with either anti-BMP-2 mAb or isotype matched control mAb (Figure 1(c)). The marginal gingiva was then approximated to achieve primary wound closure with nonresorbable polytetrafluoroethylene (PTFE) monofilament suture (4-0 Cytoplast™



(a)

FIGURE 2: Continued.

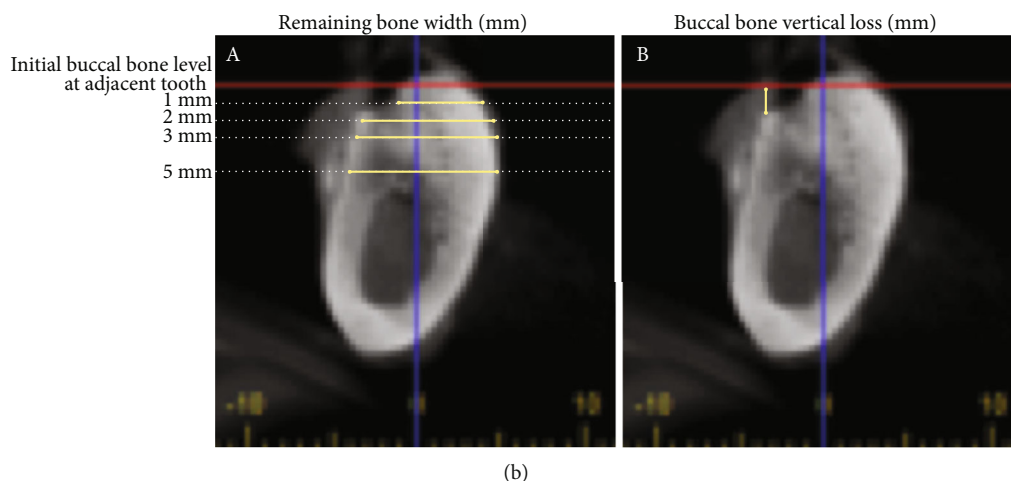


FIGURE 2: Repeatabile anatomical structures such as the adjacent crest level (red line in upper image) and long axis of the adjacent tooth (blue line in lower two images) were used as references to measure dimensional alveolar bone change. (a) Remaining bone width at different levels of 1 mm, 2 mm, 3 mm, and 5 mm from the bone crest at the adjacent tooth and (b) buccal bone height level relative to bone crest at the adjacent tooth were measured at the buccal thirds of the examined alveolus.

suture; Osteogenics, Lubbock, TX, USA). Three of the coauthors (S.M., O.K., and C.G.) performed all surgical procedures. The eight extraction socket sites were then randomly assigned to either of the two experimental treatment groups: (1) test ($N = 4$): anti-BMP-2 mAb+ABBM-C+CM and (2) control ($N = 4$): isotype matched control mAb+ABBM-C+CM.

2.2.3. Postoperative Care. After surgery, the animals were maintained on a soft diet. On alternate days, oral hygiene was performed by applying chlorhexidine gluconate (0.12% solution) with an ultrasoft toothbrush. Postoperative analgesia was administered 2 times per day for 2 days (buprenorphine, 0.05 mg/kg weight), after which the comfort level of the animals was assessed and additional analgesia was provided as needed. Sutures were removed 14 days later. At 12 weeks after tooth extraction, the animals were euthanized so that cone beam computed tomography (CBCT) and histologic and histomorphometric analyses could be conducted. The mandible of each dog was block resected, labeled, and fixed for 10 days in a 10% buffered formalin solution.

2.2.4. CBCT Analysis. Resected mandibles were imaged with CBCT (J. Morita Veraviewepocs® 3D F40, J Morita USA, Irvine, CA, USA), followed by quantitative analysis to measure mineralized tissue detected at defined locations within the grafted sites. Each of the specimens was placed in a sample holder and was scanned using high resolution. After scanning, the acquired data were imported into 3D image analysis software (i-Dixel 2.0 software, J Morita USA, Irvine, CA, USA) for quantitative analysis. A global thresholding procedure was used to segment the bone tissues. Bone tissues within the defects were defined using a threshold equal to -360 HU. The proportion of bone volume occupying the defect virtual space was measured, allowing quantitative comparisons between the test and control groups. CBCT linear measurements were made at 12 weeks postsurgery, as follows: (1) remaining bone width at different levels (1, 2, 3, and

5 mm relative to the bone crest of the adjacent first molar tooth (Figure 2(a)) and (2) buccal bone vertical level relative to the crestal bone of the adjacent first molar (Figure 2(b)). One coauthor (S.M.) performed all CBCT measurements. Repeated measurements were conducted on 10% of the sites selected randomly. The first and second measurements differed by less than 5%, demonstrating intrarater reproducibility of the analysis.

2.2.5. Histologic and Histomorphometric Analyses. Harvested biopsy samples were fixed in 4% paraformaldehyde followed by decalcification in 10% EDTA for 14 days. Excised specimens were embedded in paraffin and then serially sectioned (4 μ m thickness) and placed on glass slides. Deparaffinization was performed by immersing in xylene, followed by decreasing ethanol concentrations and washing with water. Azan-Mallory staining was applied to the sections. Images were qualitatively examined under a microscope (CX21® Olympus Optical Co., Tokyo, Japan). Histomicrographs were captured with a digital camera and analyzed by using image analysis software (Soft Image System GmbH, Münster, Germany). NIH ImageJ software (U.S. National Institutes of Health, Bethesda, Maryland, USA) was used for histomorphometric analysis to measure the total tissue volume within different areas at 0-1 mm coronal to the lingual bone crest and at 0-1 mm, 1-2 mm, and 2-3 mm apical to the lingual bone crest (Figure 3). One coauthor (T. K.) performed all histomorphometric measurements. Standard methods and nomenclature of the American Society for Bone and Mineral Research (ASBMR) were utilized to define various components of the specimens [58].

2.2.6. Statistical Analysis. The mean and standard deviations were calculated for CBCT and histomorphometric analysis. The Mann-Whitney U test was used for pairwise comparisons of the remaining bone width and buccal bone height, and total tissue volume was calculated at different locations. The SPSS software program (IBM SPSS statistics 23, IBM,

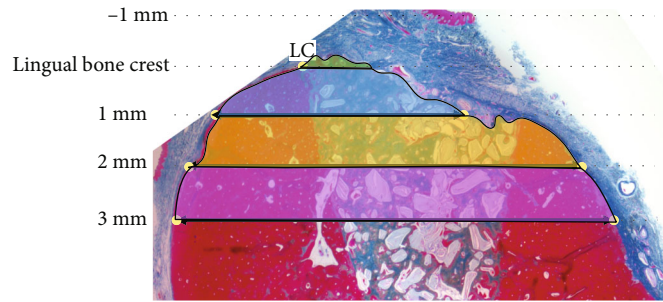


FIGURE 3: Landmarks for histomorphometric analysis, showing lingual crest (LC) as a relatively stable reference. Additional landmarks relative to the LC are represented at 1 mm coronal (i.e., -1 mm) and 1, 2, and 3 mm apical to the LC. The amounts of total tissue volume in different zones relative to the LC (0-1 mm coronal, 0-1 mm apical, 1-2 mm apical, and 2-3 mm apical) were measured.

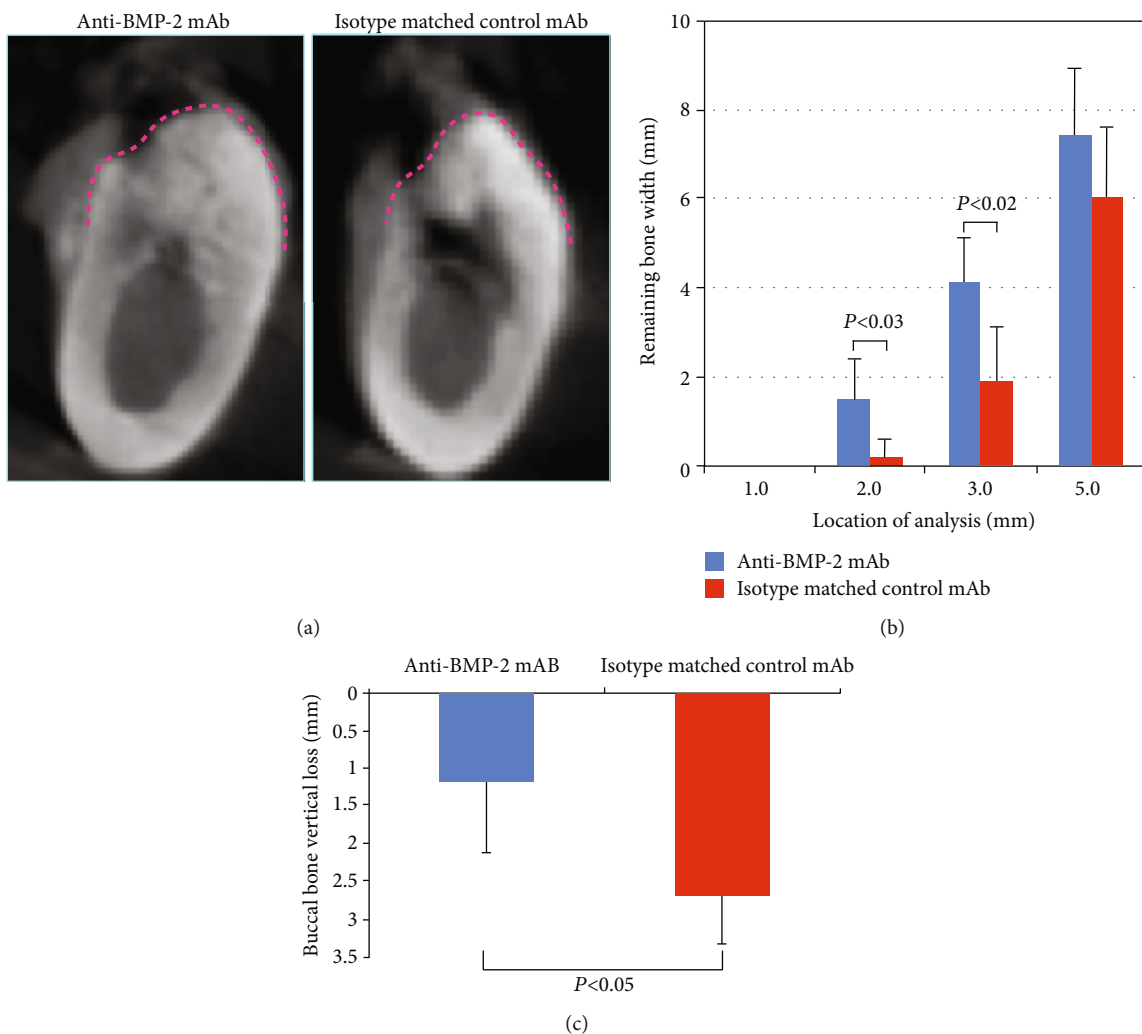


FIGURE 4: (a) Representative cone beam computed tomography (CBCT) images of anti-bone morphogenetic protein 2 monoclonal antibody- (anti-BMP-2 mAb-) treated site and isotype matched control mAb-treated site. (b) Remaining bone width at 1, 2, 3, and 5 mm from the bone crest at the adjacent tooth: a statistically significant difference in remaining bone width at 2 mm and 3 mm was found between the test group ($N = 4$) and control group ($N = 4$) ($P = 0.03$, $P = 0.02$, respectively). (c) Bone height level at buccal aspect (mm): the amounts of buccal bone height loss in the anti-BMP-2 mAb-treated sites ($N = 4$) and the isotype matched control mAb-treated sites ($N = 4$) were 1.17 ± 0.94 mm and 2.69 ± 0.63 mm, respectively, and were statistically significantly different ($P = 0.03$).

TABLE 1: Remaining bone width at 1, 2, 3, and 5 mm relative to the adjacent crestal bone.

Treatment group	Remaining bone width (mm, mean \pm SD) at four test sites			
	1 mm	2 mm	3 mm	5 mm
Anti-BMP-2 mAb	0.0 \pm 0.0	1.5 \pm 0.9*	4.1 \pm 1.0 [†]	7.4 \pm 1.5
Isotype matched control mAb	0.0 \pm 0.0	0.2 \pm 0.4	1.9 \pm 1.2	6.0 \pm 1.6

For anti-BMP-2-treated sites vs. control sites: * $P=0.03$ and [†] $P=0.02$. Anti-BMP-2 mAb: anti-bone morphogenetic protein 2 monoclonal antibody; SD: standard deviation.

Armonk, NY, USA) was used for statistical analysis and $P < 0.05$ was considered to be statistically significant.

3. Results

3.1. Clinical Observations. All surgical sites healed uneventfully with minimal inflammation and no signs of infection.

3.2. CBCT Analysis. Representative CBCT images illustrate wider alveolar crest in experimental sites treated with scaffold and membrane functionalized with anti-BMP-2, compared with control sites (Figure 4(a)). The alveolar crest also appears to have higher density in the experimental site.

3.3. Quantitative Analysis of Bone Width. For anti-BMP-2 mAb, the remaining mean bone widths in test sites at 1, 2, 3, and 5 mm relative to the adjacent crestal bone were 0.0 \pm 0.0 mm, 1.5 \pm 0.9 mm, 4.1 \pm 1.0 mm, and 7.4 \pm 1.5 mm, respectively (Figure 4(b), Table 1). Comparatively, the residual mean bone widths of control sites were 0.0 \pm 0.0 mm, 0.2 \pm 0.4 mm, 1.9 \pm 1.2 mm, and 6.0 \pm 1.6 mm, respectively. The remaining bone widths at anti-BMP-2-treated sites were statistically significantly higher at 2 and 3 mm compared with control sites ($P = 0.03$, $P = 0.02$, respectively).

3.4. Quantitative Analysis of Buccal Bone Height. For anti-BMP-2 mAb, the buccal crest of anti-BMP-2-treated sites was located 1.17 \pm 0.94 mm apical to the crestal bone of adjacent teeth. In contrast, the buccal crest of control sites treated with isotype matched control mAb was located 2.69 \pm 0.63 mm apical to that of adjacent teeth (Figure 4(c), Table 2). A statistically significant difference was found between anti-BMP-2-treated sites and control sites ($P = 0.03$).

3.5. Histologic Observation. Histologic examination revealed well-defined extraction socket defects with clear demarcation between the woven bone and more mature lamellar bone by Azan-Mallory staining of both anti-BMP-2 mAb-treated sites and control sites (Figures 5(a) and 5(b)). The barrier CM persisted underneath mucosal tissues overlying the extraction orifice of test sites treated with anti-BMP-2 mAb (green dotted lines). In contrast, the CM in control sites appeared to have been significantly more resorbed, accompanied by in-growth of mucosal tissues into the graft. The superficial ABBM particles in control sites appeared to be mostly encapsulated in fibrous tissue (Figures 5(b) and 5(d)). The area underneath the CM in anti-BMP-2 mAb-treated sites was characterized by an abundance of osteoid bone surrounding residual graft particles, as well as vascular tissue (Figures 5(a) and 5(c)). The new bone found within

TABLE 2: Location of buccal crest relative to crestal bone of the adjacent teeth.

Treatment group	Buccal bone height (mm, mean \pm SD)
Anti-BMP-2 mAb	1.17 \pm 0.94*
Isotype matched control mAb	2.69 \pm 0.63

* $P = 0.03$ for anti-BMP-2-treated sites vs. control sites. Anti-BMP-2 mAb: anti-bone morphogenetic protein 2 monoclonal antibody.

test sites appeared to be characterized by reversal lines, marking the remodeling stage of osteogenesis. In contrast, the bone within control sites was more sparse and consisted of less mature woven bone (Figures 5(b) and 5(d)).

Osteogenesis was observed within the entire extraction socket of both the test and control sites (Figures 5(a) and 5(b)). A polarized pattern of osteogenesis was observed with the most mature bone in the apical region, gradually transitioning to less mature woven bone near the alveolar crest (Figures 5(a) and 5(b)).

3.6. Quantitative Histomorphometric Analysis. The landmarks used for quantitative histomorphometric analysis are shown in Figure 3. The results shown in Figure 6 and Table 3 demonstrated that sites treated with scaffold and CM functionalized with anti-BMP-2 (test), but not sites treated with isotype matched control mAb, had bone growth coronal to the alveolar lingual crest ($P = 0.01$). In the zone up to 1 mm apical to the bone crest, there was significantly more bone volume in anti-BMP-2 mAb-treated sites than in control sites ($P = 0.02$).

4. Discussion

A variety of graft materials including autogenous [18, 19], xenogenic [18, 21–25], allogenic [20], and alloplastic [24, 26–28] materials have been used for grafting of extraction sockets for ridge preservation. In addition to these traditional grafts, newer scaffolds and biologics developed for tissue engineering have been adopted for ridge preservation [59–62]. These biologics have included growth factors and platelet concentrates [63–65].

One of the most investigated biologics is rhBMP-2, which was approved by the U.S. Food and Drug Administration (FDA) for clinical use to repair bone defects [66–68]. The growing clinical use of rhBMP-2 has been associated with numerous complications such as graft migration [69], formation of neutralizing antibodies against BMP-2 [69], and extreme edema that may obstruct the airway or affect critical

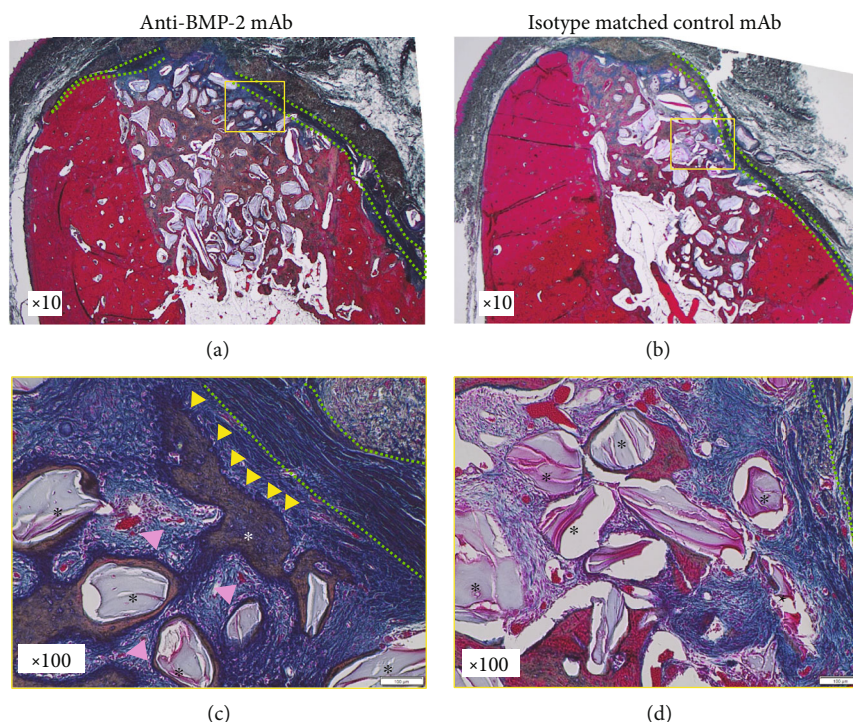


FIGURE 5: Histology at low magnification in the (a) anti-bone morphogenetic protein 2 monoclonal antibody- (anti-BMP-2 mAb-) treated site and (b) isotype matched control mAb site. Outline of alveolar bone in control sites appeared as a knife-edged shape due to buccal bone loss. The residual barrier collagen membrane (CM) was observed in both test and control sites (green dotted lines). Osteogenesis was observed within the entire extraction socket of both test and control sites. Histology at high magnification in (c) anti-BMP-2 mAb-treated and (d) isotype matched control mAb sites. The micrographs showed osteoblast-like cells (yellow arrowheads) as well as blood vessels (pink arrowheads) participating in active bone formation. The superficial anorganic bovine bone mineral (ABBM) particles (black asterisks in d) in control sites showed fibrotic encapsulation, while osteogenic cells as well as osteoid bone formation around residual ABBM graft particles were noted in test sites (white asterisk in c).

structures [46]. Additional disadvantages of exogenous growth factors (e.g., rhBMP-2) include a short biological half-life and lower biologic activity compared to the autogenous analog [70] that necessitates the use of high doses of rhBMP-2 to achieve the therapeutic effect.

To circumvent some of the problems associated with exogenous growth factors, a novel tissue engineering approach for bone regeneration known as AMOR was developed [49]. We previously reported that anti-BMP2-mAb induced osteogenic differentiation *in vitro* and *de novo* bone formation *in vivo*, by using different types of bone defects in animal models that have shown the ability of anti-BMP2-mAb to mediate bone regeneration including rat [49, 50, 52], rabbit [51], canine, and nonhuman primate [56, 57].

The current study is the first to investigate the efficacy of a scaffold and barrier membrane functionalized with anti-BMP-2 mAb for ridge preservation in a canine model.

Following tooth extraction, the anti-BMP-2 mAb immobilized on the ABBM-C was implanted into an extraction socket and was protected by anti-BMP-2 mAb immobilized on a CM.

The present study showed that the anti-BMP-2 mAb-treated sites had statistically significantly greater remaining bone width and buccal bone height, as well as higher total tissue volume, compared with control mAb-treated sites. These favorable outcomes may be attributed to the ability of the

anti-BMP-2 mAb to capture endogenous BMP-2, BMP-4, and BMP-7 and increase their *in vivo* persistence [50]. The barrier CM functionalized with anti-BMP-2 mAb was utilized not only for cell occlusion properties and space-making abilities but also for bioactive properties that promote bone regeneration by capturing endogenous BMP-2, BMP-4, and BMP-7.

Radiographic assessment demonstrated that both the buccal bone height level relative to the bone crest at an adjacent tooth and the remaining bone width at 2 and 3 mm relative to the bone crest at an adjacent tooth in the anti-BMP-2 mAb-treated site was statistically significantly higher than that of the control mAb-treated site ($P = 0.03$). Furthermore, histologic observations in the anti-BMP-2 mAb-treated site revealed the presence of bone formation with deposition of active osteogenic cells, including osteoblast-like cells as well as osteoclast-like cells beneath the remaining barrier CM.

One of major findings from this study was that histomorphometric analysis showed a statistically significantly higher total tissue volume at 0-1 mm coronal as well as at 0-1 mm apical to the lingual bone crest in the anti-BMP-2 mAb-treated site compared to that in the control mAb-treated site ($P < 0.05$). The alveolar crest contour in the anti-BMP-2 mAb-treated sites was restored more significantly compared with that in the control mAb-treated sites. Therefore, the current data demonstrated that the use of a scaffold and barrier

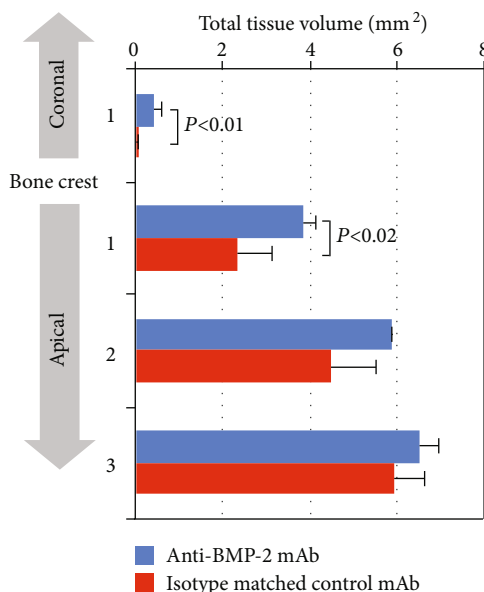


FIGURE 6: The amounts of total tissue volume within the extraction socket at 0-1 mm coronal to the lingual crest and at 0-1 mm, 1-2 mm, and 2-3 mm apical to the lingual crest. The anti-bone morphogenetic protein 2 monoclonal antibody- (anti-BMP-2 mAb-) treated sites ($N = 4$) revealed a statistically significant higher amount of total tissue volume at 0-1 mm coronal as well as at 0-1 mm apical of the alveolar bone crest relative to the lingual crest compared with the isotype matched control mAb-treated sites ($N = 4$) ($P = 0.01$, $P = 0.02$, respectively). Landmarks used for the analysis are shown in Figure 3.

TABLE 3: Quantitative histomorphometric analysis of sites treated with scaffold and collagen membrane (CM) functionalized with anti-BMP-2 mAb.

Treatment group	Total tissue volume (pixels, mean \pm SD)			
	0-1 mm coronal	0-1 mm apical	1-2 mm apical	2-3 mm apical
Anti-BMP-2 mAb	0.45 \pm 0.16*	3.85 \pm 0.30 [†]	5.87 \pm 0.03	6.54 \pm 0.42
Isotype matched control mAb	0.02 \pm 0.05	2.32 \pm 0.82	4.48 \pm 1.04	5.93 \pm 0.72

For anti-BMP-2-treated sites vs. control sites: * $P = 0.01$ and [†] $P = 0.02$. Landmarks used for the analysis are shown in Figure 3. Anti-BMP-2 mAb: anti-bone morphogenetic protein 2 monoclonal antibody; SD: standard deviation.

membrane functionalized with anti-BMP-2 mAb enhanced bone regeneration for ridge preservation. It is also worthwhile to note that in the present study, AMOR showed no signs of a severe inflammation reaction. This finding can possibly be attributed to the low concentration of anti-BMP-2 mAb that is needed to capture endogenous BMP-2 to enhance bone regeneration within the extraction socket.

The present study has a number of limitations, including a small sample size and lack of multiple time points to examine the kinetics of wound healing. We have plans to initiate additional studies with a larger sample size and longer duration to investigate the utility of AMOR for management of complex tooth extractions.

5. Conclusion

This study investigated the functionalization of a scaffold and barrier membrane with anti-BMP-2 mAb for extraction socket grafting in a canine model. The application of AMOR for socket grafting was accompanied by increased bone volume and more mature bone formation within the extraction sockets.

Data Availability

The data used to support the findings of this study are available from the corresponding author upon request.

Disclosure

This study was presented as a poster on April 4, 2018, at the University of Southern California Research Day by Dr. Taewan Kim.

Conflicts of Interest

The authors declare no conflicts of interest.

Acknowledgments

The authors would like to acknowledge Dr. Homayoun Zadeh for his assistance with the experiments described in this manuscript. This study was supported by a grant to Seiko Min from the Osteology Foundation (#13-019).

References

- [1] K. Johnson, "A study of the dimensional changes occurring in the maxilla following tooth extraction," *Australian Dental Journal*, vol. 14, no. 4, pp. 241–244, 1969.
- [2] J. Pietrokovski and M. Massler, "Alveolar ridge resorption following tooth extraction," *The Journal of Prosthetic Dentistry*, vol. 17, no. 1, pp. 21–27, 1967.
- [3] L. Schropp, A. Wenzel, L. Kostopoulos, and T. Karring, "Bone healing and soft tissue contour changes following single-tooth extraction: a clinical and radiographic 12-month prospective study," *The International Journal of Periodontics & Restorative Dentistry*, vol. 23, no. 4, pp. 313–323, 2003.
- [4] M. G. Araújo and J. Lindhe, "Dimensional ridge alterations following tooth extraction. An experimental study in the dog," *Journal of Clinical Periodontology*, vol. 32, no. 2, pp. 212–218, 2005.
- [5] J. M. Ten Heggeler, D. E. Slot, and G. A. Van der Weijden, "Effect of socket preservation therapies following tooth extraction in non-molar regions in humans: a systematic review," *Clinical Oral Implants Research*, vol. 22, no. 8, pp. 779–788, 2011.
- [6] V. Chappuis, O. Engel, K. Shahim, M. Reyes, C. Katsaros, and D. Buser, "Soft tissue alterations in esthetic postextraction sites: a 3-dimensional analysis," *Journal of Dental Research*, vol. 94, Supplement 9, pp. 187S–193S, 2015.
- [7] K. H. Ryu, S. Min, H. K. You et al., "Alveolar ridge dimensional changes following ridge preservation procedure using Socket-KAP™: exploratory study of serial cone-beam computed tomography and histologic analysis in canine model," *Clinical Oral Implants Research*, vol. 27, no. 9, pp. 1144–1151, 2016.
- [8] S. Min, Y. Liu, J. Tang et al., "Alveolar ridge dimensional changes following ridge preservation procedure with novel devices: part 1–CBCT linear analysis in non-human primate model," *Clinical Oral Implants Research*, vol. 27, no. 1, pp. 97–105, 2016.
- [9] M. Omran, S. Min, A. Abdelhamid, Y. Liu, and H. H. Zadeh, "Alveolar ridge dimensional changes following ridge preservation procedure: part-2 - CBCT 3D analysis in non-human primate model," *Clinical Oral Implants Research*, vol. 27, no. 7, pp. 859–866, 2016.
- [10] A. Abdelhamid, M. Omran, and N. Bakhshalian, "An open randomized controlled clinical trial to evaluate ridge preservation and repair using SocketKAP™ and SocketKAGE™: part 2 - three-dimensional alveolar bone volumetric analysis of CBCT imaging," *Clinical Oral Implants Research*, vol. 27, no. 6, pp. 631–639, 2016.
- [11] Y. Su, J. Tang, S. Min et al., "Alveolar ridge dimensional changes following ridge preservation procedure with novel devices: part 3 - histological analysis in non-human primate model," *Clinical Oral Implants Research*, vol. 28, no. 11, pp. e252–e261, 2017.
- [12] W. L. Tan, T. L. T. Wong, M. C. M. Wong, and N. P. Lang, "A systematic review of post-extraction alveolar hard and soft tissue dimensional changes in humans," *Clinical Oral Implants Research*, vol. 23, pp. 1–21, 2012.
- [13] H. H. Zadeh, A. Abdelhamid, M. Omran, N. Bakhshalian, and D. Tarnow, "An open randomized controlled clinical trial to evaluate ridge preservation and repair using SocketKAP™ and SocketKAGE™: part 1-three-dimensional volumetric soft tissue analysis of study casts," *Clinical Oral Implants Research*, vol. 27, no. 6, pp. 640–649, 2016.
- [14] A. L. Januário, W. R. Duarte, M. Barriviera, J. C. Mesti, M. G. Araújo, and J. Lindhe, "Dimension of the facial bone wall in the anterior maxilla: a cone-beam computed tomography study," *Clinical Oral Implants Research*, vol. 22, no. 10, pp. 1168–1171, 2011.
- [15] A. Monje, P. Galindo-Moreno, T. F. Tözüm, F. Suárez-López del Amo, and H. L. Wang, "Into the paradigm of local factors as contributors for peri-implant disease: short communication," *The International Journal of Oral & Maxillofacial Implants*, vol. 31, no. 2, pp. 288–292, 2016.
- [16] C. H. Hämmerle, M. G. Araújo, and M. Simion, "On behalf of the osteology consensus group 2011. Evidence-based knowledge on the biology and treatment of extraction sockets," *Clinical Oral Implants Research*, vol. 23, pp. 80–82, 2011.
- [17] F. Vignoletti, P. Matesanz, D. Rodrigo, E. Figuero, C. Martin, and M. Sanz, "Surgical protocols for ridge preservation after tooth extraction. A systematic review," *Clinical Oral Implants Research*, vol. 23, pp. 22–38, 2011.
- [18] M. G. Araújo and J. Lindhe, "Socket grafting with the use of autologous bone: an experimental study in the dog," *Clinical Oral Implants Research*, vol. 22, no. 1, pp. 9–13, 2011.
- [19] W. Becker, B. E. Becker, and R. Caffesse, "A comparison of demineralized freeze-dried bone and autologous bone to induce bone formation in human extraction sockets," *Journal of Periodontology*, vol. 65, no. 12, pp. 1128–1133, 1994.
- [20] J. M. Iasella, H. Greenwell, R. L. Miller et al., "Ridge preservation with freeze-dried bone allograft and a collagen membrane compared to extraction alone for implant site development: a clinical and histologic study in humans," *Journal of Periodontology*, vol. 74, no. 7, pp. 990–999, 2003.
- [21] D. Carmagnola, P. Adriaens, and T. Berglundh, "Healing of human extraction sockets filled with Bio-Oss," *Clinical Oral Implants Research*, vol. 14, no. 2, pp. 137–143, 2003.
- [22] D. Cardaropoli, L. Tamagnone, A. Roffredo, L. Gaveglio, and G. Cardaropoli, "Socket preservation using bovine bone mineral and collagen membrane: a randomized controlled clinical trial with histologic analysis," *The International Journal of Periodontics & Restorative Dentistry*, vol. 32, no. 4, pp. 421–430, 2012.
- [23] D. Cardaropoli, L. Tamagnone, A. Roffredo, and L. Gaveglio, "Relationship between the buccal bone plate thickness and the healing of postextraction sockets with/without ridge preservation," *The International Journal of Periodontics & Restorative Dentistry*, vol. 34, no. 2, pp. 211–217, 2014.
- [24] G. A. Kotsakis, M. Salama, V. Chrepa, J. E. Hinrichs, and P. Gaillard, "A randomized, blinded, controlled clinical study of particulate anorganic bovine bone mineral and calcium phosphosilicate putty bone substitutes for socket preservation," *The International Journal of Oral & Maxillofacial Implants*, vol. 29, no. 1, pp. 141–151, 2014.
- [25] A. Barone, P. Toti, A. Quaranta et al., "Clinical and histological changes after ridge preservation with two xenografts: preliminary results from a multicentre randomized controlled clinical trial," *Journal of Clinical Periodontology*, vol. 44, no. 2, pp. 204–214, 2017.
- [26] M. R. Norton and J. Wilson, "Dental implants placed in extraction sites implanted with bioactive glass: human histology and clinical outcome," *The International Journal of Oral & Maxillofacial Implants*, vol. 17, no. 2, pp. 249–257, 2002.
- [27] P. M. Camargo, V. Lekovic, M. Weinlaender et al., "Influence of bioactive glass on changes in alveolar process dimensions after exodontia," *Oral Surgery, Oral Medicine, Oral Pathology,*

- Oral Radiology, and Endodontics*, vol. 90, no. 5, pp. 581–586, 2000.
- [28] R. E. Jung, A. Philipp, B. M. Annen et al., “Radiographic evaluation of different techniques for ridge preservation after tooth extraction: a randomized controlled clinical trial,” *Journal of Clinical Periodontology*, vol. 40, no. 1, pp. 90–98, 2013.
- [29] G. Favero, N. P. Lang, E. De Santis, B. G. Gonzalez, M. T. Schweikert, and D. Botticelli, “Ridge preservation at implants installed immediately after molar extraction. An experimental study in the dog,” *Clinical Oral Implants Research*, vol. 24, no. 3, pp. 255–261, 2013.
- [30] E. T. Scheyer, P. Schupbach, and M. K. McGuire, “A histologic and clinical evaluation of ridge preservation following grafting with demineralized bone matrix, cancellous bone chips, and resorbable extracellular matrix membrane,” *The International Journal of Periodontics & Restorative Dentistry*, vol. 32, no. 5, pp. 543–552, 2012.
- [31] B. K. Barteel, “Evaluation of a new polytetrafluoroethylene guided tissue regeneration membrane in healing extraction sites,” *The Compendium of Continuing Education in Dentistry*, vol. 19, pp. 1256–1258, 1998.
- [32] R. E. Jung, D. W. Siegenthaler, and C. H. Hämmerle, “Postextraction tissue management: a soft tissue punch technique,” *The International Journal of Periodontics & Restorative Dentistry*, vol. 24, no. 6, pp. 545–553, 2004.
- [33] L. Krishnan, L. B. Priddy, C. Esancy et al., “Hydrogel-based delivery of rhBMP-2 improves healing of large bone defects compared with autograft,” *Clinical Orthopaedics and Related Research*, vol. 473, no. 9, pp. 2885–2897, 2015.
- [34] G. Guven, B. A. Gultekin, G. S. Guven, E. Guzel, S. Furat, and S. Ersanli, “Histologic and histomorphometric comparison of bone regeneration between bone morphogenetic protein-2 and platelet-derived growth factor-BB in experimental groups,” *The Journal of Craniofacial Surgery*, vol. 27, no. 3, pp. 805–809, 2016.
- [35] W. Li, S. Zhu, and J. Hu, “Bone regeneration is promoted by orally administered bovine lactoferrin in a rabbit tibial distraction osteogenesis model,” *Clinical Orthopaedics and Related Research*, vol. 473, no. 7, pp. 2383–2393, 2015.
- [36] E. G. Machado, J. P. M. Issa, F. A. T. de Figueiredo et al., “A new heterologous fibrin sealant as scaffold to recombinant human bone morphogenetic protein-2 (rhBMP-2) and natural latex proteins for the repair of tibial bone defects,” *Acta Histochemica*, vol. 117, no. 3, pp. 288–296, 2015.
- [37] S. Subramanian, A. Mitchell, W. Yu, S. Snyder, K. Uhrich, and J. P. O’Connor, “Salicylic acid-based polymers for guided bone regeneration using bone morphogenetic protein-2,” *Tissue Engineering. Part A*, vol. 21, no. 13–14, pp. 2013–2024, 2015.
- [38] B. Skovrlj, S. M. Koehler, P. A. Anderson et al., “Association between BMP-2 and carcinogenicity,” *Spine*, vol. 40, no. 23, pp. 1862–1871, 2015.
- [39] J. W. Savage, M. P. Kelly, S. A. Ellison, and P. A. Anderson, “A population-based review of bone morphogenetic protein: associated complication and reoperation rates after lumbar spinal fusion,” *Neurosurgical Focus*, vol. 39, no. 4, article E13, 2015.
- [40] C. P. Hofstetter, A. S. Hofer, and A. D. Levi, “Exploratory meta-analysis on dose-related efficacy and morbidity of bone morphogenetic protein in spinal arthrodesis surgery,” *Journal of Neurosurgery. Spine*, vol. 24, no. 3, pp. 457–475, 2016.
- [41] P. S. Brannan, R. G. Gaston, B. J. Loeffler, and D. R. Lewis, “Complications with the use of BMP-2 in scaphoid nonunion surgery,” *The Journal of Hand Surgery*, vol. 41, no. 5, pp. 602–608, 2016.
- [42] M. Bannwarth, J. C. Kleiber, B. Marlier, C. Eap, J. Duntze, and C. F. Litre, “Ectopic bone formation with joint impingement after posterior lumbar fusion with rhBMP-2,” *Orthopaedics & Traumatology, Surgery & Research*, vol. 102, no. 2, pp. 255–256, 2016.
- [43] L. Shi, W. Sun, F. Gao, L. Cheng, and Z. Li, “Heterotopic ossification related to the use of recombinant human BMP-2 in osteonecrosis of femoral head,” *Medicine (Baltimore)*, vol. 96, no. 27, article e7413, 2017.
- [44] J. Z. Guzman, R. K. Merrill, J. S. Kim et al., “Bone morphogenetic protein use in spine surgery in the United States: how have we responded to the warnings?,” *The Spine Journal*, vol. 17, no. 9, pp. 1247–1254, 2017.
- [45] F. Y. Liu, D. L. Yang, W. Z. Huang et al., “Risk factors for dysphagia after anterior cervical spine surgery: a meta-analysis,” *Medicine (Baltimore)*, vol. 96, no. 10, article e6267, 2017.
- [46] N. Stiel, T. N. Hissnauer, M. Rupprecht et al., “Evaluation of complications associated with off-label use of recombinant human bone morphogenetic protein-2 (rhBMP-2) in pediatric orthopaedics,” *Journal of Materials Science. Materials in Medicine*, vol. 27, no. 12, p. 184, 2016.
- [47] A. T. Villavicencio and S. Burneikiene, “RhBMP-2-induced radiculitis in patients undergoing transforaminal lumbar interbody fusion: relationship to dose,” *The Spine Journal*, vol. 16, no. 10, pp. 1208–1213, 2016.
- [48] A. L. Laurie, Y. Chen, R. Chou, and R. Fu, “Meta-analysis of the impact of patient characteristics on estimates of effectiveness and harms of recombinant human bone morphogenetic Protein-2 in lumbar spinal fusion,” *Spine (Phila Pa 1976)*, vol. 41, no. 18, pp. E1115–E1123, 2016.
- [49] M. O. Freire, H. K. You, J. K. Kook, J. H. Choi, and H. H. Zadeh, “Antibody-mediated osseous regeneration: a novel strategy for bioengineering bone by immobilized anti-bone morphogenetic protein-2 antibodies,” *Tissue Engineering. Part A*, vol. 17, no. 23–24, pp. 2911–2918, 2011.
- [50] M. O. Freire, H. K. Kim, J. K. Kook, A. Nguyen, and H. H. Zadeh, “Antibody-mediated osseous regeneration: the early events in the healing response,” *Tissue Engineering. Part A*, vol. 19, no. 9–10, pp. 1165–1174, 2013.
- [51] M. Freire, J.-H. Choi, A. Nguyen et al., “Application of AMOR in craniofacial rabbit bone bioengineering,” *BioMed Research International*, vol. 2015, Article ID 628769, 7 pages, 2015.
- [52] A. Moshaverinia, S. Ansari, C. Chen et al., “Co-encapsulation of anti-BMP2 monoclonal antibody and mesenchymal stem cells in alginate microspheres for bone tissue engineering,” *Biomaterials*, vol. 34, no. 28, pp. 6572–6579, 2013.
- [53] S. Ansari, A. Moshaverinia, S. H. Pi, A. Han, A. I. Abdelhamid, and H. H. Zadeh, “Functionalization of scaffolds with chimeric anti-BMP-2 monoclonal antibodies for osseous regeneration,” *Biomaterials*, vol. 34, no. 38, pp. 10191–10198, 2013.
- [54] S. Ansari, M. O. Freire, E.-K. Pang, A. I. Abdelhamid, M. Almohaimeed, and H. H. Zadeh, “Immobilization of murine anti-BMP-2 monoclonal antibody on various biomaterials for bone tissue engineering,” *BioMed Research International*, vol. 2014, Article ID 940860, 10 pages, 2014.
- [55] S. Ansari, J. H. Phark, S. Duarte Jr. et al., “Biomechanical analysis of engineered bone with anti-BMP2 antibody immobilized on different scaffolds,” *Journal of Biomedical Materials*

- Research. Part B, Applied Biomaterials*, vol. 104, no. 7, pp. 1465–1473, 2016.
- [56] Y. Xie, Y. Su, S. Min et al., “Collagen sponge functionalized with chimeric anti-BMP-2 monoclonal antibody mediates repair of critical-size mandibular continuity defects in a non-human primate model,” *BioMed Research International*, vol. 2017, Article ID 8094152, 11 pages, 2017.
- [57] L. Guo, S. Min, Y. Su et al., “Collagen sponge functionalized with chimeric anti-BMP-2 monoclonal antibody mediates repair of nonunion tibia defects in a nonhuman primate model: an exploratory study,” *Journal of Biomaterials Applications*, vol. 32, no. 4, pp. 425–432, 2017.
- [58] D. W. Dempster, J. E. Compston, M. K. Drezner et al., “Standardized nomenclature, symbols, and units for bone histomorphometry: a 2012 update of the report of the ASBMR Histomorphometry Nomenclature Committee,” *Journal of Bone and Mineral Research*, vol. 28, no. 1, pp. 2–17, 2013.
- [59] M. L. Nevins and M. A. Reynolds, “Tissue engineering with recombinant human platelet-derived growth factor BB for implant site development,” *The Compendium of Continuing Education in Dentistry*, vol. 32, pp. 20–27, 2011.
- [60] A. B. Castro, N. Meschi, A. Temmerman et al., “Regenerative potential of leucocyte- and platelet-rich fibrin. Part B: sinus floor elevation, alveolar ridge preservation and implant therapy. A systematic review,” *Journal of Clinical Periodontology*, vol. 44, no. 2, pp. 225–234, 2017.
- [61] E. A. Alkan, A. Parlar, B. Yildirim, and B. Sengüven, “Histological comparison of healing following tooth extraction with ridge preservation using enamel matrix derivatives versus Bio-Oss Collagen: a pilot study,” *International Journal of Oral and Maxillofacial Surgery*, vol. 42, no. 12, pp. 1522–1528, 2013.
- [62] A. M. Coomes, B. L. Mealey, G. Huynh-Ba, C. Barboza-Arguello, W. S. Moore, and D. L. Cochran, “Buccal bone formation after flapless extraction: a randomized, controlled clinical trial comparing recombinant human bone morphogenetic protein 2/absorbable collagen carrier and collagen sponge alone,” *Journal of Periodontology*, vol. 85, no. 4, pp. 525–535, 2014.
- [63] R. Alissa, M. Esposito, K. Horner, and R. Oliver, “The influence of platelet-rich plasma on the healing of extraction sockets: an explorative randomised clinical trial,” *European Journal of Oral Implantology*, vol. 3, no. 2, pp. 121–134, 2010.
- [64] E. Anitua, A. Murias-Freijo, M. H. Alkhraisat, and G. Orive, “Clinical, radiographical, and histological outcomes of plasma rich in growth factors in extraction socket: a randomized controlled clinical trial,” *Clinical Oral Investigations*, vol. 19, no. 3, pp. 589–600, 2015.
- [65] M. Mozzati, G. Galesio, S. di Romana, L. Bergamasco, and R. Pol, “Efficacy of plasma-rich growth factor in the healing of postextraction sockets in patients affected by insulin-dependent diabetes mellitus,” *Journal of Oral and Maxillofacial Surgery*, vol. 72, no. 3, pp. 456–462, 2014.
- [66] G. Chen, C. Deng, and Y. P. Li, “TGF- β and BMP signaling in osteoblast differentiation and bone formation,” *International Journal of Biological Sciences*, vol. 8, no. 2, pp. 272–288, 2012.
- [67] W. K. Hsu and J. C. Wang, “The use of bone morphogenetic protein in spine fusion,” *The Spine Journal*, vol. 8, no. 3, pp. 419–425, 2008.
- [68] A. L. Jones, R. W. Bucholz, M. J. Bosse et al., “Recombinant human BMP-2 and allograft compared with autogenous bone graft for reconstruction of diaphyseal tibial fractures with cortical DEFECTS,” *The Journal of Bone and Joint Surgery. American Volume*, vol. 88, no. 7, pp. 1431–1441, 2006.
- [69] K. S. Cahill, J. H. Chi, A. Day, and E. B. Claus, “Prevalence, complications, and hospital charges associated with use of bone-morphogenetic proteins in spinal fusion procedures,” *JAMA*, vol. 302, no. 1, pp. 58–66, 2009.
- [70] G. M. Calori, D. Donati, C. Di Bella, and L. Tagliabue, “Bone morphogenetic proteins and tissue engineering: future directions,” *Injury*, vol. 40, pp. S67–S76, 2009.

Research Article

Failure Modes and Survival of Anterior Crowns Supported by Narrow Implant Systems

Edmara T. P. Bergamo ¹, Everardo N. S. de Araújo-Júnior ¹, Adolfo C. O. Lopes ¹,
Paulo G. Coelho ^{2,3,4}, Abbas Zahoui ¹, Ernesto B. Benalcázar Jalkh ^{1,2},
and Estevam A. Bonfante ¹

¹Department of Prosthodontics and Periodontology, Bauru School of Dentistry-University of Sao Paulo, Bauru 17012-980, Brazil

²Department of Biomaterials and Biomimetics, New York University College of Dentistry, USA

³Department of Biomedical Engineering, New York University Tandon School of Engineering Brooklyn, USA

⁴Hansjörg Wyss Department of Plastic Surgery, New York University Grossman School of Medicine, New York City, 10010 NY, USA

Correspondence should be addressed to Edmara T. P. Bergamo; edmaratatiely@gmail.com

Received 19 June 2020; Accepted 12 August 2020; Published 8 September 2020

Guest Editor: Henriette Lerner

Copyright © 2020 Edmara T. P. Bergamo et al. This is an open access article distributed under the Creative Commons Attribution License, which permits unrestricted use, distribution, and reproduction in any medium, provided the original work is properly cited.

The reduced hardware design of narrow implants increases the risk of fracture not only of the implant itself but also of the prosthetic constituents. Hence, the current study is aimed at estimating the probability of survival of anterior crowns supported by different narrow implant systems. Three different narrow implant systems of internal conical connections were evaluated ($\text{Ø}3.5 \times 10 \text{ mm}$): (i) Active (Nobel Biocare), (ii) Epikut (S.I.N. Implant System), and (iii) BLX (Straumann). Abutments were torqued to the implants, and standardized maxillary incisor crowns were cemented. The assemblies were subjected to step-stress accelerated life testing (SSALT) in water through load application of 30 degrees off-axis lingually at the incisal edge of the crowns using a flat tungsten carbide indenter until fracture or suspension. The use level probability Weibull curves and reliability for completion of a mission of 100,000 cycles at 80 N and 120 N were calculated and plotted. Weibull modulus and characteristic strength were also calculated and plotted. Fractured samples were analyzed in a stereomicroscope. The beta (β) values were 1.6 (0.9-3.1) and 1.4 (0.9-2.2) for BLX and Active implants, respectively, and 0.5 (0.3-0.8) for the Epikut implant, indicating that failures were mainly associated with fatigue damage accumulation in the formers, but more likely associated with material strength in the latter. All narrow implant systems showed high probability of survival ($\geq 95\%$, CI: 85-100%) at 80 and 120 N, without significant difference between them. Weibull modulus ranged from 6 to 14. The characteristic strength of Active, Epikut, and BLX was 271 (260-282) N, 216 (205-228) N, and 275 (264-285) N, respectively. The failure mode predominantly involved abutment and/or abutment screw fracture, whereas no narrow implant was fractured. Therefore, all narrow implant systems exhibited a high probability of survival for anterior physiologic masticatory forces, and failures were restricted to abutment and abutment screw.

1. Introduction

Endosseous implants are common therapeutic approaches in oral rehabilitation that support the reconstruction of damaged tissues due to trauma/pathology by employing implant-supported prosthetic devices [1, 2], restoring patients' quality of life through natural-like esthetic appearance and masticatory function [3, 4]. Osseointegrated implants have been indicated for over 50 years to rehabilitate

from single to full-arch edentulism with high implant survival rates, approximately 95%, and stability of soft and hard peri-implant tissue, and marginal bone loss of approximately 0.50 mm, after 10 years of follow-up [5-7]. Current implant-supported reconstructions have been centered on the use of metal-ceramic, polymeric, and all-ceramic prostheses screwed and/or cemented to prefabricated metallic abutments, with approximately 90% survival rates up to 10 years in function [5, 8-11]. Such increasingly convincing

clinical data and bioengineering improvements have encouraged the indication of dental implants in more challenging clinical conditions than originally planned [12, 13], such as in the maxilla where there is less cortical bone to provide initial stability [14, 15]. Similarly, implant loading has been indicated steadily earlier with similar success rates to delayed loading, higher than 90% [16, 17]. Although high survival rates are reported for immediate loading, the indication of this protocol has shown to become less predictive when implant fixtures are placed in critical clinical scenarios, including postextraction sites and nonsplinted single crowns [18].

The interplay between implant macrogeometry and surgical instrumentation, bone availability, and quality have a profound influence on the achievement of optimal primary stability, favoring an undisturbed peri-implant healing, which can render the system a temporal load-bearing capability [19–23]. The characteristics of the implant design, especially the body and apex shape and thread profile, regulate bone response during implant placement, controlling the stress distribution to the surrounding bone and implant stabilization [23–26]. Therefore, implant geometry has significantly evolved over the years to maximize the biomechanical performance, especially in compromised bone scenarios [19–21].

Irrespective of implant design, an optimal three-dimensional implant positioning has to be assured to achieve long-term success, avoiding functional, biological, and esthetic complications [27, 28]. Clinical scenarios of anatomic paucity of the bone (alveolar crest atrophy) and/or compromised osteotomy walls resulting from tooth extractions, where the limited bone availability compromises the use of standard-diameter implants ($\theta \geq 3.75$ mm to $\theta < 5.0$ mm) [29], often require bone grafting procedures prior to implant surgery, which prolong treatment time and increase costs, increase morbidity, and frequently compromise immediate or early implant loading [30, 31]. Therefore, alternative concepts such as the use of narrow diameter implants ($\theta < 3.75$ to $\theta \geq 3.0$ mm) have raised as potential clinical options to rehabilitate areas with limited prosthetic space [29], with approximately 10% reduction in the need for bone tissue manipulation and respecting the minimum requirements for adequate papillary fill [27, 28, 31–35]. Narrow implants have shown similar survival rates to standard diameter implants, higher than 95%, and marginal bone loss of approximately 2 mm after an average 4 years of follow-up [36–38]. Moreover, reduced diameter implants have been successfully indicated in immediate loading protocols, with no implant loss and approximately 0.2 mm marginal bone loss after 2 years, which requires further long-term investigations [39].

Despite the high survival rates, caution has been advised in the use of narrow implant systems, where not only the implant itself but also the prosthetic constituents might be more prone to fatigue damage accumulation and fracture as a result of their reduced hardware design [40–43]. Moreover, the smaller stress distribution area of narrow implants may have a major impact on the ability to withstand biting forces, leading to bone overloading [40].

To the authors' knowledge, there is currently no study evaluating the biomechanical performance of newly developed implant systems, comprising of a narrower conical body shape and reduced neck diameter. Considering that complex mechanical loading scenarios play a significant role in the strength degradation of implant systems in the oral environment, a laboratory fatigue testing that reproduces clinical failures, such as step-stress accelerated life testing (SSALT), becomes an important tool to predict the lifetime of the implant-abutment-prosthesis reconstructions [42, 44–47]. Hence, the present study used SSALT to estimate the probability of survival and failure mode of the recently developed narrow implant systems. The postulated null hypothesis was that different narrow implant systems would not result in different probability of survival.

2. Materials and Methods

2.1. Sample Preparation. Three narrow implant systems of internal conical connections were evaluated in the current study ($\text{Ø}3.5 \times 10$ mm/ $n = 21$ /implant system): (i) Active (Nobel BioCare, Zürich, Switzerland), (ii) Epikut (S.I.N Implants, Sao Paulo, SP, Brazil), and (iii) BLX (Straumann, Basel, Switzerland). Such implant systems consisted of a narrower conical body shape with a reduced neck diameter as well as a large thread pitch, deep and wide threads, with the ability to cut the bone (the sharpness varies according to the length of the implant) (Figure 1).

Sixty-three implants were fixed in a surveyor (B2, Bio-ART, Sao Carlos, SP, Brazil) to standardize the position and embedded using polymethylmethacrylate acrylic resin (Orthodontic Resin, Dentsply, York, PA, USA) into a 15 mm diameter matrix at the same level of the implant platform. Proprietary Ti-base abutments (Pillar Snappy, Nobel; Duotech, S.I.N. Implant System; Variobase, Straumann) were torqued to the implants' respective groups, using a digital torque gauge (Tohnichi BTG150CN-S, Tohnichi America, Buffalo Grove, IL, USA), following the manufacturer's instruction.

Standardized maxillary central incisor crowns were virtually designed; the wax was pattern milled and casted using cobalt-chrome alloy (Wirobond 280, BEGO, Lincoln, RI, USA). The crowns were cemented on the abutments using a self-adhesive dual-curing resin cement (Rely X U200, 3 M Oral Care, St. Paul, MN, USA), following manufacturer's instructions.

2.2. Fatigue Testing. Single load-to-failure (SLF) testing was performed in three specimens of each group to design the stress profiles for the step-stress accelerated life testing (SSALT). An uniaxial compression load was applied 30 degrees off-axis lingually at the incisal edge of the crown using a flat tungsten carbide indenter at a crosshead speed of 1 mm/min (ElectroPuls™ E3000 Linear-Torsion System, Instron, Norwood, MA, USA) [41, 45, 47, 48]. The remaining eighteen specimens per implant system were assigned to the three stress profiles following the ratio distribution of 3 : 2 : 1, where 9 were allocated in the mild, 6 in the moderate,

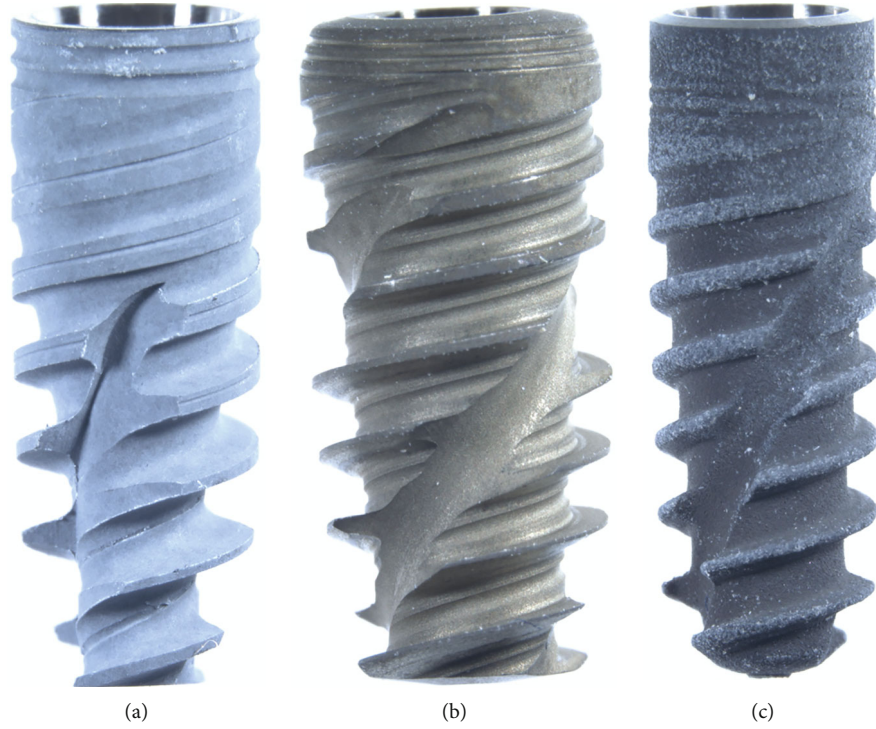


FIGURE 1: Representative images of the implants' macrogeometry: Active (a), Epikut (b), and BLX (c).

and 3 in the aggressive, as detailed elsewhere [41, 45, 47, 48]. These profiles are named based on the load increase rapidness, in which a specimen will be fatigued throughout the cycles until a certain load level. It means that specimens allocated in the mild profile will be cycled for a longer time to reach the same load level of a specimen assigned to the moderate or aggressive profiles.

SSALT was performed using the same all-electric dynamic test equipment, where the load was also applied 30 degrees off-axis lingually at the incisal edge of the crown using the same flat tungsten carbide indenter at a frequency of 15 Hz in water until specimen failure (considered a fracture or bending of the abutment, abutment screw, or implant) or survival (no failure at the end of the step-stress profiles when testing was suspended), until a maximum load of 500 N. The findings were recorded as stress profile, load at failure, and number of cycles.

Based on the failure distribution, the data was analyzed using an underlying life distribution to describe the life data collected at different stress levels and a life-stress relationship to quantify the manner in which the life distribution changed across different stress levels [45, 49–51]. Thus, the Weibull Distribution was chosen to fit the life data collected in SSALT and its probability density functions (pdfs) was given by (Equation (1)):

$$\int(T) = \frac{\beta}{\eta} \left(\frac{T}{\eta}\right)^{\beta-1} e^{-(T/\eta)^\beta}, \quad (1)$$

where η is the scale parameter and β is the shape parameter. Considering the time-varying stress model ($x(t)$), the inverse

power law relationship (IPL) was selected to extrapolate a use level condition considering the cumulative effect of the applied stresses, commonly referred as the cumulative damage model. In such a model, the IPL would be given by (Equation (2)):

$$L(x(t)) = \frac{\alpha}{x(t)}^\eta, \quad (2)$$

where L is the life data and $x(t)$ is the stress. Then, the IPL-Weibull pdf (where η is replaced by the IPL) was given by (Equation (3)):

$$\int(t, x(t)) = \beta \left(\frac{x(t)}{\alpha}\right)^\eta \left(\int_0^t \left(\frac{x(t)}{\alpha}\right)^\eta du\right)^{\beta-1} e^{-((x(t)/\alpha)^\eta du)^\beta}. \quad (3)$$

From the extrapolated use level pdf, a variety of functions was derived, including reliability (Equation (4)):

$$R(t, x(t)) = e^{-((x(t)/\alpha)^\eta du)^\beta}. \quad (4)$$

Parameter estimation for all analyses was calculated via MLE method, and 90% two-sided confidence interval (90% CI) was approximated using the Fisher matrix approach. Hence, the use level probability Weibull curves (probability of failure versus number of cycles) with a set load of 100 N were calculated and plotted (Synthesis 9, Alta Pro, Reliasoft, Tucson, AZ, USA). The reliability was calculated for the completion of a mission of 100,000 cycles at 80 and 120 N, and the differences between groups were identified based

on the nonoverlap of the CI. The use level probability Weibull analysis provides the beta (β) value, which describes the failure rate behavior over time ($\beta < 1$ indicates that failure rate decreased over time, $\beta \sim 1$ failure rate does not vary over time, and $\beta > 1$ means that failure rate increased over time) [45]. As the calculated use level probability Weibull β parameter of the Epikut group was < 1 , a Weibull 2-parameter calculation of the Weibull modulus, a unitless parameter that measures the variability of the results and the characteristic strength, load at which 63.2% of the specimens would fail, was presented using the final load to failure or survival (Weibull 9++, Reliasoft) [45, 50, 51]. Weibull 2-parameter contour plot (Weibull modulus vs. characteristic strength) was graphed to determine statistical differences through the nonoverlap of CI.

All failed specimens were evaluated in a polarized light stereomicroscope (AxioZoom V16, Zeiss, Oberkochen, Germany) using Z-stack mode which automates sequential imaging along the z-plane and sticks them within the same depth of focus (ZEN 2.3 PRO, Zeiss) to depict fracture planes and allow fractographic analysis under higher magnifications (up to 260x) and classified according to the failure criteria.

3. Results

All specimens failed during step-stress accelerated life testing (SSALT) testing. The use level probability Weibull curves calculated from the SSALT data for a use level load of 100 N are plotted in Figure 2. The mean beta (β) values derived from use level probability Weibull calculation were $\beta = 1.6$ (0.9-3.1) and $\beta = 1.4$ (0.9-2.2) for the BLX and Active implants, indicating that failures were mainly dictated by fatigue damage accumulation and tended to increase over time, while the lower bound values of the confidence interval also suggest the influence of material strength. In contrast, the Epikut implant presented $\beta = 0.5$ (0.3-0.8), indicating that failures were most likely dictated by material strength rather than damage accumulation and tended to decrease over time.

The calculated probability of survival with the corresponding 90% confidence intervals for a determined mission of 100,000 at 80 and 120 N is presented in Table 1. All narrow implant systems investigated, Active (99% and 96%), Epikut (99% and 95%), and BLX (100% and 99%), demonstrated high probability of survival for set missions (80 and 120 N, respectively) that represent above human bite forces (14.5 N) [52], without statistically significant difference between them.

There was no statistically significant difference between narrow implant systems for all estimated missions.

The calculated Weibull modulus and characteristic strength are depicted in Figure 3. Active (10, 7.4-13.8), Epikut (8.2, 6.1-10.9), and BLX (11.6, 7.9-14.8) implants exhibited similar Weibull modulus. In contrast, Active (271, 260-282 N) and BLX (275, 264-285 N) implants demonstrated statistically significant higher characteristic strength relative to the Epikut implant (216, 205-228 N); however, all values were higher than the maximum voluntary bite forces reported in the anterior region, approximately 200 N [53].

Representative failed specimens are depicted in Figures 4–6. The failure mode predominantly involved abutment and/or abutment screw fracture, mainly from lingual to buccal where forces physiologically take place, whereas no narrow implant was fractured. While Active and BLX implant fractures were more restricted to the abutment, Epikut fracture predominantly involved abutment, at the connection with the implant and also at the abutment platform where the crown is seated, and abutment screw (Figure 7).

4. Discussion

Previous studies have demonstrated that not only narrow implants but also the respective prosthetic components may be more prone to fatigue damage accumulation and fracture due to their smaller hardware design [40–43, 48], which has not yet been investigated for the newly developed implant systems, whose original strategy suggests a narrower bulk design with a more pronounced thread profile. Hence, the current study sought to estimate the fatigue lifetime and probability of survival of anterior crowns supported by recently developed narrow implant systems. From a fatigue perspective, all narrow implant systems showed high probability of survival for determined missions equivalent to anterior physiologic masticatory forces; thus, the postulated null hypothesis that different narrow implant systems would not result in different probability of survival failed to be rejected.

The current biomechanical findings obtained after fatigue testing the narrow implant systems have been related to the combination of degradation mechanisms associated with repeated loading and damage accumulation as well as strength of the weakest component of the implant-supported reconstruction, the abutment and/or abutment screw [45]. While fatigue predominantly accelerated the failure of BLX and Active narrow implant systems, there has also been an evidence of the influence of the material strength based on lower bound values of the confidence interval. In contrast, the failures of the Epikut system were mainly attributed to material strength rather than fatigue damage accumulation. In fact, flaws intrinsic to material processing can cause a meaningful variation in the fracture load from sample to sample, and the Weibull modulus (m , the shape parameter of Weibull distribution) is a dimensionless material-specific parameter used as an indicator of strength variation or asymmetric strength distribution a result of flaw population within the material structure. Higher m values indicate a more homogeneous flaw size distribution throughout the material, narrower strength scattering, and, consequently, greater structural reliability [54, 55]. The opposite association is expected from lower m values. In the current study, all groups present similar Weibull modulus, indicating similar structural reliability, and the values, ranging from 6 to 14, also corroborated with the results of previous studies evaluating different narrow implant systems under similar fatigue methodology, approximately 6 [41, 48].

At a given mission of 80 N and 120 N, all narrow implant systems evidenced high probability of survival, almost 100%. This data suggests that the newly proposed implant design,

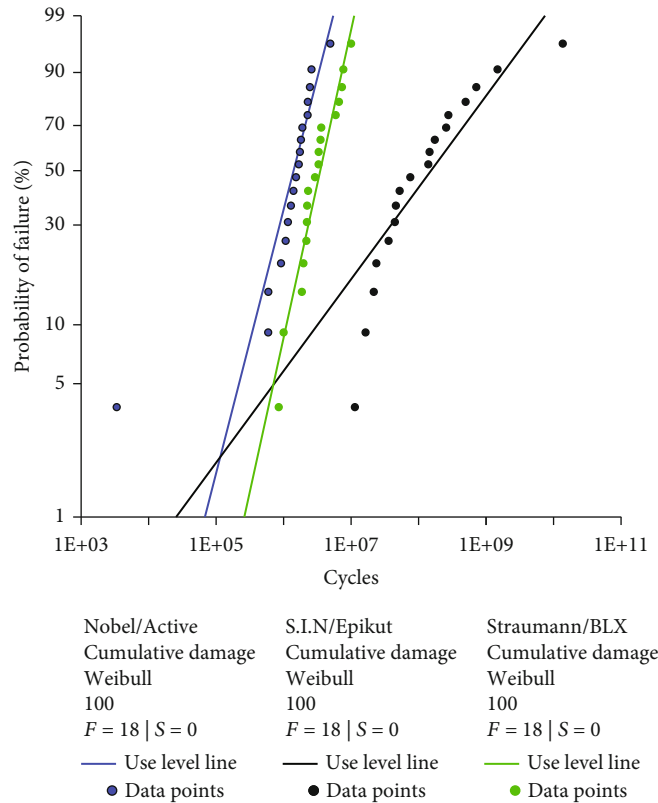


FIGURE 2: Use level probability Weibull curves at a set load of 100 N showing the probability of failure (%) as a function of cycles of the different narrow implant systems.

TABLE 1: Probability of survival (%) with the corresponding 95% CI for a mission of 100,000 cycles and at 80 and 120 N of the different implant systems.

	Active	Epikut	BLX
Upper bound	100	100	100
Probability of survival (80 N)	99	99	100
Lower bound	95	96	99
Upper bound	99	98	100
Probability of survival (120 N)	96	95	99
Lower bound	87	85	97

irrespective of commercial system, can be a reliable option to replace incisors since mean physiologic masticatory forces in these regions vary within the estimated range (14.5 N) [52]. If one considers maximum voluntary bite force values, although BLX and Active implant have shown significantly higher characteristic strength than Epikut, all systems resulted in higher values (>200 N) than the maximum forces reported in the literature for incisors, approximately 200 N [53]. Previous studies investigating the fatigue lifetime of conventional narrow implant systems using SSALT under similar methodology have also demonstrated high probability of survival for similar estimated missions, approximately 99% [41, 48]. The probability of survival of narrow implants has also been compared to standard-diameter implants, with significant differences in the biomechanical behavior being

reported only when hexagonal connections were evaluated [48]. This fact endorses the favorable results described in the current study, where the improved stability and stress distribution inherent to the internal conical connection of the different narrow implant systems supported a high survival prediction to the implant and prosthetic constituents, even in the laboratory reproduction of a challenging clinical scenario through off-axis incisal edge loading. Therefore, it can be assumed that the critical determinant of clinical survivability when smaller-diameter implants are taken into consideration should be centered on the proper selection of the implant connection rather than macrogeometry and thread design differences.

In fact, it has been well-established that mechanical complications are increased for external hexagon connection implants as a result of the reduced screw joint stability and resistance to oblique loads [47, 48]. Internal implant connections, such as the internal conical connections, have been suggested to improve the joint strength increasing lateral and rotational stability as a function of a deeper engagement on the implant-abutment interface, shielding the rehabilitation from mechanical overloading during function [56, 57]. Moreover, the increased contact area of the abutment with the implant internal walls, potentially decreasing the micro-motion at the interface and deeply distributing the intraoral forces along the implant longitudinal axis, has also shown to protect the implant itself from fracture, even in a narrow diameter design, as observed in the current study where no

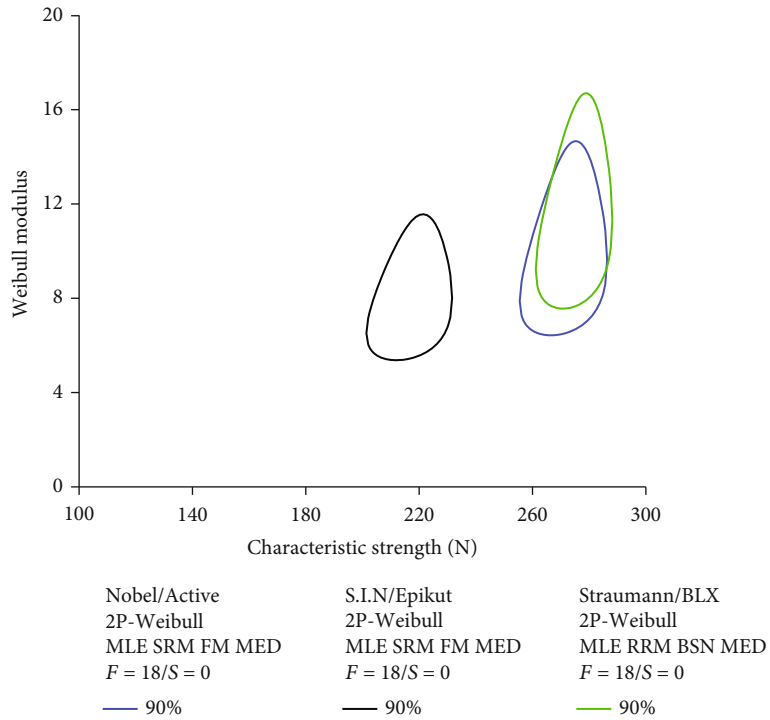


FIGURE 3: Contour plot showing the Weibull modulus (m) as a function of characteristic strength (N). The nonoverlap between contours indicates statistical difference.

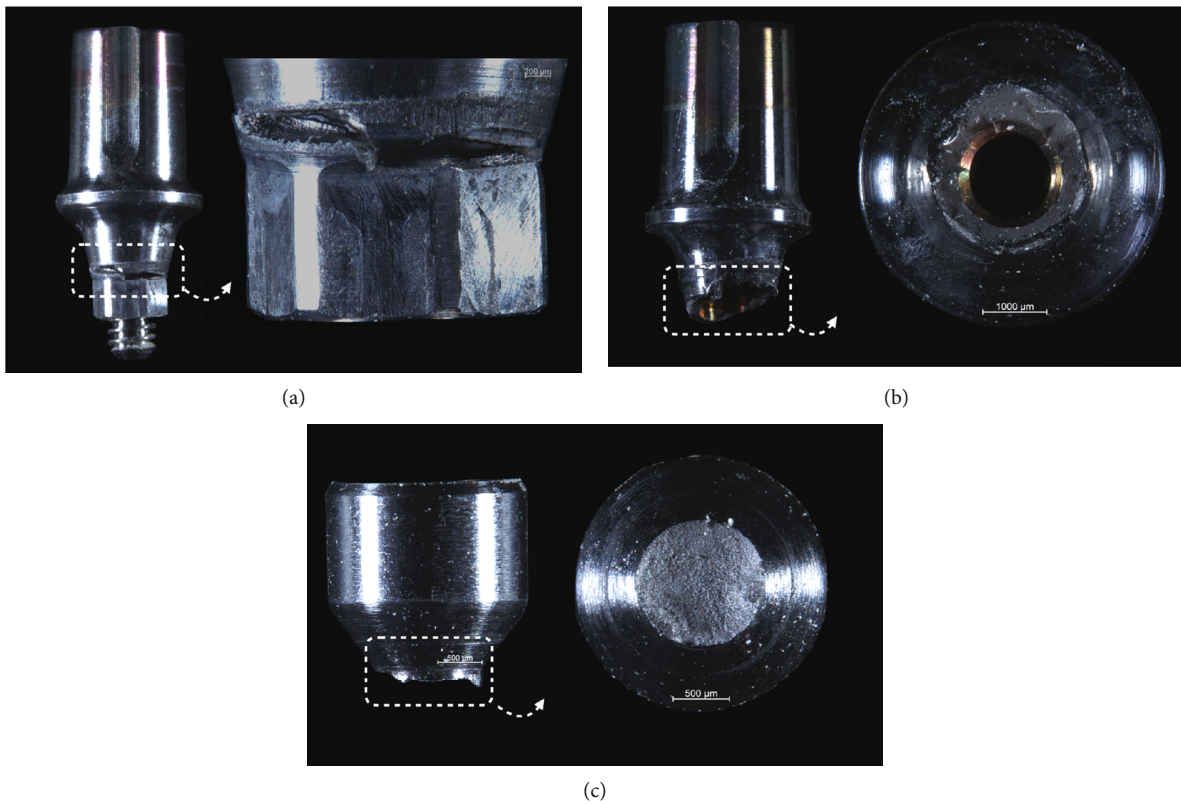


FIGURE 4: Active group implant failure modes represented by abutment fracture in the area of connection with the implant (a and b) and/or abutment screw fracture (c).

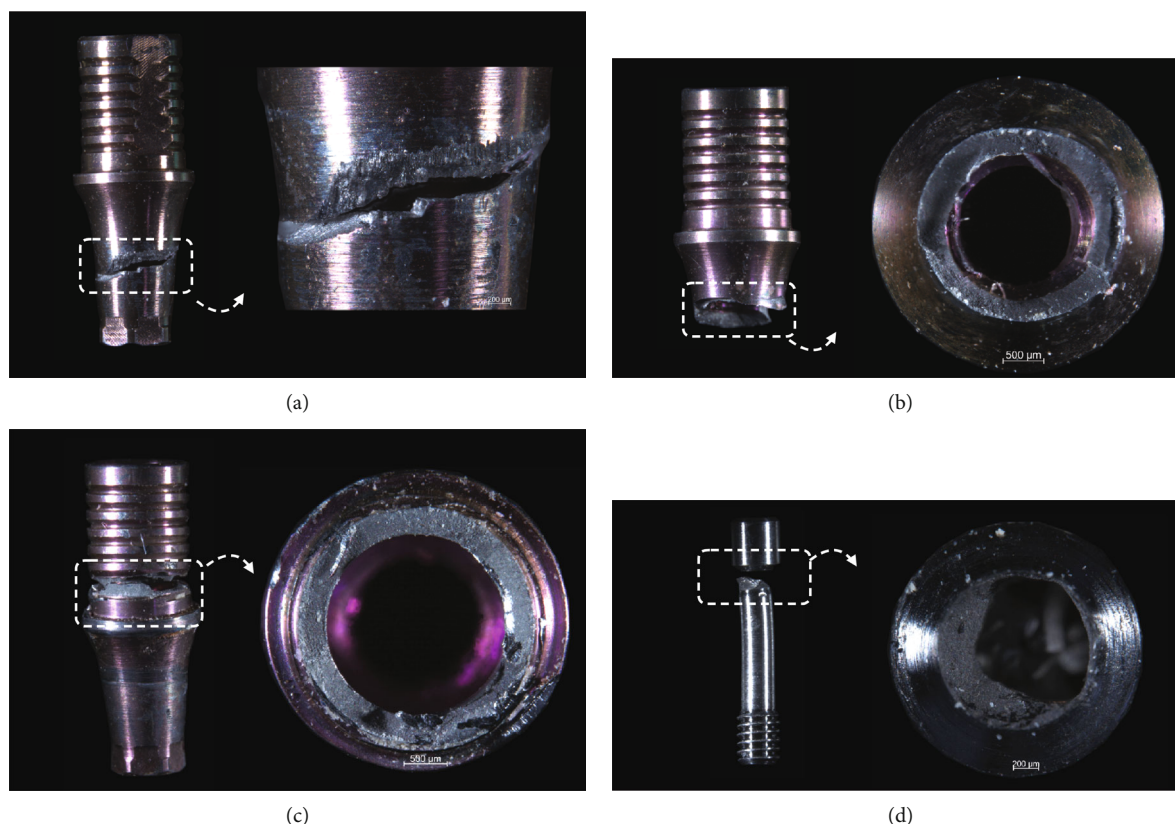
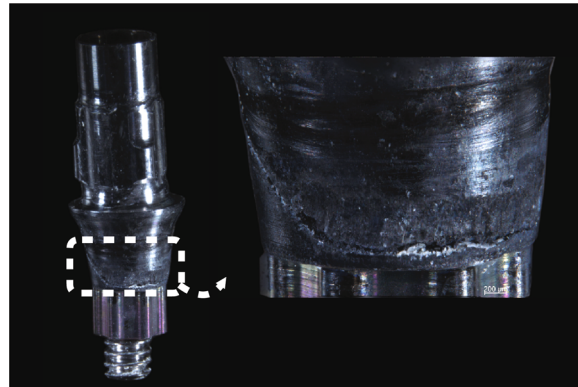


FIGURE 5: Epikut implant failure modes represented by abutment fracture in the area of connection with the implant (a and b) or the abutment platform where crown is settled (c) and/or abutment screw fracture (d).

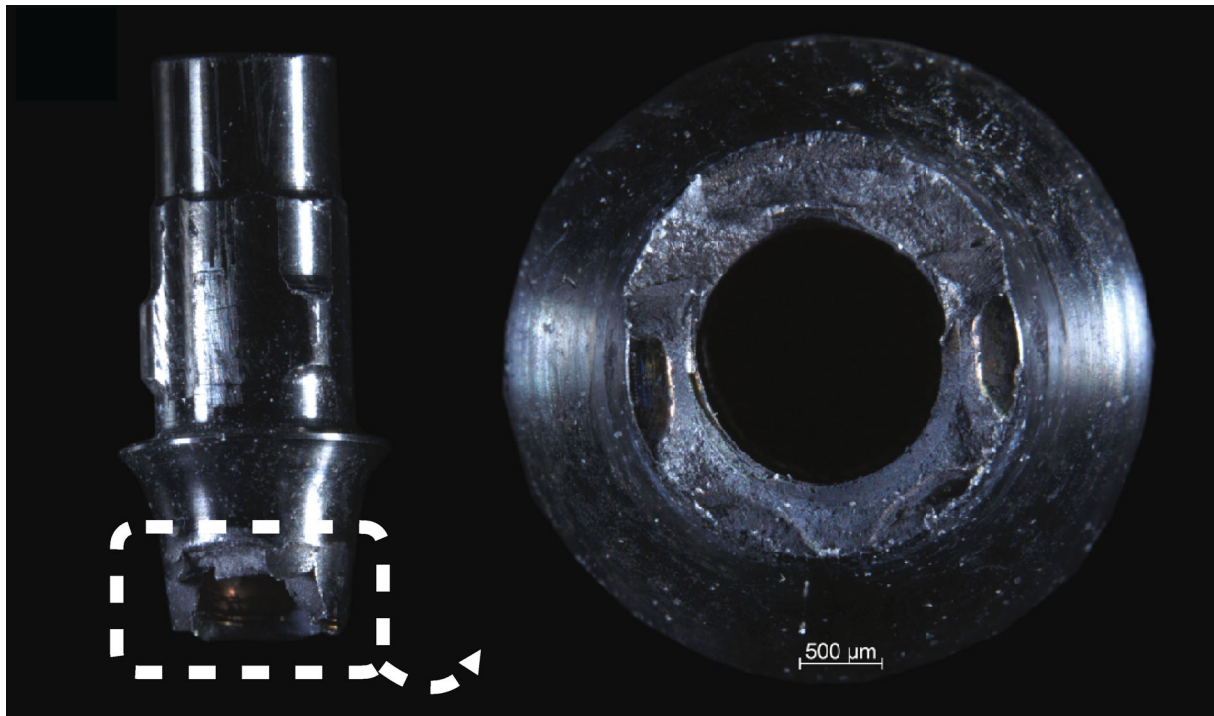
implant fracture has been observed [41, 44, 58]. In fact, the current results indicated that the implant-supported rehabilitation strength was limited by the abutment and/or abutment screw fracture for all narrow implant systems, where the high stress concentrated at the implant-abutment connection as cycles elapsed and load increased during fatigue exceeded their yield strength, leading to fracture. To overcome the strength limitation of two-piece abutments, the use of monolithic abutments connected to internal conical implants has suggested to provide a potential improved biomechanical performance [41, 59, 60], which warrants further investigation for the novel implant design, especially in a scenario of narrow diameter implants where competing failure modes are likely to occur between the thin implant wall and the bulkier abutment [41]. A noteworthy aspect to be discussed in the narrow implant failure modes of the current study is the presence of abutment platform fracture in the Epikut implant, indicating that the stress concentration exceeded the material strength in such area. Thicker abutment cone walls without compromise final superstructure anatomy may be indicated, and an improved biomechanical behavior could be expected for the prosthetic constituents, which also requires further investigations. Finally, given the positive finding of no implant fractures observed for all groups, it can be assumed that grade IV commercially pure cold worked titanium (Active and Epikut) and titanium-zirconium alloy (BLX, 85%Ti-15%Zr) were equally effective in shifting failures toward

prosthetic components, which can be replaced with less morbidity compared to removal of a fractured implant and placement of a new one.

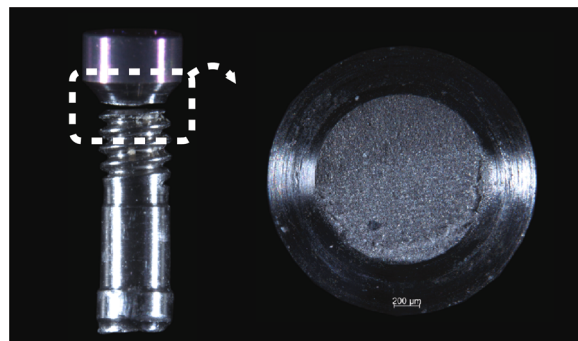
The main challenge in the development of new implant-abutment designs relies not only on the improvement of bone and soft tissue response, hastening osseointegration, but also on reducing and/or eliminating the incidence of biological and mechanical failures in the implant-prosthetic devices when in function; however, such biomechanical innovations require a profound preclinical investigation before their wide indication in the clinical setting to understand the potential complications over time. The step-stress accelerated life testing (SSALT) has been widely used in biomaterial science in order to evaluate the failure behavior of design modifications proposed for implant-supported rehabilitations [41, 42, 44–47]. The results of this type of in vitro study extrapolate clinical failure patterns in a timely way allowing the comparison of the mechanical performance of different systems and/or biomaterials [45]. Thus, the current characterization of the fatigue lifetime and failure modes of the recently developed narrow implant design provided an insight into their biomechanical behavior in a highly demanding anterior reconstruction, where single crowns that are not splinted were subjected to a worst-case loading, challenging the structural integrity of either the prosthesis components or implants; however, caution is also advised in the use of narrow implant systems in particularly challenging scenarios, such as patients with parafunction, since



(a)



(b)



(c)

FIGURE 6: BLX implant failure modes represented by abutment fracture in the area of connection with the implant (a and b) and/or abutment screw fracture (c).

previous studies have demonstrated that narrow implant systems can be more prone to failure relative to standard-diameter implants [42, 43], which may be related to the

implant-abutment connection design [44, 47], bulk material [61], and prosthesis fixation mode [62], among others [45], and require further comparisons for the novel systems.

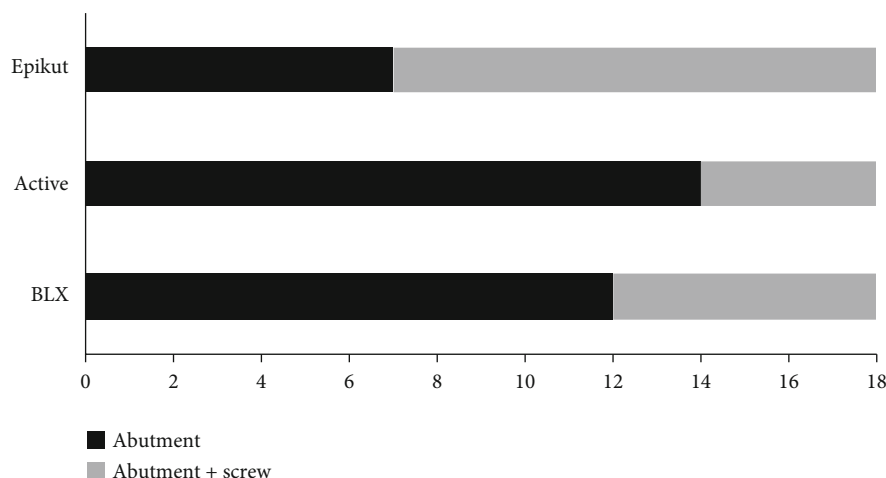


FIGURE 7: Failure distribution as a function of the narrow implant system.

Moreover, the mechanical testing was limited to single restorations and such assumptions need to be investigated in posterior restorations, fixed dental prostheses, or full-arch reconstructions, where units are splinted. Future clinical trials are highly recommended to support the indication of such implants and benefit patients through reducing the indication of difficult and costly bone grafting procedures.

5. Conclusions

From an accelerated fatigue testing perspective, it can be concluded that

- (i) all narrow implant systems exhibited high probability of survival for anterior physiologic masticatory forces
- (ii) the failure mode was similar for all implants, restricted to abutment and abutment screw fracture

Data Availability

Data will be available upon request.

Conflicts of Interest

The authors declare that there is no conflict of interest regarding the publication of this paper.

Acknowledgments

This study was supported by Fundação de Amparo a Pesquisa do Estado de São Paulo (FAPESP) Young Investigators Award grant (2012/19078-7), EMU (2016/18818-8), FAPESP (2019/08693-1, 2019/14798-0, and 2018/03072-6), and BEPE (2019/00452-5); by Conselho Nacional de Desenvolvimento Científico e Tecnológico (CNPq) (grant no. 304589/2017-9); and by CAPES finance code 001.

References

- [1] D. Morton, G. Gallucci, W. S. Lin et al., "Group 2ITI Consensus report: prosthodontics and implant dentistry," *Clinical Oral Implants Research*, vol. 29, no. S16, Supplement 16, pp. 215–223, 2018.
- [2] I. Sailer, S. Muhlemann, R. J. Kohal et al., "Reconstructive aspects: summary and consensus statements of group 3. The 5(th) EAO Consensus Conference 2018," *Clinical Oral Implants Research*, vol. 29, Supplement 18, pp. 237–242, 2018.
- [3] Y. Kumar, P. Chand, V. Arora et al., "Comparison of rehabilitating missing mandibular first molars with implant- or tooth-supported prostheses using masticatory efficiency and patient satisfaction outcomes," *Journal of Prosthodontics*, vol. 26, no. 5, pp. 376–380, 2017.
- [4] S. T. Chen and D. Buser, "Esthetic outcomes following immediate and early implant placement in the anterior maxilla—a systematic review," *The International Journal of Oral & Maxillofacial Implants*, vol. 29, Supplement, pp. 186–215, 2014.
- [5] L. Hjalmarsson, M. Gheisarifar, and T. Jemt, "A systematic review of survival of single implants as presented in longitudinal studies with a follow-up of at least 10 years," *European Journal of Oral Implantology*, vol. 9, no. 2, Supplement 1, pp. 155–162, 2016.
- [6] I. K. Karoussis, U. Bragger, G. E. Salvi, W. Burgin, and N. P. Lang, "Effect of implant design on survival and success rates of titanium oral implants: a 10-year prospective cohort study of the ITI Dental Implant System," *Clinical Oral Implants Research*, vol. 15, no. 1, pp. 8–17, 2004.
- [7] M. Rocuzzo, G. Grasso, and P. Dalmaso, "Keratinized mucosa around implants in partially edentulous posterior mandible: 10-year results of a prospective comparative study," *Clinical Oral Implants Research*, vol. 27, no. 4, pp. 491–496, 2016.
- [8] S. Pieralli, R. J. Kohal, K. Rabel, M. von Stein-Lausnitz, K. Vach, and B. C. Spies, "Clinical outcomes of partial and full-arch all-ceramic implant-supported fixed dental prostheses. A systematic review and meta-analysis," *Clinical Oral Implants Research*, vol. 29, Supplement 18, pp. 224–236, 2018.
- [9] B. E. Pjetursson, N. A. Valente, M. Strassling, M. Zwahlen, S. Liu, and I. Sailer, "A systematic review of the survival and complication rates of zirconia-ceramic and metal-ceramic

- single crowns," *Clinical Oral Implants Research*, vol. 29, no. S16, Supplement 16, pp. 199–214, 2018.
- [10] K. Rabel, B. C. Spies, S. Pieralli, K. Vach, and R. J. Kohal, "The clinical performance of all-ceramic implant-supported single crowns: a systematic review and meta-analysis," *Clinical Oral Implants Research*, vol. 29, Supplement 18, pp. 196–223, 2018.
- [11] I. Sailer, M. Strasing, N. A. Valente, M. Zwahlen, S. Liu, and B. E. Pjetursson, "A systematic review of the survival and complication rates of zirconia-ceramic and metal-ceramic multiple-unit fixed dental prostheses," *Clinical Oral Implants Research*, vol. 29, Supplement 16, pp. 184–198, 2018.
- [12] P. I. Branemark, R. Adell, T. Albrektsson, U. Lekholm, S. Lundkvist, and B. Rockler, "Osseointegrated titanium fixtures in the treatment of edentulousness," *Biomaterials*, vol. 4, no. 1, pp. 25–28, 1983.
- [13] P. I. Branemark, B. O. Hansson, R. Adell et al., "Osseointegrated implants in the treatment of the edentulous jaw. Experience from a 10-year period," *Scandinavian Journal of Plastic and Reconstructive Surgery Supplementum*, vol. 16, pp. 1–132, 1977.
- [14] J. J. Romero-Millan, J. Aizcorbe-Vicente, M. Penarrocha-Diago, P. Galindo-Moreno, L. Canullo, and D. Penarrocha-Oltra, "Implants in the posterior maxilla: open sinus lift versus conventional implant placement. A systematic review," *The International Journal of Oral & Maxillofacial Implants*, vol. 34, no. 4, pp. e65–e76, 2019.
- [15] S. S. Al-Johany, "Survival rates of short dental implants ($\leq 6.5\text{ mm}$) placed in posterior edentulous ridges and factors affecting their survival after a 12-month follow-up period: a systematic review," *The International Journal of Oral & Maxillofacial Implants*, vol. 34, no. 3, pp. 605–621, 2019.
- [16] Q. Cheng, Y. Y. Su, X. Wang, and S. Chen, "Clinical outcomes following immediate loading of single-tooth implants in the esthetic zone: a systematic review and meta-analysis," *The International Journal of Oral & Maxillofacial Implants*, vol. 35, no. 1, pp. 167–177, 2020.
- [17] Y. N. R. Gallardo, I. R. da Silva-Olivio, L. Gonzaga, N. Sesma, and W. Martin, "A systematic review of clinical outcomes on patients rehabilitated with complete-arch fixed implant-supported prostheses according to the time of loading," *Journal of Prosthodontics*, vol. 28, no. 9, pp. 958–968, 2019.
- [18] I. Sanz-Sanchez, I. Sanz-Martin, E. Figuero, and M. Sanz, "Clinical efficacy of immediate implant loading protocols compared to conventional loading depending on the type of the restoration: a systematic review," *Clinical Oral Implants Research*, vol. 26, no. 8, pp. 964–982, 2015.
- [19] E. A. Bonfante, R. Jimbo, L. Witek et al., "Biomaterial and biomechanical considerations to prevent risks in implant therapy," *Periodontology 2000*, vol. 81, no. 1, pp. 139–151, 2019.
- [20] P. G. Coelho and R. Jimbo, "Osseointegration of metallic devices: current trends based on implant hardware design," *Archives of Biochemistry and Biophysics*, vol. 561, pp. 99–108, 2014.
- [21] P. G. Coelho, R. Jimbo, N. Tovar, and E. A. Bonfante, "Osseointegration: hierarchical designing encompassing the micrometer, micrometer, and nanometer length scales," *Dental Materials*, vol. 31, no. 1, pp. 37–52, 2015.
- [22] F. Faot, A. M. Bielemann, A. J. Schuster et al., "Influence of insertion torque on clinical and biological outcomes before and after loading of mandibular implant-retained overdentures in atrophic edentulous mandibles," *BioMed Research International*, vol. 2019, Article ID 8132520, 14 pages, 2019.
- [23] F. Javed, H. B. Ahmed, R. Crespi, and G. E. Romanos, "Role of primary stability for successful osseointegration of dental implants: factors of influence and evaluation," *Interventional Medicine and Applied Science*, vol. 5, no. 4, pp. 162–167, 2013.
- [24] R. Jimbo, N. Tovar, R. B. Anchieta et al., "The combined effects of undersized drilling and implant macrogeometry on bone healing around dental implants: an experimental study," *International Journal of Oral and Maxillofacial Surgery*, vol. 43, no. 10, pp. 1269–1275, 2014.
- [25] H. Abuhussein, G. Pagni, A. Rebaudi, and H. L. Wang, "The effect of thread pattern upon implant osseointegration," *Clinical Oral Implants Research*, vol. 21, no. 2, pp. 129–136, 2010.
- [26] L. Kong, B. L. Liu, K. J. Hu et al., "Optimized thread pitch design and stress analysis of the cylinder screwed dental implant," *Hua Xi Kou Qiang Yi Xue Za Zhi*, vol. 24, no. 6, pp. 509–12, 515, 2006.
- [27] G. I. Benic, M. Mokti, C. J. Chen, H. P. Weber, C. H. Hammerle, and G. O. Gallucci, "Dimensions of buccal bone and mucosa at immediately placed implants after 7 years: a clinical and cone beam computed tomography study," *Clinical Oral Implants Research*, vol. 23, no. 5, pp. 560–566, 2012.
- [28] W. Teughels, J. Merheb, and M. Quirynen, "Critical horizontal dimensions of interproximal and buccal bone around implants for optimal aesthetic outcomes: a systematic review," *Clinical Oral Implants Research*, vol. 20, Supplement 4, pp. 134–145, 2009.
- [29] S. S. Al-Johany, M. D. Al Amri, S. Alsaeed, and B. Alalola, "Dental implant length and diameter: a proposed classification scheme," *Journal of Prosthodontics*, vol. 26, no. 3, pp. 252–260, 2017.
- [30] J. N. Walton and M. I. MacEntee, "Choosing or refusing oral implants: a prospective study of edentulous volunteers for a clinical trial," *The International Journal of Prosthodontics*, vol. 18, no. 6, pp. 483–488, 2005.
- [31] B. Zinsli, T. Sagesser, E. Mericske, and R. Mericske-Stern, "Clinical evaluation of small-diameter ITI implants: a prospective study," *The International Journal of Oral & Maxillofacial Implants*, vol. 19, no. 1, pp. 92–99, 2004.
- [32] E. Andersen, E. Saxegaard, B. M. Knutsen, and H. R. Haanaes, "A prospective clinical study evaluating the safety and effectiveness of narrow-diameter threaded implants in the anterior region of the maxilla," *The International Journal of Oral & Maxillofacial Implants*, vol. 16, no. 2, pp. 217–224, 2001.
- [33] D. E. Papadimitriou, B. Friedland, C. Gannam, S. Salari, and G. O. Gallucci, "Narrow-diameter versus standard-diameter implants and their effect on the need for guided bone regeneration: a virtual three-dimensional study," *Clinical Implant Dentistry and Related Research*, vol. 17, no. 6, pp. 1127–1133, 2015.
- [34] E. Mijiritsky, Z. Mazor, A. Lorean, and L. Levin, "Implant diameter and length influence on survival," *Implant Dentistry*, vol. 22, no. 4, pp. 394–398, 2013.
- [35] R. Penmetsa and K. R. Venkatesh Murthy, "Replacement of a molar with two narrow-diameter dental implants," *Journal of Indian Society of Periodontology*, vol. 20, no. 6, pp. 651–654, 2016.
- [36] P. Malo and M. de Araujo Nobre, "Implants (3.3 mm diameter) for the rehabilitation of edentulous posterior regions: a retrospective clinical study with up to 11 years of follow-up," *Clinical Implant Dentistry and Related Research*, vol. 13, no. 2, pp. 95–103, 2011.

- [37] E. Schiegnitz and B. Al-Nawas, "Narrow-diameter implants: a systematic review and meta-analysis," *Clinical Oral Implants Research*, vol. 29, no. S16, Supplement 16, pp. 21–40, 2018.
- [38] M. O. Klein, E. Schiegnitz, and B. Al-Nawas, "Systematic review on success of narrow-diameter dental implants," *The International Journal of Oral & Maxillofacial Implants*, vol. 29, Supplement, pp. 43–54, 2014.
- [39] C. Peron and G. Romanos, "Immediate provisionalization of single narrow implants in fresh extraction sockets and healed sites: clinical and radiographic outcomes of 2 years follow-up," *The International Journal of Periodontics & Restorative Dentistry*, vol. 40, no. 3, pp. 417–424, 2020.
- [40] S. R. Allum, R. A. Tomlinson, and R. Joshi, "The impact of loads on standard diameter, small diameter and mini implants: a comparative laboratory study," *Clinical Oral Implants Research*, vol. 19, no. 6, pp. 553–559, 2008.
- [41] D. Bordin, L. Witek, V. P. Fardin, E. A. Bonfante, and P. G. Coelho, "Fatigue failure of narrow implants with different implant-abutment connection designs," *Journal of Prosthodontics*, vol. 27, no. 7, pp. 659–664, 2018.
- [42] E. A. Bonfante, E. O. Almeida, F. C. Lorenzoni, and P. G. Coelho, "Effects of implant diameter and prosthesis retention system on the reliability of single crowns," *The International Journal of Oral & Maxillofacial Implants*, vol. 30, no. 1, pp. 95–101, 2015.
- [43] J. A. Griggs, "Dental implants," *Dental Clinics of North America*, vol. 61, no. 4, pp. 857–871, 2017.
- [44] E. O. Almeida, A. C. Freitas Jr., E. A. Bonfante, L. Marotta, N. R. Silva, and P. G. Coelho, "Mechanical testing of implant-supported anterior crowns with different implant/abutment connections," *The International Journal of Oral & Maxillofacial Implants*, vol. 28, no. 1, pp. 103–108, 2013.
- [45] E. A. Bonfante and P. G. Coelho, "A critical perspective on mechanical testing of implants and prostheses," *Advances in Dental Research*, vol. 28, no. 1, pp. 18–27, 2016.
- [46] A. C. Freitas-Junior, E. P. Rocha, E. A. Bonfante et al., "Biomechanical evaluation of internal and external hexagon platform switched implant-abutment connections: an in vitro laboratory and three-dimensional finite element analysis," *Dental Materials*, vol. 28, no. 10, pp. e218–e228, 2012.
- [47] L. S. Machado, E. A. Bonfante, R. B. Anchieta, S. Yamaguchi, and P. G. Coelho, "Implant-abutment connection designs for anterior crowns: reliability and failure modes," *Implant Dentistry*, vol. 22, no. 5, pp. 540–545, 2013.
- [48] G. P. Freitas, R. Hirata, E. A. Bonfante, N. Tovar, and P. G. Coelho, "Survival probability of narrow and standard-diameter implants with different implant-abutment connection designs," *The International Journal of Prosthodontics*, vol. 29, no. 2, pp. 179–185, 2016.
- [49] E. T. P. Bergamo, D. Bordin, I. S. Ramalho et al., "Zirconia-reinforced lithium silicate crowns: effect of thickness on survival and failure mode," *Dental Materials*, vol. 35, no. 7, pp. 1007–1016, 2019.
- [50] W. Nelson, *Accelerated testing: statistical models, test plans and data analysis*, John Wiley & Sons, Hoboken, New Jersey, USA, 2004.
- [51] W. E. Zhao and E. A. Elsayed, "A general accelerated life model for step-stress testing," *IIE Transactions*, vol. 37, no. 11, pp. 1059–1069, 2005.
- [52] Y. Hattori, C. Satoh, T. Kunieda, R. Endoh, H. Hisamatsu, and M. Watanabe, "Bite forces and their resultants during forceful intercuspal clenching in humans," *Journal of Biomechanics*, vol. 42, no. 10, pp. 1533–1538, 2009.
- [53] G. Hellsing, "On the regulation of interincisor bite force in man," *Journal of Oral Rehabilitation*, vol. 7, no. 5, pp. 403–411, 1980.
- [54] J. B. Quinn and G. D. Quinn, "A practical and systematic review of Weibull statistics for reporting strengths of dental materials," *Dental Materials*, vol. 26, no. 2, pp. 135–147, 2010.
- [55] J. E. Ritter, "Predicting lifetimes of materials and material structures," *Dental Materials*, vol. 11, no. 2, pp. 142–146, 1995.
- [56] P. P. Binon and M. J. McHugh, "The effect of eliminating implant/abutment rotational misfit on screw joint stability," *International Journal of Prosthodontics*, vol. 9, no. 6, 1996.
- [57] I. M. Finger, P. Castellon, M. Block, and N. Elian, "The evolution of external and internal implant/abutment connections," *Practical procedures & aesthetic dentistry: PPAD*, vol. 15, no. 8, pp. 625–32; quiz 634, 2003.
- [58] B. R. Merz, S. Hunenbart, and U. C. Belser, "Mechanics of the implant-abutment connection: an 8-degree taper compared to a butt joint connection," *The International Journal of Oral & Maxillofacial Implants*, vol. 15, no. 4, pp. 519–526, 2000.
- [59] D. Bordin, E. T. P. Bergamo, E. A. Bonfante, V. P. Fardin, and P. G. Coelho, "Influence of platform diameter in the reliability and failure mode of extra-short dental implants," *Journal of the Mechanical Behavior of Biomedical Materials*, vol. 77, pp. 470–474, 2018.
- [60] D. Bordin, E. T. P. Bergamo, V. P. Fardin, P. G. Coelho, and E. A. Bonfante, "Fracture strength and probability of survival of narrow and extra-narrow dental implants after fatigue testing: in vitro and in silico analysis," *Journal of the Mechanical Behavior of Biomedical Materials*, vol. 71, pp. 244–249, 2017.
- [61] R. Hirata, E. A. Bonfante, L. S. Machado, N. Tovar, and P. G. Coelho, "Mechanical evaluation of two grades of titanium used in implant dentistry," *The International Journal of Oral & Maxillofacial Implants*, vol. 30, no. 4, pp. 800–805, 2015.
- [62] A. C. Freitas Jr., E. A. Bonfante, E. P. Rocha, N. R. Silva, L. Marotta, and P. G. Coelho, "Effect of implant connection and restoration design (screwed vs. cemented) in reliability and failure modes of anterior crowns," *European Journal of Oral Sciences*, vol. 119, no. 4, pp. 323–330, 2011.

Research Article

An Antibacterial Strategy of Mg-Cu Bone Grafting in Infection-Mediated Periodontics

Xue Zhao,¹ Peng Wan,² Hongyan Wang,¹ Shuwei Zhang,¹ Jingbo Liu,¹ Chunrong Chang,¹ Ke Yang ,³ and Yaping Pan ,^{1,4}

¹Department of Periodontics, School and Hospital of Stomatology, China Medical University, Liaoning Provincial Key Laboratory of Oral Disease, Shenyang, Liaoning 110002, China

²School of Materials Science and Engineering, Dongguan University of Technology, Dongguan, Guangdong 523808, China

³Institute of Metal Research, Chinese Academic of Sciences, Shenyang, Liaoning 110016, China

⁴Department of Oral Biology, School and Hospital of Stomatology, China Medical University, Liaoning Provincial Key Laboratory of Oral Disease, Shenyang, Liaoning 110002, China

Correspondence should be addressed to Ke Yang; kyang@imr.ac.cn and Yaping Pan; yppan@cmu.edu.cn

Received 11 June 2020; Accepted 3 August 2020; Published 28 August 2020

Guest Editor: Henriette Lerner

Copyright © 2020 Xue Zhao et al. This is an open access article distributed under the Creative Commons Attribution License, which permits unrestricted use, distribution, and reproduction in any medium, provided the original work is properly cited.

Periodontal diseases are mainly the results of infections and inflammation of the gum and bone that surround and support the teeth. In this study, the alveolar bone destruction in periodontitis is hypothesized to be treated with novel Mg-Cu alloy grafts due to their antimicrobial and osteopromotive properties. In order to study this new strategy using Mg-Cu alloy grafts as a periodontal bone substitute, the *in vitro* degradation and antibacterial performance were examined. The pH variation and Mg²⁺ and Cu²⁺ release of Mg-Cu alloy extracts were measured. *Porphyromonas gingivalis* (*P. gingivalis*) and *Aggregatibacter actinomycetemcomitans* (*A. actinomycetemcomitans*), two common bacteria associated with periodontal disease, were cultured in Mg-Cu alloy extracts, and bacterial survival rate was evaluated. The changes of bacterial biofilm and its structure were revealed by scanning electron microscopy (SEM) and transmission electronic microscopy (TEM), respectively. The results showed that the Mg-Cu alloy could significantly decrease the survival rates of both *P. gingivalis* and *A. actinomycetemcomitans*. Furthermore, the bacterial biofilms were completely destroyed in Mg-Cu alloy extracts, and the bacterial cell membranes were damaged, finally leading to bacterial apoptosis. These results indicate that the Mg-Cu alloy can effectively eliminate periodontal pathogens, and the use of Mg-Cu in periodontal bone grafts has a great potential to prevent infections after periodontal surgery.

1. Introduction

Periodontal disease (PD) is one of the most common diseases in humans. Approximately 750,847 million people are suffering from PD worldwide according to the global burden of disease study in 2016 [1, 2]. It is characterized by progressive destruction of the tooth-supporting apparatus [3], especially loss of alveolar bone, which is naturally irreversible. Therefore, periodontal bone grafting, a medical device promoting periodontal bone regeneration, has been widely used in periodontal regeneration surgery [4].

Nowadays, numerous bone grafts are used in periodontal surgeries, showing good biocompatibility and osteogenesis.

Autogenous bone graft, as the gold standard bone graft currently, often requires a second invasive surgical procedure on the donor site. However, the limited source and volume of the harvested bones and unpredictable resorption rate among patients are main shortcomings. Alternatives to autografts are allografts and xenografts, but they may cause disease transmission and bring risks of infection [5]. The limitations of the above two approaches can be overcome by the use of synthesized bone grafts. Recently, biodegradable magnesium (Mg) alloy implants have received tremendous attention, since they have demonstrated good biocompatibility and similar mechanical properties to natural bone [6, 7]. Compared with other traditional metallic bone implants,

the elastic modulus of Mg is much closer to the natural bone [8]. What is more, Mg has an ideal desorption rate and can be gradually consumed or excreted in the human body and then disappear after the healing of bone tissues [9–11].

Mg alloys have been reported to have an antibacterial ability due to the large amount of OH^- produced during degradation resulting in a strong alkaline environment [12–15]. However, high pH can be balanced in body fluid when a Mg alloy device is implanted, and hence, the antibacterial ability will be diminished. Thus, it can be meaningful to explore the possibility of adding a proper metal element with antibacterial effect in magnesium.

Copper (Cu) has been found to have antibacterial ability since 1885 [16]. Nowadays, Cu has been added into medical metal materials to offer antimicrobial activities in stainless steels [17, 18], titanium alloys [19], and cobalt-based alloys [20]. Our previous studies have demonstrated the biocompatibility and osteogenic promotion of the Mg-Cu alloy as a biodegradable bone implant [21, 22]. Many studies have proven that addition of Cu in implant material could both kill bacteria and stimulate biological responses to mesenchymal stem cells like proliferation and osteogenic differentiation [23]. These properties make the Mg-Cu alloy an attractive implant material for preventing infections.

Meanwhile, the oral environment is known for the coexistence of various bacteria, with more than 300 distinct bacterial species in the human gingival crevice. It has been proven that periodontal bacteria exist as biofilms composed of very complex mixtures of bacterial species, and their formation is highly ordered. Streptococci such as *Streptococcus gordonii* (*S. gordonii*) represent the primary colonizing bacteria which can adhere to saliva-coated teeth and gingiva surfaces and provide a base for subsequent colonization of other bacterial species [24]. *Fusobacterium nucleatum* (*F. nucleatum*) plays a role as a bridging organism connecting early and late colonizing bacteria such as *Porphyromonas gingivalis* (*P. gingivalis*) and *Aggregatibacter actinomycetemcomitans* (*A. actinomycetemcomitans*) [25]. *P. gingivalis* is known as a keystone bacteria in periodontal diseases as a part of the red complex of periodontal pathogens [26–28]. *A. actinomycetemcomitans* is regarded as the main periodontopathogen in aggressive periodontitis and peri-implantitis [29–31]. Both *P. gingivalis* and *A. actinomycetemcomitans* are capable of invading the gingival epithelial cell and then produce virulence factors to disrupt host-microbial homeostasis, resulting in inflammation and bone loss.

At present, no clinically used natural or synthesized grafts display antibacterial ability. Periodontists thus rely heavily on the myriad antibiotic administration to prevent postoperative infections, leading to a worldwide antibiotic abuse problem [32]. For this reason, an antibacterial bone graft which is unlikely to cause the development of drug resistance is undeniably beneficial [33, 34].

Based on the primary studies, we supposed the biodegradable Mg-Cu alloy as a grafting material to fill the infrabony pocket of periodontal bone resorption. The objective of this study was to explore the antibacterial abilities of Mg-Cu against periodontal anaerobic bacteria in order to provide more evidence for clinical application of this novel material.

2. Material and Experimental Methods

2.1. Material Preparation. Three Mg-Cu alloys with gradient contents of 0.1, 0.2, and 0.4 wt.% Cu were prepared by conventional melting technique, which were assigned as Mg-0.1Cu, Mg-0.2Cu, and Mg-0.4Cu, respectively. The Mg-Cu alloys were cut into disks with size of $\varnothing 10 \text{ mm} \times 3 \text{ mm}$, grounded and polished with SiC papers, and finally ultrasonically cleaned with acetone and ethanol. Pure Mg and β -TCP (β -tricalcium phosphate) were used as control groups.

2.2. Material Extract Preparation. Extracts of the Mg-Cu alloys were prepared according to ISO 10993-5. The ratio of surface area to extraction medium was $1.25 \text{ cm}^2/\text{mL}$. Samples were immersed in brain heart infusion (BHI) broth in a humidified atmosphere with 5% CO_2 at $37 \pm 0.5^\circ\text{C}$ for 3 h, 6 h, 12 h, 24 h, 48 h, and 72 h. Then, the extracts were filtered and refrigerated at 4°C .

2.3. pH and Ion Release Measurements. The pH value of extracts was measured at intervals. Concentration of Mg^{2+} and Cu^{2+} in the extracts was measured using ICP-OES at each time point. The measurements were performed in triplicate.

2.4. In Vitro Antibacterial Effect Evaluation

2.4.1. Bacterial Strain Preparation. The bacterial strains used for the present study were *Streptococcus gordonii* Challis CH1 (*S. gordonii*), *Fusobacterium nucleatum* ATCC25586 (*F. nucleatum*), *Porphyromonas gingivalis* ATCC 33277 (*P. gingivalis*), and *Aggregatibacter actinomycetemcomitans* ATCC 43718 (*A. actinomycetemcomitans*), which represent the early, middle, and late colonizers of the bacterial accretion in the periodontal plaque biofilm. All the bacteria in the test were obtained from the Department of Oral Biology, School of Stomatology, China Medical University.

Bacterial strains of *P. gingivalis*, *A. actinomycetemcomitans*, and *F. nucleatum* were cultured in a freshly prepared brain heart infusion (BHI) agar plate (Difco Laboratories, MI) supplemented with 5% sterile defibrinated sheep blood, 1% hemin, and 0.1% menadione in a chamber under anaerobic conditions of 80% N_2 , 10% H_2 , and 10% CO_2 . *S. gordonii* was cultured aerobically in freshly prepared BHI agar plate supplemented with 1% yeast extract for 16 h at 37°C .

All the bacterial suspensions for the test were suspended in a BHI broth until reaching a final density of 1×10^7 colony forming units (CFU)/mL.

2.4.2. Bacterial Concentration and Living Rate Measurements. The antibacterial activity was determined using the indirect method by culturing bacteria in the Mg-Cu alloy extracts. Tested bacteria were diluted by extracts into 1×10^5 CFU/mL, which were then cultured in anaerobic conditions for 24 h. The BHI broth was served as the blank group. The concentration of extracts cultured with bacterial suspensions was determined by real-time PCR assay. The number of living bacteria was determined by the bacterial counting method. The bacterial suspensions were diluted to 1×10^3 CFU/mL, 0.1 mL of which was spread on nutrition agar plates evenly, followed by further incubation at 37°C

for 72 h before counting the bacteria colonies. All the tests were conducted three times.

2.4.3. Live/Dead Staining. Tested bacteria were diluted by extracts into 1×10^5 CFU/mL, which were then cultured in anaerobic conditions for 24 h. The bacterial biofilms attached on the base of the plates were fixed by 1% paraformaldehyde for 1 h and then stained with $2.5 \mu\text{L/mL}$ propidium iodide (PI) for 30 min. The viability of the bacteria was examined with fluorescence microscope.

2.4.4. SEM Analysis. Tested bacteria were diluted by extracts into 1×10^5 CFU/mL, which were then cultured in anaerobic conditions for 24 h. The bacterial biofilms attached on the base of the plates were fixed with 2.5% glutaraldehyde in PBS (pH = 7.4) for 1 h at room temperature, then washed with PBS for three times and gradually dehydrated with ethanol. The processed samples were smeared onto a copper plate followed by gold sputtering, and images were acquired on a scanning electron microscope (SEM, Inspect F50, FEI Company, USA).

2.4.5. TEM Analysis. Tested bacteria were diluted by extracts into 1×10^7 CFU/mL, which were then cultured in anaerobic conditions for 24 h. The cocultured bacterial suspensions were centrifuged at 5000 rpm for 20 min, and the bacteria were fixed with 2.5% glutaraldehyde. After dehydration with ethanol, the bacteria were embedded with LR white medium (EMS, PA), which was then cut into sections. The sections were contrasted with uranyl acetate and were examined under a transmission electron microscopy (TEM, H7650 Hitachi, Japan).

3. Results

3.1. pH Variation and Ion Release. Figure 1(a) shows the pH values of the medium immersed with Mg-Cu alloys compared with pure Mg. The results were in line with the immersion time. The pH value was increased with the increase of Cu content in the Mg-Cu alloy, indicating higher degradation rate. For all the Mg-Cu groups, the pH values increased quickly in the first 6 h and then remained stable above 10 afterwards.

The release of Mg^{2+} and Cu^{2+} after immersion is plotted in Figures 1(b) and 1(c). The higher the pH value was, the more the Mg^{2+} and Cu^{2+} released from Mg-Cu alloy extracts. For the Mg-0.1Cu alloy, the concentration of Mg^{2+} showed no significant difference with pure Mg at 72 h. As the concentration of Cu^{2+} was positively related to the Cu content in the alloy, the Mg-0.4Cu alloy released much more Cu^{2+} than the other Mg-Cu alloys.

3.2. Bacterial Survival. One of the most attractive behaviors of the Mg-Cu alloy system is its remarkable antibacterial activity. In this study, *P. gingivalis* and *A. actinomycetemcomitans*, two common bacteria associated with PD, were used to evaluate the antibacterial activity of the Mg-Cu alloy for bone graft application. As shown in Figure 2, Mg-Cu alloys demonstrated significant inhibition of growths of both *P. gingivalis* (Figures 2(a)–2(c)) and *A. actinomycetemcomitans*

(Figures 2(d)–2(f)) ($P < 0.05$). The β -TCP group did not show any antibacterial effect as expected. A series of extracts were prepared by incubating samples with bacterial culture medium for different time intervals. For pure Mg and Mg-Cu alloy groups, both the bacterial concentration (Figures 2(a) and 2(d)) and the live bacterial colony (Figures 2(b) and 2(e)) were decreased with increase of incubation time. It should also be noted that the bacterial concentration and colony number for Mg-Cu groups were always less than those of pure Mg, indicating that the release of Cu^{2+} further enhanced the antibacterial ability of Mg. But the three Mg-Cu alloy groups did not show difference in both bacterial concentration and live bacterial colony. *P. gingivalis* and *A. actinomycetemcomitans* reacted differently to the extract of Mg-Cu alloys. For *P. gingivalis*, the inhibition started to become noticeable in the extract with 3 h incubation; however, for *A. actinomycetemcomitans*, the same effect started in the extract after 12 h incubation. The optical images of the *P. gingivalis* (Figure 2(c)) and *A. actinomycetemcomitans* (Figure 2(f)) in nutrition agar plates show the similar results, i.e., for pure Mg and Mg-Cu groups, the numbers of bacterial colonies were much smaller than those of the control group.

3.3. Confocal Fluorescence Microscope Analysis. The activities of *P. gingivalis* and *A. actinomycetemcomitans* single-species bacterial biofilms were assessed by live/dead staining (Figure 3). A confocal fluorescence microscope was used to image both *P. gingivalis* and *A. actinomycetemcomitans* after incubation with the Mg-Cu alloy extract for 24 h. For the blank and β -TCP (positive) groups, amounts of live bacteria were observed, showing a thick biofilm compared with the pure Mg group. Approximate fifty–fifty live and dead bacteria were found in the pure Mg group. However, for the Mg-0.1Cu group, only few live bacteria could be found.

3.4. Scanning Electron Microscope Analysis. To further explore the antibacterial mechanism of Mg-Cu alloys, the status of the bacterial biofilm was assessed by SEM (Figure 4). For single-species biofilms of *P. gingivalis* and *A. actinomycetemcomitans* (Figure 4(a)), continuous biofilms with smooth surface were formed on both the blank and β -TCP groups. In the pure Mg group, bacteria were able to connect but did not form a continuous biofilm. Comparatively, the Mg-0.1Cu group showed few of the individual bacteria without formation of a biofilm. Similar results were observed in the multispecies biofilm model (Figure 4(b)). A large scale of smooth biofilm was only seen in the blank and β -TCP groups. The pure Mg group showed less biofilm formation, while the bacteria in the Mg-0.1Cu group lost connection with each other and the biofilm collapsed completely due to apoptosis of bacteria.

3.5. Transmission Electron Microscope Analysis. TEM observation showed the change of cell membranes and structures of *P. gingivalis* and *A. actinomycetemcomitans* after coculturing in different groups for 24 h (Figure 5). In blank and β -TCP groups, the integrity of the bacterial cells was unchanged, and bacterial cytoplasm was clear. Comparatively, the cell

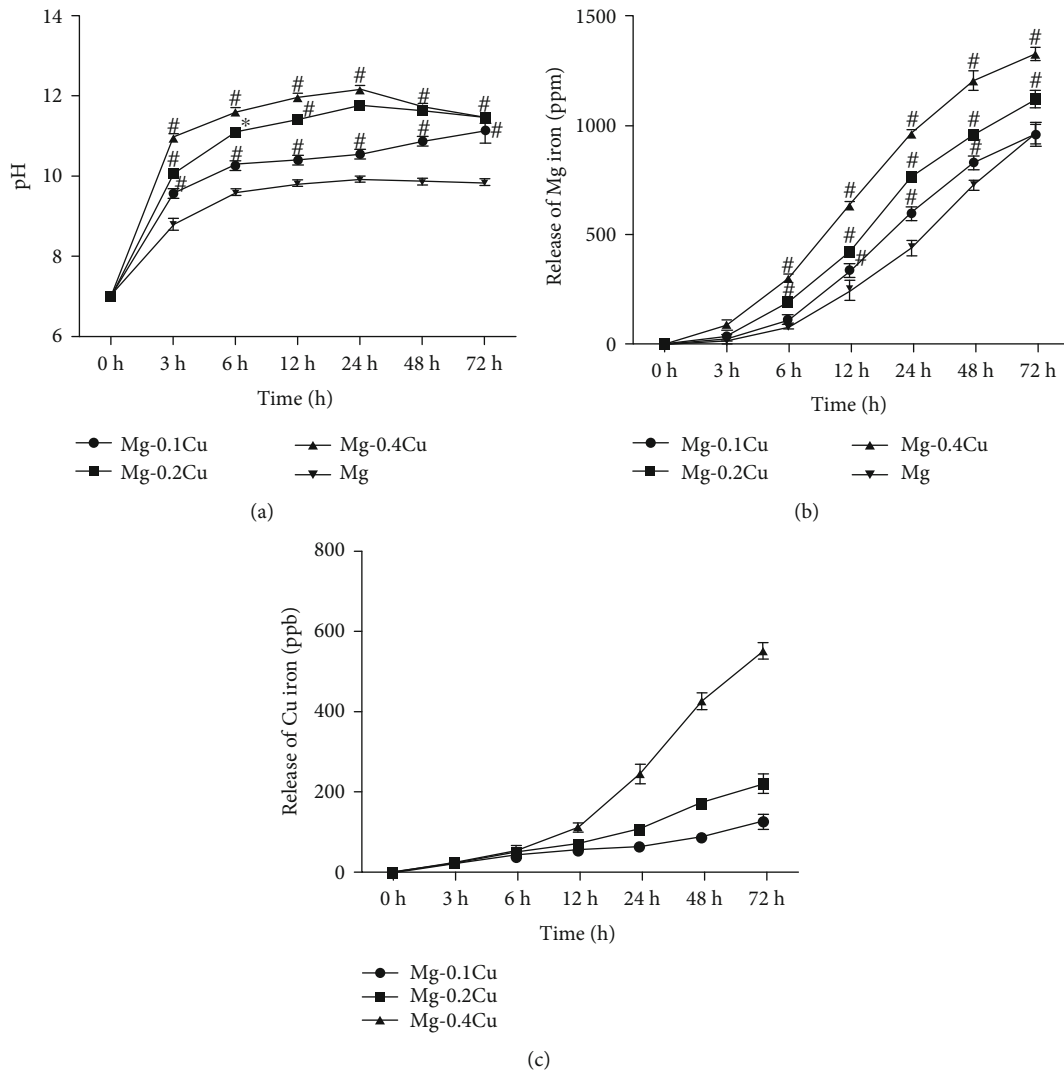


FIGURE 1: (a) pH value of the Mg-Cu alloy and Mg extracts. The results are in line with the immersion time. (b) Mg^{2+} concentration in the Mg-Cu alloy and Mg extracts and (c) Cu^{2+} concentration in Mg-Cu alloy extracts. The concentration of Cu^{2+} was positively related to the Cu content in the Mg-Cu alloy. The Mg-0.4Cu alloy released much more Cu^{2+} than the other Mg-Cu alloys. # refers to a significant difference between Mg-Cu alloy groups and the Mg group ($P < 0.05$, $n = 3$).

membrane showed folds and stratification in the pure Mg group, where the membrane was separated from the cytoplasm, while in the Mg-0.1Cu group, the dead bacteria showed almost intact cell membranes with little cytoplasm remaining.

4. Discussion

This study was designed to explore a potential treatment strategy for periodontal disease with novel Mg-Cu grafts which possessed the antibacterial ability against *P. gingivalis* and *A. actinomycetemcomitans*.

Periodontal bone grafting is a widely used surgery to promote periodontal regeneration, while inflammation control after surgery is an intricate problem in the clinic. Since bone substitutes have no antimicrobial properties, routine use of antibiotics was reported for guided bone regeneration by 97% of the survey respondents, with penicillin and doxycy-

cline which are frequently used. The antibiotic uses before and after surgery with time length vary from 7 days to 10 days [35]. However, antibiotic abuse is currently a global challenge since the number of bacterial strains that are resistant to multiple types of antibiotics has dramatically increased each year worldwide [36]. In that case, it is urgent to find an alternate to reduce the use of antibiotics after periodontal surgery.

The Mg-Cu alloy which is considered to inhibit bacteria growth was proposed and investigated systematically in previous studies [22, 37]. It has been proven that Cu alloying in Mg exhibited long-lasting antibacterial effect against *Staphylococcus aureus* by the synergistic effects of Mg degradation and Cu ion release [21]. Furthermore, there was no cytotoxicity to both HUVECs and MC3T3-E1 cells during the degradation of the Mg-Cu alloy, and the proper release of Mg and Cu ions provided favorable promotion to osteogenesis

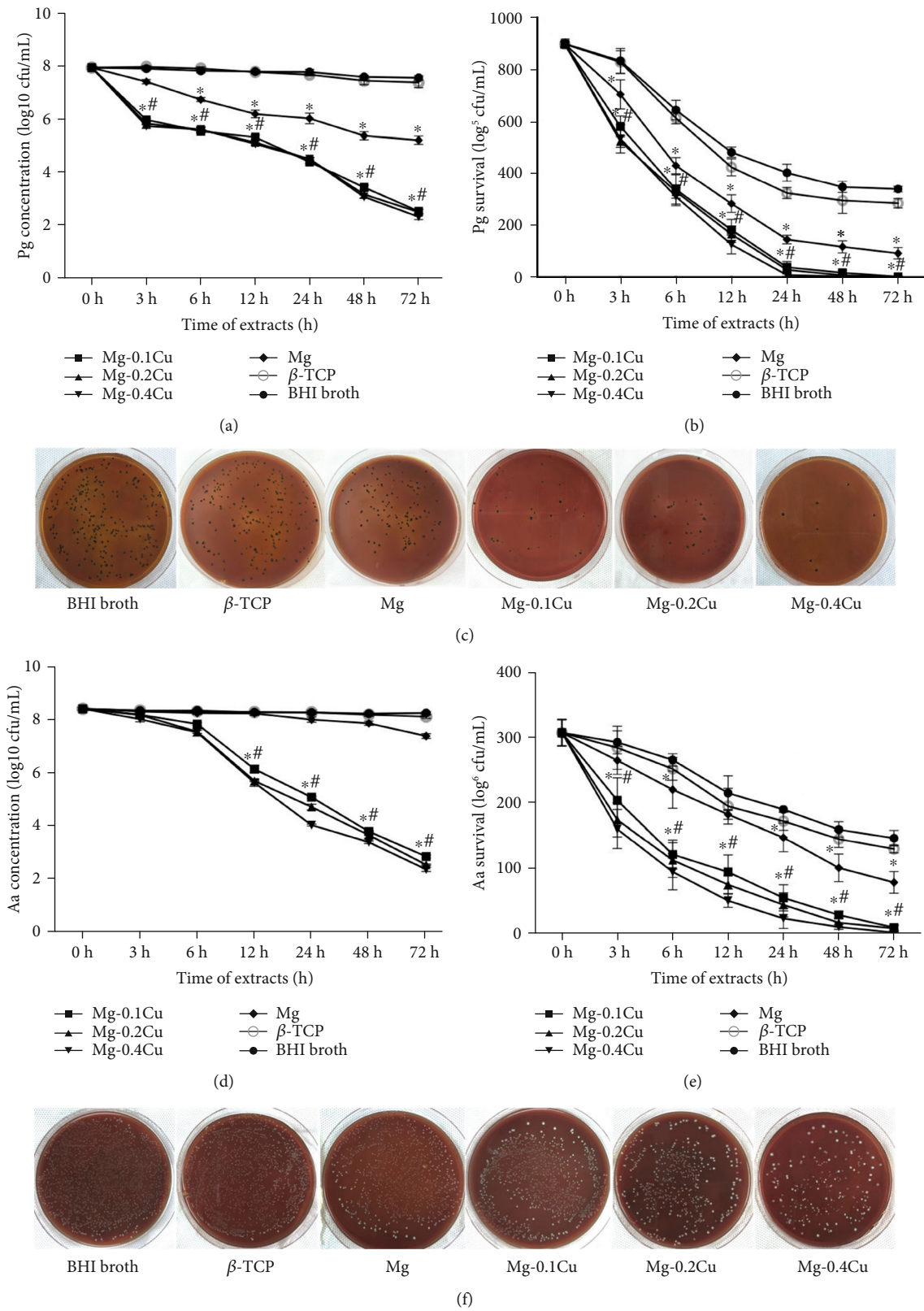


FIGURE 2: The responses of *P. gingivalis* (Pg) to the Mg-Cu alloy and Mg and β-TCP extracts: (a) bacterial concentration; (b) live bacterial colonies; (c) optical images of the bacterial colonies in nutrition agar plates and the responses of *A. actinomycetemcomitans* (*Aa*) to the Mg-Cu alloy and Mg and β-TCP extracts; (d) bacterial concentration; (e) live bacterial colonies; (f) optical images of the bacterial colonies in nutrition agar plates. * refers to a significant difference between Mg-Cu alloy groups (Mg-0.1Cu, Mg-0.2Cu, and Mg-0.3Cu) and the BHI broth and β-TCP groups. # refers to a significant difference between Mg-Cu alloy groups and the Mg group ($P < 0.05$, $n = 3$).

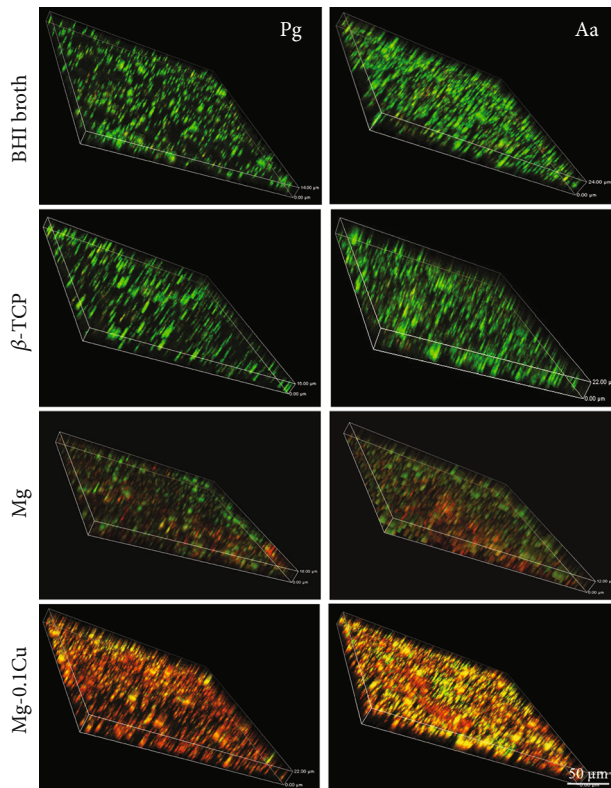


FIGURE 3: Live/dead imaging of Pg and Aa after culturing in Mg-0.1Cu extracts for 24 h under a confocal fluorescence microscope. The green color indicates live bacterial while the red color indicates dead bacterial. Majorities of both Pg and Aa were dead in the Mg-0.1Cu alloy extract after culturing for 24 h.

and angiogenesis, indicating a great potential in bone grafting application. However, most PD-related bacteria are anaerobic, which have different growth characteristics from *Staphylococcus aureus*. In order to prove the efficacy of the Mg-Cu alloy on periodontal pathogens, anaerobic bacteria such as *P. gingivalis* and *A. actinomycetemcomitans* were selected in this study.

The pH value was positively correlated to the Cu content in the Mg-Cu alloy (Figure 1(a)) due to severe galvanic corrosion. The pH value for the pure Mg extract was the lowest followed by Mg-0.1Cu, Mg-0.2Cu, and Mg-0.4Cu alloys in sequence. The survival of most PD-related bacteria depends on the pH homeostasis, since most proteins including enzymes only behave their functions in a neutral range of pH values. Exposure to a higher alkaline environment would pose stress on the bacterial cytoplasmic pH homeostasis [38]. Other studies also implied the antibacterial properties of Mg and its alloys [13, 14]. However, the present study raised two drawbacks of pH enhancement-induced antibacterial effect. First, when an Mg alloy device is implanted, change of the pH value will easily be balanced by body fluid. Therefore, the antibacterial ability of the Mg alloy *in vivo* is questionable. When the increase of pH is balanced, the antibacterial property would disappear as demonstrated in the previous study [18]. Second, high alkalinity circumstance may only switch the normal bacteria to a nonmetabolically

active state. Many studies have proven that bacteria could survive in the extreme environment by switching to inactive status [39, 40]. In this study, the live/dead imaging (Figure 3) also indicated that high percentages of both *P. gingivalis* and *A. actinomycetemcomitans* were still alive in the pure Mg group.

Due to the drawbacks mentioned above, the introduction of antimicrobial metal elements such as Ag and Cu into the Mg alloy has gained more attention [37, 41]. Cu ion is known to cause multiple toxic effects such as generation of reactive oxygen species, lipid peroxidation, protein oxidation, and DNA degradation [42]. With higher content of Cu, more Cu ions are eluted from the implant material and bonded to the surface of bacteria, which eventually damage the cell membranes and kill the bacteria. Cu ions can hardly be balanced by human body fluid nor diluted by surrounding medium after releasing from the implant. Thus, the antibacterial activity will be maintained for the Mg-Cu alloy after implantation *in vivo*. In addition, the live/dead staining demonstrated that the release of Cu ions led to the necrosis of both *P. gingivalis* and *A. actinomycetemcomitans* (Figure 3) instead of switching them to the inactive state. The TEM observation showed that only the bacteria membrane changed in the pure Mg group, while the cytoplasm was lost completely in the Mg-Cu group with almost intact membranes. This indicates that the antibacterial mechanism of Cu should be different from that of the high pH value. It has previously been shown that Cu ions exert an antimicrobial activity, leading to increased influx of Cu^{2+} into bacteria and generation of reactive oxygen species, which results in inhibition of respiration and degradation of DNA and loss of cytoplasm [43].

The biofilm is critical for the microbial to attach to the material surface for survival [44, 45]. Both *P. gingivalis* and *A. actinomycetemcomitans* were not able to form a continuous biofilm as single species or multispecies (Figure 4) and were only observed as individual cells when incubated in the Mg-Cu alloy extracts. Without the protection from the biofilm, the cell membrane was destroyed directly and all the intracellular structures leaked outside (Figure 5), leading to bacterial apoptosis eventually. Another study also showed that on the surface of a Cu-implanted alloy, the shapes of *Escherichia coli* and *Staphylococcus aureus* changed obviously and their membranes were damaged [46]. Thus, Cu played a very important antibacterial role in the Mg-Cu extracts.

In the previous study [21], it has been demonstrated that the Mg-Cu alloy with the lowest Cu content could also enhance the cell viability, alkaline phosphatase activity, and osteogenesis-related gene and protein expressions. Thus, the biodegradable Mg-Cu alloy with osteogenesis, angiogenesis, and favorable antibacterial ability to PD-related bacteria is considered as a promising bone graft in periodontal regeneration. It is supposed that the Mg-Cu bone grafts in the form of particles can be filled into the alveolar bone pocket to treat the periodontal disease and enhance the possible regeneration of alveolar bone as well. The antibacterial and osteopromotive properties of Mg-Cu grafts will be further verified *in vivo* on a clinical relevant PD infection animal model.

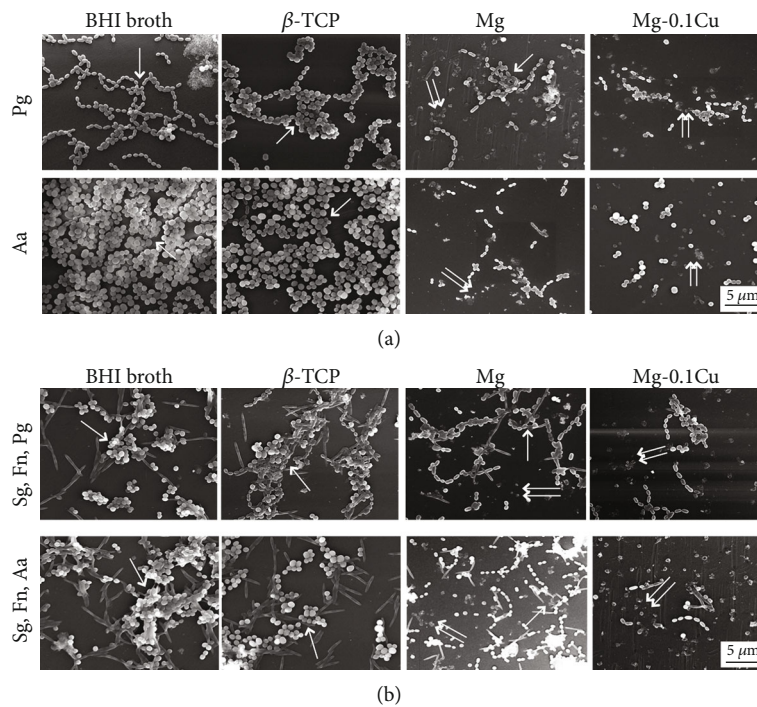


FIGURE 4: SEM images of bacterial biofilm after culturing in the extract for 24 h. (a) Single-species biofilm of *Pg* and *Aa*, (b) multispecies biofilm of *Sg, Fn*, and *Pg* and *Sg, Fn*, and *Aa*, scale bar = 5 μ m. Single arrow shows the normal bacterial biofilm. Double arrows show the damaged bacterial biofilm. The bacteria in the Mg-0.1Cu alloy group lost connection with each other, and the biofilm collapsed completely due to death of bacteria.

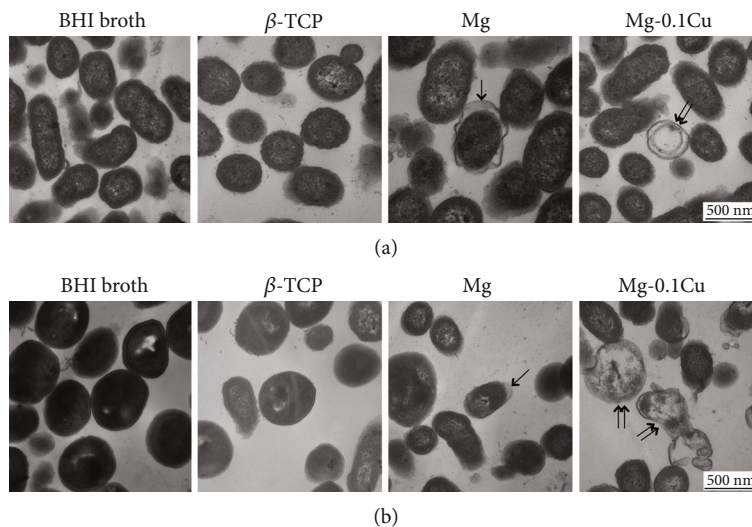


FIGURE 5: TEM images of the cell membrane and structure of *Pg* (a) and *Aa* (b) after culturing in extracts and BHI broth for 24 h, scale bar = 500 μ m. Single arrow shows the change of bacterial membrane in the Mg group. The cell membrane showed folds and stratification in the pure Mg group, where the membrane was separated from cytoplasm. Double arrows show the bacteria change in the Mg-Cu alloy group. The dead bacteria showed almost intact cell membranes with little cytoplasm remaining.

5. Conclusions

The results in this study showed that with increase of the Cu content in the Mg-Cu alloy, the survival rates of both *P. gingivalis* and *A. actinomycetemcomitans* in the Mg-Cu alloy

extracts were decreased significantly, and the bacteria cells and bacterial biofilms were destroyed obviously. The results are in agreement with other studies on Cu-bearing metals, indicating that the Mg-Cu alloy as potential bone grafts can effectively prevent infections in periodontal surgery.

Data Availability

I have published all the data in the paper on Figshare (<https://doi.org/10.6084/m9.figshare.12587297.v1>).

Conflicts of Interest

The authors declare that they have no conflicts of interest.

Acknowledgments

The authors gratefully acknowledge the financial support from the Talents Plant for Liaoning Development (No. XLYC1802129), Natural Science Foundation of China (No. 51631009) and Research Start-Up Funds of DGUT (No. GC300501-082).

References

- [1] J. M. Albandar, "Epidemiology and risk factors of periodontal diseases," *Dental Clinics of North America*, vol. 49, no. 3, pp. 517–532, 2005.
- [2] B. Zhu, L. C. Macleod, E. Newsome, J. Liu, and P. Xu, "Aggregatibacter actinomycetemcomitans mediates protection of Porphyromonas gingivalis from Streptococcus sanguinis hydrogen peroxide production in multi-species biofilms," *Scientific Reports*, vol. 9, no. 1, p. 4944, 2019.
- [3] F. M. Chen and Y. Jin, "Periodontal tissue engineering and regeneration: current approaches and expanding opportunities," *Tissue Engineering. Part B, Reviews*, vol. 16, no. 2, pp. 219–255, 2010.
- [4] M. A. Reynolds, M. E. Aichelmann-Reidy, G. L. Branch-Mays, and J. C. Gunsolley, "The efficacy of bone replacement grafts in the treatment of periodontal osseous defects. A systematic review," *Annals of Periodontology*, vol. 8, no. 1, pp. 227–265, 2003.
- [5] R. Yunus Basha, S. K. TS, and M. Doble, "Design of biocomposite materials for bone tissue regeneration," *Materials Science & Engineering. C, Materials for Biological Applications*, vol. 57, pp. 452–463, 2015.
- [6] D. Hong, P. Saha, D. T. Chou et al., "In vitro degradation and cytotoxicity response of Mg-4% Zn-0.5% Zr (ZK40) alloy as a potential biodegradable material," *Acta Biomaterialia*, vol. 9, no. 10, pp. 8534–8547, 2013.
- [7] D. T. Chou, D. Hong, P. Saha et al., "In vitro and in vivo corrosion, cytocompatibility and mechanical properties of biodegradable Mg-Y-Ca-Zr alloys as implant materials," *Acta Biomaterialia*, vol. 9, no. 10, pp. 8518–8533, 2013.
- [8] Z. Z. Yin, W. C. Qi, R. C. Zeng et al., "Advances in coatings on biodegradable magnesium alloys," *Journal of Magnesium and Alloys*, vol. 8, no. 1, pp. 42–65, 2020.
- [9] A. F. Cipriano, T. Zhao, I. Johnson, R. G. Guan, S. Garcia, and H. Liu, "In vitro degradation of four magnesium-zinc-strontium alloys and their cytocompatibility with human embryonic stem cells," *Journal of Materials Science Materials in Medicine*, vol. 24, no. 4, pp. 989–1003, 2013.
- [10] F. Witte, J. Fischer, J. Nellesen et al., "In vitro and in vivo corrosion measurements of magnesium alloys," *Biomaterials*, vol. 27, no. 7, pp. 1013–1018, 2006.
- [11] L. Xu, G. Yu, E. Zhang, F. Pan, and K. Yang, "In vivo corrosion behavior of Mg-Mn-Zn alloy for bone implant application," *Journal of biomedical materials research Part A*, vol. 83, no. 3, pp. 703–711, 2007.
- [12] H. Qin, Y. Zhao, Z. An et al., "Enhanced antibacterial properties, biocompatibility, and corrosion resistance of degradable Mg-Nd-Zn-Zr alloy," *Biomaterials*, vol. 53, pp. 211–220, 2015.
- [13] J. Y. Lock, E. Wyatt, S. Upadhyayula et al., "Degradation and antibacterial properties of magnesium alloys in artificial urine for potential resorbable ureteral stent applications," *Journal of biomedical materials research Part A*, vol. 102, no. 3, pp. 781–792, 2014.
- [14] D. A. Robinson, R. W. Griffith, D. Shechtman, R. B. Evans, and M. G. Conzemijs, "In vitro antibacterial properties of magnesium metal against Escherichia coli, Pseudomonas aeruginosa and Staphylococcus aureus," *Acta Biomaterialia*, vol. 6, no. 5, pp. 1869–1877, 2010.
- [15] S. Mukherjee, S. Barman, N. C. Mandal, and S. Bhattacharya, "Anti-bacterial activity of Achatina CRP and its mechanism of action," *Indian Journal of Experimental Biology*, vol. 52, no. 7, pp. 692–704, 2014.
- [16] P. Szymanski, T. Fraczek, M. Markowicz, and E. Mikiciuk-Olasik, "Development of copper based drugs, radiopharmaceuticals and medical materials," *Biometals*, vol. 25, no. 6, pp. 1089–1112, 2012.
- [17] L. Ren, K. Yang, L. Guo, and H. W. Chai, "Preliminary study of anti-infective function of a copper-bearing stainless steel," *Materials Science and Engineering: C*, vol. 32, no. 5, pp. 1204–1209, 2012.
- [18] H. Chai, L. Guo, X. Wang et al., "Antibacterial effect of 317L stainless steel contained copper in prevention of implant-related infection in vitro and in vivo," *Journal of Materials Science Materials in Medicine*, vol. 22, no. 11, pp. 2525–2535, 2011.
- [19] S. Wang, Z. Ma, Z. Liao, J. Song, K. Yang, and W. Liu, "Study on improved tribological properties by alloying copper to CP-Ti and Ti-6Al-4V alloy," *Materials Science & Engineering. C, Materials for Biological Applications*, vol. 57, pp. 123–132, 2015.
- [20] Z. K. Ghouri, N. A. M. Barakat, and H. Y. Kim, "Influence of copper content on the electrocatalytic activity toward methanol oxidation of Co_xCu_y alloy nanoparticles-decorated CNFs," *Scientific Reports*, vol. 5, no. 1, 2015.
- [21] C. Liu, X. Fu, H. Pan et al., "Biodegradable Mg-Cu alloys with enhanced osteogenesis, angiogenesis, and long-lasting antibacterial effects," *Scientific Reports*, vol. 6, no. 1, 2016.
- [22] Y. Li, L. Liu, P. Wan et al., "Biodegradable Mg-Cu alloy implants with antibacterial activity for the treatment of osteomyelitis: in vitro and in vivo evaluations," *Biomaterials*, vol. 106, pp. 250–263, 2016.
- [23] I. Burghardt, F. Luthen, C. Prinz et al., "A dual function of copper in designing regenerative implants," *Biomaterials*, vol. 44, pp. 36–44, 2015.
- [24] M. Y. Mahmoud, S. Sapare, K. C. Curry, D. R. Demuth, and J. M. Steinbach-Rankins, "Rapid release polymeric fibers for inhibition of Porphyromonas gingivalis adherence to Streptococcus gordonii," *Frontiers in Chemistry*, vol. 7, 2020.
- [25] F. Wang, W. Qiao, B. Bao et al., "Effect of IgY on periodontitis and halitosis induced by Fusobacterium nucleatum," *Journal of Microbiology and Biotechnology*, vol. 29, no. 2, pp. 311–320, 2019.
- [26] O. Chigasaki, Y. Takeuchi, A. Aoki et al., "A cross-sectional study on the periodontal status and prevalence of red complex

- periodontal pathogens in a Japanese population,” *Journal of Oral Science*, vol. 60, no. 2, pp. 293–303, 2018.
- [27] G. Hajishengallis, “Periodontitis: from microbial immune subversion to systemic inflammation,” *Nature Reviews Immunology*, vol. 15, no. 1, pp. 30–44, 2015.
- [28] B. Malinowski, A. Wesierska, K. Zalewska et al., “The role of *Tannerella forsythia* and *Porphyromonas gingivalis* in pathogenesis of esophageal cancer,” *Infectious Agents and Cancer*, vol. 14, no. 1, 2019.
- [29] I. Olsen and O. Yilmaz, “Modulation of inflammasome activity by *Porphyromonas gingivalis* in periodontitis and associated systemic diseases,” *Journal of Oral Microbiology*, vol. 8, no. 1, 2016.
- [30] P. J. Ezzo and C. W. Cutler, “Microorganisms as risk indicators for periodontal disease,” *Periodontology 2000*, vol. 32, no. 1, pp. 24–35, 2003.
- [31] B. A. Herbert, C. M. Novince, and K. L. Kirkwood, “Aggregatibacter actinomycetemcomitans, a potent immunoregulator of the periodontal host defense system and alveolar bone homeostasis,” *Molecular Oral Microbiology*, vol. 31, no. 3, pp. 207–227, 2016.
- [32] R. E. Hancock and A. Patrzykat, “Clinical development of cationic antimicrobial peptides: from natural to novel antibiotics,” *Current Drug Targets. Infectious Disorders*, vol. 2, no. 1, pp. 79–83, 2002.
- [33] U. Theuretzbacher, “Future antibiotics scenarios: is the tide starting to turn?,” *International Journal of Antimicrobial Agents*, vol. 34, no. 1, pp. 15–20, 2009.
- [34] Y. Shao, R. C. Zeng, S. Q. Li et al., “Advance in antibacterial magnesium alloys and surface coatings on magnesium alloys: a review,” *Acta Metallurgica Sinica (English Letters)*, vol. 33, no. 5, pp. 615–629, 2020.
- [35] S. J. Froum and M. A. Weinberg, “An evaluation of antibiotic use in periodontal and implant practices,” *The International Journal of Periodontics & Restorative Dentistry*, vol. 35, no. 4, pp. 481–487, 2015.
- [36] C. Gonzalez-Bello, “Antibiotic adjuvants - a strategy to unlock bacterial resistance to antibiotics,” *Bioorganic & Medicinal Chemistry Letters*, vol. 27, no. 18, pp. 4221–4228, 2017.
- [37] X. Yan, P. Wan, L. Tan, M. Zhao, L. Qin, and K. Yang, “Corrosion and biological performance of biodegradable magnesium alloys mediated by low copper addition and processing,” *Materials Science & Engineering. C, Materials for Biological Applications*, vol. 93, pp. 565–581, 2018.
- [38] T. A. Krulwich, G. Sachs, and E. Padan, “Molecular aspects of bacterial pH sensing and homeostasis,” *Nature Reviews. Microbiology*, vol. 9, no. 5, pp. 330–343, 2011.
- [39] G. Wegrzyn and A. Wegrzyn, “Stress responses and replication of plasmids in bacterial cells,” *Microbial Cell Factories*, vol. 1, no. 1, p. 2, 2002.
- [40] R. Trastoy, T. Manso, L. Fernández-García et al., “Mechanisms of bacterial tolerance and persistence in the gastrointestinal and respiratory environments,” *Clinical Microbiology Reviews*, vol. 31, no. 4, 2018.
- [41] D. Tie, F. Feyerabend, W. D. Muller et al., “Antibacterial biodegradable Mg-Ag alloys,” *European Cells & Materials*, vol. 25, pp. 284–298, 2013, discussion 98.
- [42] A. K. Chatterjee, R. Chakraborty, and T. Basu, “Mechanism of antibacterial activity of copper nanoparticles,” *Nanotechnology*, vol. 25, no. 13, p. 135101, 2014.
- [43] S. L. Warnes, V. Caves, and C. W. Keevil, “Mechanism of copper surface toxicity in *Escherichia coli* O157:H7 and *Salmonella* involves immediate membrane depolarization followed by slower rate of DNA destruction which differs from that observed for Gram-positive bacteria,” *Environmental Microbiology*, vol. 14, no. 7, pp. 1730–1743, 2012.
- [44] R. Roy, M. Tiwari, G. Donelli, and V. Tiwari, “Strategies for combating bacterial biofilms: a focus on anti-biofilm agents and their mechanisms of action,” *Virulence*, vol. 9, no. 1, pp. 522–554, 2018.
- [45] V. S. Bhinu, “Insight into biofilm-associated microbial life,” *Journal of Molecular Microbiology and Biotechnology*, vol. 10, no. 1, pp. 15–21, 2006.
- [46] Z. Ding, Y. Wang, Q. Zhou et al., “Microstructure, wettability, corrosion resistance and antibacterial property of Cu-MTa₂O₅ multilayer composite coatings with different Cu incorporation contents,” *Biomolecules*, vol. 10, no. 1, p. 68, 2020.

Review Article

Scientific Production in Dentistry: The National Panorama through a Bibliometric Study of Italian Academies

Felice Lorusso ¹, Francesco Inchingolo,² and Antonio Scarano ¹

¹Department of Medical, Oral and Biotechnological Sciences, University of Chieti-Pescara, Via dei Vestini, 31, 66100 Chieti, Italy

²Department of Interdisciplinary Medicine, University of Bari "Aldo Moro", 70121 Bari, Italy

Correspondence should be addressed to Antonio Scarano; ascarano@unich.it

Received 10 June 2020; Revised 10 July 2020; Accepted 22 July 2020; Published 6 August 2020

Guest Editor: Paolo Pesce

Copyright © 2020 Felice Lorusso et al. This is an open access article distributed under the Creative Commons Attribution License, which permits unrestricted use, distribution, and reproduction in any medium, provided the original work is properly cited.

Background. The academic scientific research in the field of dentistry has rapidly increased in the last 20 years under the pressure of the multidisciplinary technological advancements and the growing demand for new predictable and cost-effective techniques and materials. The aim of the present investigation was to analyze the academic scientific production conducted by Italian Academies and Dental Schools. **Methods.** The list of MED/28 academic researchers, associate and full professors, and academic affiliations was collected from the national database of CINECA to evaluate the scientific output of the Italian Universities. The complete list of scientific contributions and the bibliometric parameters were recorded in the Scopus database. **Results.** The scientific production of 37 Italian Universities, 416 researchers, and 23689 papers was evaluated. The measurement of total academic papers, citations, h-index, and relative citation ratio (RCR) was calculated. The study data showed an increase of the academic scientific production over the last 5 years. **Conclusions.** The results presented show how scientific research is increasingly pursued by dental clinicians.

1. Introduction

In recent years, the progress of scientific research in medicine and dentistry is growing due to the technological advances in techniques and materials that are improving the quality of life [1–3].

The academic scientific research has gradually increased in the last years following the world trend and today represents an important element for university academic careers in the bibliometric disciplines [4, 5]. Scientometrics is the discipline that evaluates the quality of the scientific production by techniques and indicators able to measure the bibliographic data and the process of scholarly communication [6–9].

Moreover, the bibliometric research provides a key role for the evaluation of the scholarly chain by measuring methodologies of the scientific productivity of researchers, academies, and scientific associations [10–12]. An extended national bibliometric evaluation represents a

valuable methodology able to create a demographic and trend analysis [13–15].

In fact, the evaluation of the scientific production of a single researcher or an institution can be done through access to one of the dedicated databases existing in the network [16, 17]. One of the main problems of those approaches is represented by the potential systematic bias [11, 16, 18, 19].

Several assessment parameters have been proposed for this scope, such as the journal impact factor citation count, the h-index, and the contemporary h-index that are based on paper citation rate calculation [8, 10].

Dentistry discipline is focused on the prevention, diagnosis, and treatment of oral diseases and disorders and maintenance of oral health [3, 20–22]. This clinical activity is centered on hard and soft tissues, oral mucosa, teeth, maxillofacial bones, temporomandibular, and other supporting structures [23–26].

Moreover, the therapeutic approaches, materials, and protocols need to be convalidated, updated, and constantly

TABLE 1: Demographic evaluation of the academics of the 37 Italian Universities evaluated.

Academic positions	Total	Total papers	Mean h-index	Total citations	Papers published (2015-2020)
Researchers	153	2666	7.4 ± 5.1	29441	1425
Associate professors	175	11372	15.7 ± 8.4	175378	6583
Full professors	88	9500	21.2 ± 11.4	168089	4369

TABLE 2: Distribution of the academics in the 37 Italian Universities evaluated.

Universities	Researchers	Associate professors	Full professors
Bari	3	4	2
Bologna	9	4	3
Brescia	5	6	2
Cagliari	1	3	2
Campania-“L. Vanvitelli”	4	7	5
Catania	6	0	1
Catanzaro	1	3	0
Roma Cattolica del Sacro Cuore	5	3	2
Chieti-Pescara	5	6	8
Ferrara	0	5	3
Firenze	4	4	1
Foggia	2	4	1
Genova	2	4	1
Insubria	2	2	2
L’Aquila	2	0	5
Messina	3	6	0
Milano	6	12	6
Milano-Bicocca	4	0	1
Modena e Reggio Emilia	3	4	0
Napoli Federico II	8	12	7
Padova	2	4	1
Palermo	8	4	4
Parma	5	3	2
Pavia	5	2	3
Perugia	4	0	3
Piemonte Orientale	0	2	1
Pisa	2	1	3
Politecnica delle Marche	2	5	2
Roma “La Sapienza”	12	18	4
Roma “Tor Vergata”	20	5	5
S. Raffaele Milano	1	7	1
Salerno	0	1	1
Sassari	2	3	1
Siena	2	5	1
Torino	6	12	3
Trieste	6	6	1
Verona	1	8	0

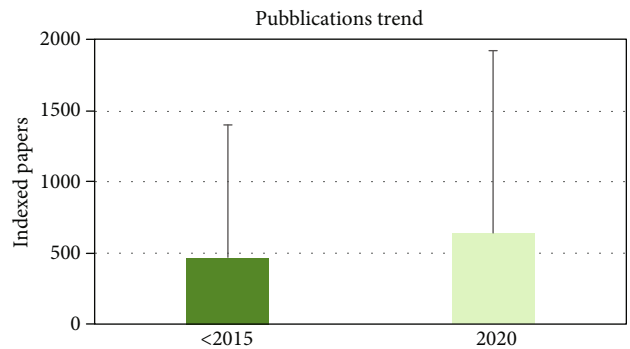


FIGURE 1: Scientific production trends of the academics in the last 5 years.

revised to increase the predictability of the outcomes in clinical practices [27, 28].

The aim of the present investigation was to perform a bibliometric analysis of the scientific academic production of the public and private Italian Universities.

2. Materials and Methods

2.1. Selection of the Sample. The bibliometric quantitative evaluation and content analysis was performed in accordance with the Standards for Reporting Qualitative Research (SRQR) [27].

A list of academic researchers of the Italian Universities was obtained from the national institutional database CINECA (<https://www.cineca.it>) and recorded by two expert specialists (F.L.) into a special dedicated electronic database by the Excel software package (Microsoft Corporation, Redmond, Washington, USA). The recordings were classified and indexed as researchers, associate professors, and full professors affiliated to the academic medical-disciplinary sector odontostomatological diseases (MED/28) for demographic evaluations. For the present investigation, also the position of a researcher at a determined time was considered for the bibliometric evaluation.

2.2. Data Collection. The study data were found and recorded from March 2 to April 8, 2020, from the researcher list of Italian Academics, then analyzed and included in this study.

The database chosen for the bibliometric data evaluation was SciVerse® Scopus (<https://www.scopus.com>). The bibliometric data collection was performed by two operators with experience in the field of literature search (L.F. and A.S.). The author search was performed on the electronic database and included the following data: surname and initial of first name. The authors entered only the initial of the name to

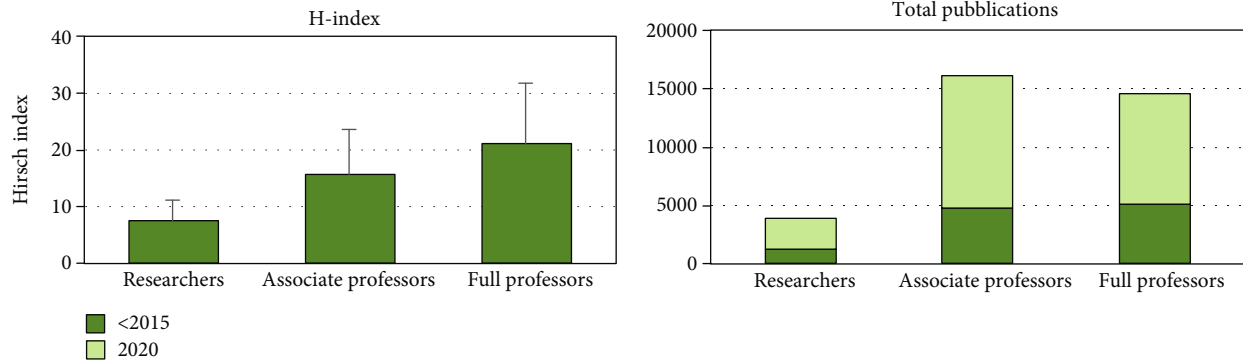


FIGURE 2: Total paper production and mean h-index of the academics evaluated.

avoid possible loss of data, due to the fact that in some publications the full name of the author does not appear. In case of a disambiguation mismatch, the results of the research were excluded. For the bibliometrical analysis, all contribution types recorded in the database (such as proceedings, review, article, and letter) were considered.

2.3. Scientific Production Assessment. For each academic author search, the total number of papers, total citations, and h-index was computed. Moreover, the last ten-year publications were considered to evaluate the trend in scientific production. All data were included in a spreadsheet Office Excel 2007 (Microsoft Corporation) and processed to calculate the mean, the median, and the interquartile range (Iqr) and the percentage change between the individual values where required. The most cited papers for each academic professional were collected for the academic cumulative mean, and the indexed papers, h-index, and total citations were calculated.

3. Results

3.1. Study Population. For the present investigation, a total of 37 Italian universities, 416 academics (153 researchers, 175 associate professors, and 88 full professors), and 23538 indexed papers were evaluated for demographic and statistical analysis (Table 1).

The distribution of the academics is presented in Table 2 (total range between 29 and 2).

The researchers ranged from 29 to 0 (mean: 5.5 ± 4.7), the associated professors ranged between 18 and 3 (mean: 7.1 ± 4.1), and the full professors between 29 and 2 (mean: 4.2 ± 2.7).

3.2. Academics Scientific Production. An increase of the scientific production was reported during the last 5 years for all academics (2015-2020) (Figure 1).

A full professor mean h-index was reported higher if compared to associate professors and researchers, while the researchers' increase of indexed papers was 53.4%, the associate professors' increase was 57.8%, and the full professors' increase was 45.5%.

An increase of the academic scientific papers was reported in the last 5 years, with an augmented production

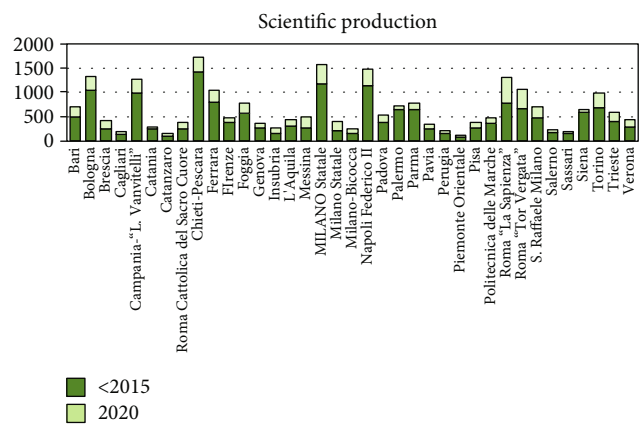


FIGURE 3: Scientific production trends referring to the 37 universities evaluated.

index ranging between 52.4% and 91.7% (Figure 2) and a distribution of the publications between the three professional categories (Figure 3).

The summary of the bibliometric parameters of the Italian schools of dentistry are presented in Table 3, with the total count of indexed papers, h-index, total citations, and cumulative most cited paper value.

A heterogeneity of the amount of indexed paper (Figure 4), mean h-index (Figure 5), and mean citations count (Figure 6) are reported between the academic categories of the universities evaluated.

4. Discussion

The scholastic institution in the field of dentistry in Italy presents a more recent historical course if compared to the other medical sectors [28].

In Italy, the dentistry profession is currently practiced by three different figures: the graduate in Medicine and specialized in Odontostomatology; the graduate in Medicine and Surgery who is not a specialist but registered in the National Register of Dentists; and the graduate in Dentistry. In the same way, the researchers' careers afferent to the academic medical-disciplinary sector, odontostomatological diseases (MED/28), require a degree in medicine and dentistry.

TABLE 3: Summary of the Italian Academies investigated (tot: total cumulative count; mean: average amount; sd: standard deviation, Icq: interquartile range).

Universities		Indexed papers	h-index	Citations	Papers (2015-2020)	Most cited paper
Bari	Tot	707.0	153.0	8780.0	218.0	724.0
	Mean	70.7	15.3	878.0	21.8	72.4
	sd	51.1	6.7	829.1	14.1	48.3
	Irq	63.0	9.5	979.3	19.5	78.5
Bologna	Tot	1334.0	321.0	33299.0	292.0	2661.0
	Mean	95.3	22.9	2378.5	20.9	190.1
	sd	69.6	14.0	2848.5	17.8	160.5
	Irq	77.8	16.3	2019.8	26.0	111.8
Brescia	Tot	408.0	125.0	4606.0	156.0	841.0
	Mean	31.4	9.6	354.3	12.0	64.7
	sd	21.5	4.6	407.9	9.9	61.9
	Irq	28.0	6.0	278.0	13.0	22.0
Cagliari	Tot	182.0	59.0	2162.0	60.0	350.0
	Mean	30.3	9.8	360.3	10.0	58.3
	sd	17.4	4.6	302.9	8.5	34.3
	Irq	20.8	6.3	348.5	13.3	44.5
Campania- "L. Vanvitelli"	Tot	1272.0	282.0	20096.0	284.0	2274.0
	Mean	84.8	18.8	1339.7	18.9	151.6
	sd	55.0	8.1	1006.0	17.8	108.1
	Irq	65.0	11.5	1406.0	14.5	194.0
Catania	Tot	283.0	54.0	3390.0	32.0	276.0
	Mean	56.6	10.8	678.0	6.4	55.2
	sd	87.8	11.6	1168.2	13.2	37.9
	Irq	18.0	6.0	346.0	1.0	60.0
Catanzaro	Tot	143.0	31.0	873.0	50.0	114.0
	Mean	47.7	10.3	291.0	16.7	38.0
	sd	8.5	2.3	64.6	8.4	5.6
	Irq	8.5	2.0	61.5	7.5	5.5
Roma Cattolica del Sacro Cuore	Tot	381.0	98.0	5040.0	140.0	1965.0
	Mean	42.3	10.9	560.0	15.6	218.3
	sd	18.4	4.5	410.2	10.6	285.8
	Irq	24.0	5.0	706.0	15.0	252.0
Chieti-Pescara	Tot	1729.0	391.0	33835.0	294.0	2995.0
	Mean	96.1	21.7	1879.7	16.3	166.4
	sd	77.6	10.4	2088.3	17.5	119.7
	Irq	68.5	14.8	1590.3	18.3	190.5
Ferrara	Tot	1054.0	162.0	18314.0	247.0	1036.0
	Mean	131.8	20.3	2289.3	30.9	129.5
	sd	146.9	14.5	3210.8	27.2	83.1
	Irq	99.3	11.0	1318.0	43.5	82.5
Firenze	Tot	466.0	100.0	9317.0	90.0	923.0
	Mean	77.7	16.7	1552.8	15.0	153.8
	sd	92.1	11.9	2528.0	25.1	167.7
	Irq	18.5	3.5	348.0	4.8	73.5

TABLE 3: Continued.

Universities		Indexed papers	h-index	Citations	Papers (2015-2020)	Most cited paper
Foggia	Tot	778.0	126.0	14294.0	202.0	758.0
	Mean	129.7	21.0	2382.3	33.7	126.3
	sd	173.0	14.3	3549.0	38.2	77.4
	Irq	23.5	11.8	1217.3	24.3	77.0
Genova	Tot	360.0	83.0	3857.0	101.0	320.0
	Mean	60.0	13.8	642.8	16.8	53.3
	sd	28.9	6.9	403.7	9.5	28.3
	Irq	39.0	3.8	410.8	8.3	11.0
Insubria	Tot	266.0	60.0	2366.0	122.0	186.0
	Mean	66.5	15.0	591.5	30.5	46.5
	sd	21.5	2.9	296.5	14.4	25.5
	Irq	25.0	2.5	358.5	11.0	24.5
L'Aquila	Tot	443.0	88.0	5189.0	137.0	368.0
	Mean	73.8	14.7	864.8	22.8	61.3
	sd	43.7	7.4	675.4	17.8	21.3
	Irq	61.8	13.8	1169.8	24.3	32.8
Messina	Tot	500.0	135.0	6639.0	235.0	422.0
	Mean	62.5	16.9	829.9	29.4	52.8
	sd	52.6	8.7	737.2	31.5	17.8
	Irq	26.5	7.5	606.3	12.0	16.3
Milano	Tot	1581.0	352.0	30365.0	393.0	2675.0
	Mean	87.8	19.6	1686.9	21.8	148.6
	sd	67.5	12.3	1615.1	21.5	119.7
	Irq	61.3	16.0	2160.0	25.8	170.0
Milano-Bicocca	Tot	391.0	66.0	4080.0	186.0	466.0
	Mean	78.2	13.2	816.0	37.2	93.2
	sd	77.7	9.9	1064.7	54.7	56.9
	Irq	45.0	7.0	584.0	9.0	68.0
Modena e Reggio Emilia	Tot	237.0	58.0	1584.0	88.0	248.0
	Mean	39.5	9.7	264.0	14.7	41.3
	sd	8.6	2.9	149.0	9.7	11.4
	Irq	11.0	3.0	117.0	12.8	12.5
Napoli Federico II	Tot	1487.0	330.0	27739.0	348.0	6555.0
	Mean	78.3	17.4	1459.9	18.3	345.0
	sd	53.1	8.5	1710.8	14.9	917.9
	Irq	68.0	13.5	1625.0	20.0	157.0
Padova	Tot	527.0	100.0	5518.0	143.0	455.0
	Mean	87.8	16.7	919.7	23.8	75.8
	sd	26.1	4.5	436.8	11.6	29.3
	Irq	14.8	5.0	478.0	17.8	27.5
Palermo	Tot	730.0	166.0	10123.0	81.0	1154.0
	Mean	52.1	11.9	723.1	5.8	82.4
	sd	52.3	9.8	1220.1	7.5	56.8
	Irq	50.5	10.0	508.0	5.8	71.8

TABLE 3: Continued.

Universities		Indexed papers	h-index	Citations	Papers (2015-2020)	Most cited paper
Parma	Tot	777.0	118.0	10109.0	126.0	913.0
	Mean	129.5	19.7	1684.8	21.0	152.2
	sd	127.7	7.1	1542.6	11.8	94.6
	Irq	80.3	8.0	922.3	7.0	144.8
Pavia	Tot	341.0	89.0	3581.0	96.0	516.0
	Mean	42.6	11.1	447.6	12.0	64.5
	sd	29.2	5.9	372.6	11.4	31.7
	Irq	49.3	7.3	338.5	17.5	34.5
Perugia	Tot	198.0	31.0	687.0	50.0	189.0
	Mean	33.0	5.2	114.5	8.3	31.5
	sd	29.5	3.5	110.1	7.6	29.7
	Irq	27.8	5.8	185.3	11.5	40.8
Piemonte Orientale	Tot	108.0	20.0	482.0	39.0	85.0
	Mean	36.0	6.7	160.7	13.0	28.3
	sd	18.0	1.5	136.6	8.9	23.3
	Irq	17.5	1.5	131.0	8.5	21.5
Pisa	Tot	373.0	100.0	8028.0	103.0	802.0
	Mean	74.6	20.0	1605.6	20.6	160.4
	sd	52.1	12.3	1265.2	15.8	113.5
	Irq	8.0	10.0	1511.0	19.0	183.0
Politecnica delle Marche	Tot	475.0	115.0	6705.0	114.0	887.0
	Mean	52.8	12.8	745.0	12.7	98.6
	sd	35.9	7.6	821.9	9.9	94.4
	Irq	49.0	8.0	742.0	18.0	66.0
Roma "La Sapienza"	Tot	1315.0	274.0	12994.0	539.0	1603.0
	Mean	48.7	10.1	481.3	20.0	59.4
	sd	47.0	6.8	657.5	20.8	48.8
	Irq	23.0	7.5	504.0	16.5	42.5
Roma "Tor Vergata"	Tot	1061.0	251.0	10298.0	391.0	2393.0
	Mean	36.6	8.7	355.1	13.5	82.5
	sd	39.7	5.6	399.8	15.3	82.5
	Irq	36.0	7.0	317.0	18.0	67.0
S. Raffaele Milano	Tot	709.0	165.0	10981.0	240.0	911.0
	Mean	88.6	20.6	1372.6	30.0	113.9
	sd	63.4	7.1	839.5	22.5	57.6
	Irq	37.8	12.0	960.0	27.5	79.0
Salerno	Tot	218.0	36.0	2206.0	45.0	237.0
	Mean	109.0	18.0	1103.0	22.5	118.5
	sd	1.4	5.7	769.3	12.0	108.2
	Irq	1.0	4.0	544.0	8.5	76.5
Sassari	Tot	194.0	50.0	2858.0	49.0	430.0
	Mean	38.8	10.0	571.6	9.8	86.0
	sd	49.0	8.9	748.8	13.2	75.8
	Irq	14.0	6.0	263.0	11.0	133.0

TABLE 3: Continued.

Universities		Indexed papers	h-index	Citations	Papers (2015-2020)	Most cited paper
Siena	Tot	644.0	166.0	22226.0	53.0	1299.0
	Mean	80.5	20.8	2778.3	6.6	162.4
	sd	98.2	22.0	4437.1	8.4	142.5
	Irq	73.3	26.0	3163.5	7.3	199.8
Torino	Tot	984.0	281.0	16305.0	298.0	1937.0
	Mean	54.7	15.6	905.8	16.6	107.6
	sd	28.1	6.6	620.6	12.4	58.8
	Irq	32.8	10.0	833.0	22.5	79.3
Trieste	Tot	594.0	138.0	11181.0	188.0	2015.0
	Mean	54.0	12.5	1016.5	17.1	183.2
	sd	55.4	11.9	1523.0	16.0	260.2
	Irq	55.5	12.5	1046.0	18.0	190.5
Verona	Tot	439.0	93.0	4018.0	161.0	771.0
	Mean	54.9	11.6	502.3	20.1	96.4
	sd	41.0	3.6	143.6	19.8	65.0
	Irq	55.0	4.5	168.3	26.8	54.5

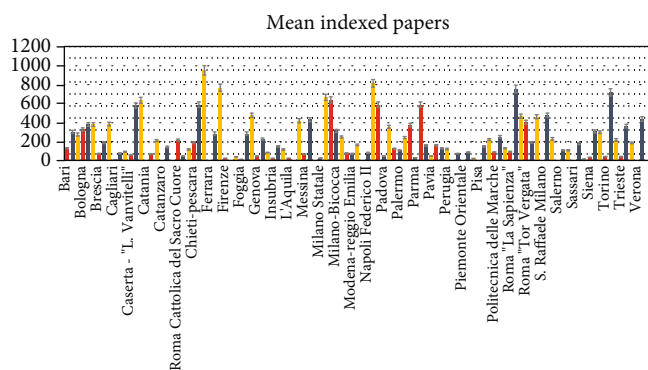


FIGURE 4: Indexed papers distribution of the researchers (red), associates (blue), and full professors (yellow) investigated.

Nowadays, the clinical and research activity in dental practice covers several different specialties such as oral surgery and implantology, odontostomatology, orthodontics, pediatric, restorative, and prosthetic dentistry. As a result, dental research has shown a worldwide increase of scientific production output in the last decades [29].

Pulgar et al. reported a quantitative analysis of the scientific production on electronic database, investigating Dentistry, Oral Surgery, and Medicine (DOSM) publications and Non-DOSM production. The percentage of dental papers, including surgery manuscripts, compared to total production was 0.89% during the last three decades, with a Non-DOSM/DOSM ratio of 17% [29].

Moreover, the Italian scientific production was considered among the top 20 countries with an increase of 4.43% of DOSM publications during the same period [29].

In the present investigation, the academics of the Italian Universities registered in the national institutional

database were considered for evaluating the scientific production trend.

However, this methodology does not consider the scientific contribution offered by the private practitioners and hospital dental employees, who represent a consistent part of the dental health care in Italy [30].

The present investigation was not extended to health workers of hospitals and public assistance structures, where the bibliometric parameters are not institutional indicators for the careers of the clinicians in the public healthcare structures.

In this way, the adoption of new research strategies of quality scientific production could improve the researchers' activity in studying new approaches and therapeutic treatments for oral and jaw diseases and for a better knowledge of their etiopathogenesis [1, 31, 32].

In a previous research, Zizzari et al. investigated the scientific production of 252 active members of Italian associations of Oral Surgery throughout three periods of 5 years each, covering a total of 15 years [33]. The study showed that the nonacademic scientific production produced from 2886 to 5679 papers during the period between 2003 and 2008, 7865 from 2009 to 2013, with an increase of 172.52% manuscripts.

One of the most important limits of the research design is represented by the systematic research bias [29, 34]. In fact, the disambiguation of authors represents the weak point of the of the present methodology.

Moreover, a comparison of the investigation results with the international academic scientific production is a possible perspective, but the high risk of bias is present in relation to the extensive differences between the nations' academic systems and institutional affiliations in medicine and dentistry. Probably the presence of a common European and international researchers register can

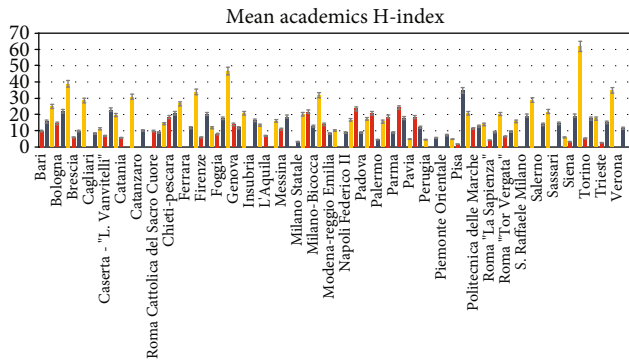


FIGURE 5: Mean h-index distribution between the researchers (red), associates (blue), and full professors (yellow).

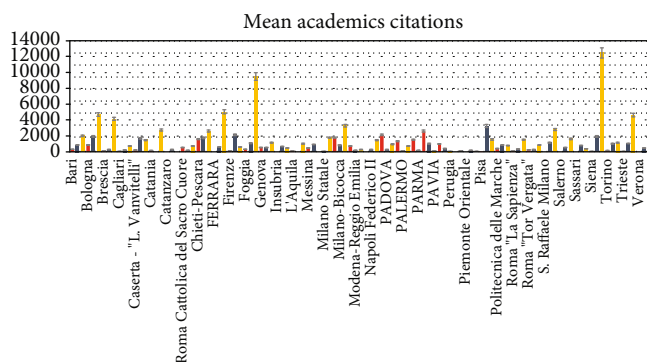


FIGURE 6: Mean citation amount distribution of the academic professionals referring to the universities investigated. Researcher (red), associated (blue), and full professors (yellow).

facilitate the check of the academics for a supranational bibliometric comparison.

Scopus provides the most complete database with the largest scientific bibliography and citations system, with over 18000 journal sources registered, covering several fields, such as medicine, engineering, humanities, and social disciplines [19, 35].

In the present study, the institutions with an increased amount of academics showed the higher level of scientific production, in terms of total published papers. On the contrary, the other quality production indexes such as citation count and h-index showed a great heterogeneity of the output, with a production index that exceeded 90% in the last 5 years.

However, clinical research in dental practice of the Italian academics concerned the different disciplines of dentistry: oral surgery and implantology, odontostomatology, orthodontics, pediatric, restorative, and prosthetic dentistry. In fact, the recent research activity in dentistry showed a significant increase of scientific production output in the last decades, following the advances in new materials, clinical protocols, technical procedures, and technologies in the relative disciplines.

Today, the scientific production represents an important element of evaluation for the university researchers' careers

in the bibliometric disciplines and probably a substantial incentive to enhance the present activity.

Moreover, the bibliometric parameters used do not represent the outline of the years of activity of the individual academics that could influence the quality trends of the younger researchers [36–38].

In this way, a normalized citation index should be introduced to overcome this activity difference and reduce the potential confounding factor between the researchers, associate professors, and full professors to a more equal evaluation trend [6, 12, 15, 30].

5. Conclusions

The existing databases represent valuable tools for measuring the quality and quantity of the institutional scientific production according to an appropriate interpretation of the data, with a growth in the last 5 years in the trend of academic activity with a high scientific-impact indices output.

Conflicts of Interest

The authors declare no conflict of interest for the present research.

Authors' Contributions

Conceptualization was done by AS and FL, methodology by FL and AS, software by FL, validation by AS and FL, formal analysis by AS, investigation by AS, data curation by AS and FL, writing—original draft preparation—by FL, writing—review and editing—by FL, AS, and FI, and supervision by AS.

References

- [1] A. R. Amini, C. T. Laurencin, and S. P. Nukavarapu, "Bone tissue engineering: recent advances and challenges," *Critical Reviews in Biomedical Engineering*, vol. 40, no. 5, pp. 363–408, 2012.
- [2] H. N. Chia and B. M. Wu, "Recent advances in 3D printing of biomaterials," *Journal of Biological Engineering*, vol. 9, no. 1, p. 4, 2015.
- [3] S. Tandon, A. Venkiteswaran, S. M. Baliga, and U. A. Nayak, "Recent research trends in dentistry," *Journal of the Indian Society of Pedodontics and Preventive Dentistry*, vol. 35, no. 2, pp. 102–105, 2017.
- [4] C. J. F. Waaijer, NVMO Special Interest Group on Scientific Education, B. W. C. Ommering, L. J. van der Wurff, T. N. van Leeuwen, and F. W. Dekker, "Scientific activity by medical students: the relationship between academic publishing during medical school and publication careers after graduation," *Perspectives on Medical Education*, vol. 8, no. 4, pp. 223–229, 2019.
- [5] V. T. Warren, B. Patel, and C. J. Boyd, "Analyzing the relationship between Altmetric score and literature citations in the Implantology literature," *Clinical Implant Dentistry and Related Research*, vol. 22, no. 1, pp. 54–58, 2020.
- [6] I. Masic, "Medical publication and scientometrics," *Journal of Research in Medical Sciences*, vol. 18, no. 6, pp. 516–521, 2013.
- [7] M. S. Shaikh, R. Ullah, M. A. Lone, H. Matabdin, F. Khan, and M. S. Zafar, "Periodontal regeneration: a bibliometric analysis

- of the most influential studies," *Regenerative Medicine*, vol. 14, no. 12, pp. 1121–1136, 2019.
- [8] W. Liu, L. Ma, C. Song, C. Li, Z. Shen, and L. Shi, "Research trends and characteristics of oral lichen planus: A bibliometric study of the top-100 cited articles," *Medicine*, vol. 99, no. 2, article e18578, 2020.
- [9] S. S. Patil, S. C. Sarode, G. S. Sarode et al., "A bibliometric analysis of the 100 most cited articles on Early Childhood Caries," *International Journal of Paediatric Dentistry*, vol. 3, 2020.
- [10] A. Cabezas-Clavijo and E. Delgado-López-Cózar, "Google Scholar and the h-index in biomedicine: the popularization of bibliometric assessment," *Medicina Intensiva*, vol. 37, no. 5, pp. 343–354, 2013.
- [11] I. Masic, E. Begic, and N. Begic, "Validity of scientometric analysis of medical research output," *Studies in Health Technology and Informatics*, vol. 238, pp. 246–249, 2017.
- [12] A. Alonso-Arroyo, J. G. de Dios, C. Calvo, Á. Caldúch-Losa, and R. Aleixandre-Benavent, "Scientific impact and bibliometric contextualisation of Paediatrics compared to other specialities," *Anales de Pediatría (English Edition)*, vol. 92, no. 3, pp. 172.e1–172.e12, 2020.
- [13] G. Buela-Casal, M. P. Bermúdez, J. C. Sierra, R. Quevedo-Blasco, A. Castro, and A. Guillén-Riquelme, "Ranking 2010 in production and research productivity in Spanish public universities," *Psicothema*, vol. 23, no. 4, pp. 527–536, 2011.
- [14] M. De la Flor-Martínez, P. Galindo-Moreno, E. Sánchez-Fernández, E. Abadal, M.-J. Cobo, and E. Herrera-Viedma, "Evaluation of scientific output in Dentistry in Spanish Universities," *Medicina Oral Patología Oral y Cirugía Bucal*, vol. 22, pp. e491–e499, 2015.
- [15] R. R. de Moraes, L. L. Morel, M. B. Correa, and G. da Silveira Lima, "A bibliometric analysis of articles published in Brazilian dental journal over 30 years," *Brazilian Dental Journal*, vol. 31, no. 1, pp. 10–18, 2020.
- [16] M. E. Falagas, E. I. Pitsouni, G. A. Malietzis, and G. Pappas, "Comparison of PubMed, Scopus, Web of Science, and Google Scholar: strengths and weaknesses," *The FASEB Journal*, vol. 22, pp. 338–342, 2007.
- [17] S. Baykoucheva, "Selecting a database for drug literature retrieval: a comparison of MEDLINE, Scopus, and Web of Science," *Science & Technology Libraries*, vol. 29, no. 4, pp. 276–288, 2010.
- [18] P. Jacso, "Testing the calculation of a realistic h-index in Google Scholar, Scopus, and Web of Science for F. W. Lancaster," *Library Trends*, vol. 56, no. 4, pp. 784–815, 2008.
- [19] L. I. Meho and C. R. Sugimoto, "Assessing the scholarly impact of information studies: a tale of two citation databases—Scopus and Web of Science," *Journal of the American Society for Information Science and Technology*, vol. 60, no. 12, pp. 2499–2508, 2009.
- [20] G. Prato, F. Cairo, C. Tinti, P. Cortellini, L. Muzzi, and E. Mancini, "Prevention of alveolar ridge deformities and reconstruction of lost anatomy: a review of surgical approaches," *The International Journal of Periodontics & Restorative Dentistry*, vol. 24, no. 5, pp. 434–445, 2004.
- [21] S. P. Pilipchuk, A. B. Plonka, A. Monje et al., "Tissue engineering for bone regeneration and osseointegration in the oral cavity," *Dental Materials*, vol. 31, no. 4, pp. 317–338, 2015.
- [22] M. B. Stephens, J. P. Wiedemer, and G. M. Kushner, "Dental problems in primary care," *American Family Physician*, vol. 98, no. 11, pp. 654–660, 2018.
- [23] K. M. Reich, C. D. Huber, W. R. Lippnig, C. Ulm, G. Watzek, and S. Tangl, "Atrophy of the residual alveolar ridge following tooth loss in an historical population," *Oral Diseases*, vol. 17, no. 1, pp. 33–44, 2011.
- [24] A. Scarano, G. Murmura, G. Vantaggiato et al., "Delayed expansion of atrophic mandible (deam): a case report," *Oral & Implantology*, vol. 10, no. 2, pp. 190–196, 2017.
- [25] G. Isola, L. Perillo, M. Migliorati et al., "The impact of temporomandibular joint arthritis on functional disability and global health in patients with juvenile idiopathic arthritis," *European Journal of Orthodontics*, vol. 41, pp. 117–124, 2019.
- [26] L. Nibali, V. P. Koidou, M. Nieri, L. Barbato, U. Pagliaro, and F. Cairo, "Regenerative surgery versus access flap for the treatment of intra-bony periodontal defects: A systematic review and meta-analysis," *Journal of Clinical Periodontology*, vol. 47, no. S22, pp. 320–351, 2020.
- [27] B. C. O'Brien, I. B. Harris, T. J. Beckman, D. A. Reed, and D. A. Cook, "Standards for reporting qualitative research: a synthesis of recommendations," *Academic Medicine*, vol. 89, no. 9, pp. 1245–1251, 2014.
- [28] P. Zampetti and G. Barbon, Cento anni di odontoiatria in Italia: 1912–2012.
- [29] R. Pulgar, I. Jiménez-Fernández, E. Jiménez-Contreras, D. Torres-Salinas, and C. Lucena-Martín, "Trends in world dental research: an overview of the last three decades using the Web of Science," *Clinical Oral Investigations*, vol. 17, no. 7, pp. 1773–1783, 2013.
- [30] R. J. Dinis-Oliveira, "The h-index in life and health sciences: advantages, drawbacks and challenging opportunities," *Current Drug Research Reviews*, vol. 11, no. 2, pp. 82–84, 2019.
- [31] P. I. Brånemark, P. Engstrand, L. O. Öhrnell et al., "Brånemark Novum: a new treatment concept for rehabilitation of the edentulous mandible. Preliminary results from a prospective clinical follow-up study," *Clinical Implant Dentistry and Related Research*, vol. 1, no. 1, pp. 2–16, 1999.
- [32] B. Pjetursson, A. Asgeirsson, M. Zwahlen, and I. Sailer, "Improvements in implant dentistry over the last decade: comparison of survival and complication rates in older and newer publications," *The International Journal of Oral & Maxillofacial Implants*, vol. 29, Supplement, pp. 308–324, 2014.
- [33] V. L. Zizzari, A. De Carlo, F. Lorusso, S. Tetè, and A. Piattelli, "Evaluation of scientific production in oral surgery in Italy from 1998 to 2012," *Minerva Stomatologica*, vol. 63, no. 5, pp. 155–165, 2014.
- [34] Y. Gallardo Sánchez, R. L. Gallardo Arzuaga, M. Fonseca Arias, and M. E. Pérez Atencio, "Scientometric characterization of Medwave's scientific production 2010–2014," *Medwave*, vol. 16, no. 8, article e6538, 2016.
- [35] S. Tetè, V. L. Zizzari, A. De Carlo et al., "Characterizing scientific production of Italian Oral Surgery professionals through evaluation of bibliometric indices," *Annali di Stomatologia*, vol. 5, no. 1, pp. 23–29, 2014.
- [36] M. A. Islam, R. M. Talukder, R. Taheri, and A. Dutta, "Pharmacy relative to other health professions in interprofessional education: a bibliometric study," *Journal of National Black Nurses' Association*, vol. 30, no. 2, pp. 38–43, 2019.

- [37] P. Ahmad, J. A. Asif, M. K. Alam, and J. Slots, "A bibliometric analysis of Periodontology 2000," *Periodontology 2000*, vol. 82, no. 1, pp. 286–297, 2019.
- [38] P. Ahmad, P. Vincent Abbott, M. Khursheed Alam, and J. Ahmed Asif, "A bibliometric analysis of the top 50 most cited articles published in the dental traumatology," *Dental Traumatology*, vol. 36, no. 2, pp. 89–99, 2019.

Research Article

Influence of Implant Thread Morphology on Primary Stability: A Prospective Clinical Study

Maria Menini,¹ Francesco Bagnasco,¹ Ivan Calimodio,¹ Nicolò Di Tullio,¹ Francesca Delucchi ¹ Domenico Baldi,¹ and Francesco Pera²

¹Department of Surgical Sciences (DISC), Implant and Prosthetic Dentistry Unit, University of Genoa, Ospedale S. Martino (pad. 4), L. Rosanna Benzi 10, 16132 Genoa, Italy

²Interdepartmental Research Center, Dental-School, University of Turin, Turin, Italy

Correspondence should be addressed to Francesca Delucchi; dafne.1995@libero.it

Received 24 April 2020; Accepted 1 July 2020; Published 5 August 2020

Academic Editor: Dong-Wook Han

Copyright © 2020 Maria Menini et al. This is an open access article distributed under the Creative Commons Attribution License, which permits unrestricted use, distribution, and reproduction in any medium, provided the original work is properly cited.

Objectives. The purpose of this study was to evaluate the primary stability of two implants with the same macro- and micromorphology but different thread design and analyze their clinical outcomes over a one-year period. **Materials and Methods.** 14 patients needing a partial rehabilitation with a delayed loading approach (DEL group: 9 patients) or a full-arch rehabilitation treated with immediately loaded fixed prostheses supported by 4 implants following the Columbus Bridge Protocol (CBP) (IL group: 5 patients) were included. In each patient, at least one SY (implant with standard threads) and one SL implant (implant with an augmented depth of the threads) were randomly inserted. Primary outcome measures were the number of threads exposed at a torque of 30 Ncm and 50 Ncm and final insertion torque. Secondary outcome measures were implant and prosthetic failure, peri-implant bone resorption, and periodontal parameters: bleeding on probing (BoP), plaque index (PI), and probing depth (PD) evaluated at 3, 6, and 12 months of healing. **Results.** Nineteen SY and 19 SL implants were inserted in 14 patients. Twenty implants (10 SL and 10 SY) were inserted in the IL group, while 18 (9 SL and 9 SY) were inserted in the DEL group and followed-up for 12 months. No patients dropped out. No implants and prostheses failed. No biological complications were identified. No significant differences were found between SY and SL implants comparing the number of exposed threads when inserting the implant with a torque insertion of 30 N (T student test $p = .142$ and U test $p = .164$). At 50 N, no threads were visible in either groups. Final torque insertion values were higher for SL (mean: 48.42 Ncm) compared to SY implants (mean: 43.42 Ncm) without a statistically significant difference. All the implants showed good clinical outcomes at the 1-year-in-function visit. **Conclusions.** After 12 months of function, both implant types provided good clinical outcomes without statistically significant differences between the two groups. A difference in insertion torque (even if not statistically significant) was found with higher insertion torque values for SL implants with a larger thread depth.

1. Introduction

Dental implant rehabilitation is considered a highly predictable method to replace missing teeth, with a success rate ranging around 95% [1]. Adequate implant stability with a close connection between residual peri-implant bone and the implant itself, avoiding micromovements of the implants, is a fundamental prerequisite to achieve successful osseointegration [2, 3].

Primary implant stability, that is, the mechanical stability of the implant at placement, is a mechanical phenomenon that can be determined by measuring insertion torque values [4]. It mainly depends on three factors [5]:

- (1) biomechanical properties of bone (quality and quantity of the receiving bone)
- (2) preparation technique of the implant site (diameter of the largest drill used, length of the preparation,

morphology of the drill, and tapping or not of the implant site)

- (3) macrostructure of the implant (diameter, length, and shape)

While bone characteristics are not modifiable, the surgical technique and the macrostructure of the implant (that is, the macroscopic shape of the implant, including diameter, length, shape, and thread design) and the microstructure of the implant (that is, implant surface characteristics) can be modulated by the clinician to optimize primary stability. Moreover, after implantation, and even once osseointegration has been reached, bone undergoes a constant remodeling which is also influenced by occlusal loads, abutment characteristics, platform switching, etc. [5–9].

Reaching optimal primary stability is a prerequisite particularly important in full-arch immediate loading rehabilitations. In this case, primary stability is considered a key factor together with the use of a rigid framework in order to avoid micromotions of the implants and achieve osseointegration [10–13].

Implant design is one of the key factors to modulate primary stability and stress distribution to peri-implant bone. The geometric features of an implant strongly affect its surface area, and as a consequence, they influence the amount of bone-implant contact (BIC). Implants with deeper threads, small pitch, and reduced helix angle were shown to enhance primary stability by achieving higher bone to implant contact while reducing osseocompression [14, 15].

Implant geometry also plays an important role on stress distribution at the bone-implant interface and on implant capacity to withstand forces during the process of osseointegration. Therefore, implant thread design affects both the obtainment and maintenance of osseointegration through multiple mechanisms [5, 14].

Clinically, implant stability can be measured with torque insertion force or resonance frequency analysis. Insertion torque values are very important for the clinical determination of primary stability levels and the absence of micromovement whenever an immediate load is applied [16].

The purpose of the present study was to evaluate the primary stability of two implants with the same micro- and macromorphology but different thread designs and investigate the relation of implant thread design with clinical outcomes over a one-year period. The null hypothesis tested was that there was a difference neither in torque insertion nor in 1-year clinical outcomes between dental implants with standard and increased depth of the threads.

2. Materials and Methods

In the period between May 2017 and March 2019, patients referring to the Implant and Prosthetic Dentistry Unit of the Department of Surgical Sciences (DISC) of Genoa University were selected if they required the insertion of at least two implants. This prospective study was performed following the principles outlined in the Declaration of Helsinki on experimentation involving human subjects. All patients were

thoroughly informed about the procedures and signed an informed consent form.

Exclusion criteria were as follows:

- (i) patients with a history of bisphosphonate therapy
- (ii) patients with uncontrolled diabetes (HbA1c > 6%, glycemic level > 110 mg/dL)
- (iii) patients with relevant medical conditions contraindicating oral surgery
- (iv) patients without sufficient native bone needing regenerative procedures

2.1. Implant Characteristics. The titanium implants analyzed (Syra and Syra SL, Sweden & Martina, Due Carrare PD, Italy) presented an external hexagon connection, a conical morphology, and a surface sand-blasted with zirconia oxide and etched with mineral acid (Figure 1). The neck was machined for the height of 1.00 mm and presented a divergent shape with different angles according to the implant diameter, in order to use the same prosthetic component on all implant diameters:

- (i) Implant diameter of 3.80 mm and platform diameter of 4.10 mm → collar divergence of 14°
- (ii) Implant diameter of 4.25 mm and platform diameter of 4.10 mm → collar divergence of 7.5°
- (iii) Implant diameter of 5.00 mm and platform diameter of 5.00 mm → collar divergence of 7.5°

The SYRA implant (SY) had a constant thread depth of 0.25 mm along the whole body of the fixture, keeping the maximum external profile of the implant conical.

Syra SL (SL) implants differ from SY for two factors:

- (i) Depth of the threads: it gradually increases from 0.25 mm in the coronal part of the implant body to 0.70 mm in the apical part, making the maximum profile of the implant cylindrical
- (ii) Shape of the threads: trapezoidal in the loops in the upper part of the implant (such as SY implants) and triangular shape in the apical part. On the contrary, SY implants present a trapezoidal shape of the threads throughout their entire length

Patients were divided into two groups depending on the rehabilitation required:

- (i) DEL group: patients needing a partial rehabilitation with a delayed loading approach
- (ii) IL group: patients needing a full-arch rehabilitation treated with immediate loading full-arch fixed prostheses supported by implants ($n = 4-6$ for an arch) following the Columbus Bridge Protocol (CBP) [10, 13]

In each patient, at least one SY and one SL implant were randomly inserted applying a split-mouth methodology

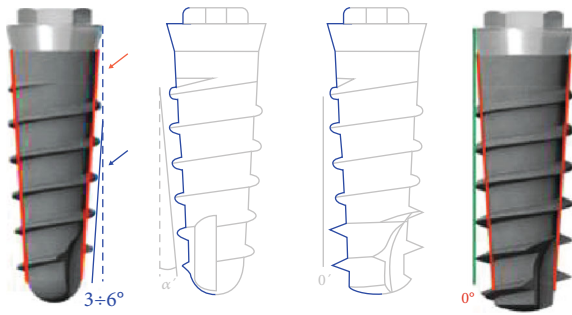


FIGURE 1: Design of the two tested implants: SY on the left and SL on the right.

(Figure 2). In the IL group, one hemiarch was treated with 2 SY implants and the contralateral hemiarch was treated with 2 SL implants. Each hemiarch was randomly allocated to the SY or SL treatment. In the DEL group, one SL implant and one SY implant were inserted one next to the other into an edentulous area, and their position in the adjacent osteotomies was randomly allocated. Implant length ranged between 10 and 18 mm (10-13 mm in the DEL group and 10-18 mm in the IL group), and implant diameter was 3.8 mm or 4.25 mm depending on available bone.

Under local anesthesia, a crestal incision and a full-thickness flap elevation were performed. The implant sites were prepared starting with a pilot drill followed by the sequence of burs provided by the implant manufacturer. Bone quality was evaluated, and the site preparation protocol was chosen accordingly. Bone was considered according to the Misch [17] classification which is based on the microstructural characteristics of the two components of bone (cortical and spongy bone) and dividing bone quality into 4 types: D1 (dense cortical bone and poor spongy bone), D2 (thick spongy and narrow-meshed cortical bone), D3 (thin-meshed spongy cancellous bone), and D4 (loose cancellous bone). Implants were inserted using the Implantmed electronic surgical drilling unit with torque control (Implantmed, W&H). The device was first set at 30 Ncm, and the implant insertion procedure was stopped when the 30 Ncm insertion torque was reached in order to record the number of exposed threads at 30 Ncm; that is to say, the number of threads above the bone crest was recorded. The same procedure was conducted at 50 Ncm. If the implant was still not in its final position, a manual insertion device was then used and the final insertion torque was registered. The implant threads were observed on the vestibular side of each implant.

2.2. DEL Rehabilitation. In the DEL group, a one-stage technique was applied. After implant insertion, transmucosal titanium healing abutments were immediately connected to the implants and soft tissues were approximated and sutured around them. Patients were prescribed analgesics and antibiotic coverage (amoxicillin 2 g/daily or in case of allergy clindamycin 600 mg/daily) for 7 days from the day before surgery, as well as oral rinses of 0.12% chlorhexidine gluconate for 7 days from the day following implant placement. Three months after surgery, a traditional impression was

taken, and definitive screw-retained prostheses provided with a metal framework and composite resin veneering material were delivered. All the restorations were splinted; no single crowns were realized.

2.3. IL Rehabilitation. In the case of full-arch immediate loading rehabilitations, the Columbus Bridge Protocol was applied [10-13].

The CBP is a surgical and prosthodontic protocol developed for rehabilitation of atrophic, edentulous maxillae, and mandibles using distal tilted implants (upper jaw: implants placed parallel to the anterior sinus wall; lower jaw: implants placed obliquely angled above the mental foramen). The surgical and prosthetic protocol was the same used in already published papers [10-13].

Conical abutments with a 0, 15, or 30 degrees inclination (P.A.D, Sweden & Martina, Due Carrare, Padova) were placed onto the implants immediately after implant insertion, prior to suturing the mucoperiosteal flaps, and a pick-up impression was taken using impression plaster [18]. The fixed screw-retained prostheses delivered 24 hours after surgery were fabricated with a rigid metal framework in order to provide increased strength and rigidity to the prostheses and a composite resin veneering material [2].

The prostheses did not present distal cantilevered extensions.

The drug therapy prescribed was the same as in the delayed loading group. After implant placement, all patients received oral and written recommendations to improve healing: liquid/soft diet for 40 days and hygienic instruments and techniques appropriate to the stage of healing [19].

2.4. Outcomes. Primary outcome measures were as follows:

- (i) number of threads exposed at a torque of 30 and 50 Ncm
- (ii) final insertion torque

Secondary outcome measures were as follows:

- (i) implant and prosthetic failure
- (ii) peri-implant bone resorption calculated using intraoral digital periapical radiographs at the following time points: at implant insertion (T0), at 3, 6, and 12 months of healing. Radiographs were obtained with a parallel long-cone technique. The implant-abutment interface was used as the reference point for bone level measurements. Interproximal bone levels were assessed from these reference points to the most coronal bone levels at the mesial and distal surfaces of each implant. Digital software (OrisWin DG, FONADental, Assago, Italy) was used to perform measurements. The software was calibrated for every image using the implant diameter as a reference. Two of the authors (FB and IC) performed all MBL measurements on the mesial and distal surfaces of each implant after a calibration exercise demonstrating 95.9% concordance within ± 0.5 mm for

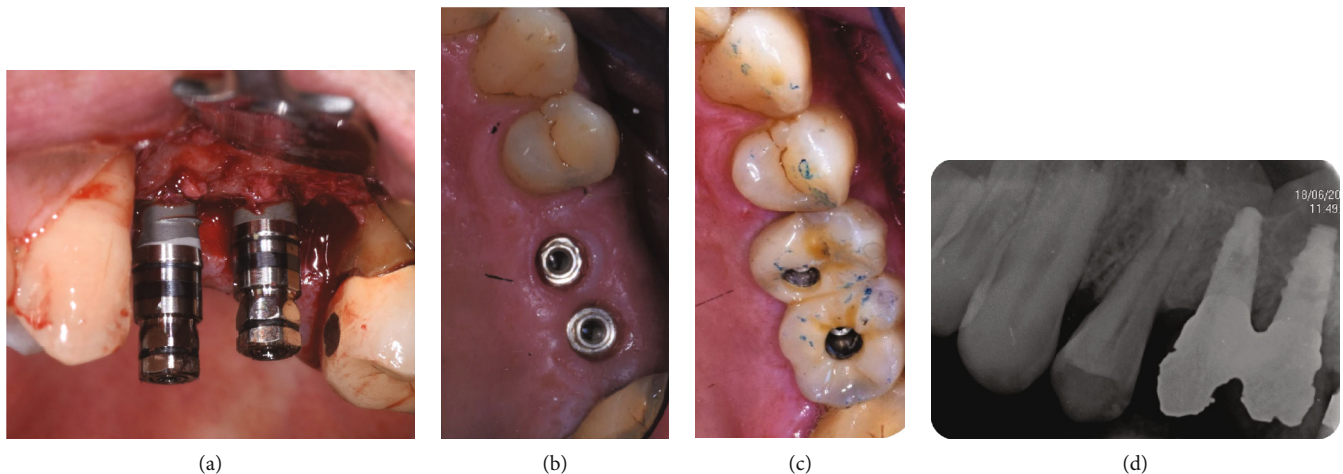


FIGURE 2: Clinical pictures of one of the patients included in the present research (DEL group): (a) clinical image of insertion of the 2 implants at 30 Ncm (T0); (b) healing phase (3 months after implant insertion); (c) delivery of the fixed prosthesis (14 weeks after implant insertion); (d) radiographic image (1 year after implant insertion).

measurements. The examiners were not blinded because the different implant thread morphologies were visible on the radiograph; measurement differences were discussed among examiners until an agreement was found

- (iii) periodontal parameters: bleeding on probing (BoP), suppuration, plaque index (PI), and probing depth (PD) evaluated at 3, 6, and 12 months of healing. BoP was defined as the presence of bleeding (yes/no) evaluated at four points for each implant (mesial, distal, buccal, and lingual) using a nonmetallic probe. PI was defined as the presence of plaque (yes/no) on four points using an erythrosine gel. Therefore, for PI and BoP, values from 0 to 4 were recorded for each implant site. PD was assessed at four points for each implant

2.5. Statistical Methods. The descriptive statistical analysis included age, gender, loading type, implant position, implant length, bone quality, and implant type (SY or SL). Moreover, peri-implant health parameters such as BOP, PD, PI, suppuration, and bone resorption were analyzed. The main outcomes of the study, i.e., the insertion strength (expressed in Ncm) and the implant exposition at a torque of 30 and 50 Ncm (expressed in a number of threads), were considered. The nonparametric Mann-Whitney test was performed to analyze all evaluated criteria among the groups at each time point. The Kruskal-Wallis test was applied too. ANOVA was used to assess intergroup variability. Linear mixed models were used to investigate differences over time. A significance level of 5% was adopted in all tests, and SPSS IBM (version 25) was used.

3. Results

Fourteen patients (8 males and 6 females, mean age: 61.7 years) fulfilled the inclusion criteria and were enrolled in

the present research. All the patients attended the follow-up appointments and were followed-up for at least 12 months.

Five patients were rehabilitated in the IL group, while 9 in the DEL group. Baseline characteristics are reported in Table 1.

Twenty implants (10 SL and 10 SY) were inserted in the IL group, while 18 (9 SL and 9 SY) were inserted in the DEL group. In the IL group, two patients rehabilitated the inferior arch and three the upper arch. In the DEL group, 5 patients rehabilitated the upper arch and 4 the lower arch.

The chi-square approximation of the Kruskal-Wallis test did not find significant differences in torque insertion between bone sites with different bone qualities ($p = .559$). An analysis between classes was carried on, and no value was statistically different (Table 2).

Torque insertion data are reported in Table 3. Parametric and nonparametric tests showed a not significant difference between SYRA and SYRA SL in the number of visible threads when inserting the implant with an insertion torque of 30 Ncm (T student test: $p = .142$; U test: $p = .164$). At 50 Ncm, all the implants had reached their final position in the implant site and no threads were visible in either of the groups.

Parametric and nonparametric tests showed a relevant but not significant difference between SYRA and SYRA SL in final torque insertion values (T student test: $p = .055$; U test: $p = .063$).

No prosthetic nor implant failures occurred during the follow-up period, and no technical nor biological complications were encountered. Mean peri-implant health parameters are reported in Table 4.

As a consequence, it can be stated that the null hypothesis has not been rejected. In fact, no significant differences were found between SL and SY implants.

Linear mixed model (interaction time * loading protocol) was used to investigate the difference in bone resorption over time between DEL and IL. The relationship was significantly different ($p = .040$). DEL showed higher values of bone resorption over time compared to IL (Figure 3).

TABLE 1: Main demographic data.

	Mean	SD	% (cases/tot)
Age (years)	61.7 (range: 48-72)	8.0	
Gender (M)			57 (8/14)
Loading (DEL)			64 (9/14)
Bone quality			D1: 18 (7/38)
			D2: 40 (15/38)
			D3: 42 (16/38)
			D4: 0
Implants			Syra: 50 (19/38)
			Syra SL: 50 (19/38)

TABLE 2: Correlation between insertion torque and bone quality.

	Final insertion torque (Ncm)			<i>p</i>
	Mean	SD	<i>N</i>	
Bone quality 1	48.57	3.78	7	<i>p</i> = .286
vs. bone quality 2	45.67	8.63	15	
Bone quality 3	45.00	8.76	16	<i>p</i> = .833
vs. bone quality 2	45.67	8.63	15	
Bone quality 3	45.00	8.76	16	<i>p</i> = .316
vs. bone quality 1	48.57	3.78	7	

4. Discussion

The results of the present research identified a difference, even if not statistically significant, of torque insertion values between the two implant morphologies. Applying an insertion torque of 30 Ncm, SL implants presented a greater number of exposed threads compared to SY implants, and the final insertion torque was higher for SL implants (48.42 vs. 43.42 Ncm). This indicates that with the same bone quality and the same bone site preparation, implant insertion is easier when using a reduced thread depth while implants with a larger thread diameter need higher insertion torque values and thus reach greater primary stability. This might be due to their increased surface area.

Periodontal parameters were similar for the two implants, and no cases of peri-implantitis or mucositis were noted [20, 21]; no differences in bone resorption were found among the two implants; however, it is interesting to note a significant correlation between bone resorption and loading protocol, with greater bone resorption in the DEL group. At 12 months of postimplant insertion, our analysis reported mean bone resorption of 1.909 mm in the DEL group and 1.440 mm in the IL group. However, it must be considered that only 5 patients were included in the IL group. Moreover, loading time was not the unique difference between DEL and IL groups. The two groups also differed in implant length (longer implants in the immediate loading rehabilitation) and in the type of rehabilitation (partial vs. full-arch prostheses). In addition, in the DEL group, bone resorption around one of the implants might have influenced bone level next to the adjacent implant.

The SY and SL implants used in the present research have a conical shape and, as concerns SL implant, an aggressive design of the threads: this macrostructure has the aim of improving primary stability. The divergent shape of SY and SL implant collar has the purpose of further increasing primary stability while impacting cortical bone. This is in contrast with modern implants with convergent collars aimed at providing greater space for peri-implant tissue in the transmucosal area, in order to favour soft tissue thickness and aesthetic [22].

Primary stability is one of the main factors to be sought in implant insertion in order to favour osseointegration in both single and full-arch rehabilitations. An ideal implant design should provide a balance between compressive and tensile forces while minimizing shear force generation [23, 24].

As reported by McCullough and Klokkevold, implant macrogeometry plays a fundamental role: variations in implant length, diameter, number of threads, thread depth, pitch, and helix angle may strongly influence primary stability [25]. The threads of the implants seem to have a huge relevance in the obtainment of implant osseointegration improving initial stability, maximizing BIC, and favouring stress distribution at the bone-implant interface.

In a FEM study, Huang et al. showed that implant thread morphology is important both during the insertion of the implant to allow its sliding into the implant site and to reduce the stress of peri-implant bone, increasing implant stability and long-term survival [26].

Similar results were provided by Lee et al. [15] showing that implants with greater thread depth provide higher primary stability, especially in low-quality bone. The use of implants with a greater depth of the threads seems also to induce an increased condensation of peri-implant bone. This is in accordance with the results of the present research reporting a greater insertion torque when using SL implants.

In a study by Makary et al., it is reported that the use of large-thread implants turns out to be an advantage only in implant rehabilitations with bone type D3 and D4, while in D1, it appeared to be a disadvantage because of the necessity of an excessive surgical preparation to which bone should be subjected [27].

However, it is difficult to understand what the ideal depth of the threads should be in function of bone density to ensure high primary stability and a better distribution of the stresses into the peri-implant bone.

Ao et al. in a FEM analysis evaluated the behaviour of implants with a depth of threads ranging from 0.2 to 0.6 mm. The study showed that larger threads tend to have a better distribution of peri-implant stress than the narrower ones. The threads with a depth greater than 0.44 mm showed a better biomechanical behaviour, reaching the best results with a depth between 0.34 and 0.5 mm [28].

It is important to note that not only the depth but also the shape of the threads can influence the primary stability of the implant and peri-implant bone resorption. Several studies have shown that immediately after implant placement, occlusal loads are mainly concentrated at the bone next to the first thread, indicating that the implant width and the wires can create a reduction of loads [14, 15].

TABLE 3: Insertion torque outcomes. The number of exposed threads at 30 and 50 Ncm and the final insertion torque are reported.

	Total		SYRA		SYRA SL	
	Mean	SD	Mean	SD	Mean	SD
30 Ncm (n. visible threads)	1.11	0.66	0.95	0.74	1.26	0.54
50 Ncm (n. visible threads)	0.00	0.00	0.00	0.00	0.00	0.00
Final torque (Ncm)	45.92	7.96	43.42	10.01	48.42	4.10

TABLE 4: Peri-implant health parameters.

Mean (SD)	3 months		6 months		12 months	
	SYRA	SYRA SL	SYRA	SYRA SL	SYRA	SYRA SL
BOP	0.16 (0.38)	0.05 (0.23)	0.32 (0.48)	0.26 (0.45)	0.37 (0.50)	0.58 (0.77)
PD (mm)	1.11 (0.74)	0.95 (0.78)	1.45 (0.57)	1.40 (0.56)	2.01 (0.62)	1.73 (0.79)
PI	0.37 (0.60)	0.32 (0.58)	0.61 (0.64)	0.61 (0.64)	0.74 (0.99)	0.68 (1.00)
Bone resorption (mm)	0.86 (0.78)	0.88 (0.83)	1.17 (0.91)	1.18 (0.92)	1.61 (0.76)	1.72 (1.16)

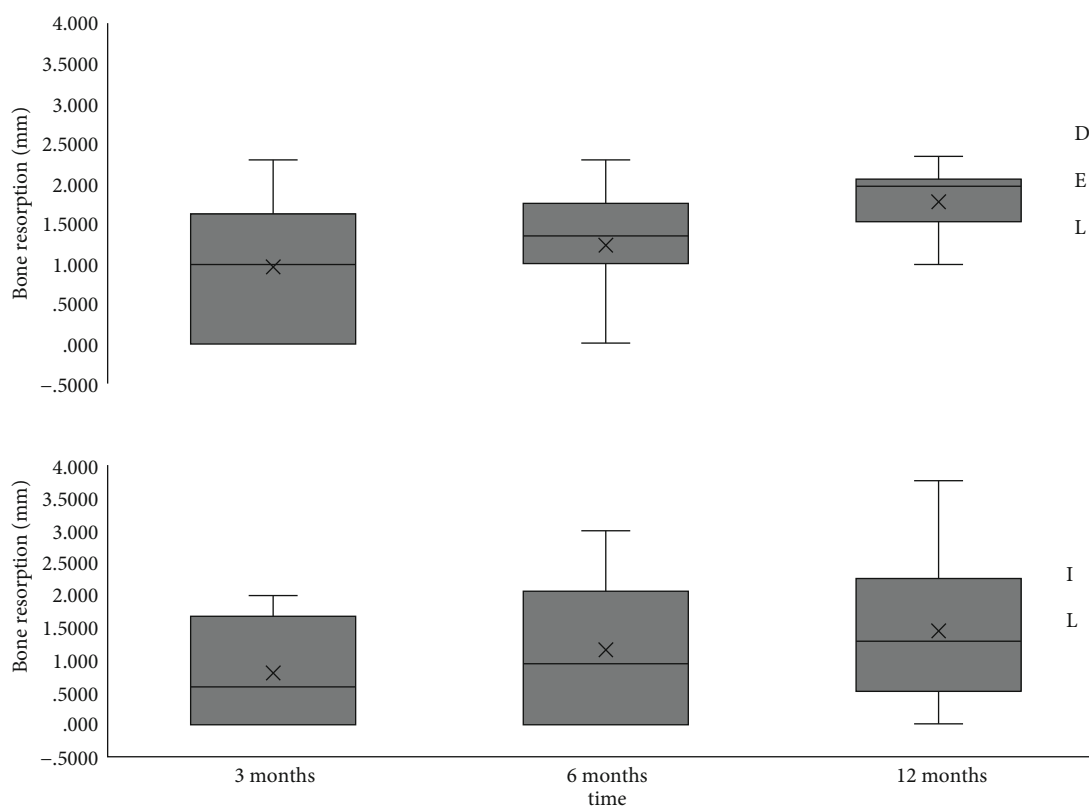


FIGURE 3: Bone resorption trend over time grouping for DEL and IL rehabilitations. Mean value (X), median value (line in the box), inter 2nd and 3rd quartile range (box), and max and min values (whiskers).

Some studies have analyzed how a different morphology of the threads can determine a different distribution of the loads into peri-implant bone. A more squared shape of the threads allows to increase the BIC and to dissipate loads on a greater bone surface, allowing a better distribution especially of the lateral forces. A V-shape of the threads in the most apical part of the implant determines a greater aggressiveness of the implant, especially in a poor-quality bone, managing to obtain greater mechanical stability of the

implant and greater resistance to vertical forces [14, 20, 29]. It must be noted that in the present study, SY and SL implants did not differ for thread depth only. In fact, SY implants present a trapezoidal thread shape throughout their entire length, while SL implant threads show a trapezoidal shape in the coronal portion and a more aggressive triangular shape in the apical part.

Our research failed to find a difference in bone resorption between SY and SL implants. However, SL implants

presented greater primary stability, and this may help in reaching good stability in poor quality bone. This is particularly important in immediate loading rehabilitations.

In the present research, the drilling protocol varied according to bone quality as proposed by the manufacturer's guidelines, and the same identical drilling procedure was applied for SL and SY implants in the same patient. This was done in order to reduce possible bias related to bone quality and to the osteotomy preparation. The degree of underpreparation was standardized on the base of implant dimensions and bone quality. Undersized osteotomies showed a greater remodeling of peri-implant cortical bone during the early healing period compared to nonundersized preparations as demonstrated by Stocchero et al. [30].

Some limits of the present research must be acknowledged: the limited sample size and the primary stability evaluated only on the base of insertion torque values and without resonance frequency analysis can be considered limiting factors [31, 32]. Further research including a greater sample size and a longer follow-up period would be useful to confirm the present outcomes.

5. Conclusions

The outcomes of the present research highlighted that dental implants with an increased depth of the threads presented higher insertion torque values without a statistically significant difference compared with standard threads. No differences in bone resorption over time were noted among the two implant morphologies. Deeper threads might be useful in implant sites with low bone quality and in immediate loading rehabilitations when the obtainment of primary stability is a fundamental prerequisite.

Data Availability

Readers can access the data supporting the conclusions of the study by requesting them to the corresponding authors.

Conflicts of Interest

The authors declare no conflict of interest.

Acknowledgments

The study was partly funded by Sweden and Martina (Due Carrare PD, Italy).

References

- [1] P. A. Fugazzotto, "Success and failure rates of osseointegrated implants in function in regenerated bone for 72 to 133 months," *The International Journal of Oral & Maxillofacial Implants*, vol. 20, pp. 77–83, 2020.
- [2] S. Szmukler-Moncler, H. Salama, Y. Reingewirtz, and J. H. Dubruille, "Timing of loading and effect of micromotion on bone-dental implant interface: review of experimental literature," *Journal of Biomedical Materials Research*, vol. 43, no. 2, pp. 192–203, 1998.
- [3] T. Albrektsson, P.-I. Brånemark, H.-A. Hansson, and J. Lindström, "Osseointegrated titanium implants. Requirements for ensuring a long-lasting, direct bone-to-implant anchorage in man," *Acta Orthopaedica Scandinavica*, vol. 52, no. 2, pp. 155–170, 2009.
- [4] M. Atsumi, S. H. Park, and H. L. Wang, "Methods used to assess implant stability: current status," *The International Journal of Oral & Maxillofacial Implants*, vol. 22, no. 5, pp. 743–754, 2007.
- [5] H. S. Ryu, C. Namgung, J. H. Lee, and Y. J. Lim, "The influence of thread geometry on implant osseointegration under immediate loading: a literature review," *The Journal of Advanced Prosthodontics*, vol. 6, no. 6, pp. 547–554, 2014.
- [6] P. Pesce, M. Menini, G. Tommasato, R. Patini, and L. Canullo, "Influence of modified titanium abutment surface on peri-implant soft tissue behaviour: a systematic review of histological findings," *International Journal of Oral Implantology*, vol. 12, no. 4, pp. 419–429, 2019.
- [7] L. Canullo, Y. Omori, Y. Amari, G. Iannello, and P. Pesce, "Five-year cohort prospective study on single implants in the esthetic area restored using one-abutment/one-time prosthetic approach," *Clinical Implant Dentistry and Related Research*, vol. 20, no. 5, pp. 668–673, 2018.
- [8] L. Canullo, P. Pesce, M. Tronchi, J. Fiorellini, Y. Amari, and D. Penarrocha, "Marginal soft tissue stability around conical abutments inserted with the one abutment-one time protocol after 5 years of prosthetic loading," *Clinical Implant Dentistry and Related Research*, vol. 20, no. 6, pp. 976–982, 2018.
- [9] L. Canullo, G. R. Fedele, G. Iannello, and S. Jepsen, "Platform switching and marginal bone-level alterations: the results of a randomized-controlled trial," *Clinical Oral Implants Research*, vol. 21, no. 1, pp. 115–121, 2010.
- [10] T. Tealdo, M. Menini, M. Bevilacqua et al., "Immediate versus delayed loading of dental implants in edentulous patients' maxillae: a 6-year prospective study," *The International Journal of Prosthodontics*, vol. 27, no. 3, pp. 207–214, 2014.
- [11] M. Menini, P. Pesce, M. Bevilacqua et al., "Effect of framework in an implant-supported full-arch fixed prosthesis: 3D finite element analysis," *The International Journal of Prosthodontics*, vol. 28, no. 6, pp. 627–630, 2015.
- [12] P. Pesce, F. Pera, D. Bruno, and M. Menini, "Survival rate and bone resorption in immediate loading of atrophic maxillary arches using normal and long implants: a pilot observational study," *The International Journal of Prosthodontics*, vol. 31, no. 6, pp. 580–583, 2018.
- [13] P. Pera, M. Menini, P. Pesce, M. Bevilacqua, F. Pera, and T. Tealdo, "Immediate versus delayed loading of dental implants supporting fixed full-arch maxillary prostheses: a 10-year follow-up report," *The International Journal of Prosthodontics*, vol. 32, no. 1, pp. 27–31, 2019.
- [14] H. Abuhussein, G. Pagni, A. Rebaudi, and H.-L. Wang, "The effect of thread pattern upon implant osseointegration," *Clinical Oral Implants Research*, vol. 21, no. 2, pp. 129–136, 2010.
- [15] S. Y. Lee, S. J. Kim, H. W. An et al., "The effect of the thread depth on the mechanical properties of the dental implant," *The Journal of Advanced Prosthodontics*, vol. 7, no. 2, pp. 115–121, 2015.
- [16] C. Makary, A. Rebaudi, G. Sammartino, and N. Naaman, "Implant primary stability determined by resonance frequency analysis: correlation with insertion torque, histologic bone volume, and torsional stability at 6 weeks," *Implant Dentistry*, vol. 21, no. 6, pp. 474–480, 2012.

- [17] C. E. Misch, "Density of bone: effect on treatment plans, surgical approach, healing, and progressive boen loading," *The International Journal of Oral Implantology*, vol. 6, no. 2, pp. 23–31, 1990.
- [18] M. Menini, P. Setti, F. Pera, P. Pera, and P. Pesce, "Accuracy of multi-unit implant impression: traditional techniques versus a digital procedure," *Clinical Oral Investigations*, vol. 22, no. 3, pp. 1253–1262, 2018.
- [19] M. Menini, E. Dellepiane, P. Pesce et al., "Hygienic and dietetic guidelines for implant-supported full-arch immediate loading prostheses," *International Journal of Oral and Dental Health*, vol. 1, pp. 1–5, 2015.
- [20] P. Pesce, M. Menini, T. Tealdo, M. Bevilacqua, F. Pera, and P. Pera, "Peri-implantitis: a systematic review of recently published papers," *The International Journal of Prosthodontics*, vol. 27, no. 1, pp. 15–25, 2014.
- [21] P. Pesce, L. Canullo, M. G. Grusovin, H. de Bruyn, J. Cosyn, and P. Pera, "Systematic review of some prosthetic risk factors for periimplantitis," *The Journal of Prosthetic Dentistry*, vol. 114, no. 3, pp. 346–350, 2015.
- [22] L. Canullo, M. Menini, U. Covani, and P. Pesce, "Clinical outcomes of using a prosthetic protocol to rehabilitate tissue-level implants with a convergent collar in the esthetic zone: a 3-year prospective study," *The Journal of Prosthetic Dentistry*, vol. 123, no. 2, pp. 246–251, 2020.
- [23] C. E. Misch, T. Strong, and M. W. Bidez, "Scientific rationale for dental implant design," in *Contemporary Implant Dentistry*, C. E. Misch, Ed., pp. 200–229, Mosby, St. Louis, 3rd edition, 2008.
- [24] T. H. Lan, J. K. Du, C. Y. Pan, H. E. Lee, and W. H. Chung, "Biomechanical analysis of alveolar bone stress around implants with different thread designs and pitches in the mandibular molar area," *Clinical Oral Investigations*, vol. 16, no. 2, pp. 363–369, 2012.
- [25] J. J. McCullough and P. R. Klokkevold, "The effect of implant macro-thread design on implant stability in the early post-operative period: a randomized, controlled pilot study," *Clinical Oral Implants Research*, vol. 28, no. 10, pp. 1218–1226, 2017.
- [26] H.-L. Huang, J.-T. Hsu, L.-J. Fuh, M.-G. Tu, C.-C. Ko, and Y.-W. Shen, "Bone stress and interfacial sliding analysis of implant designs on an immediately loaded maxillary implant: a non-linear finite element study," *Journal of Dentistry*, vol. 36, no. 6, pp. 409–417, 2008.
- [27] C. Makary, A. Menhall, C. Zammarie et al., "Primary stability optimization by using fixtures with different thread depth according to bone density: a clinical prospective study on early loaded implants," *Materials*, vol. 12, no. 15, p. 2398, 2019.
- [28] J. Ao, T. Li, Y. Liu et al., "Optimal design of thread height and width on an immediately loaded cylinder implant: a finite element analysis," *Computers in Biology and Medicine*, vol. 40, no. 8, pp. 681–686, 2010.
- [29] S. Hansson and M. Werke, "The implant thread as a retention element in cortical bone: the effect of thread size and thread profile: a finite element study," *Journal of Biomechanics*, vol. 36, no. 9, pp. 1247–1258, 2003.
- [30] M. Stocchero, M. Toia, Y. Jinno et al., "Influence of different drilling preparation on cortical bone: a biomechanical, histological, and micro-CT study on sheep," *Clinical Oral Implants Research*, vol. 29, no. 7, pp. 707–715, 2018.
- [31] E. Corvino, P. Pesce, F. Camodeca, O. Moses, G. Iannello, and L. Canullo, "Clinical and radiological outcomes of implants with two different connection configurations, a RCT," *International Journal of Oral Implantology*, 2020.
- [32] D. Baldi, T. Lombardi, J. Colombo et al., "Correlation between insertion torque and implant stability quotient in tapered implants with knife-edge thread design," *BioMed Research International*, vol. 2018, Article ID 7201093, 7 pages, 2018.

Research Article

Impact of Matching Point Selections on Image Registration Accuracy between Optical Scan and Computed Tomography

Hai Yen Mai ¹ and Du-Hyeong Lee ^{1,2}

¹Department of Prosthodontics, School of Dentistry, Kyungpook National University, 2177 Dalgubeoldae-ro, Jung-Gu, Daegu 41940, Republic of Korea

²Institute for Translational Research in Dentistry, Kyungpook National University, Daegu 41940, Republic of Korea

Correspondence should be addressed to Du-Hyeong Lee; dewylee@knu.ac.kr

Received 17 June 2020; Accepted 21 July 2020; Published 5 August 2020

Guest Editor: Henriette Lerner

Copyright © 2020 Hai Yen Mai and Du-Hyeong Lee. This is an open access article distributed under the Creative Commons Attribution License, which permits unrestricted use, distribution, and reproduction in any medium, provided the original work is properly cited.

The point-based surface registration method involves the manual selection process of paired matching points on the data of computed tomography and optical scan. The purpose of this study was to investigate the impact of selection error and distribution of fiducial points on the accuracy of image matching between 3-dimensional (3D) images in dental planning software programs. Computed tomography and optical scan images of a partial edentulous dental arch were obtained. Image registration of the optical scan image to computed tomography was performed using the point-based surface registration method in planning software programs under different conditions of 3 fiducial points: point selection error (0, 1, or 2 mm), point distribution (unilateral, bilateral), and planning software (Implant Studio, Blue Bio Plan) ($n = 5$ per condition, $N = 60$). The accuracy of image registration at each condition was evaluated by measuring linear discrepancies between matched images at X , Y , and Z axes. Kruskal-Wallis test, Mann-Whitney U test with Bonferroni correction, and 3-way analysis of variance were used to statistically analyse the measurement data ($\alpha = 0.05$). No statistically significant difference was exhibited between the 0 and 1 mm point mismatch conditions in either unilateral or bilateral point distributions. The discrepancy values in the 2 mm mismatch condition were significantly different from the other mismatch conditions, especially in the unilateral point distribution ($P < 0.05$). Strong interactions among point selection error, distribution, and software programs on the image registration were found ($P < 0.001$). Minor matching point selection error did not influence the accuracy of point-based automatic image registration in the software programs. When the fiducial points are distributed unilaterally with large point selection error, the image matching accuracy could be decreased.

1. Introduction

Three-dimensional (3D) imaging technologies have enhanced the diagnostic modalities and treatment planning for implant, maxillofacial surgery, and orthodontic fields [1, 2]. Cone-beam computed tomography (CBCT) is representative, and the 3D image data that it produces are commonly used to evaluate the underlying bone and identifying critical anatomical structures, such as the inferior alveolar nerve, the maxillary sinus, and the roots of neighbouring teeth [3]. Slices of CBCT radiographic images can be reconstructed into a 3D image model [4], but the resolution of the 3D image is limited because of the voxel size of raw radiographic data

available in CBCT devices [5, 6]. Thus, to make a 3D model with soft and hard tissue, image merging with optical scan data of the oral cavity surface is recommended [7, 8].

Image registration is the process of matching the optical scan image to the 3D-reconstructed CBCT image [9, 10]. Accurate image registration is essential to replicate the exact relationship of underlying bone and oral cavity surface data [11, 12]. Errors in the image alignment in this step could cause unexpected surgical complications because of discrepancies between the planning in the virtual model and the actual results at the surgical site [13]. Contemporary image registration techniques for 3D data are divided into voxel-based and surface-based method [14]. The voxel based-

registration utilizes the grey-scale difference of the voxels to align the images, achieving the least difference in the total grey-scale density [14]. Because the voxel-based registration uses the image intensity in the entire volume, the presence of image artifacts caused by metallic prostheses in the radiographic data could deteriorate precise image matching by masking the fiducial anatomic structures [5]. Meanwhile, the surface-based registration uses the geometric shape of 3D object surfaces to match images [15]. The computer algorithm of iterative closest points (ICPs) locates optimal positions of pair images by computing the 3D coordinates of image surface point clouds [14]. The accuracy of image superimposition by graphic processing has been validated [16], and currently, point-based surface matching is widely used in the dental planning and inspection computer software programs for the enhancement of efficiency and accuracy of matching [9].

When performing the point-based surface registration, the congruent areas between the 3D reconstructed radiographic image and optical scan image are designated in pair [17]. In the dentate jaws, because the tooth is discernible in both images, the outline of the tooth is generally used as the fiducial area of image superimposition [17]. Three pair points have been used for image matching [18], and wide distribution of points in the arch is recommended [19]. It was also suggested to choose the matching points close to the edentulous area [19, 20]. Although several protocols for image registration have been suggested, the paired points could be selected differently because this process basically depends on the operator's visual observations. Human error in selecting matching points could affect the accuracy of subsequent automatic image matching processes. The recommended positions of the matching points also have not been clarified. The purpose of this study was to assess the impact of selection error and distribution of fiducial points on the accuracy of image matching between 3D radiographic and optical scan images in planning software programs. The proposed null hypothesis was that the mismatch in paired fiducial points, and the different distribution of points would not influence the accuracy of image registration of the 3D optical scan image to the reconstructed radiographic data.

2. Materials and Methods

The workflow of this study is described in Figure 1. A patient missing the second premolar and first molar on the maxilla was selected for this study. The patient had no severe defect or metal restorations in the remaining teeth on the arch. Computed tomographic images of the patient were obtained by using a CBCT scanner (Pax-i3D Smart, Vatech, Hwaseong, Korea) with 80 kVp, 8 mA, 24 s pulsed scan, field of view of 100×80 mm, and slice thickness of 0.2 mm. An optical scan image of the oral cavity surface was obtained by digitizing the stone model using a lab-based scanner (IDC S1, Amann Girrbach, Koblach, Austria). The stone model was fabricated using the conventional silicone impression and stone pouring technique. The scan file was transferred to a reverse engineering software program (Geomagic Design X, 3D Systems, Rock Hill, SC, USA) where indexing markers

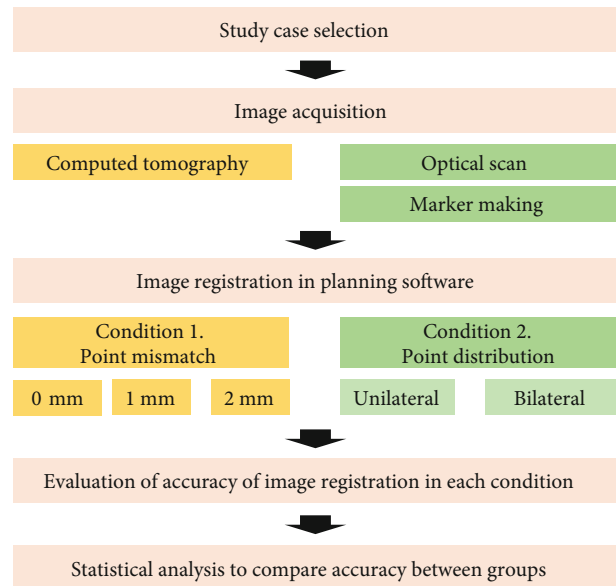


FIGURE 1: Workflow of this study.

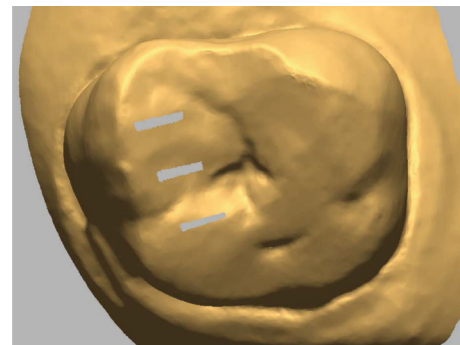


FIGURE 2: Indexing markers at intervals of 1 mm to guide the operator in placing matching points at different levels of error selection.

for indicating matching points were made on the occlusal surface of teeth by deleting the surface of the image in the strip shape at 1 mm intervals (Figure 2). Consequently, the radiographic and optical-scan data were delivered to planning computer software programs, Implant Studio (3Shape, Copenhagen, Denmark) and Blue Sky Plan (Blue Sky Bio, LLC, Grayslake, IL, USA), for merging the images.

The experimental factors of this study were selection error in pair points and the distribution of fiducial points in the image registration process. The selection error was set at 3 levels (0, 1, and 2 mm; Figure 3), and the distribution of points was set at 2 levels (unilateral and bilateral; Figure 4). In all matching conditions, 3 matching points were used in pairs in both radiographic and optical-scan images, and the positions of points were designated in reference to the indexing markers to provide the standardized error in point selection [17, 20]. The central incisor, first premolar, and second premolars were used for the image matching in the unilateral and bilateral distribution conditions. After the point designation in each condition, the point-based best-fit algorithm was run in the software programs. All image

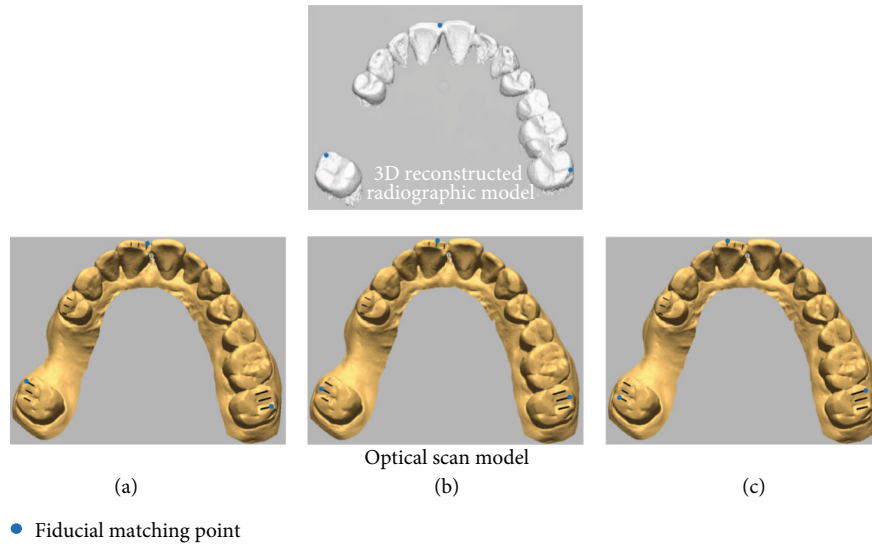


FIGURE 3: Mismatch conditioning of paired matching points between radiographic and optical scan images: (a) no mismatch, (b) 1 mm mismatch, and (c) 2 mm mismatch.

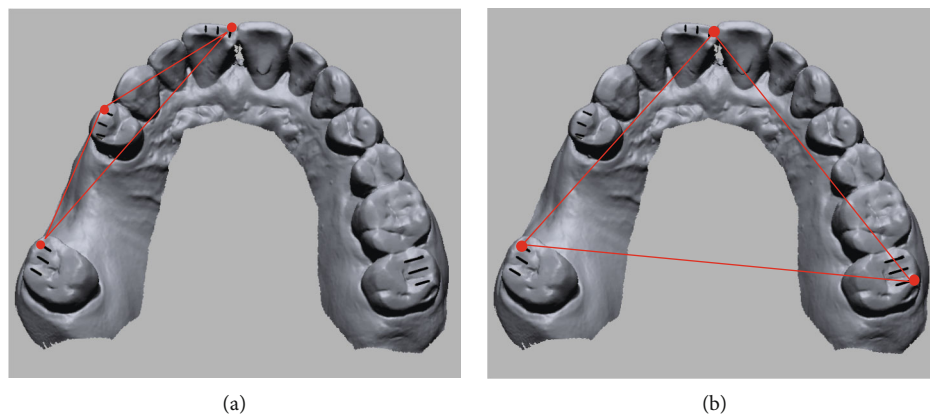


FIGURE 4: Conditioning of distribution of matching points: (a) unilateral and (b) bilateral.

registrations were carried out 5 times in each condition by a single operator who had experience in image registration and was blinded to the purpose of this study.

The resulting accuracy of each condition’s image registration was evaluated by measuring the positional discrepancy between the radiographic and optical-scan images in the X-, Y-, and Z-axes (Figure 5). The assessments were performed in the cross-sectional images of central incisor and second molar areas using the measurement function of the planning software programs. A single investigator carried out all the measurements to avoid errors that can arise when using different examiners.

The mean and standard deviation of linear discrepancies in each condition were calculated by averaging the measurement values collected in the anterior and posterior areas. Kruskal-Wallis test and a post hoc Mann-Whitney *U* test with Bonferroni correction were used to compare the accuracy of image registration between groups. Three-way analysis of variance (ANOVA) was used to investigate how interactions between factors, such as the point selection

error, point distribution, and planning software, affected image registration accuracy. All statistical analyses were performed by using the Statistical Package for the Social Sciences (SPSS) software program (SPSS version 25.0; IBM Inc., Armonk, NY, USA) with the statistical significance level of 0.05.

3. Results

The linear discrepancy between the radiographic and optical-scan images after the image registration process at different matching conditions is shown in Table 1. In general, no statistically significant difference was found between the 0 and 1 mm point mismatch conditions; however, the discrepancy values in the 2 mm mismatch condition were significantly different from the other mismatch conditions. In particular, when the 2 mm point mismatch condition was applied in the unilateral point distribution in the Blue Sky Plan software, markedly high discrepancy was observed (9.92 mm in

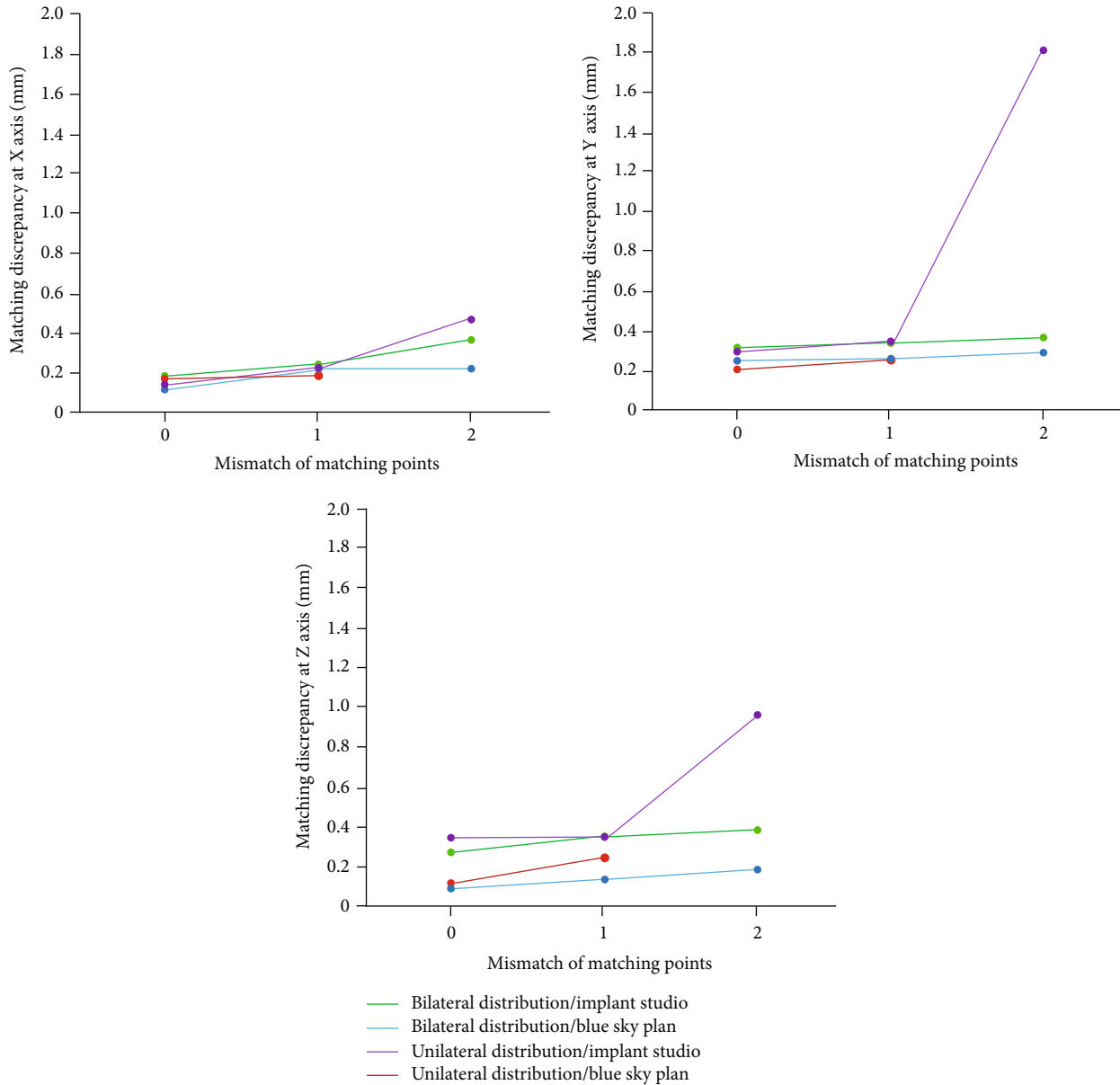


FIGURE 5: Line graphs showing the effect of the mismatch of matching points on the accuracy of image registration in different point distribution and software programs at X-, Y-, and Z-axes.

the X-axis, 2.52 mm in the Y-axis, and 4.19 mm in the Z-axis).

The pattern of point distribution did not make a statistically significant difference in the matching discrepancy in the 0 and 1 mm point mismatch conditions, but it did make significant differences in the 2 mm mismatch condition in both planning software programs.

Three-way ANOVA results showed that each factor has strong interactions with different factors, which affects the outcome of image matching, as shown in Table 2 ($P < 0.001$; adjusted $R^2 = 0.958$).

4. Discussion

The purpose of this study was to elucidate the impact of the matching point selection process on the accuracy of optical

scan image registration to radiographic images for image merging. Variations in the process of manual point designation were designed by controlling the factors, such as the disagreement in paired points and the distribution of points. The overall results of this study showed that minor errors in matching point selection did not influence the accuracy of image registration regardless of whether the distribution pattern was unilateral or bilateral. However, the discrepancy was significantly different when there was large point mismatch. Thus, the null hypothesis that the mismatch in paired fiducial points and the different distribution of points would not influence the accuracy of image registration was rejected.

The image matching method used in the study was point-based surface registration. Polygonal 3D mesh images were aligned with each other in the closest position using the best-fit algorithm based on the fiducial points designated by

TABLE 1: Mean and standard deviation of linear discrepancy of image matching at each condition (mm).

Coordinate	Distribution	Implant studio Point mismatch			<i>P</i>	Blue Sky Plan Point mismatch			<i>P</i>
		0	1	2		0	1	2	
X	Bilateral	0.20 ± 0.03 ^a	0.22 ± 0.02 ^{ab}	0.24 ± 0.03 ^b	0.101	0.12 ± 0.07 ^a	0.21 ± 0.08 ^{ab}	0.21 ± 0.11 ^b	0.055
	Unilateral	0.18 ± 0.02 ^a	0.21 ± 0.02 ^a	0.46 ± 0.14 ^b	<0.001	0.18 ± 0.06 ^a	0.19 ± 0.04 ^a	9.92 ± 4.43 ^b	<0.001
	<i>P</i>	0.205	.141	.006		0.096	.543	<0.001	
Y	Bilateral	0.31 ± 0.05	0.33 ± 0.07	0.37 ± 0.13	0.258	0.24 ± 0.17	0.25 ± 0.18	0.27 ± 0.32	0.901
	Unilateral	0.29 ± 0.08 ^a	0.34 ± 0.10 ^a	1.79 ± 0.21 ^b	<0.001	0.20 ± 0.19 ^a	0.24 ± 0.20 ^a	2.52 ± 1.43 ^b	<0.001
	<i>P</i>	0.951	0.651	<0.001		0.936	0.689	<0.001	
Z	Bilateral	0.30 ± 0.04 ^a	0.35 ± 0.02 ^b	0.39 ± 0.03 ^b	<0.001	0.11 ± 0.02 ^a	0.14 ± 0.04 ^b	0.19 ± 0.01 ^c	<0.001
	Unilateral	0.34 ± 0.04 ^a	0.35 ± 0.02 ^a	0.96 ± 0.47 ^b	0.002	0.12 ± 0.02 ^a	0.22 ± 0.03 ^a	4.19 ± 2.54 ^b	<0.001
	<i>P</i>	0.067	0.576	0.036		0.090	0.052	<0.001	

Values with the same letter are not statistically different based on Kruskal-Wallis test at $P < 0.05$.

TABLE 2: Variations between different affecting factors and interactions in the accuracy of image registration by 3-way analysis of variance.

Source	Type III sum of squares	d.f.	Mean square	<i>F</i>	<i>P</i>
Corrected model	1142.827	11	103.893	370.319	<0.001
Intercept	209.693	1	209.693	747.433	<0.001
Distribution	123.936	1	123.936	441.758	<0.001
Software	76.649	1	76.649	273.210	<0.001
Mismatch	257.151	2	128.576	458.297	<0.001
Mismatch × distribution	241.687	2	120.844	430.737	<0.001
Mismatch × software	174.877	2	87.439	311.668	<0.001
Distribution × software	90.653	1	90.653	323.124	<0.001
Mismatch × distribution × software	177.873	2	88.937	317.007	<0.001
Error	47.133	168	0.281		
Total	1399.652	180			
Corrected Total	1189.959	179			

Adjusted $R^2 = 0.958$.

the operator [21]. The results of this study showed that minor errors in the point selection did not affect the quality of image superimposition of paired images. This accurate matching algorithm not only reduces the influence of iatrogenic mistakes in the image superimposition for treatment planning but also can be used for result analyses and research purposes in various medical fields [22, 23]. Because the matching method is based on mathematical calculations, it is assumed that there is no matching error when the matching is performed in ideal conditions. However, in the present study, there was some discrepancy when there was no point selection error. This phenomenon might be due to the differences in forms of 3D restructured radiographic and optical scan images. Shape deformation has been reported in the conversion process from radiographic raw data to 3D mesh image because of the partial volume effect [24–26]. The optical scan model could also have dimensional errors depending on scanner performance and scanning strategy [27, 28]. Thus, operators should be aware of the errors that inevitably occur because of the morphological differences between matched

images, and they should focus on minimizing additional operator errors caused by inappropriate manual works.

In this study, point-based surface registration was performed in planning software programs that are widely used in guided implant surgery [9]. The general results were similar in the 2 software programs. However, the matching results were different in unilateral point distribution with 2 mm selection error. In the Implant Studio, the optical scan image was approximately located near the corresponding radiographic image, but in the Blue Sky Plan, the image matching failed completely. The malfunctioning of the best-fit algorithm might be due to the fact that the level of point mismatch in a certain point distribution was beyond the condition that is needed for the automatic image matching to operate normally. Based on the findings of the present study, it seems that the maximum allowance limit that enables normal operation of best-fit image matching might be different according to different computer software programs. Scherer [23] reported that the accuracy of outcomes could vary depending on the software programs used. Further studies

on the capability of image matching in different commercial software programs are needed.

The conventional procedures of silicone impression taking and gypsum cast fabrication in this study could be sources of error in replicating the morphology of the oral cavity because of the physical and chemical characteristics of the materials [29]. Intraoral optical scanning can be considered to directly obtain image data from the oral cavity, eliminating the drawbacks of analog methods [30]. A partially edentulous dental arch case was chosen for this study. Considering the clinical variability in the size of dental arches, positions and spans of the edentulous area, and tooth morphology, various clinical cases should be included in future studies to generalize the results of the present study. Cases with metallic restorations also need to be included to investigate the effects of metal artifact images on the accuracy of image registration. The proficiency of the operator in the image matching could be another influencing factor. The operator factor was controlled in the present study by recruiting operators who had the same amount of experience in using planning computer software. Clinically, given that operator's experience varies, it will be necessary to examine the relationship between experience and point selection error in related future studies.

5. Conclusions

Within the limitations of this study, the following conclusions were drawn:

- (1) A matching point selection error of 1 mm did not affect the accuracy of optical scan image registration to radiographic image in either unilateral or bilateral point distributions
- (2) Whether the fiducial points were distributed unilaterally or bilaterally did not affect the accuracy of image registration when there was no or 1 mm point selection error
- (3) The accuracy of image registration was significantly different between software programs when the fiducial points were distributed unilaterally with a 2 mm selection error

Data Availability

The data used to support the findings of this study are included within the article.

Conflicts of Interest

The authors declare that there is no conflict of interest regarding the publication of this paper.

Authors' Contributions

HY Mai contributed to the conceptualization of the study, data curation, formal analysis, investigation, and writing of the manuscript. DH Lee was involved in the methodology,

data curation, supervision, and critical revision of the manuscript. All authors have read and approved the final manuscript.

Acknowledgments

The authors thank Hang-Nga Mai and Yong-Do Choi for obtaining data for this experiment.

References

- [1] G. Orentlicher, D. Goldsmith, and A. Horowitz, "Applications of 3-dimensional virtual computerized tomography technology in oral and maxillofacial surgery: current therapy," *Journal of Oral and Maxillofacial Surgery*, vol. 68, no. 8, pp. 1933–1959, 2010.
- [2] E. Honda, J. L. Prince, and V. R. C. Fontanella, "State-of-the-art digital imaging in dentistry: advanced research of MRI, CT, CBCT, and digital intraoral imaging," *BioMed Research International*, vol. 2018, Article ID 9057120, 2018.
- [3] M. Bornstein, W. Scarfe, V. Vaughn, and R. Jacobs, "Cone beam computed tomography in implant dentistry: a systematic review focusing on guidelines, indications, and radiation dose risks," *International Journal of Oral and Maxillofacial Implants*, vol. 29, Supplement, pp. 55–77, 2014.
- [4] T. Kulczyk, M. Rychlik, D. Lorkiewicz-Muszyńska, M. Abreu-Głowacka, A. Czajka-Jakubowska, and A. Przysańska, "Computed tomography versus optical scanning: a comparison of different methods of 3D data acquisition for tooth replication," *BioMed Research International*, vol. 2019, Article ID 4985121, 7 pages, 2019.
- [5] G. R. J. Swennen, E.-L. Barth, C. Eulzer, and F. Schutyser, "The use of a new 3D splint and double CT scan procedure to obtain an accurate anatomic virtual augmented model of the skull," *International Journal of Oral and Maxillofacial Surgery*, vol. 36, no. 2, pp. 146–152, 2007.
- [6] G. R. J. Swennen, M. Y. Mommaerts, J. Abeloos et al., "The use of a wax bite wafer and a double computed tomography scan procedure to obtain a three-dimensional augmented virtual skull model," *Journal of Craniofacial Surgery*, vol. 18, no. 3, pp. 533–539, 2007.
- [7] T. V. Flügge, K. Nelson, R. Schmelzeisen, and M. C. Metzger, "Three-dimensional plotting and printing of an implant drilling guide: simplifying guided implant surgery," *Journal of Oral and Maxillofacial Surgery*, vol. 71, no. 8, pp. 1340–1346, 2013.
- [8] T. V. Flügge, S. Schlager, K. Nelson, S. Nahles, and M. C. Metzger, "Precision of intraoral digital dental impressions with iTero and extraoral digitization with the iTero and a model scanner," *American Journal of Orthodontics and Dentofacial Orthopedics*, vol. 144, no. 3, pp. 471–478, 2013.
- [9] C. C. Lin, C. Z. Wu, M. S. Huang, C. F. Huang, H. C. Cheng, and D. P. Wang, "Fully digital workflow for planning static guided implant surgery: a prospective accuracy study," *Journal of Clinical Medicine*, vol. 9, no. 4, p. 980, 2020.
- [10] H.-N. Mai, S.-Y. Choi, S.-T. Lee, and D.-H. Lee, "Optimizing accuracy in computer-guided implant surgery with a superimposition- anchor microscrew system: A clinical report," *Journal of Prosthetic Dentistry*, vol. 120, no. 5, pp. 789.e1–789.e5, 2018.
- [11] L. Ritter, S. D. Reiz, D. Rothamel et al., "Registration accuracy of three-dimensional surface and cone beam computed

- tomography data for virtual implant planning,” *Clinical Oral Implants Research*, vol. 23, no. 4, pp. 447–452, 2012.
- [12] D. H. Lee, “Strategic use of microscrews for enhancing the accuracy of computer-guided implant surgery in fully edentulous arches: a case history report,” *International Journal of Prosthodontics*, vol. 31, no. 3, pp. 262–263, 2018.
- [13] M. Vercruyssen, T. Fortin, G. Widmann, R. Jacobs, and M. Quirynen, “Different techniques of static/dynamic guided implant surgery: modalities and indications,” *Periodontology 2000*, vol. 66, no. 1, pp. 214–227, 2014.
- [14] A. Almukhtar, X. Ju, B. Khambay, J. McDonald, and A. Ayoub, “Comparison of the accuracy of voxel based registration and surface based registration for 3D assessment of surgical change following orthognathic surgery,” *PLoS One*, vol. 9, no. 4, p. e93402, 2014.
- [15] F. A. Rangel, T. J. J. Maal, M. J. J. de Koning, E. M. Bronkhorst, S. J. Bergé, and A. M. Kuijpers-Jagtman, “Integration of digital dental casts in cone beam computed tomography scans—a clinical validation study,” *Clinical Oral Investigations*, vol. 22, no. 3, pp. 1215–1222, 2018.
- [16] H. H. Lin, W. C. Chiang, L. J. Lo, S. Sheng-Pin Hsu, C. H. Wang, and S. Y. Wan, “Artifact-resistant superimposition of digital dental models and cone-beam computed tomography images,” *Journal of Oral and Maxillofacial Surgery*, vol. 71, no. 11, pp. 1933–1947, 2013.
- [17] T. Flügge, W. Derksen, J. Te Poel, B. Hassan, K. Nelson, and D. Wismeijer, “Registration of cone beam computed tomography data and intraoral surface scans - a prerequisite for guided implant surgery with CAD/CAM drilling guides,” *Clinical Oral Implants Research*, vol. 28, no. 9, pp. 1113–1118, 2017.
- [18] D.-H. Lee, S.-Y. An, M.-H. Hong, K.-B. Jeon, and K.-B. Lee, “Accuracy of a direct drill-guiding system with minimal tolerance of surgical instruments used for implant surgery: a prospective clinical study,” *The Journal of Advanced Prosthodontics*, vol. 8, no. 3, pp. 207–213, 2016.
- [19] F. Z. Jamjoom, D. G. Kim, D. J. Lee, E. A. McGlumphy, and B. Yilmaz, “Effect of length and location of edentulous area on the accuracy of prosthetic treatment plan incorporation into cone-beam computed tomography scans,” *Clinical Implant Dentistry and Related Research*, vol. 20, no. 3, pp. 300–307, 2018.
- [20] F. Z. Jamjoom, B. Yilmaz, and W. M. Johnston, “Impact of number of registration points on the positional accuracy of a prosthetic treatment plan incorporated into a cone beam computed tomography scan by surface scan registration: an in vitro study,” *Clinical Oral Implants Research*, vol. 30, no. 8, pp. 826–832, 2019.
- [21] S. Akyalcin, D. J. Dyer, J. D. English, and C. Sar, “Comparison of 3-dimensional dental models from different sources: diagnostic accuracy and surface registration analysis,” *American Journal of Orthodontics and Dentofacial Orthopedics*, vol. 144, no. 6, pp. 831–837, 2013.
- [22] X. Lin, T. Chen, J. Liu, T. Jiang, D. Yu, and S. G. F. Shen, “Point-based superimposition of a digital dental model on to a three-dimensional computed tomographic skull: an accuracy study in vitro,” *British Journal of Oral and Maxillofacial Surgery*, vol. 53, no. 1, pp. 28–33, 2015.
- [23] M. D. Scherer, “Presurgical implant-site assessment and restoratively driven digital planning,” *Dental Clinics of North America*, vol. 58, no. 3, pp. 561–595, 2014.
- [24] C. E. Cann, “Quantitative CT for determination of bone mineral density: a review,” *Radiology*, vol. 166, no. 2, pp. 509–522, 1988.
- [25] M. R. Norton and C. Gamble, “Bone classification: an objective scale of bone density using the computerized tomography scan,” *Clinical Oral Implants Research*, vol. 12, no. 1, pp. 79–84, 2001.
- [26] O. Watzke and W. A. Kalender, “A pragmatic approach to metal artifact reduction in CT: merging of metal artifact reduced images,” *European Radiology*, vol. 14, no. 5, pp. 849–856, 2004.
- [27] H.-Y. Feng, Y. Liu, and F. Xi, “Analysis of digitizing errors of a laser scanning system,” *Precision Engineering*, vol. 25, no. 3, pp. 185–191, 2001.
- [28] A. Suomalainen, T. Vehmas, M. Kortseniemi, S. Robinson, and J. Peltola, “Accuracy of linear measurements using dental cone beam and conventional multislice computed tomography,” *Dentomaxillofacial Radiology*, vol. 37, no. 1, pp. 10–17, 2008.
- [29] F. Teraoka and J. Takahashi, “Dimensional changes and pressure of dental stones set in silicone rubber impressions,” *Dental Materials*, vol. 16, no. 2, pp. 145–149, 2000.
- [30] A. Di Fiore, P. Vigolo, L. Graiff, and E. Stellini, “Digital vs conventional workflow for screw-retained single-implant crowns: a comparison of key considerations,” *The International Journal of Prosthodontics*, vol. 31, no. 6, pp. 577–579, 2018.

Research Article

The Effects of Titanium Surfaces Modified with an Antimicrobial Peptide GL13K by Silanization on Polarization, Anti-Inflammatory, and Proinflammatory Properties of Macrophages

Xuxi Chen ¹, Lin Zhou,² Dong Wu,³ Wenxiu Huang ⁴, Yanjun Lin,⁵ Bowei Zhou,⁶ and Jiang Chen ⁷

¹Fujian Key Laboratory of Oral Diseases, School and Hospital of Stomatology, Fujian Medical University, China

²Fujian Provincial Engineering Research Center of Oral Biomaterial, School and Hospital of Stomatology, Fujian Medical University, China

³Stomatological Key Lab of Fujian College and University, School and Hospital of Stomatology, Fujian Medical University, China

⁴Research Center of Dental and Craniofacial Implant, School and Hospital of Stomatology, Fujian Medical University, China

⁵Institute of Stomatology, School and Hospital of Stomatology, Fujian Medical University, China

⁶Department of Oral Implantology, School and Hospital of Stomatology, Fujian Medical University, China

⁷Institute of Stomatology & Research Center of Dental and Craniofacial Implant, School and Hospital of Stomatology, Fujian Medical University, China

Correspondence should be addressed to Wenxiu Huang; hwx706@126.com and Jiang Chen; dentistjiang@126.com

Received 9 April 2020; Revised 4 June 2020; Accepted 25 June 2020; Published 24 July 2020

Guest Editor: Paolo Pesce

Copyright © 2020 Xuxi Chen et al. This is an open access article distributed under the Creative Commons Attribution License, which permits unrestricted use, distribution, and reproduction in any medium, provided the original work is properly cited.

The polarization of macrophages and its anti-inflammatory and proinflammatory properties play a significant role in host response after implant placement to determine the outcome of osseointegration and long-term survival. In the previous study, we immobilized an antimicrobial peptide, GL13K, onto titanium surfaces to provide immune regulation property. In the herein presented study, we aimed at investigating whether GL13K immobilized titanium surface could improve osteogenesis and reduce the inflammatory reaction around the biomaterials by altering macrophage response. We evaluated the cell proliferation of the different phenotypes of macrophages seeded in GL13K-coated titanium surface, which indicated an inhibition of M1 macrophages and a good cytocompatibility to M2 macrophages. Then, we measured the inflammatory and anti-inflammatory activity of the M1 and M2 macrophages seeded on the GL13K-coated titanium surfaces. The results of the enzyme-linked immunosorbent assay and quantitative reverse transcription-polymerase chain reaction showed that the group with the GL13K modified surface had a downregulation in the expression level of the tumor necrosis factor- α and interleukin-1 β in M1 macrophages and an upregulation of IL-10 and transforming growth factor- β 3 (TGF- β 3) levels in M2 macrophages. This study demonstrated that the GL13K modified titanium surfaces can regulate macrophages' polarization and the expression of inflammatory and anti-inflammatory effects, reducing the effects of the inflammatory process, which may promote the process of bone regeneration and osseointegration.

1. Introduction

Based on the developing of dental implant technology and biomaterials, dental implant has become an increasingly popular treatment for missing teeth. The success of the osseointegration and the subsequent implant survival depend from multiple causal factors, such as physiological conditions

of the recipient, implant site preparation, implant design, and implant surface properties. Dental implant is a prosthetic device made of alloplastic material such as titanium and its alloys like Ti-6Al-4V for its excellent physical and chemical properties and biocompatibility. On the other hand, furthermore factors such as nature of the implant surface and implant placement procedure also contribute to the final

success of osseointegration. However, both the implant operation as a traumatic operation and the implant as a foreign body inevitably lead to a significant immune response and the consequent biological behavior of bone cells, which finally determine the fate of the dental implant. Therefore, the immune response may become an important factor that has a potentially effect on the osteogenic capability of bone biomaterial. However, the current research on implants and bone biomaterials mainly focuses on promoting implant osseointegration and inducing osteogenesis, but ignores the important role of immune-inflammatory response in this process, which often leads to conflicts and disagreements between in vivo and in vitro studies. In order to improve this situation, many new researches began to try to incorporate immune cells into the in vitro evaluation system for osteogenic performance of implants and bone biomaterials in recent years, and good progress was made [1–4]. In vivo and in vitro matching results are also helpful for the research and development of implant and bone biomaterials.

The immune system plays an important role in the host response after implant placement to determine the outcome of osseointegration and long-term survival. As part of the immune system, macrophages receive the most attention due to their vital roles in the regulation of inflammation and tissue regeneration. Studies have shown the high plasticity and multiple effects of macrophages during the healing phase [5]. At the inflammatory site, macrophages activated by infectious microorganism-related molecules and inflammation-related cytokines can switch into different phenotypes, secrete many cytokines, and create a different immune environment [6]. In a specific immune microenvironment, macrophages can polarize into M1/M2 phenotypes characterized by their different functions, surface markers, and inducers that mirror the Th1/Th2 nomenclature of T helper cells [7]. M1 macrophages, known as classically activated inflammatory phenotype, express high levels of the cytokine interleukin- (IL-) 12 as well as the cytokine IL-23. On the contrary, the expression level of the cytokine IL-10 is low in the M1 macrophages. They also secrete many kinds of proinflammatory cytokines including tumor necrosis factor- α (TNF- α), IL-6, and IL-1 β , and produce toxic effector molecules, like reactive oxygen species (ROS), and nitric oxide (NO) [8]. Alternative activated M2 macrophages are characterized by having a high level of scavenger-, mannose, and galactose-type receptors and expressing a high level of IL-10 and low level of IL-12 and IL-23 [9].

The development of osteoimmunology has revealed the multiple functions of macrophages in the bone regeneration process. For example, M1 macrophages secrete many cytokines (TNF- α , IL-6, IL-1 β), which are generally recognized to be inflammatory and have properties of inducing osteoclastogenesis and leading to bone resorption. However, some recent researches have demonstrated the enhancement of osteogenesis in the response of M1 macrophages, rather than M2 [10], while in a wound healing environment, M2 macrophages seem to be related to the late stage of tissue healing. They secrete not only osteogenic cytokines which contributed to osteogenesis, such as (BMP2) and (VEGF), but complicated inflammatory and fibrous agents as well, like TGF- β ,

which lead to inflammation and forming of fibrous capsules [11]. It seems that M2 macrophages play a more important role in the repair reaction compared with M1 macrophages, while the M1 macrophages can determine the pattern of cytokines secreted by M2 macrophages during the early phase of bone regeneration. Prolonged M1 polarization results in the release of fibrosis-related cytokines. Conversely, an effective and timely switch in M1 polarization can lead to osteogenesis-enhancing cytokines release pattern of M2 macrophages [12]. Accordingly, it is probable that both macrophage phenotypes play indispensable roles during the bone regeneration process, and that the switch pattern of macrophage determines the fate of bone biomaterials. Therefore, we can modulate the response of macrophages to biomaterials and affect the bone formation process. An advanced generation of the biomaterials for implants ought to have a property of regulating the local immune environment to improve osseointegration and osteogenesis around the implant.

Antimicrobial peptides (AMPs) have received extensive attention in the area of biomaterials in recent years because of their broad-spectrum antibacterial activity, reduced cytotoxicity, nonselection of resistant mutants, and anti-inflammatory activity, especially when immobilized onto a titanium surface [13, 14]. Our previous research about titanium surface immobilized with antimicrobial peptide GL13K using silane as a chemical linker demonstrated its good antibacterial activity against *Porphyromonas gingivalis* and *Staphylococcus epidermidis* with no cytotoxicity to human gingival fibroblasts and osteoblasts [15, 16]. The GL13K immobilized titanium surface has a property of reducing the effects of the inflammatory process through the downregulation of the main proinflammatory cytokine expression and upregulation of the anti-inflammatory cytokine expression without any influence on cell attachment and proliferation [17]. The immunomodulation property of the titanium surface immobilized with AMP GL13K to macrophage polarization still requires clarification.

According to our previous works, we immobilized an antimicrobial peptide, GL13K, onto titanium surfaces to prepare a potential bone biomaterial and observed a porous network on the GL13K coated surface with greater roughness nanotopography. This study aimed at exploring the impact of the surface-immobilized GL13K to the macrophage polarization and analyzing the proliferation and secretion of different macrophage phenotypes on the titanium surface immobilized with GL13K so as to explain the immunomodulation property of this biomaterial surface in the host inflammatory process and the macrophage polarization. This research provides rationales for the osteoimmunomodulation and osteogenesis promotion of the new generation of implant biomaterials.

2. Materials and Methods

2.1. Titanium and the Modification of the Titanium Surfaces with the AMP GL13K. We used pure titanium foils supplied by Alfa Aesar as the sample in control groups. And the antimicrobial peptides (GL13KGIKLLKASLKLCONH₂, MW = 1424 g/mol) which were used to immobilize the titanium surfaces were provided by China peptides Co. Ltd.

(Shanghai, China). The experimental groups were made by modifying the same pure titanium foils with antimicrobial peptide GL13K. We use 3-(chloropropyl)-triethoxysilane (CPTES, 95%) which was supplied by Sigma-Aldrich (St. Louis, MO, USA) as a linker to modify the titanium surface with the antimicrobial peptide GL13K, as mentioned in our previous study [15]. In simple terms, the immobilization can be immobilized while treated by NaOH and dipped in a mixture, which contained 0.6 ml of diisopropylethylamine, 1.2 ml of 3-(chloropropyl)-triethoxysilane, and 7 ml of anhydrous pentane for silanization. Then, silanized titanium foils obtained were used in Sil-Ti groups. After that, we modified the titanium surface with the antimicrobial peptide GL13K by dipping in a mixed solution which contained AMP GL13K and Na_2CO_3 overnight. Ethanol was used to disinfect all samples for 2 h. Then, the material surfaces were washed with deionized water and dried before using in the GL13K-Ti groups in further assays. We set 0.1 mM as the appropriate saturation concentration of AMP GL13K as we suggested in our previous research [17]. Five samples which were both 10×10 mm square, and 0.25 mm thick were used in each group for this study.

2.2. Cell Culture. RAW 264.7 cells, a murine leukemic monocyte cell line obtained from the American Type Culture Collection (ATCC), were used in this study. RAW 264.7 cells were incubated at 37°C under a humidified $5\% \text{CO}_2$ atmosphere with high glucose Dulbecco's Modified Eagle's Medium (DMEM) (Hyclone, USA) supplemented with 1% penicillin/streptomycin ($100 \times$, Beyotime, China) and 10% fetal bovine serum (Hyclone, USA). RAW 264.7 cells were passaged by gently scraping the cells off while the RAW 264.7 cells reached the confluence of approximately 70%. ALL the RAW 264.7 cells used for the assays were from third to fifth passages.

2.3. Macrophage Activation. When activated cells were needed, Raw 264.7 cells were cultured with the stimulation of 100 ng/ml of ultra-pure lipopolysaccharides (LPS, E. coli, Invivogen, USA) after incubating as described previously to prepared M1 macrophages, and M2 macrophages were obtained by receiving the stimulation of 50 ng/ml of recombinant murine IL-4 (E. coli, PeproTech Inc., USA) after early incubation.

2.4. Macrophage Polarization. The polarization of the macrophages in different groups was evaluated by flow cytometry. After culturing for 24 h, 72 h, and 7 d, macrophages were collected and transferred into 2 groups. The cells in the first group, classified as M1 identification, were incubated with the CD11c antibody marked by PE-Cy7. The cells in the second group, classified as M2 identification, were incubated with the CD206 antibody marked by Alexa Fluor 647. After 1 h of incubation on ice, the detection was performed on the BD FACSCanto™ II system to analyze the surface marker expression of different macrophage polarizations.

2.5. Macrophage Proliferation. The proliferation of the macrophages with different polarizations after culturing on the biomaterial surfaces for 24 h, 48 h, and 72 h was evaluated

by the Cell Counting Kit-8 (CCK-8). At each culturing time point, the old medium was replaced with $500 \mu\text{l}$ of fresh culture medium and $50 \mu\text{l}$ of CCK-8 solution in each group which were incubated for 2 h at 37°C . The optical absorbance value of the solution was measured by a microplate reader at a wavelength of 450 nm.

2.6. Inflammatory and Anti-Inflammatory Cytokines Expression. The inflammatory and anti-inflammatory cytokines expressions of macrophages with different polarizations in different groups were detected by enzyme-linked immunosorbent assay (ELISA). After 24 h culturing on the different surfaces and activated as described previously when cells reached the confluence of 80%, the collected culture medium was centrifuged at 4°C . Extracellular levels of $\text{TNF}\alpha$, $\text{IL-1}\beta$ of M1 macrophages and IL-10, IL-1ra of M2 macrophages were evaluated by ELISA according to the manufacturer's instructions (ABclonal, USA).

2.7. Inflammatory and Anti-Inflammatory Gene Expression. The expression level of inflammation-related and anti-inflammatory genes were measured by quantitative reverse transcription-polymerase chain reaction (qRT-PCR) in the M1 macrophage and M2 macrophage groups, respectively, and the results were normalized to the expression of house-keeping gene glyceraldehyde 3-phosphate dehydrogenase (GAPDH). After the macrophages with different polarizations were seeded onto different surfaces in 6-well plates for 3 days, the total RNA of the treated macrophages with different polarizations was isolated from the different groups following a conventional method. Then, the extracted RNA was transcribed into cDNA by the PrimeScript RT Reagents Kit (Takara) following the manufacturer's instructions after the purity and concentration. The real-time qPCR was performed using the SYBR Premix Ex Taq (Takara) and conducted on a Roche LightCycler 480 System. After the completion of the reaction, the expression level of each gene was calculated by the software of the instrument using the $2^{-\Delta\Delta\text{CT}}$ method. The values were expressed as mean \pm standard deviation. The primer sequences and genes studied in this section are all listed in Table 1.

2.8. Statistical Analysis. The mean values \pm standard deviation was used to express the data of this study. Statistical analysis was carried out with SPSS statistics version (IBM USA) on different samples. All the data were analyzed with a one-way analysis of variance (ANOVA), and the least significant difference (LSD) method was used for comparison. A difference of p value < 0.05 was considered as statistically significant.

3. Results

3.1. Macrophage Polarization. After culturing on different surfaces for 24 h, 72 h, and 7 d, the expression of the macrophage surface marker evaluated by flow cytometry showed higher expression level of the M2 marker CD206 and lower expression level of the M1 marker CD11c by the RAW264.7 cells in the GL13K groups in comparison with those in the titanium groups (Figure 1). These results suggested that GL13K-coated titanium surface has a better

TABLE 1: Inflammatory and anti-inflammatory gene primer sequences used in the qRT-PCR.

GAPDH	Forward primer	5'-CTCCCACTCTTCCACCTTCG-3'
	Reverse primer	5'-TTGCTGTAGCCGTATTCATT-3'
TNF- α	Forward primer	5'-CTGAACTTCGGGGTGATCGG-3'
	Reverse primer	5'-GGCTTGCACTCGAATTTTGA-3'
IL-1 β	Forward primer	5'-TGGAGAGTGTGGATCCCAAG-3'
	Reverse primer	5'-GGTGCTGATGTACCAGTTGG-3'
IL-6	Forward primer	5'-ATAGTCCTTCCACCCCAATTTCC-3'
	Reverse primer	5'-GATGAATTGGATGGTCTTGGTCC-3'
IL-10	Forward primer	5'-GAGAAGCATGGCCAGAAATC-3'
	Reverse primer	5'-GAGAAATCGATGACAGCGCC-3'
IL-1ra	Forward primer	5'-CTCCAGCTGGAGGAAGTTAAC-3'
	Reverse primer	5'-CTGACTCAAAGCTGGTGGTG-3'
TGF- β 1	Forward primer	5'-CAGTACAGCAAGGTCCTTGC-3'
	Reverse primer	5'-ACGTAGTAGACGATGGGCAG-3'
TGF- β 3	Forward primer	5'-CAACACCCTGAACCCAGAG-3'
	Reverse primer	5'-CTTACCACCATGTTGGACAG-3'

property of reducing the M1 polarization of macrophages and increasing the M2 polarization of macrophages then the titanium surface.

3.2. Macrophage Proliferation. The proliferation of macrophages was measured by using CCK-8 in different groups. The results in Figure 2 showed the difference of the optical density (OD) values in different groups. For the macrophages with the M1 polarization, the statistically significant differences can be found between the results on the titanium surface and GL13K-coated titanium surface at both 48 h and 72 h. By contrast, the results for the macrophages with M2 polarization showed no statistically significant difference between the two groups which mean that they were almost identical in the 3 time periods. Taken together, all these results show that GL13K immobilized titanium surface may inhibit the proliferation of M1 macrophages and have a great biocompatibility for M2 macrophages.

3.3. Inflammatory and Anti-Inflammatory Cytokine Expression. ELISA was used to evaluate the extracellular secretion level of cytokines TNF- α , IL-1 β in macrophages with M1 polarization, and the cytokines IL-10 and IL-1ra in macrophages with M2 polarization. While comparing with the macrophages in the control group without any additional stimulation, the results in Figure 3 revealed that releasing cytokines IL-1 β and IL-1ra had no statistically significant difference in the GL13K-coated titanium group by M1 and M2 macrophages, respectively, but a significant difference can be seen that M1 macrophages seeded on the GL13K-coated surface released a lower level of proinflammatory cytokine TNF- α , and M2 macrophages released a higher level of IL-10 than those in the control group. While comparing with the macrophages in the titanium group, M1 and M2

macrophages seeded on the GL13K-coated surface also shows the decreasing expression level of cytokine TNF- α and increasing level of cytokine IL10, respectively. This result suggested that GL13K-coated titanium not only regulates macrophage polarization but also regulates the secretion of inflammatory cytokines by different types of macrophage.

3.4. Inflammatory and Anti-Inflammatory Gene Expression. The mRNA expression of the cytokines IL-1 β TNF- α , and IL-6 in macrophages with M1 polarization and the cytokines IL-10, IL-1ra, TGF- β 1, and TGF- β 3 in macrophages with M2 polarization which were cultured on different samples was investigated by qRT-PCR at 72 h. Figure 4 shows the down-regulation of proinflammatory genes TNF- α and IL-6 in M1 macrophages after being seeded on the GL13K-coated Ti surface. Whereas this surface also significantly improved the expression level of anti-inflammatory genes IL-10 and TGF- β 3 in M2 macrophages after being seeded on the GL13K-coated Ti surface. This result also proved that GL13K-coated titanium surface has a property of regulating the cytokine release by macrophages, and it can be seen that this specified surface performed better than titanium surface.

4. Discussion

Macrophages play multiple significant roles in the process of osteogenesis and osseointegration after implantation. In the local environment of injured tissue, macrophages first exhibit M1 phenotypes, secreting a large amount of TNF- α , IL-1 β , and IL-6, which can activate inflammatory responses and the tissue regeneration process. However, if these cytokines exist for a long time in healing tissue, they inhibit the expression of BMP-2 receptors and affect the chemotaxis and migration of osteoblasts, thereby affecting the bone formation [18].

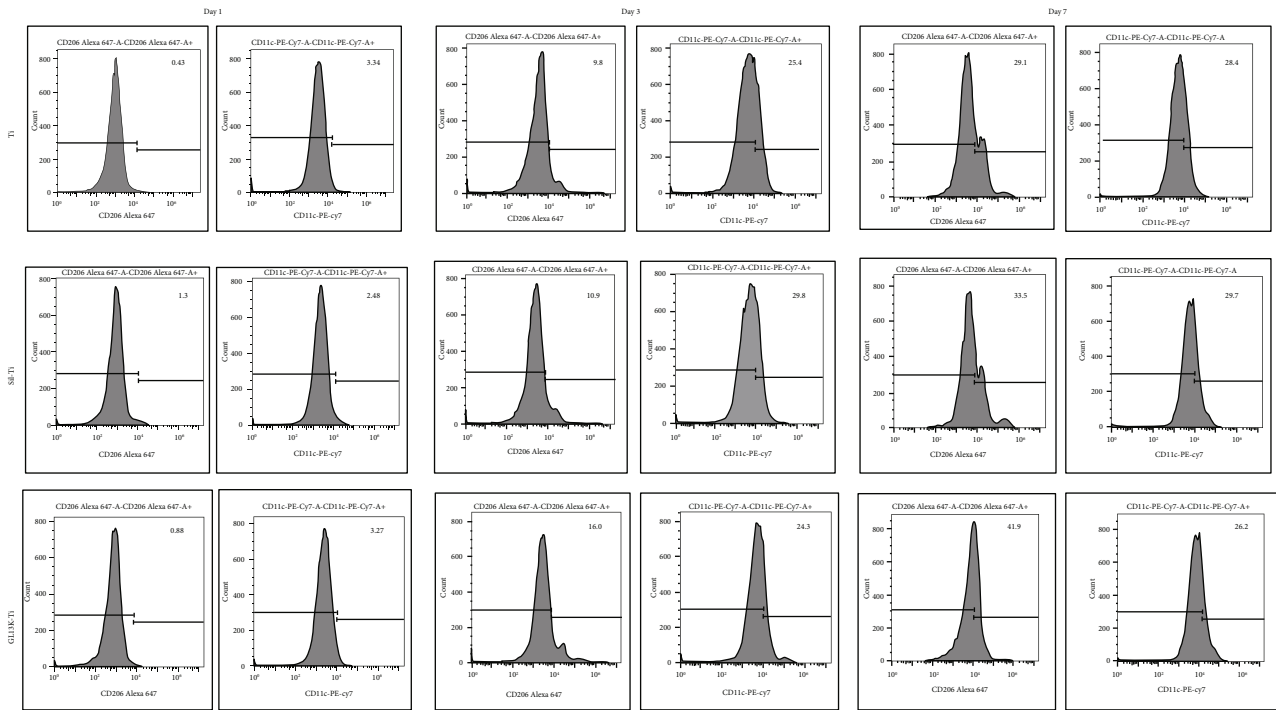


FIGURE 1: FACS results of RAW264.7 cells cultured on the titanium surface, the silanized titanium surface, and the GL13K-coated titanium surface for 24 h, 72 h, and 7 d. After being seeded onto GL13K-coated titanium surfaces, the mean expression level of CD206 was increased in comparison to that in the titanium groups, while the mean expression level of CD11c was reduced in the cells cultured on the GL13K-coated titanium compared with the titanium group.

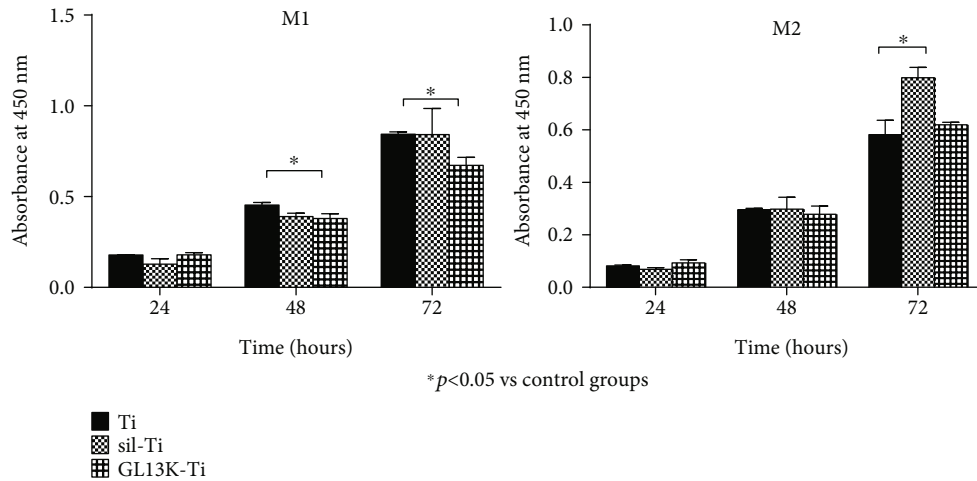


FIGURE 2: Cell proliferation of M1 macrophages and M2 macrophages after culturing on the titanium surface, the silanized titanium surface, and the GL13K-coated surface for 24, 48, and 72 h. Error bars represent mean \pm SD for $n = 5$. A statistically significant difference exists between GL13K-coated Ti groups and Ti groups at 48 h ($p < 0.001$) and 72 h ($p < 0.05$).

In contrast, moderate M2 polarization promotes osteogenesis, while excessive M2 macrophage polarization induces fibrocysts that prevent the inflammatory sites from bone formation. Therefore, the moderate transformation of macrophages from the proinflammatory phenotype M1 to the immune regulation or anti-inflammatory phenotype M2 is considered an important aspect to promote the bone healing

process, that is, to promote the functional recovery rather than the formation of scar tissue [19–24].

Our study shows that when the macrophages were cultured on GL13K-coated titanium surfaces, the surface markers of M1 polarization macrophage were reduced and M2 macrophage polarization surface markers were increased compared with those cultured on the titanium surface, which

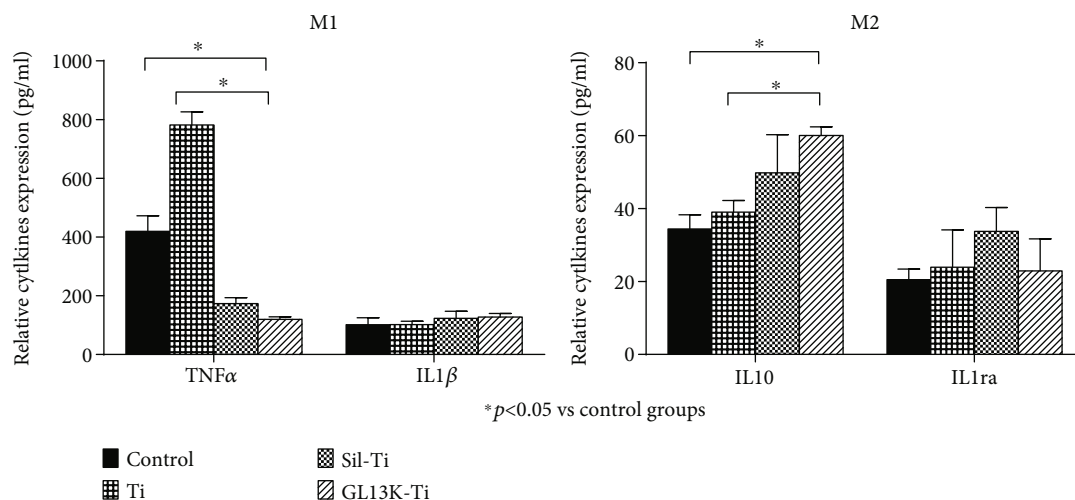


FIGURE 3: ELISA analysis of the secretion of IL-1 β and TNF- α in macrophages with M1 polarization and IL-10 and IL-1ra in macrophages with M2 polarization cultured on the titanium surface, the silanized titanium surface, and the GL13K-coated surface at 24 h. Error bars represent mean \pm SD for $n = 5$. The downregulation of the secretion level of cytokines TNF- α ($p < 0.001$) and the upregulation of cytokines IL-10 ($p = 0.002$) were detected in the GL13K immobilized titanium group.

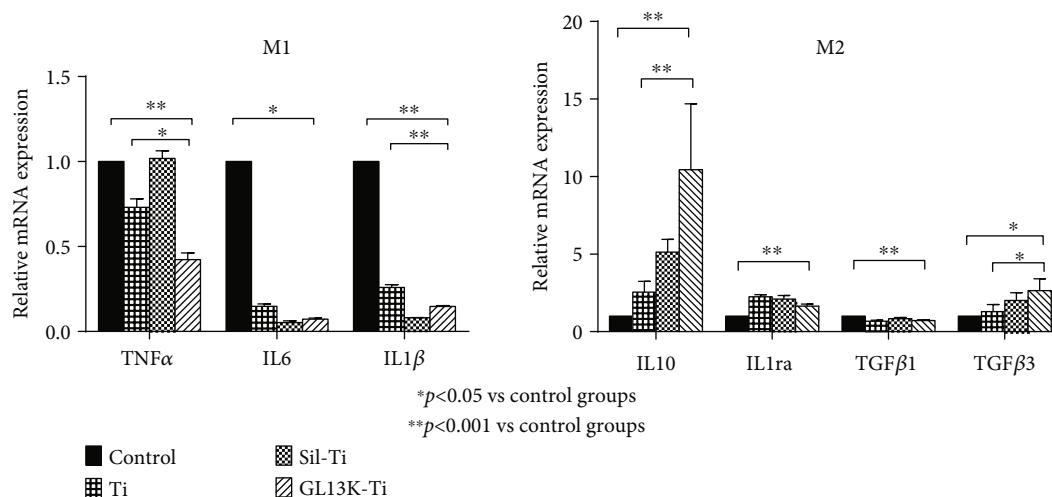


FIGURE 4: Quantitative analysis of the secretion of TNF- α , IL-6, and IL-1 β of macrophages with M1 polarization and IL-10, IL-1ra, TGF- β 1, and TGF- β 3 of macrophages with M2 polarization after culturing on the titanium surface, the silanized titanium surface, and the GL13K-coated surface for 3 days. Error bars represent mean \pm SD for $n = 5$. A downregulation of the relative mRNA expression of TNF- α ($p = 0.001$) and IL-1 β ($p < 0.001$) was detected in the groups of GL13K immobilized titanium, while the expression of IL-10 ($p < 0.001$) and TGF- β 3 ($p = 0.003$) levels were upregulated in these groups.

means macrophages can be promoted from the M1 polarization state toward the M2 polarization state while stimulated by GL13K-coated titanium surface. In the cell proliferation experiment of M1 and M2 macrophages, GL13K-coated titanium surfaces were found to inhibit the M1 macrophage polarization and have a good biocompatibility for the polarization of the M2 macrophages. It can be suggested that the regulation of the polarization state of macrophages on the surface of GL13K modified titanium material is due to its different proliferation promotion and inhibition effects on macrophages with different polarization phenotypes. Thanks to the moderation of the promotion effect in M2 macro-

phages, the GL13K-coated titanium surface can modulate the switch pattern of macrophages by transforming the M1 polarization to M2 polarization mildly without resulting in excessive M2 polarization [19].

In this study, it was also found that the immunoregulatory function of GL13K-coated titanium surface for the expression of anti-inflammatory and proinflammatory factors in macrophages not only derives from its regulation on the transformation of M1/M2 polarized phenotype in macrophages but also from its regulation on the secretion of cytokines by macrophages with different polarized phenotypes. In comparison to M1 macrophages cultured on the

titanium surface, those cultured on the surface of GL13K-coated titanium have decreased levels of the inflammatory cytokine TNF- α , which has been observed to suppress the differentiation of osteoblastic cells by inhibiting the release of BMP-2 and inducing apoptosis effects on osteoblasts [25, 26]. On the other hand, M2 macrophages released more IL-10 after culturing on the GL13K-coated titanium surfaces. Moreover, compared with the titanium surface, after being cultured on the GL13K immobilized titanium surface for 3 days, the expression levels of mRNA TNF- α and IL-1 β of M1 macrophages decreased, while the mRNA IL10 and TGF- β 3 expressed by M2 macrophages significantly increased. The inhibitory effect of GL13K-coated titanium surface to the M1 macrophages may be one of the reasons for this, but it also shows that the GL13K immobilized titanium surface can regulate the release of cytokines from macrophages. It can inhibit the proinflammatory factor secreting by M1 macrophages and promote the anti-inflammatory factor releasing of M2 macrophages, thus promoting the transformation of inflammatory processes to the tissue healing process. This result is corresponding with some other researchers that suggested the properties of the antimicrobial peptides to suppress the secretion of inflammation-related cytokines [27].

It is worth noting that the silanized titanium surface also shows some potential of immune regulation in this study. After culturing on this surface for 72 h, M2 macrophage proliferation is promoted ($p < 0.001$), and the silanized titanium surface also showed inhibition in the expression of the cytokine TNF- α and mRNA IL-1 β . As a chemical linker between the biomaterial substrate and the biomolecules, the silanes have been thoroughly studied. Based on silanes, bioactive molecules can covalently attach to surfaces with self-assembled monolayers [28], and we can improve the biological properties of the biomaterial coating using silanes that induce specific cell responses, such as cell proliferation, cell differentiation [29], or antibacterial effects [30, 31]. However, research on the biological properties of these silanized surfaces remains scarce. Previous studies have shown that silanization can improve the surface properties of titanium [32], improve its antibacterial properties [33], and even increase the expression of osteoblastic cell differentiation markers to provide osteoinductive properties [34]. This indicates that it had certain regulation effects on the biological behavior of cells, suggesting that part of the biological function of the GL13K-modified titanium surface was derived from silanization treatment.

In summary, the GL13K immobilized titanium surface was showed the properties for the regulation of macrophages' polarization and the expression of inflammatory and anti-inflammatory effects within the limits of our research. However, further researches are still needed to investigate the mechanism for the biomaterials to regulate the immune responses and induce bone regeneration. In recent years, miRNAs have been demonstrated to be pivotal players actively participating in the macrophage polarization, inflammatory, anti-inflammatory, and tissue healing activities [35]. Moreover, specific miRNA expression profiles have been found to predict specific clinical outcomes, which means miRNAs

may be reliable markers and important regulatory elements in the interaction between biomaterials and tissues [36, 37]. This may provide a favorable complement to our future research. It is also worth noting that as every in vitro study, the translation of the results from these studies to the clinical situation is limited. Further researches are still needed to accurately simulate the complex in vivo environment by investigating the involvement of more immunocytes and bone cells.

5. Conclusion

In the present study, the GL13K immobilized titanium surface showed the inhibition of the M1 macrophage polarization and a good biocompatibility for the polarization of the M2 macrophages, and it regulates the properties of the inflammatory and anti-inflammatory cytokines, respectively, secreted by M1 and M2 macrophages. Moreover, compared with the titanium surface, the GL13K immobilized titanium surface can regulate the expression of proinflammatory and anti-inflammatory relative genes in M1 and M2 macrophages, resulting in less time in the inflammatory process and more time in the tissue healing process.

Data Availability

All data used during this study are available from the corresponding author by request.

Conflicts of Interest

The authors declare that they have no conflicts of interest.

Authors' Contributions

Xuxi Chen and Lin Zhou should be considered joint first authors.

Acknowledgments

The works were financially supported by the National Natural Science Foundation of China (NSFC) (No. 81771126) and the Fujian provincial healthy and family planning commission program (No. 2017-2-37).

References

- [1] C. Wu, Z. Chen, D. Yi, J. Chang, and Y. Xiao, "Multidirectional effects of Sr-, Mg-, and Si-containing bioceramic coatings with high bonding strength on inflammation, osteoclastogenesis, and osteogenesis," *ACS Applied Materials & Interfaces*, vol. 6, no. 6, pp. 4264–4276, 2014.
- [2] Z. Chen, D. Yi, X. Zheng, J. Chang, C. Wu, and Y. Xiao, "Nutrient element-based bioceramic coatings on titanium alloy stimulating osteogenesis by inducing beneficial osteoimmunomodulation," *Journal of Materials Chemistry B*, vol. 2, no. 36, pp. 6030–6043, 2014.
- [3] M. Shi, Z. Chen, S. Farnaghi et al., "Copper-doped mesoporous silica nanospheres, a promising immunomodulatory agent for inducing osteogenesis," *Acta Biomaterialia*, vol. 30, pp. 334–344, 2016.

- [4] W. Zhang, F. Zhao, D. Huang, X. Fu, X. Li, and X. Chen, "Strontium-substituted submicrometer bioactive glasses modulate macrophage responses for improved bone regeneration," *ACS Applied Materials & Interfaces*, vol. 8, no. 45, pp. 30747–30758, 2016.
- [5] Z. Chen, T. Klein, R. Z. Murray et al., "Osteoimmunomodulation for the development of advanced bone biomaterials," *Materials Today*, vol. 19, no. 6, pp. 304–321, 2016.
- [6] P. Italiani and D. Boraschi, "From monocytes to M1/M2 macrophages: phenotypical vs. functional Differentiation," *Frontiers in Immunology*, vol. 5, 2014.
- [7] C. D. Mills, K. Kincaid, J. M. Alt, M. J. Heilman, and A. M. Hill, "Pillars Article: M-1/M-2 Macrophages and the Th1/Th2 Paradigm. *J. Immunol.* 2000. 164: 6166–6173," *The Journal of Immunology*, vol. 199, no. 7, pp. 2194–2201, 2017.
- [8] S. Gordon and P. R. Taylor, "Monocyte and macrophage heterogeneity," *Nature Reviews Immunology*, vol. 5, no. 12, pp. 953–964, 2005.
- [9] A. Sica and A. Mantovani, "Macrophage plasticity and polarization: in vivo veritas," *The Journal of Clinical Investigation*, vol. 122, no. 3, pp. 787–795, 2012.
- [10] P. Guihard, Y. Danger, B. Brounais et al., "Induction of osteogenesis in mesenchymal stem cells by activated monocytes/macrophages depends on oncostatin M signaling," *Bone*, vol. 50, no. 4, pp. S83–S83, 2012.
- [11] D. O. Freytes, J. W. Kang, I. Marcos-Campos, and G. Vunjak-Novakovic, "Macrophages modulate the viability and growth of human mesenchymal stem cells," *Journal of Cellular Biochemistry*, vol. 114, no. 1, pp. 220–229, 2013.
- [12] Z. Chen, J. Yuen, R. Crawford, J. Chang, C. Wu, and Y. Xiao, "The effect of osteoimmunomodulation on the osteogenic effects of cobalt incorporated β -tricalcium phosphate," *Biomaterials*, vol. 61, pp. 126–138, 2015.
- [13] M. Kazemzadeh-Narbat, J. Kindrachuk, K. Duan, H. Jenssen, R. E. W. Hancock, and R. Wang, "Antimicrobial peptides on calcium phosphate-coated titanium for the prevention of implant-associated infections," *Biomaterials*, vol. 31, no. 36, pp. 9519–9526, 2010.
- [14] P. H. Warnke, E. Voss, P. A. J. Russo et al., "Antimicrobial peptide coating of dental implants: biocompatibility assessment of recombinant human beta defensin-2 for human cells," *The International Journal of Oral & Maxillofacial Implants*, vol. 28, no. 4, pp. 982–988, 2013.
- [15] L. Zhou, Y. Lai, W. Huang et al., "Biofunctionalization of microgroove titanium surfaces with an antimicrobial peptide to enhance their bactericidal activity and cytocompatibility," *Colloids and Surfaces B: Biointerfaces*, vol. 128, pp. 552–560, 2015.
- [16] K. V. Holmberg, M. Abdolhosseini, Y. Li, X. Chen, S. U. Gorr, and C. Aparicio, "Bio-inspired stable antimicrobial peptide coatings for dental applications," *Acta Biomaterialia*, vol. 9, no. 9, pp. 8224–8231, 2013.
- [17] L. Zhou, Z. Lin, J. Ding, W. Huang, J. Chen, and D. Wu, "Inflammatory and biocompatibility evaluation of antimicrobial peptide GL13K immobilized onto titanium by silanization," *Colloids and Surfaces B: Biointerfaces*, vol. 160, pp. 581–588, 2017.
- [18] N. E. Hengartner, J. Fiedler, A. Ignatius, and R. E. Brenner, "IL-1 β inhibits human osteoblast migration," *Molecular Medicine*, vol. 19, no. 1, pp. 36–42, 2013.
- [19] B. N. Brown, R. Londono, S. Tottey et al., "Macrophage phenotype as a predictor of constructive remodeling following the implantation of biologically derived surgical mesh materials," *Acta Biomaterialia*, vol. 8, no. 3, pp. 978–987, 2012.
- [20] E. M. Sussman, M. C. Halpin, J. Muster, R. T. Moon, and B. D. Ratner, "Porous implants modulate healing and induce shifts in local macrophage polarization in the foreign body reaction," *Annals of Biomedical Engineering*, vol. 42, no. 7, pp. 1508–1516, 2014.
- [21] R. Guo, A. R. Merkel, J. A. Sterling, J. M. Davidson, and S. A. Guelcher, "Substrate modulus of 3D-printed scaffolds regulates the regenerative response in subcutaneous implants through the macrophage phenotype and Wnt signaling," *Biomaterials*, vol. 73, pp. 85–95, 2015.
- [22] B. V. Fearing and M. E. Van Dyke, "In vitro response of macrophage polarization to a keratin biomaterial," *Acta Biomaterialia*, vol. 10, no. 7, pp. 3136–3144, 2014.
- [23] B. N. Brown, J. E. Valentin, A. M. Stewart-Akers, G. P. McCabe, and S. F. Badylak, "Macrophage phenotype and remodeling outcomes in response to biologic scaffolds with and without a cellular component," *Biomaterials*, vol. 30, no. 8, pp. 1482–1491, 2009.
- [24] L. R. Madden, D. J. Mortisen, E. M. Sussman et al., "Proangiogenic scaffolds as functional templates for cardiac tissue engineering," *Proceedings of the National Academy of Sciences of the United States of America*, vol. 107, no. 34, pp. 15211–15216, 2010.
- [25] L. Gilbert, X. He, P. Farmer et al., "Inhibition of osteoblast differentiation by tumor necrosis factor- α ," *Endocrinology*, vol. 141, no. 11, pp. 3956–3964, 2000.
- [26] M. Feldmann and R. N. Maini, "Anti-TNF therapy, from rationale to standard of care: what lessons has it taught us?," *Journal of Immunology*, vol. 185, no. 2, pp. 791–794, 2010.
- [27] Y. Liu, X. Xia, L. Xu, and Y. Z. Wang, "Design of hybrid β -hairpin peptides with enhanced cell specificity and potent anti-inflammatory activity," *Biomaterials*, vol. 34, no. 1, pp. 237–250, 2013.
- [28] S. Bauer, P. Schmuki, K. von der Mark, and J. Park, "Engineering biocompatible implant surfaces," *Progress in Materials Science*, vol. 58, no. 3, pp. 261–326, 2013.
- [29] G. K. Toworfe, S. Bhattacharyya, R. J. Composto, C. S. Adams, I. M. Shapiro, and P. Ducheyne, "Effect of functional end groups of silane self-assembled monolayer surfaces on apatite formation, fibronectin adsorption and osteoblast cell function," *Journal of Tissue Engineering and Regenerative Medicine*, vol. 3, no. 1, pp. 26–36, 2009.
- [30] Y. Ma, M. Chen, J. E. Jones, A. C. Ritts, Q. Yu, and H. Sun, "Inhibition of *Staphylococcus epidermidis* biofilm by trimethylsilane plasma coating," *Antimicrobial Agents and Chemotherapy*, vol. 56, no. 11, pp. 5923–5937, 2012.
- [31] M. G. Katsikogianni and Y. F. Missirlis, "Interactions of bacteria with specific biomaterial surface chemistries under flow conditions," *Acta Biomaterialia*, vol. 6, no. 3, pp. 1107–1118, 2010.
- [32] J. P. Matinlinna, J. K. H. Tsoi, J. de Vries, and H. J. Busscher, "Characterization of novel silane coatings on titanium implant surfaces," *Clinical Oral Implants Research*, vol. 24, no. 6, pp. 688–697, 2013.
- [33] N. Villard, C. Seneviratne, J. K. H. Tsoi, M. Heinonen, and J. Matinlinna, "Candida albicans aspects of novel silane system-coated titanium and zirconia implant surfaces," *Clinical Oral Implants Research*, vol. 26, no. 3, pp. 332–341, 2015.

- [34] M. Godoy-Gallardo, J. Guillem-Marti, P. Sevilla, J. M. Manero, F. J. Gil, and D. Rodriguez, "Anhydride-functional silane immobilized onto titanium surfaces induces osteoblast cell differentiation and reduces bacterial adhesion and biofilm formation," *Materials Science and Engineering: C*, vol. 59, no. 5, pp. 524–532, 2016.
- [35] G. Curtale, M. Rubino, and M. Locati, "MicroRNAs as molecular switches in macrophage activation," *Frontiers in Immunology*, vol. 10, p. 799, 2019.
- [36] M. Menini, P. Pesce, D. Baldi, G. Coronel Vargas, P. Pera, and A. Izzotti, "Prediction of titanium implant success by analysis of microRNA expression in peri-implant tissue. A 5-year follow-up study," *Journal of Clinical Medicine*, vol. 8, no. 6, p. 888, 2019.
- [37] M. Menini, E. Dellepiane, D. Baldi, M. G. Longobardi, P. Pera, and A. Izzotti, "Microarray expression in peri-implant tissue next to different titanium implant surfaces predicts clinical outcomes: a split-mouth study," *Clinical Oral Implants Research*, vol. 28, no. 9, pp. e121–e134, 2017.